DEVELOPING IN-VITRO SYNTHETIC BLOOD CLOT MODELS FOR TESTING THROMBOLYTIC DRUGS

by

Ziqian Zeng

A Dissertation

Submitted to the Faculty of Purdue University

In Partial Fulfillment of the Requirements for the degree of

Doctor of Philosophy

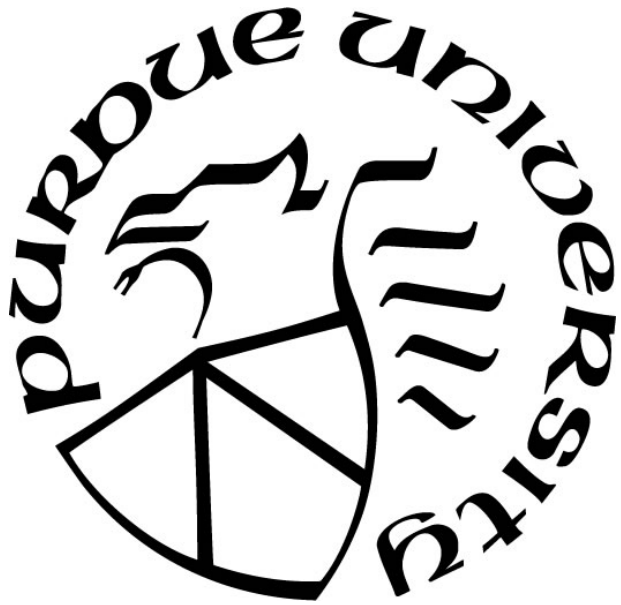

Weldon School of Biomedical Engineering

West Lafayette, Indiana

May 2022

THE PURDUE UNIVERSITY GRADUATE SCHOOL
STATEMENT OF COMMITTEE APPROVAL

Dr. Nathan J. Alves, Co-Chair
Emergency Medicine Department
Indiana University School of Medicine

Dr. Sherry L. Harbin, Co-Chair
Weldon School of Biomedical Engineering

Dr. Julie C. Liu
Weldon School of Biomedical Engineering

Dr. Vitaliy L. Rayz
Weldon School of Biomedical Engineering

Approved by:
Dr. Tamara L. Kinzer-Ursem

Dedicated to my family and friends

ACKNOWLEDGMENTS

I would like to express my appreciation to all the individuals that have helped me during my Ph.D. career. I would like to first thank my lovely wife for the unfailing support and love that has guided me through the difficult times. I thank my advisor Dr. Nathan Alves who has offered me the excellent opportunity to work on such a fantastic project. Dr. Alves has provided invaluable insights and advice that genuinely enlightened my understanding of science and guided my research and life. I also thank my co-advisor, Dr. Sherry Harbin, and committee members, Dr. Vitaliy Rayz and Dr. Julie Liu, for constructive feedback on my project. I also want to acknowledge my collaborators, Dr. Amelia Linnemann and Dr. Mouhamad Alloosh at IUSM, for sharing resources and instruments. I am also grateful to my lab mates and friends, Tanmaye and Alexei. I thank you both for the support and encouragement inside and outside the lab. I also want to thank the lab manager Abigail Hall and all other colleagues, friends, professors, and collaborators who have helped me throughout my Ph.D. career.

TABLE OF CONTENTS

LIST OF TABLES 9
LIST OF FIGURES 10
ABSTRACT 15
1. INTRODUCTION 16
2. BACKGROUND 19
2.1 Thrombus Formation and Dissolution 21
2.2 Thrombus Stability and Hemodynamics 22
2.3 Animal Thrombosis Models 24
2.4 Diagnostic Assays 27
2.5 *in-vitro* Thrombosis Models 29
2.5.1 Flow Chamber-based Model 30
2.5.2 Chandler Loop Model 31
2.6 Conclusion 32
2.7 References 33
3. CHARACTERIZATION OF FIBRIN UNDER VARIOUS CLOTTING CONDITIONS ... 47
3.1 Abstract 47
3.2 Introduction 48
3.3 Material and Methods 51
3.3.1 Materials 51
3.3.2 Sample Preparation 51
3.3.3 Thromboelastography Assays 52
3.3.4 Varying Ionic Strength 52
3.3.5 Varying pH 53
3.3.6 Statistical Analysis 53
3.4 Results and Discussion 54
3.4.1 Factor Contamination Study 55
3.4.2 Effects of Fibrinogen Concentration on Clot Formation 58
3.4.3 Effects of Thrombin Concentration on Clot Formation 59
3.4.4 Effects of Ionic Strength on Clot Formation 61

3.4.5 Effects of pH on Clot Formation 63
3.4.6 Effects of Albumin Concentration on Clot Formation 64
3.4.7 Cross-Species Fibrin Deposition 65
3.5 Conclusions 67
3.6 References 68
4. FLUORESCENTLY CONJUGATED ANNULAR FIBRIN CLOT FOR MULTIPLEXED REAL-TIME DIGESTION ANALYSIS 72
4.1 Abstract 73
4.2 Introduction 74
4.3 Materials and Methods 77
4.3.1 FITC-Fibrinogen Conjugation 77
4.3.2 Clotting Solution Preparation 80
4.3.3 FITC-Fibrin Turbidity and TEG Assays 80
4.3.4 Scanning Electron Microscopy 80
4.3.5 Confocal Microscopy 81
4.3.6 Fibrin Clot Stability After Storage 81
4.3.7 Annular Clot Fabrication 81
4.3.8 Dose Response Experiment 82
4.3.9 Annular Clot Lysis Assay 82
4.3.10 S2251 Chromogenic Assay 82
4.3.11 Statistical Analysis 83
4.4 Results and Discussion 83
4.4.1 Effect of Fibrinogen Tagging on Clot Formation 83
4.4.2 Fibrin clot Morphology via SEM 86
4.4.3 Tagging Consistency via Confocal Microscopy 88
4.4.4 Annular Clot Formation 90
4.4.5 Effects of Fibrinogen Tagging on Plasmin Clot Digestion 91
4.4.6 Varying Plasminogen and tPA levels on Annular Clot Digestion 95
4.5 Conclusion 99
4.6 References 100

5. EFFECT OF CHANDLER LOOP SHEAR AND TUBING SIZE ON CLOT ARCHITECTURE 105
5.1 Abstract 105
5.2 Introduction 106
5.3 Materials and Methods 108
5.3.1 Materials 108
5.3.2 Chandler Loop Clot Formation 108
5.3.3 Clot Properties and Histology 109
5.3.4 Scanning Electron Microscopy 109
5.3.5 Statistical Analysis 110
5.4 Results 110
5.4.1 Clot Formation 110
5.4.2 Clot Appearance and Weight 110
5.4.3 Histologic Composition 112
5.4.4 Shear Effects on Clot Composition 114
5.4.5 Scanning Electron Microscopy 116
5.5 Discussion 117
5.6 Conclusions 119
5.7 References 120
6. REAL-TIME TRACKING OF FIBRINOLYSIS UNDER PHYSIOLOGIC SHEAR IN AN IN-VITRO THROMBOLYSIS MODEL 124
6.1 Abstract 125
6.2 Introduction 125
6.3 Materials and Methods 128
6.3.1 Whole Blood and Plasma Processing 128
6.3.2 FITC-Fibrinogen Synthesis 128
6.3.3 Thromboelastography 128
6.3.4 Whole Blood Clot Analog Formation 129
6.3.5 Hematoxylin & Eosin Staining and Epifluorescence 129
6.3.6 Static Digestion 130
6.3.7 Chandler Loop Digestion 130

6.3.8 RT-FluFF Assay Construction 131
6.3.9 RT-FluFF Digestion Assay 132
6.3.10 Shear-Stretch Analysis 132
6.3.11 Statistical Analysis 132
6.4 Results 133
6.4.1 Generating a Physiologically Relevant Clot Analog 133
6.4.2 RT-FluFF Assay Device Characterization 135
6.4.3 Quantifying Fibrinolysis in Real-Time 139
6.5 Discussion 142
6.5.1 Optimization of FITC-labeling 142
6.5.2 Thrombolysis and Fluorometric Monitoring of Fibrinolysis 144
6.5.3 Limitations of the *in-vitro* Thrombolysis Model 145
6.6 Conclusions 146
6.7 References 147
7. PULSATILE EFFECT ON THROMBOLYTIC DRUG EFFICACY 151
7.1 Abstract 151
7.2 Introduction 152
7.3 Materials and Methods 154
7.3.1 Pulsatile RT-FluFF Model Setup 154
7.3.2 Clot Formation and Digestion 156
7.3.3 Statistical Analysis 156
7.4 Results 157
7.5 Discussion 160
7.6 Conclusions 161
7.7 References 161
8. FUTURE DIRECTIONS 164
8.1 Reference 166
APPENDIX 168
PUBLICATIONS 186

LIST OF TABLES

Table 3.1. Reproducibility test of TEG varying fibrinogen concentration in fibrin..... 54

Table 4.1. Total pore area and fiber diameter of clot at different fibrinogen to 12FhF ratios 88

Table 7.1. Flow Parameters of RT-FluFF model to mimic MPA..... 155

LIST OF FIGURES

Figure 2.1. Coagulation cascade and fibrinolysis..... 22

Figure 2.2. The Chandler Loop, human blood is perfused in an end-joined loop, which is fixed on a plate. The shaft through the center of the plate can be spun to a desired speed to mimic the in vivo hemodynamic changes. 32

Figure 3.1. (A) Turbidity and (B) TEG tracing curves. After a lag period following the clot initiation, clot absorbance (turbidity assay) and clot amplitude (TEG assay) increase over time and level off at the end of clot formation. The symmetrical shaped trajectory in the TEG assay is a result of the dual-direction rotation and sensing by the pin. 55

Figure 3.2. Standard curve of Technochrom® FXIII kit (A) and Factor XIII activity in bovine and human 3 mg/mL fibrinogen stock (B). Triplicates were performed using different aliquots on different days with data represented as means ± std. 56

Figure 3.3. Comparison of RT (non-dialyzed), dialyzed, RT+Ca and Dialyzied+Ca groups for bovine fibrin TEG^{Max} (A) and TEG^{Time} (C) and human fibrin TEG^{Max} (B) and TEG^{Time} (D). RT and dialyzed groups showed little difference in TEG^{Max} and TEG^{Time} for both bovine and human. Experiments were performed in triplicates using different aliquots and dialysis cassettes on different days. 57

Figure 3.4. Turbidity (A) and TEG assays (B) on bovine and human fibrin clots with different fibrinogen concentrations (1, 2, 3, 4, 5 mg/mL) at constant 1U/mL thrombin. $Turb^{max}$ and TEG^{Max} on primary axis; $Turb^{Time}$ and TEG^{Time} on secondary axis. All comparisons were made using averages. Raw tracing curves of turbidity and TEG shown in Figure A.1 and Figure A.2 with V_{max}, Lag time, α angle and R included in Table A.1. 59

Figure 3.5. Turbidity (A) and TEG assays (B) on bovine and human fibrin clots at 3 mg/mL fibrinogen with different thrombin concentrations (0.1, 0.3, 0.6, 0.8, 1, 2.5, 5, 10 U/mL). $Turb^{max}$ and TEG^{Max} on primary axis; $Turb^{Time}$ and TEG^{Time} on secondary axis. All comparisons were made using averages. Raw tracing curves of turbidity and TEG shown in Figure A.3 and Figure A.4 with V_{max}, Lag time, α angle and R included in Table A.2. 60

Figure 3.6. Turbidity assays (A) and TEG assays (B) on bovine and human fibrin clots at 3 mg/mL fibrinogen with 1U/mL thrombin at different ionic strength in PBS (0.05, 0.13, 0.14, 0.15, 0.16, 0.17, 0.3M). $Turb^{max}$ and TEG^{Max} on primary axis; $Turb^{Time}$ and TEG^{Time} on secondary axis. All comparisons were made using averages. Raw tracing curves of turbidity and TEG shown in Figure A.5 and Figure A.6 with V_{max}, Lag time, α angle and R included in Table A.3. 62

Figure 3.7. Turbidity assays (A) and TEG assays (B) on bovine and human fibrin clots at 3 mg/mL fibrinogen with 1U/mL thrombin in PBS at different pH (5.8-8.0). $Turb^{max}$ and TEG^{Max} on primary axis; $Turb^{Time}$ and TEG^{Time} on secondary axis. All comparisons were made using averages. Raw tracing curves of turbidity and TEG shown in Figure A.6 and Figure A.7 with V_{max}, Lag time, α angle and R included in Table A.4. 63

Figure 3.8. Turbidity assays (A) and TEG assays (B) on bovine and human fibrin clots at 3 mg/mL fibrinogen with 1 U/mL thrombin with the addition of different amount of albumin (0, 20, 40, 50, 60, 80, 100 mg/mL in final solution). $Turb^{max}$ and TEG^{Max} on primary axis; $Turb^{Time}$ and TEG^{Time} on secondary axis. All comparisons were made using averages. Raw tracing curves of turbidity and TEG shown in Figure A.8 and Figure A.9 with V_{max}, Lag time, α angle and R included in Table A.5. 65

Figure 3.9. Turbidity assays (A, C) and TEG assays (B, D) on clots formed by four different thrombin and fibrinogen combinations: bovine thrombin and fibrinogen, bovine thrombin with human fibrinogen, human thrombin and fibrinogen, and human thrombin with bovine fibrinogen ($Turb^{max}$ (A), TEG^{Max} (B), $Turb^{Time}$ (C) and TEG^{Time} (D)). In all groups, 1 U/mL thrombin and 1, 2, 3, 4, 5 mg/mL fibrinogen concentrations were used. All comparisons were made using averages. Tracing curves of turbidity and TEG for this experiment were shown in Figure A.11 and Figure A.12 with V_{max}, Lag time, α angle and R included in Table A.6. 67

Figure 4.1. (A) The schematic of the 3D molding 3 X 2 insert and the printed product. (B) The schematic of annular clot formation in the well and the actual annular clot prepared by the 3 X 2 insert in the 96-well plate (C) Side and top views of the setup in the well. 77

Figure 4.2. (A) Comparison of relative size of FITC and fibrinogen molecule (B) FITC-Fibrinogen conjugation reaction and standard procedure for ultra-filtration. 78

Figure 4.3. 12FITC-Fibrinogen (FhF) molecular and fluorescent stability after 4 freeze-thaw cycles. Three tubes of product were examined at (A, B, C) absorbance 280nm and 494 nm of stock aliquots at 20-fold dilution, (D, E, F) fluorescence endpoint Ex 495nm and Em 519 nm of stock aliquots at 400-fold dilution, and (G, H, I) additional fluorescent emission spectrum (Ex 495 nm, Em 450 - 650 nm, 400-fold dilution). No significant difference was found for product absorbance after 3 cycles (n=3, p_280 nm=0.1089, p_494nm=0.0897) and no significant difference were observed for emission spectrum as well as fluorescence endpoint after 4 cycles (n=3, p=0.2312). In addition, FhF aliquots were examined over storage time using the same metric. Both (J) absorbance spectrum and (K) fluorescence (Ex 495 nm, Em 450 - 650 nm, 400-fold dilution) showed consistent values over 31 days. This result indicates fluorescence intensity of FITC-Fbg product is stable after vigorous freeze-thaw cycles and storage. 79

Figure 4.4. (A) Representative FITC conjugation sites on fibrinogen crystal structure displaying widespread FITC labels across the surface of fibrinogen. (B) Forming FITC labeled fibrin clot using thrombin-cleaved unmodified fibrinogen and FITC-fibrinogen mixture. Representative tracing curves of (C) turbidity assay and (D) TEG assay for varying 12FITC labeled human fibrinogen (FhF) levels in 12FITC-fibrin clot. (E) $Turb^{max}$, (F) TEG^{Max} (Maximum amplitude), (G) $Turb^{Time}$, and (H) TEG^{Time} of 3, 7 and 12- FITC-fibrin clots at different FhF levels were compared. Data were normalized by values of human fibrinogen control groups. * denotes significant differences (P value < 0.05) between FhF groups and hFbg ctrl group. 85

Figure 4.5. Representative SEM Images of FITC labeled human fibrin formed by neat and unmodified fibrinogen mixed 3, 7, 12- FITC-Fibrinogen at (A) 4,000X and (B) 35,000X. Scale bars were shown as 5 μm and 500 nm, respectively. Average fiber diameter (nm), average pore size (μm^2) and total pore area (%) were reported as bar plots and data were compared with unmodified fibrin controls using *, ** and *** denoting p values < 0.05, 0.001, and 0.0001. 87

Figure 4.6. Representative SEM images of varying 12 FhF in fibrin. 4,000X (first row) and 35,000X (second row). Scale bars shown as 1 μm (first row) and 100 nm (second row). 88

Figure 4.7. Representative confocal microscope images (40X objective with 1.5X digital zoom, excitation energy at 1%) of clots formed by (A) neat 3, 7, 12 - FhF, and (B) 3FhF (10:1), 7FhF (30:1) and 12FhF (50:1). Fluorescence intensity distribution were shown for physiologically relevant FhF clots. Integrated density was shown for (C) neat FhF and (D) physiologically relevant clots in bar plots with brackets denoting pairs of groups that exhibit significant differences ($P < 0.05$). Image brightness of 12FhF (50:1) clots were adjusted to enhance structure visualization. Scale bar = 20 μm. 89

Figure 4.8. Plasmin dose-response curve by (A) initial velocity (V_0) in S2251 assay and (B) fluorescence release rate (V_{FR}) in neat and physiologically relevant (PR)- 12FhF annular clot lysis assay where data were shown at the double-logarithmic scale. (C) Analytical sensitivity determination curves of annular clot lysis assay by plotting data points below 0.05 U/mL plasmin. Analytical sensitivity of neat 12FhF and PR12FhF annular clots were 11927 and 630. (D) Fibrin degradation rate (V_{FDR}) at increasing [plasmin]. V_{FDR} of PR- and neat 12FhF were converted via multiplying their fluorescence release rates (RFU/min) by 50/12 and 1/12, respectively. All fluorescence tracing curves were shown in Figure A.15 and A.16. 94

Figure 4.9. (A) Representative fluorescence release tracing curves of physiologically relevant (PR)-12FhF at varying [plasmin] and the derivation of FLU200 for PR-12FhF at 1.5 U/mL. (B) FLU200 for PR-12FhF over varying [plasmin]. Brackets denoting pairs of groups that exhibit significant differences ($P < 0.05$). 95

Figure 4.10. Digestion rates (primary axis, Abs/min or RFU/min) and plasmin activity (secondary axis, U/mL) by (A) fixed tPA and varying PLG in S2251 assay, (B) fixed tPA and varying PLG in PR-12FhF annular clot lysis assay (C) fixed PLG and varying tPA in S2251 assay and (D) fixed PLG and varying tPA in PR-12 FhF annular clot lysis assay. FLU200 by PR-12FhF were shown in bar plots at (E) varying PLG and (F) varying tPA experiments with brackets denoting pairs that have significant differences. Plasmin activities were converted by plugging the digestion rate values in linear regression equations derived in Figure 4.8. Plasmin activities were of two orders of magnitude faster in annular clot lysis assay compared to S2251 assay. Fluorescence tracing curves were shown in Figure A.17 and A.18. 96

Figure 4.11. Comparing (A) digestion rates (initial velocity, abs/min) at 405 nm by S2251 assay and (B) converted plasmin activity at varying [tPA] (0, 200, 500, 1000 ng/mL) with or without 3 mg/mL fibrinogen at 37 °C. 98

Figure 4.12. FITC-fibrin structural stability by clot turbidity (at 550 nm) over 8 weeks. Turbidity values were normalized by starting turbidity values of each sample. (A) Unmodified and (B, C, D) physiologically relevant 3, 7, and 12 FhF FITC-fibrin clots were formed in 96 well plates and stored at both RT and 4 °C to determine the long-term stability of the formed clots. Additional untagged fibrin clot was stored in (E) 0.05% sodium azide. 99

Figure 5.1. (A) Schematic representation of the Chandler loop setup. (B) A photo of the assembled Chandler loop apparatus with blood running in the device. (C) Illustration depicting clot formation within the Chandler loop at the forward meniscus. 107

Figure 5.2. Images showing RBC morphology before and after clot formation in a hemacytometer (Bright-Line™ Hemacytometer). For RBC images after clot formation, remainder clot-free solution samples were 1:200 diluted in formalin citrate, which is an isotonic solution to preserve RBC morphology. In addition, clotted liquid volume was measured and showed an overall consistent volume ratio with respect to total solution before solution. 111

Figure 5.3. (A) Comparison of clot samples across nine groups. Clots formed at S-small, M-medium, and L-large tubing (top to bottom) at 20, 40 and 60 RPM (left to right). (B) Comparison of the average clot diameters formed in different diameter tubing. Comparison of (C) clot volume estimated through clot appearance using ImageJ and (D) clot weight across groups. Brackets denote significant differences between groups. 112

Figure 5.4. (A) Gross and 5X H&E photos of representative clots. WBCs (blue), RBCs (red), fibrin (pink). Scale bars are 5 mm in gross photos and 200 μm in 5X images. Comparing the percent area of packed RBC, fibrin-rich, and RBC infiltrated fibrin in clot samples formed at different RPMs in (B) small, (C) medium, and (D) large diameter tubing. Detailed measurements highlighting these regions of interests were included in Figure A.19. 113

Figure 5.5. Histology photos of representative clot samples at (A) low, (B) medium, and (C) high shear rates. From left to right: photos of identical spots in the fibrin-rich region under H&E versus MSB at 40X and zoomed MSB platelet-specific regions. H&E stains: WBCs (blue), RBCs (red), fibrin (pink). MSB stains: WBCs (purple), RBCs (yellow or red), fibrin (blue or red), platelets (gray). Red arrows indicate platelets in MSB (platelets) photos. Scale bars are 5 mm for photos in the first column, 200 μm for the second column and 50 μm for the rest. Remainder clot sample photos are listed in Figure A.20. 115

Figure 5.6. (A) WBC and (B) RBC percentage area in clots are shown over shear rates. Linear regression was plotted by RBC percentage area over increased shear rates. 115

Figure 5.7. Representative SEM images of clots formed at (A1-A5) low, (B1-B5) medium, and (C1-C5) high shear in each row. In each row, structures were ranked based on their high-to-low presence frequency in the sample groups, for example, A1 is the most common structure in the low shear group. Images were taken at 1000 X and spots of interests were shown at 2000X in selected images. Scale bars are 10 μm in these graphs. 116

Figure 5.8. Shear rates calculation at nine different Chandler loop conditions (20, 40 and 60 RPMs, and small, medium, and large tubing inner diameters) using an equation derived from laminar flow assumption by Gardner et al.[7] vs an empirical equation derived by computational simulating Chandler loop published by Touma et al.[29] 118

Figure 6.1. (A) Schematic representation and (B) Lab setup of Real-Time Fluorometric Flowing Fibrinolysis Assay (RT-FluFF). Components from left to right are dampener, peristaltic pump, pressure sensors (before clot), reservoir, pressure sensor (after clot), fluorometer. 127

Figure 6.2. Bar plots outlining the TEG parameters (A) TEG^{Max}, (B) TEG^{Time}, and (C) alpha angle in the various FITC-Fg groups explored during optimization. (D) Percent clot mass lost during digestion of Chandler-loop made clots utilizing various ratios of FITC-Fg. Clot digestion conducted over the course of 60-minutes with 600 ng/mL tPA. Single asterisk denotes P-value < 0.05, Double asterisk denotes P-value <0.01, Triple asterisk denotes P-value <0.001. 134

Figure 6.3. (A) Masses of clots formed in the Chandler loop utilizing the control (0:1), 50:1, 10:1, and 10:1 FhF groups. (B) Gross images of clots formed in the Chandler Loop using varying FhF ratios under room light (top row) vs UV light (bottom row). Scale bars represent 20 mm. (C) H&E and epifluorescence images acquired of Chandler loop clots from respective ratios of FhF. White arrow indicates fibrin dense regions. Note the loss of fibrin dense regions in the 5:1 group, indicating significant perturbation of clot architecture. Scales bars represent 2 mm. 135

Figure 6.4. Systolic-diastolic pressure difference outlined in (A) pressure sensor A and (B) pressure sensor B in various systemic pressure settings as well as in dampened versus undampened settings. Height (inch) refer to the displacement of output drain from the pressure sensors. Absolute systolic pressure readings at (C) pressure sensor A and (D) pressure sensor B over a wide range of pump shear rates. 136

Figure 6.5. (A) Comparison between spectrophotometer and fluorometer in quantifying fluorescence of a serial dilution of FhF. (B) Stepwise injection of Fluorescein into flowing plasma with fluorometer data acquisition. (C) Continuous infusion of either FhF or Fluorescein into plasma with fluorometer data acquisition. 138

Figure 6.6. (A) Shear-induced clot analog stretching. Individual colored bars represent 0, 300, 600, and 900 s^{-1} wall shear rate. (B) Change in clot length (%) is relative to the clot length under 0 s^{-1} shear. Note the relative uniform stretching of clots in response to varying levels of shear. 139

Figure 6.7. (A) Representative scatter plot outlining rise in fluorescence over course of thrombolysis in respective tPA conditions in the RT-FluFF assay. (B) Representative example of gross changes that clots undergo 200 ng/mL tPA digestion illuminated under UV-light. Plot of linear-phase digestion rate by spectrometer captured in (C) RT-FluFF, (D) Chandler loop, and (E) static conditions at varying tPA concentrations. 141

Figure 6.8. A) Percent clot mass lost based on various concentrations of tPA and varying thrombolysis modalities. B) Correlation analysis for static digestion. RFU as tracked by the spectrophotometer. C) Correlation analysis for Chandler loop digestion. RFU as tracked by the spectrophotometer. D) Correlation analysis for the RT-FluFF assay. RFU as tracked by the fluorometer. 142

Figure 7.1. Clot digestion slope (RFU/min) by fluorometer in the RT-FluFF model were compared across three dampeners settings at (A) 913 s^{-1}, (B) 523 s^{-1}, (C) 205 s^{-1}, and (D) 523 s^{-1} 1Hz on/off setups. Significant differences between 0 and 1000 ng/mL tPA were shown. Single asterisk denotes P-value < 0.05, double asterisk denotes P-value < 0.01, and triple asterisk denotes P-value < 0.001. 158

Figure 7.2. (A) Clot mass loss% at 30 min and (B) digestion% at 30 min in the RT-Fluff model were compared across three dampeners (60, 20, and 6 cc) at averaged shear rates of 913 s^{-1}, 523 s^{-1}, 205 s^{-1}, and 523 s^{-1} at 1 Hz on/off. 159

ABSTRACT

Thrombosis is the pathological formation of a blood clot in the body that blocks blood circulation, leading to high morbidity and mortality rates. Thrombolytic drugs that offer rapid clot dissolution are promising treatments yet current drugs are often associated with limited efficacy and high bleeding risks. While numerous animal thrombosis models have been developed for drug screening, the translation of therapeutic agents into and through clinical trials remains limited. This is largely due to animal models' poor reproducibility and distinctive physiology to that of humans. *In-vitro* flow models that utilize both human blood components and physiologically relevant flow conditions can provide for a more representative testing environment to screen thrombolytic drugs. Developing better *in-vitro* models may not eliminate the need for preclinical animal testing but can help exclude inefficient agents earlier in the drug development pipeline to expedite the drug evaluation process. Existing *in-vitro* thrombolysis flow models are not ideal as they either adopt over-simplified clot substrates or utilize small-length-scale geometries that insufficiently mimic native hemodynamics. Thus, we propose to first develop a static fluorescently labeled clot lysis assay for an initial high throughput screening of thrombolytic drugs, and ultimately engineer a highly reproducible, physiological scale, flowing clot lysis model for more human relevant drug efficacy evaluation. Developing the static clot lysis assay not only helps to understand the mechanism of how diversified clotting conditions affect clot properties but also offer a chance to well-characterize fluorescence conjugations to fibrins. The ultimate flow model combines an *in-vivo*-like fluorescence incorporated synthetic clot (FISC) and a human-relevant flow system. Guided by results from static clotting experiments diversified FISCs are fluorescently optimized and fabricated dynamically using a Chandler loop setup at various conditions. The flow system is a tubing-based structure that comprises of a peristaltic pump, and a well-controlled flow chamber to provide for physiological shear and pulsatile levels. Therefore, the proposed synthetic clot model is a versatile platform that can mimic a variety of thrombosis conditions and offer representative drug testing and dosing results across numerous thrombolytic agents.

1. INTRODUCTION

The dysregulation of a healthy hemostasis response can result in pathologic thrombosis leading to tissue death and major organ failure. Thrombolytic drugs that offer rapid clot dissolution are a promising therapy for treating thrombosis; however, current thrombolytic drugs are associated with limited efficacy and high bleeding risks. Testing novel thrombolytic agents is necessary and requires the use of representative drug screening models. Although numerous thrombolysis models have been developed for thrombolytic drug evaluation, translation of drugs into and through clinical trials has not been improved. Animal models are extensively used but they are limited by poor reproducibility and distinctive physiology to humans. Clot lysis assays can utilize human blood components, but they often lack the capacity to examine the impact of shear on thrombolysis due to their often-static setup. *In-vitro* thrombolysis flow models can offer more representative drug efficacy results because these devices can adopt human blood components together with mimicked human-relevant flow conditions. Developing better *in-vitro* models may not eliminate preclinical drug testing using animals, but early testing on more human-relevant model systems can help exclude inefficient thrombolytic agents to expedite the drug evaluation process and focus on lead compounds with higher probability of clinical translation. Parallel chamber and microfluidic assays are well-characterized *in-vitro* flow models that have been extensively utilized to model thrombosis formation. While they can be easily adapted to evaluate thrombolytic agents, these devices usually have small length scales that may not fully mimic native hemodynamics. Other *in-vitro* flow models are often over-simplified and poorly documented. To date, a highly reproducible, physiological scale, flowing clot lysis model has yet to be developed. Thus, there is a need for developing a physiologically relevant *in-vitro* model to offer representative blood flow conditions for thrombolytic drug evaluation. This dissertation proposes to engineer a thrombolytic drug evaluation model by combining an in vivo-like fluorescence incorporated synthetic clot (FISC) and a human-relevant flow system. The model described herein was extensively characterized and optimized through completion of the following aims:

Aim 1: Fabricate and characterize physiologically relevant fibrin-based fluorescence incorporated synthetic clots. Fluorescein isothiocyanate (FITC) conjugated fibrinogen were synthesized and used to form fluorescently labeled fibrin clots. FITC labeling levels were

modulated to preserve native fibrin structure through a developed characterization system by leveraging clot turbidity assay and thromboelastography (TEG). FISC were formed by expanding the optimized FITC labeled fibrin clot to include other blood components under physiological shear conditions using a Chandler loop apparatus. Clot micro-structures were further examined under scanning electron microscope (SEM) to confirm clot physiological relevance.

Aim 2: Develop and optimize an easily multiplexed fluorescence incorporated clot lysis assay to monitor sample fibrinolytic activity. A unique annular clot geometry was developed and optimized to provide for a non-disrupted real-time clot lysis monitoring platform using a spectrometer. Fluorescence labeling homogeneity of FITC-fibrin clots was evaluated to ensure accurate clot lysis tracking is achieved through consistent fluorescence release. Different levels of plasmin, tissue plasminogen activator (tPA), and other fibrinolytic factors were tested in the assay to evaluate its capability to differentiate fibrinolytic potential under diverse conditions. Results further guided fluorescence labeling in FISC and optimized the design to achieve an ideal analytic sensitivity together with its physiologically relevant clot properties.

Aim 3: Engineer an *in-vivo* like FISC thrombolytic model that mimics human-relevant flow conditions at a physiologically relevant scale. The flow model consists of a peristaltic pump and a well-controlled and macroscopic tubing loop. This setup can either offer a steady flow to evaluate drug profile under continuous shear with a help of a dampener, or adapt the oscillating flow generated by the peristaltic pump to mimic native pulsatile flow dynamics. Optimized arterial or venous FISC obtained through Aim 1 is placed inside the flow segment. Thrombolytic drugs were added to flowing plasma perfused in the model to digest the FISC. Fluorescence release was monitored to assess drug-induced thrombolysis efficacy.

The static annular fluorescently labeled clot lysis assay offers a high-throughput capacity. It can be multiplexed into a 96-well or 384-well format for initial thrombolytic drug efficacy screenings. This assay can also be adapted to assess patient plasma clinically for fibrinolytic potential in the presence or absence of therapeutic agents for personalized medicine applications. The FISC thrombolytic flow model can offer a representative drug therapeutic target and human-relevant hemodynamic conditions to study a thrombolytic drug's efficacy profile, guide the development of new drugs, and help determine therapeutic dosing. The flow setup can also be modified to assess the feasibility of novel thrombolytic drug delivery methods and study ultrasound-aided thrombolytic therapy. By perfusing hypercoagulable blood samples with the

addition of antithrombotic drugs, the model can further examine antithrombotic drug efficacy for preventing thrombosis formation. In all, the developed model system can provide for human-relevant drug testing results without relying on an animal model. This can both expedite the thrombolytic pre-clinical drug evaluation process and improve drug translation into and through clinical trials.

2. BACKGROUND

Thrombosis is a blood clot that reduces or completely obstructs blood flow leading to tissue death, major organ failure, and in some instances, death. It can be categorized into arterial and venous thrombosis based on the clot location. Arterial thrombosis, often developed through the rupture of a fatty plaque, can induce ST (a segment in an electrocardiogram) elevated myocardial infarction (STEMI) and ischemic stroke. STEMI accounts for 30% of all myocardial infarction (MI) cases while 87% of stroke cases are found to be ischemic stroke worldwide.[1, 2] The annual incidence rates are estimated to be 2 and 3 cases per 1000 people with recurrence rates of 15% at two years for STEMI and 6.9 % at three years for ischemic stroke, respectively. Venous thromboembolism (VTE), comprising deep vein thrombosis (DVT) and pulmonary embolism (PE), are the most common forms of venous thrombosis. Recent studies estimate the annual incidence of VTE to be 1-2 cases per 1000 people. In VTE cases, 5 - 7% of patients develop recurrent thrombosis within six months after the onset of their first thrombosis event. Thrombosis results in high mortality with ~11% of VTE patients ≥ 45-years old die within 28 days. Additionally, the one-year fatality rate of MI is 24% and the 30-day fatality rate of ischemic stroke is 15%.[3, 4]

Treatments for thrombosis include surgical thrombectomy, antithrombotic drugs and thrombolytic therapy. Drugs are generally preferred over surgeries because they are more easily accessible, cost-effective, and less invasive. Antithrombotic drugs are often adopted for the prophylaxis of recurrent thrombosis. Conventional vitamin K antagonists, antiplatelet and anticoagulant agents are commonly prescribed to patients as they can reduce their blood clotting tendency and prevent recurrent thrombosis events. For example, aspirin can reduce recurrent stroke risk by 13 - 22% and direct oral anticoagulants (DOACs) are highly effective at preventing recurrent VTE.[5-7] Thrombolytic therapy refers to the intravenous administration of clot-buster agents such as streptokinase, urokinase, and tissue plasminogen activator (tPA). These drugs can offer a rapid clot dissolution following agent-triggered fibrinolysis which enables a fast relief for life-threatening thrombosis events. In acute ischemic stroke studies, intravenous tPA improved clinical outcomes at three months.[8] In acute STEMI patients, thrombolytic therapy is used for reperfusion when percutaneous coronary intervention is not available.[9, 10] The rapid restoration of vessel patency also contributes to a reduction of post thrombotic syndromes in VTE patients.

87% of acute massive PE patients have achieved stabilized hemodynamics, improved resolution of hypoxia and increased survival to hospital discharge following catheter directed thrombolytic treatment.[11, 12] The global thrombolytic drug market continues to grow at a rapid pace due to increase in incidence rate of thrombosis and demand for technologically advanced products. Despite several generations of thrombolytic drugs having been developed, hemorrhage remains to be the major complication.[8, 13, 14] A thrombolytic agent that has better clot-specificity and enhanced resistance to endogenous inhibitors can improve thrombosis treatment and patient quality and duration of life.[15]

A representative drug evaluation model is critical for the development of novel thrombolytic drugs. Current evaluation of thrombolytic agents has relied on animal thrombosis models.[16, 17] Since susceptibility to clot lysis under interventions varies significantly due to different clot properties and thrombosis locations, several animal thrombosis models have been developed, for example, the Folts canine model, the Wessler rabbit model, and the AV-shunt rodent model.[18-20] Animals are useful to study in vivo drug safety, biological effect and comparative pharmacology. They are also commonly required by drug authorities, such as the FDA, prior to initiating clinical trials. However, even non-human primates, the best human analog, do not predict a reliable drug efficacy profile in humans due to their distinct physiology. To circumvent this problem, clot lysis assays using human blood components have been developed to examine drug efficacy. These assays are more reproducible and offer more human-relevant drug efficacy profiles than animal models, but often lack hemodynamic effects in their setup which reduces their clinical relevance.[21-23]

By introducing shear flow to clot lysis, *in-vitro* flow models are capable of mimicking various thrombosis conditions and provide for more representative drug evaluation environments. Despite the potential to exhibit high clinical relevance, very few *in-vitro* flow models have been designed for evaluating thrombolytic agents. A parallel flow chamber or microfluidic device belongs to a category of flow models that have been well studied. A chamber typically consists of an upper cover slide and a customized plate. The cover slide is commonly coated with collagen and tissue factors or other thrombogenic substances to facilitate platelet binding and promote thrombus formation.[24, 25] These chambers have been extensively employed for the study of thrombosis pathogenesis and evaluations of antiplatelet and anticoagulant drugs but rarely of novel thrombolytic drugs.[26-29] Only recently, a group has modified the chamber to evaluate

thrombolytic agents whereas the design has several drawbacks.[30] Small length scales and highly ordered flow patterns make flow dynamics in these devices less comparable to those in vivo. Other flow models found in the literature are usually over-simplified and require a comprehensive characterization.[31] A number of tubing-based models have been developed to examine ultrasound-aided thrombolytic therapy. While they can be used to generally explore the effects of hemodynamics, results may not be accurate to guide clinical thrombolytic therapy as neither clot substrates nor flow conditions utilized in these models exhibit significant physiological relevance. An ideal thrombolytic drug evaluation model should combine the knowledge of native thrombolytic mechanisms, hemodynamic effects, and incorporate a comprehensively characterized, physiologically relevant clot substrate. The setup should also allow for real-time clot lysis tracking via a mechanism that does not affect the fibrinolytic dynamics.

2.1 Thrombus Formation and Dissolution

Hemostasis is a healthy response to blood vessel injury. The dysregulation of this response can result in a pathologic thrombosis. The process begins with vessel constriction followed by recruiting platelets to form a plug. Coagulation factors are subsequently activated in the blood coagulation cascade through two pathways, namely the contact pathway and the tissue factor pathway. The contact pathway is activated by negatively charged substances while in the other pathway, tissue factors are secreted from the surrounding cells at the site to initiate a much faster series of protease activations. Both pathways converge upon a common route leading to the generation of thrombin. Fibrin monomers result after the proteolytic release of fibrinopeptides A and B when thrombin cleaves fibrinogen (340 kDa). The monomeric fibrin self-assembles into protofibrils which aggregate laterally and longitudinally to form fibers that branch to yield a three-dimensional insoluble fibrin mesh. The fibrin is eventually stabilized through covalent crosslinking at lysine residues of adjacent γ- and α-chains by the transglutaminase, factor XIIIa in the presence of calcium (**Figure 2.1**).[32] The fibrin mesh reinforces the platelet plug and entraps red blood cells (RBC), leukocytes and even more activated platelets to form an end product called a “clot”, or thrombus, that can effectively stop bleeding. Upon healing, the clot dissolves through a process known as fibrinolysis. The process begins with the conversion of plasminogen into plasmin (83 kDa) when they are bound to C-terminal lysine residues on fibrin. The activated protease breaks down the mesh leading to a complete clot dissolution. Tissue plasminogen

activator (tPA) and urokinase are two individual endogenous plasminogen activators with the former binding to fibrin C-terminal lysine residues. In addition, the fibrinolytic system is carefully regulated by inhibitors including type 1 plasminogen activator inhibitor (PAI-1) for tPA and urokinase, alpha 2-antiplasmin and alpha 2-macroglobulin for plasmin. Sustained generation of thrombin after injury also activates thrombin activated fibrinolysis inhibitor (TAFI), which removes tPA and plasmin fibrin binding sites to stabilize clot against fibrinolysis.

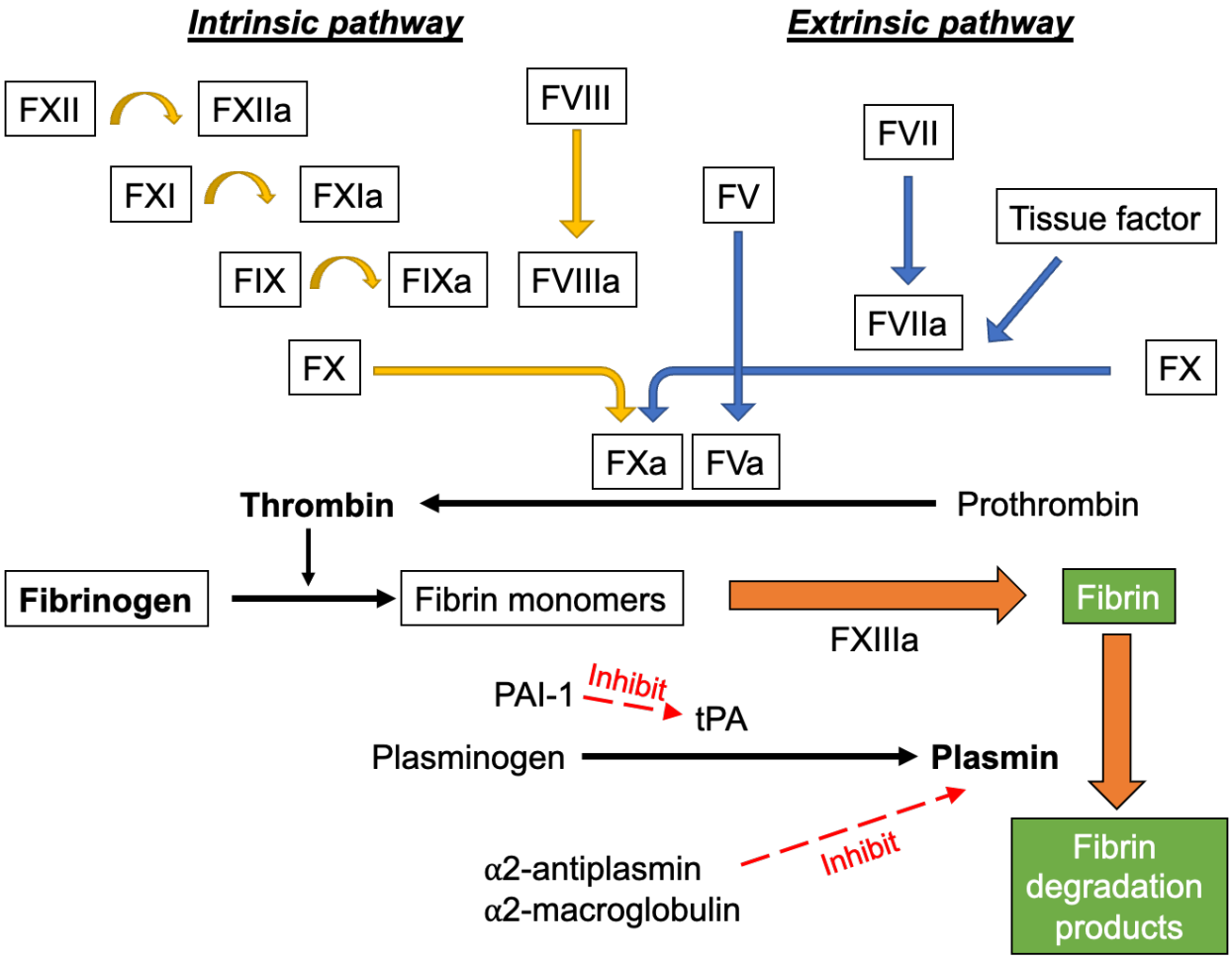

Figure 2.1. Coagulation cascade and fibrinolysis

2.2 Thrombus Stability and Hemodynamics

Understanding clot stability, or the susceptibility to lysis, is critical to design a clinically relevant model to screen drugs or provide dosing information to treat patient-specific thrombosis conditions. The clot stability depends on interactions of biology and hydrodynamics during clot

formation.[33, 34] The fibrin, as the primary protein structure in a thrombus, offers mechanical and biological supports to other blood components and together contributes significantly to the clot stability. Based on a recent clot morphology study, venous thrombus comprises fibrin content at 36% while arterial thrombus at 51%.[35] Fibrin clots composed of thick and loose fibers are known to have higher permeability leading to accelerated fibrinolysis.[36] Tight and rigid fibrin formation are more common in MI patients which has explained why a MI thrombus has higher thrombolytic resistance.[37] Platelets and RBCs are also important components in a thrombus that affect clot stability. Platelet cytoskeletal contraction results in stiffened clot structure while the RBC can reduce clot permeability by surface drag and volume occupancy.[38, 39] The physiological wall shear rate in the human body ranges from 10 s^{-1} in veins to 2500 s^{-1} in small arteries to 40,000 s^{-1} in large arteries. This large variation in shear flow affects fibrin formation, platelet aggregation and RBC incorporation leading to the formation of diversified clot structure.[40] The high wall shear rates in the artery increase platelet deposition and decrease RBC accumulation resulting in the appearance of a white thrombus. The arterial clot shows a platelet-rich head and a RBC-rich tail confirming the impact of shear flow on clot growth.[41, 42] In contrast, venous thrombus is usually large with a length from several centimeters up to 25 cm long. These clots are predisposed to have more RBC deposition due to the low shear rates found in veins. Despite both venous and arterial having a fair amount of fibrin content, the fibrin structure also differs in these thrombi due to distinct shear rates and the interactions with varying levels of other factors and blood components during formation.[43] In addition, the structure of thrombus evolves over time which creates an even bigger variation in clot properties and stability. The coronary artery thrombi obtained from STEMI patients have shown double the fibrin content and halved platelet content per additional ischemic hour within the testing period.[44] Venous thrombi have also shown a time-dependent clot hardening.[45]

Hemodynamics not only affects clot formation but also has an important role in native thrombolysis. In MI patients with hypotension, the success rate of thrombolytic treatment is generally lower.[46] Since thrombolytic agents aim at digesting fibrin in the thrombus, the efficiency of agents permeating into the fibrin clot directly affects the performance of a thrombolytic therapy. Clot permeation is a transport phenomenon that is determined by both clot permeability and the trans-thrombus pressure drop. The pressure drop can be derived by the innate blood shear rates and the severity of stenosis. For example: a 1 cm arterial thrombus can have a

trans-thrombus pressure drop ranging from 40 to 80 mm Hg/cm while a 25 cm long DVT clot has a pressure drop as low as less than <1 mm Hg/cm.[47] Thus, a thrombolytic therapy is clinically contraindicated for DVT patients due to a poor agent permeation. The wall shear rates also affect the levels of circulating proteins that are present at the lysis front. It was found that increasing wall shear rate at a fibrin surface from 25 to 500 s^{-1} causes a 2.8 fold increase in the amount of plasmin.[48] In addition, a turbulent flow could further complicate the interaction of fibrinolytic factors to clot. These situations make the clot lysis highly unpredictable and difficult to be simulated using mathematical models.[49] Moreover, the turbulent flow effect on the thrombus formation have been studied while its effect on thrombolysis requires a more thorough examination.[50-52] Additionally, the pulsatility generated by human heart contributes to more complex flow patterns than what were commonly studied in continuous shear *in-vitro* models. Understanding the effect of pulsatile flow on thrombolytic drug efficacy is also crtical for depicting a complete picture of drug therapeutic profile in humans.

2.3 Animal Thrombosis Models

Animal thrombosis models have played a crucial role in novel antithrombotic and thrombolytic drug discovery and evaluation. Animal models not only partially mimic human hemodynamics and pathological conditions during thrombus generation and dissolution but they are also useful for toxicity and indication-specific pharmacology studies.[53] Animals are primary source to evaluate bleeding risks, which is the most common side effects associated with all existing antithrombotic drugs. Recent advances in genetic knock-out animals makes it possible for phenotype studies that would benefit novel antithrombotic drug designs.[54] The selection of suitable animal thrombosis models is critical to achieve different therapeutic evaluation goals given the variety of model specificities and drug therapeutic targets. Throughout the literature, numerous animal models have been developed.[16, 17, 53] Methods used to induce thrombogenic conditions in animals essentially follow the well-known Virchow's triad that comprises local stasis, blood vessel injury, and hypercoagulable state. Diversified animal species have been adopted including small animals like rodents and rabbits, and large animals like pigs, dogs, and non-human primates. In the following context, three popular animal models will be discussed: the Folts model, the Wessler model, and the Arteriovenous (AV) shunt model.

The Folts model was first introduced in 1976 by Folts and colleagues.[18] It describes an arterial thrombosis setup in a stenosed coronary artery of an open-chest, anesthetized dog. Pigs, monkeys, and baboons were also viable options appeared in Folts model variations. Coronary artery thrombus is induced by a combination of focal stenosis via a plastic constrictor and intimal injury via a hemostatic clamp or low amperage electrical current.[17, 55] In every 2-3 minutes, the thrombus is shaken loose to restore blood flow. Cyclic flow reduction (CFR) is measured by electromagnetic probe looking at the percentage change of blood vessel occlusion in this periodic event. Magnitude and frequency of CFR are monitored and compared to study drug interventions. The formation of the platelet-rich arterial thrombus makes the Folts a good pre-clinical platform for antiplatelet drug evaluation. Aspirin is the first antiplatelet agents to be tested which entirely abolished CFRs in the dog Folts model.[18] Novel antiplatelet agents such as GP IIb/IIIa receptor antagonists and ADP receptor antagonists have also been extensively tested in this model.[56-59] Anticoagulants have also been evaluated in Folts with heparin showing only a weak effect while low molecular weight heparin showing abolished CFRs.[18, 53, 60] Overall, the Folts model stand out among all in vivo arterial thrombosis models for the several reasons: First, with a controllable severity of stenosis, the Folts model could reproduce similar pathological thrombosis conditions in different recipients. Second, due to the benefits of repetitive thrombus formation, Folts models are also eligible to study dose-responses of an agent and synergistic effects of combined therapy.[57, 61, 62] Third, as the Folts model was initially proposed to mimic the acute arterial thrombosis conditions in stenosed coronary arteries, it could guide in clinical treatments of coronary thromboembolic disorders. In fact, a handful of drugs pre-tested in the Folts model have revealed comparable effects in patients, such as the enoxaparin, abciximab, and tirofiban.[63-65]

One drawback of the Folts model is the strong resistances to thrombolytic agents which is still yet to be understood.[66, 67] Besides, the lack of a standard on the severity of stenosis and a poor documentation of experimental procedures deferred cross-study comparisons which made it difficult to draw meaningful conclusions.[60] Finally, like all animal thrombosis models, conclusions drawn from the Folts model are considered to be over-optimistic. A recent statistical study published that with drug validated in animal models, about one-third were translated into clinical trials, and only 10% could finally become available to patients.[68]

The Wessler model is a classic venous thrombosis animal model. It was introduced to study the pathogenesis of thromboembolism by Wessler and his group in the 1950s.[19] Venous

thrombosis is induced in the jugular vein of an anesthetized rabbit by a complete stasis and an influx of foreign species blood serum. Model variants involve the use of other animal species, such as rats and mouse, or the application of other thrombogenic substances like thrombin or thromboplastin to establish hypercoagulable state.[69] Due to the formation of a stable fibrin-rich venous thrombus, the Wessler model is capable of evaluating drugs for both thrombolytic and antithrombotic potency. Various endpoint measurements were adopted to quantify the effects of therapeutic interventions among which measuring a change in thrombus mass is the most common practice. Some studies have utilized a radioactively labeled clot which facilitates a dynamically trace of in vivo clot dissolution.[70, 71] This model has tested numerous antithrombotic and thrombolytic drugs, such as LMWH, heparin, rt-PA, FXa inhibitors, and thrombin inhibitors.[72-77] Advanced drug delivery methods were also tested in the Wessler model, for example, a clot lysis study by a delivery of urokinase coated nanoparticle.[78]

The Wessler model was often preferred over other venous thrombosis model types because a complete stasis in the jugular vein is more reliable and easier to achieve compared to other blood vessels or induction methods like vessel injury or partial stasis during practice.[16] Limitations of the Wessler model are also prominent. First, due to a complete isolation of the jugular vein, thrombus is formed at a static condition, and thus, the effect of hemodynamic changes that contribute significantly to thrombus structure is missing in this model. Some researchers have reported an upgraded model via the use of a thread to induce thrombosis in the flowing bloodstream.[79, 80] While the presence of a foreign substance like the thread could still affect both drug-clot interaction and clot orientation leading to a less representative drug evaluation results. Second, the lack of vascular damage during induction could result in a poor platelet recruitment to the formed thrombi which largely affects thrombolytic drug efficacy. Platelets not only aggregate to increase clot rigidity like what are mostly seen in arterial thrombi but also release thrombolytic factor inhibitors like PAI-1 to increase thrombolytic resistance.[42]

Although large animals are better analogs to humans, small sized rodents are usually picked for early-stage drug evaluations because of easy management and the need of minimized therapeutic screening quantities. Arteriovenous (AV) shunt rat model is a frequently used small animal model for novel antithrombotic agents.[81] A plastic shunt is placed in between the cannulated jugular vein and carotid artery of an anesthetized rat. A cotton thread is used to induce thrombosis in line with the shunt after blood reperfusion. Formed thrombus are rich in RBCs,

platelets, and fibrin which make the model capable of evaluating the antithrombotic effects of both anticoagulant drugs like FXa inhibitors, and antiplatelet drugs like PAR1 antagonist and ADP receptor antagonist.[58, 75, 82] The thread with thrombus is sequentially weighed, and change of thrombus mass is monitored to indicate the antithrombotic efficacy and dose-response performance of drug interventions. The AV shunt model has also been modified to utilize large animals to achieve better physiological relevance. Non-human primates, for example baboons, were utilized to evaluate anticoagulant recombinant tick peptide and FXa inhibitors.[83, 84] Since the extracorporeal shunt could be made from different materials, the AV shunt thrombosis model were also used to study the thrombogenic properties of cardiovascular prosthesis materials.[85, 86]

Animal thrombosis models are useful to indicate drug efficacy while drug bleeding risk is still unpredictable in humans. Researchers have turned to employ animals to evaluate drug bleeding tendency. Multiple animal bleeding models are found in literature, which include rabbit cuticle, rat tail, rabbit ear, and dog tongue models where bleeding time is used as the variable for bleeding risk assessment.[77, 80, 87, 88] Bleeding time estimates primary hemostasis capacity of animal blood in the presence of a drug intervention. Since almost all antithrombotic drugs reveal prolonged bleeding times, a dosage regimen with a shorter bleeding time and a competitive antithrombotic efficacy is commonly the goal for pharmacist and researchers. In fact, animal bleeding time models have already played an pivotal role in current pre-clinical drug evaluation process.[77]

2.4 Diagnostic Assays

Although animal models are well established for drug evaluation, their built-in endpoint measurement either poorly estimate drug effects or fails to provide complete therapeutic profiles, for example, CFR in the Folts model gives an indirect measurement of antithrombotic effects; Thrombus mass measured at the end of the test cannot give real-time drug activity or pharmacology. More importantly, animal physiology distinct from humans. Thus, many drug evaluation studies have adopted additional assays running with human blood samples to offer complementary efficacy results. Immunoassays and chromogenic assays are beneficial for determining levels and chemical kinetics of active coagulation and thrombolytic proteases, but they are limited in assessing their biological functions. *In-vitro* assays that are designed for clinical thrombosis diagnosis are better options for antithrombotic and thrombolytic drug evaluation because they

allow for the study of drug effects in a more human-relevant way. Examples of these assays are prothrombin time (PT), activated partial thromboplastin time (aPTT), Thromboelastography (TEG), euglobulin clot lysis test (ECLT), and Light transmission aggregometry (LTA).

The PT assay evaluates the extrinsic pathway of the coagulation cascade. It measures the time for exogenous tissue factor to induce patient plasma clotting. The extrinsic pathway is a combination of upstream coagulation factors like fibrinogen, prothrombin, FV, FVII, FX and vitamin K. And thus, PT can provide a systemic evaluation of drugs that inhibit these coagulation factors. aPTT, another coagulation assay, monitors the performance of the intrinsic pathway and is usually used in conjunction with PT. In drug evaluation studies, novel antithrombotic agents are usually compared with conventional drugs on PT and aPTT to demonstrate potency. Usually, a prolonged PT or aPTT of a drug represents a good antithrombotic potency. [75, 77, 80, 89]

TEG is a viscoelastic method that provides a comprehensive measurement of blood coagulation and clot lysis. It has played an important role in identifying blood disorders in various clinical settings. Upon a TEG assay, a thromboelastograph is generated to document a real time change of mechanical strength of the clotting sample. Reaction time, maximum amplitude, lysis at 60 minutes, and other TEG built-in variables are derived by the software. The TEG instrument can perform different assay types. For example, a standard TEG assay examines a kaolin blended whole blood sample. Resulting variables are compared with clinical normal ranges to assess the performance of patient hemostasis or determine a deficiency of a specific factor.[90] Platelet mapping assay is a different assay type that measures the inhibition of platelet function through arachidonic acid (AA) or ADP pathways. This assay monitors the effect of antiplatelet in the presence of potent aggregation stimuli like AA or ADP.[91] Compared with other common blood coagulation assays, TEG is more sensitive in detecting blood coagulation anomalies.[92] Therapeutics that has been evaluated by TEG include synthetic thrombin inhibitors, GP IIb/IIIa antagonist, and P2Y12 receptor inhibitor.[93-95]

The ECLT assay is a variant of plasma clot lysis assay that has a long history in assessing drug fibrinolytic activity in plasma.[96] Current ECLT and plasma clot lysis assay protocol involves an utilization of a spectrometer to monitor turbidity changes of blood samples over time. The ECLT assay requires to separate an euglobulin fraction from platelet-poor plasma and initiates clotting via the addition of thrombin. It is designed to estimate the activity of endogenous plasminogen activator despite that plasminogen, PAI-1, TAFI, and fibrinogen that potentially

affects ECLT are all present in the fraction.[97] Many studies have tested recombinant plasminogen activators using ECLT.[98, 99] A whole blood clot lysis assay differs from a plasma clot lysis assay or the ECLT assay. Investigators either add exogenous thrombolytic agents into a pre-formed whole blood clot or mix both clot initiation and thrombolytic agents in whole blood to achieve a non-stop coagulation-fibrinolysis. [87, 100]

Light transmission aggregometry (LTA), also known as the Born method, is the clinical standard for testing blood platelet function.[101] An increase in light transmission is measured when the antagonist aggregates platelets. This assay is typically useful in antiplatelet drug evaluation. Studies have been found to assess the antiplatelet activity of novel compounds using LTA.[102-104]

In summary, diagnostic assays are convenient to depict a picture of human-relevant drug effects as they mimic *in-vivo* processes to give indications of drug functions, for example, the clot formation process in testing anticoagulants, the platelet aggregation process in testing antiplatelets, and the fibrinolytic process in testing thrombolytics. Results are however biased due to process simplicity and limitations in physiological relevance. Two aspects of limitations are the lack of hemodynamic changes and the lack of comprehensive interplays of all blood components in the testing sample.[105]

2.5 *in-vitro* Thrombosis Models

Animal thrombosis models are not perfect albeit useful for evaluating drugs and assessing drug-associated bleeding risks. Poor model reproducibility, distinct physiology and pharmacokinetics are drawbacks that could lead to predisposed understanding and inaccurate indication of drug effects in humans. The use of preparatory agents like anesthetics also largely influence animal test results making drugs difficult for clinical translations.[106] On the other hand, if ineffective drugs were excluded earlier in the drug discovery pipeline, the entire process could be more efficient with less animal research burdens.

Compared to diagnostic assays, *in-vitro* thrombosis models are flow models that can offer human-relevant therapeutic information because of their biomimetic features including the use of human blood and the introduction of hemodynamic changes during clot formation. *In-vitro* thrombosis and thrombolysis models are often overlooked in the past as the research focus lies on animal experiments. Even fewer models have been developed or well-characterized for

thrombolytic drug evaluation purposes. Some *in-vitro* thrombosis models are found in the literature to mainly evaluate antiplatelet drugs since platelet has long been discovered as the most responsive clot components to native flow shear changes. These models usually employ small length scales, for instance, flow chamber-based models, shear-flow cytometry models, and dynamic shear platelet aggregation models. They have also been used to study the impact of flow shear on drug efficacy during the formation of a human platelet-rich thrombus. Other flow flow thrombosis model are loop based. The mostly known is the Chandler Loop model which has been used for drug evaluation since last century. In the following sections, flow chamber-based model and the Chandler loop model will be thoroughly discussed.

2.5.1 Flow Chamber-based Model

Flow chamber-based assays and more recent microfluidic assays have attracted a lot of attentions over the decades. Parallel plate flow chamber, biochips with microchannels and rectangular microcapillaries are three fluidic assays that have already been used for studying thrombosis pathogenesis and testing hemostatic functions of platelet during a thrombus formation. Since most thrombosis-related flow chamber assays have similar designs and limitations, I will discuss them as one technique in this section. Flow chambers are often seen to be surface-coated with collagen, tissue factors, and/or other thrombogenic substances.[24] As blood flows through the coatings, collagen and tissue factor facilitate platelet binding and thrombus formation, respectively.[25] Researchers pre-label platelets with fluorescent reporters to facilitate a real-time monitoring during the perfusion of buffer, plasma or blood. In some designs, one could continuously record the ongoing platelet deposition via a fluorescence microscopy or an intensity reading to study platelet accumulation, platelet disaggregation, and flow-dependent thrombus deposition. Additionally, coagulation factors such as fibrinogen, FXa and prothrombin have also been previously stained and evaluated in these setups.[107-109] Another benefit of flow chambers is that they can be adapted into bifurcated or multi-channel designs. Rheological variables like viscosity, flow rate and pressure drop can be easily controlled to study drug diffusion and permeation.[110, 111] These models have also been used to help solve physiological problems, for example, to indicate what variables make blood bypass the thrombus occlusion to another open channel or strive to develop a new flow pattern near the thrombus.[112, 113]

Flow chamber models are assuredly eligible for evaluating drug efficacy. Altered platelet activity have been monitored in the presence of antiplatelet drugs. Among which aspirin and clopidogrel showed comparable results in these chambers to those experimented *in-vivo*.[27, 28, 114] Anticoagulants such as FXa inhibitors and direct thrombin inhibitors have also shown capacity of disaggregating platelets and fibrin in these models.[115-117] However, very few publications are found for testing thrombolytic agents using flow chambers to date.[30] It could attribute to that the surface coated collagen causes the formation of platelet-rich clots, which express high resistances to thrombolytic agents.[118] With that said, current flow chamber-based assays are good *in-vitro* models to study arterial thrombosis but limited in venous thrombosis studies where platelet function is less prominent. Nonetheless, small length scales and highly ordered flow patterns make flow chambers especially microfluidic setups less appealing to mimic native flow conditions as *in-vivo* hemodynamics can be turbulent and much more diversified.

2.5.2 Chandler Loop Model

The Chandler loop is a technique designed to assess whole blood clotting in a flowing system.[119] Studies have shown that the morphology and components of the thrombi formed in the Chandler loop are similar to those formed in human bodies.[42, 120, 121] The apparatus has also been extensively used to test thrombogenicity or hemocompatibility of prosthetic materials and two examples of these applications are heparin coated polyethylene for stents and silver nanoparticles coating for medical devices (**Figure 2.2**).[122, 123] A common setup of a Chandler loop apparatus is assembled by attaching an axle through the center of an end-joined tubing loop partially filled with blood. With rotating the axle, the resulting shear stress drives blood naturally flowing against the spinning direction in the tubing. In most studies, clotting time and thrombus mass are primarily evaluated. Comparable clotting times and clot appearances via utilizing different initiation methods such as tissue factor, recalcification or non-coagulated blood in the loop. [124] The formed clot is always floating below the forward meniscus. Chandler loop has previously been used for antithrombotic and thrombolytic drug evaluation. In a study by Mutch et al., fluorescence-labeled human whole blood clots are pre-formed in the Chandler loop.[125] Thrombolytic agents like rt-PA are added into the preformed clots in the tubing loop to evaluate thrombolytic potency. As rt-PA activates plasmin in blood to triggers fibrinolysis, fluorescence is

released from the clot into the flowing serum. Fluorescence intensity of collected samples are measured by a spectrometer periodically to indicate the status of fibrinolysis and clot digestion.

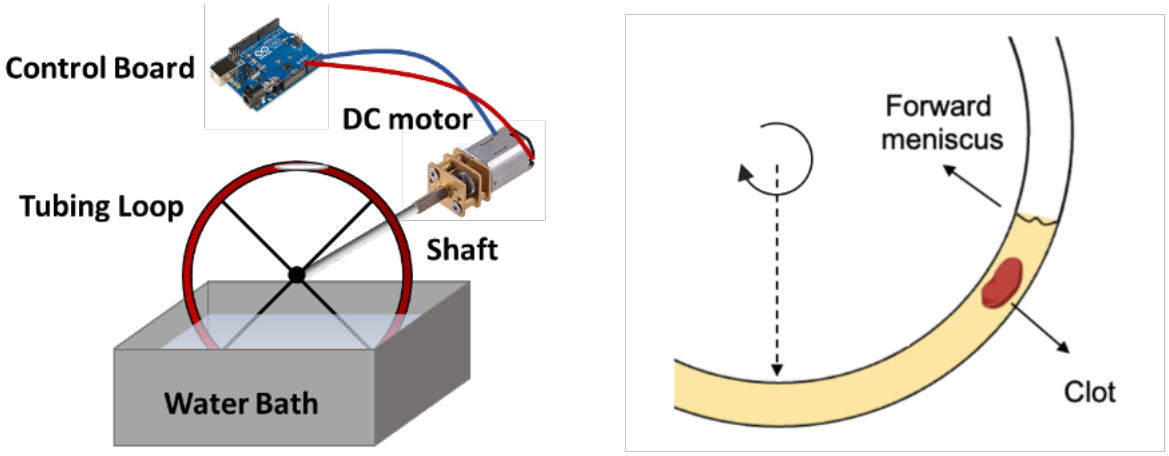

Figure 2.2. The Chandler Loop, human blood is perfused in an end-joined loop, which is fixed on a plate. The shaft through the center of the plate can be spun to a desired speed to mimic the in vivo hemodynamic changes.

In summary, Chandler loop is a simple apparatus that has many benefits as a thrombosis drug evaluation model. First, it can potentially fabricate different types of representative human thrombi analogs by varying clot forming conditions. Second, it can be used to study shear-dependent drug induced clot dissolution. As a relatively new use of the model, there exists a need to demonstrate model effectiveness through more experiments and model characterization using clinical samples. since the presence of pulsatile flow in vivo, the introduction of pulsatility to lysis in the Chandler loop can make it more representative. If a fluorescently labeled clot were to be used, the molecules introduced in the clot should not interfere with the formation of the thrombus as was reported by other studies.[126, 127] In all, the Chandler loop model demands thorough investigations to demonstrate its usefulness. A characterization of clot properties forming should be the priority step for further research.

2.6 Conclusion

Thrombosis is a leading cause of death worldwide. To date, no existing models can provide complete efficacy profiles of thrombolytic drugs and help drug translations into clinical trials. During the pre-clinical drug evaluation process, novel thrombolytic agents are tested in both

diagnostic assays and animal models to offer therapeutic information. Diagnostic assays are convenient for functional testing while animal thrombosis models are ideal for systemic drug evaluation regarding their pathophysiological relevance. Nonetheless, results from diagnostic assays are sometimes biased and drawbacks in animal models are still prominent. These facts can easily end up in a low clinical translation and a massive waste of animal resources. Current engineered *in-vitro* thrombosis models are promising in terms of biomimetic features and the use of human blood. The participation of *in-vitro* thrombosis models should expedite the drug screening process and greatly release animal research burden, although drug tests in animals cannot be entirely avoided due to regulatory rules and necessary *in vivo* side-effect checks. Limitations of current *in-vitro* thrombosis models include insufficient drug research, limited testing capacity, poor model characterization, and a lack of tunability in mimicking different pathophysiological conditions. These limitations make the refinement of current models extremely difficult as most models are not designed originally for thrombolytic drug evaluations, and a re-design process may take as much time as designing a new model. Therefore, a large demand existed for developing representative *in-vitro* thrombolysis flow models to screen novel thrombolytic agents that offer faster clot dissolution and better clot specificity. Thrombi characteristics and local hemodynamics largely affect the in vivo efficacy of thrombolytic agents. And thus, the developed model should emphasize both aspects to gain physiological relevance. In all, a thrombolytic drug evaluation model that combines an in vivo-like fluorescence incorporated synthetic clot (FISC) and human-relevant flow conditions can be a versatile and representative platform that expedite improve drug translation rates and expedite drug evaluation processes.

2.7 References

[1] A.S. Go, D. Mozaffarian, V.L. Roger, E.J. Benjamin, J.D. Berry, M.J. Blaha, S. Dai, E.S. Ford, C.S. Fox, S. Franco, H.J. Fullerton, C. Gillespie, S.M. Hailpern, J.A. Heit, V.J. Howard, M.D. Huffman, S.E. Judd, B.M. Kissela, S.J. Kittner, D.T. Lackland, J.H. Lichtman, L.D. Lisabeth, R.H. Mackey, D.J. Magid, G.M. Marcus, A. Marelli, D.B. Matchar, D.K. McGuire, E.R. Mohler, C.S. Moy, M.E. Mussolino, R.W. Neumar, G. Nichol, D.K. Pandey, N.P. Paynter, M.J. Reeves, P.D. Sorlie, J. Stein, A. Towfighi, T.N. Turan, S.S. Virani, N.D. Wong, D. Woo, M.B. Turner, Heart Disease and Stroke Statistics - 2014 Update: A report from the American Heart Association, 2014.

[2] S.Z. Goldhaber, H. Bounameaux, Pulmonary embolism and deep vein thrombosis, The Lancet 379(9828) (2012) 1835-1846.
[3] A. Kochar, A.Y. Chen, P.P. Sharma, N.J. Pagidipati, G.C. Fonarow, P.A. Cowper, M.T. Roe, E.D. Peterson, T.Y. Wang, Long-term mortality of older patients with acute myocardial infarction treated in US clinical practice, Journal of the American Heart Association 7(13) (2018).
[4] T. Gattringer, A. Posekany, K. Niederkorn, M. Knoflach, B. Poltrum, S. Mutzenbach, H.P. Haring, J. Ferrari, W. Lang, J. Willeit, S. Kiechl, C. Enzinger, F. Fazekas, Predicting Early Mortality of Acute Ischemic Stroke, Stroke 50(2) (2019) 349-356.
[5] R.D.S. Watson, B.S.P. Chin, G.Y.H. Lip, Antithrombotic therapy in acute coronary syndromes, Bmj 325(7376) (2002) 1348-1348.
[6] N.C. Chan, J.W. Eikelboom, J.I. Weitz, Evolving Treatments for Arterial and Venous Thrombosis: Role of the Direct Oral Anticoagulants, Circulation Research 118(9) (2016) 1409-1424.
[7] A. Li, D.A. Garcia, G.H. Lyman, M. Carrier, Direct oral anticoagulant (DOAC) versus low-molecular-weight heparin (LMWH) for treatment of cancer associated thrombosis (CAT): A systematic review and meta-analysis, Thrombosis Research 173(March 2018) (2019) 158-163.
[8] S.T.S. Troke, S.T.G. Roup, Tissue Plasminogen Activator for Acute Ischemic Stroke, New England Journal of Medicine 333(24) (1995) 1581-1588.
[9] L.K. Newby, W.R. Rutsch, R.M. Califf, M.L. Simoons, P.E. Aylward, P.W. Armstrong, L.H. Woodlief, K.L. Lee, E.J. Topol, F. Van De Werf, Time from symptom onset to treatment and outcomes after thrombolytic therapy, Journal of the American College of Cardiology 27(7) (1996) 1646-1655.
[10] M.J. Claeys, A. de Meester, C. Convens, P. Dubois, J. Boland, H. de Raedt, P. Vranckx, P. Coussement, S. Gevaert, P. Sinnaeve, P. Evrard, C. Beauloye, M. Renard, C. Vrints, Contemporary mortality differences between primary percutaneous coronary intervention and thrombolysis in ST-segment elevation myocardial infarction, Archives of Internal Medicine 171(6) (2011) 544-549.
[11] W.T. Kuo, M.K. Gould, J.D. Louie, J.K. Rosenberg, D.Y. Sze, L.V. Hofmann, Catheter-directed Therapy for the Treatment of Massive Pulmonary Embolism: Systematic Review and Meta-analysis of Modern Techniques, Journal of Vascular and Interventional Radiology 20(11) (2009) 1431-1440.

[12] C. Marti, G. John, S. Konstantinides, C. Combescur, O. Sanchez, M. Lankeit, G. Meyer, A. Perrier, Systemic thrombolytic therapy for acute pulmonary embolism: A systematic review and meta-analysis, European Heart Journal 36(10) (2015) 605-614.
[13] S. Chatterjee, A. Chakraborty, I. Weinberg, M. Kadakia, R.L. Wilensky, P. Sardar, D.J. Kumbhani, D. Mukherjee, M.R. Jaff, J. Giri, Thrombolysis for pulmonary embolism and risk of all-cause mortality, major bleeding, and intracranial hemorrhage: A meta-analysis, JAMA - Journal of the American Medical Association 311(23) (2014) 2414-2421.
[14] S. Vedantham, G. Piazza, A.K. Sista, N.A. Goldenberg, Guidance for the use of thrombolytic therapy for the treatment of venous thromboembolism, Journal of Thrombosis and Thrombolysis 41(1) (2016) 68-80.
[15] M. Verstraete, Third-generation thrombolytic drugs, American Journal of Medicine 109(1) (2000) 52-58.
[16] L. Chi, S. Rebello, B.R. Lucchesi, In Vivo Models of Thrombosis, 1999, pp. 101-107.
[17] S. Mousa, H. Sciences, In Vivo Models for the Evaluation of Antithrombotics and Thrombolytics, 2010, pp. 29-107.
[18] J.D. Folts, E.B. Crowell, G.G. Rowe, Platelet aggregation in partially obstructed vessels and its elimination with aspirin, Circulation 54(3) (1976) 365-370.
[19] S. Wessler, Studies in intravascular coagulation. III. The pathogenesis of serum-induced venous thrombosis, The Journal of clinical investigation 34(4) (1955) 647-651.
[20] R. Peters, C. Lees, K. Mitchell, M. Tweed, M. Talbot, R. Wallis, The Characterisation of Thrombus Development in an Improved Model of Arterio-Venous Shunt Thrombosis in the Rat and the Effects of Recombinant Desulphatohirudin (CGP 39393), Heparin, and Iloprost, Thrombosis and Haemostasis 65(03) (1991) 268-274.
[21] A.P. Cellai, D. Lami, A. Magi, A.A. Liotta, A. Rogolino, E. Antonucci, B. Bandinelli, R. Abbate, D. Prisco, Assessment of fibrinolytic activity by measuring the lysis time of a tissue factor-induced Clot: A feasibility evaluation, Clinical and Applied Thrombosis/Hemostasis 16(3) (2010) 337-344.
[22] L.T. Couto, J.L. Donato, G. de Nucci, Analysis of five streptokinase formulations using the euglobulin lysis test and the plasminogen activation assay, Brazilian Journal of Medical and Biological Research 37(12) (2004) 1889-1894.

[23] L. Summaria, Thromboelastographic Study of Fibrinolytic Agents, Seminars in Thrombosis and Hemostasis 21(S 04) (2012) 063-071.
[24] M. Roest, A. Reininger, J.J. Zwaginga, M.R. King, J.W.M. Heemskerk, Flow chamber-based assays to measure thrombus formation in vitro: Requirements for standardization, Journal of Thrombosis and Haemostasis 9(11) (2011) 2322-2324.
[25] S.L.N. Brouns, J.P. van Geffen, J.W.M. Heemskerk, High-throughput measurement of human platelet aggregation under flow: application in hemostasis and beyond, Platelets 00(00) (2018) 1-8.
[26] J.P. Bossavy, C. Thalamas, L. Sagnard, A. Barret, K. Sakariassen, B. Boneu, Y. Cadroy, A double-blind randomized comparison of combined aspirin and ticlopidine therapy versus aspirin or ticlopidine alone on experimental arterial thrombogenesis in humans, Blood 92(5) (1998) 1518-25.
[27] Y. Cadroy, J.P. Bossavy, C. Thalamas, L. Sagnard, K. Sakariassen, B. Boneu, Early Potent Antithrombotic Effect With Combined Aspirin and a Loading Dose of Clopidogrel on Experimental Arterial Thrombogenesis in Humans, Circulation 101(24) (2000) 2823-2828.
[28] M.B. Lucitt, S. O'Brien, J. Cowman, G. Meade, L. Basabe-Desmonts, M. Somers, N. Kent, A.J. Ricco, D. Kenny, Assaying the efficacy of dual-antiplatelet therapy: use of a controlled-shear-rate microfluidic device with a well-defined collagen surface to track dynamic platelet adhesion, Analytical and Bioanalytical Chemistry 405(14) (2013) 4823-4834.
[29] K. Hosokawa, T. Ohnishi, T. Kondo, M. Fukasawa, T. Koide, I. Maruyama, K.A. Tanaka, A novel automated microchip flow-chamber system to quantitatively evaluate thrombus formation and antithrombotic agents under blood flow conditions, Journal of Thrombosis and Haemostasis 9(10) (2011) 2029-2037.
[30] S. Loyau, B. Ho-Tin-noé, M.C. Bourrienne, Y. Boulaftali, M. Jandrot-Perrus, Microfluidic modeling of thrombolysis effect of antiplatelet and anticoagulant agents on tpa (tissue-type plasminogen activator)-induced fibrinolysis, Arteriosclerosis, Thrombosis, and Vascular Biology 38(11) (2018) 2626-2637.
[31] T. Huang, N. Li, J. Gao, Recent strategies on targeted delivery of thrombolytics, Asian Journal of Pharmaceutical Sciences 14(3) (2019) 233-247.
[32] J.W. Weisel, R.I. Litvinov, Fibrin Formation, Structure and Properties, 2017, pp. 405-456.

[33] S.L. Diamond, Engineering design of optimal strategies for blood clot dissolution, Annual Review of Biomedical Engineering (1) (1999) 427-461.
[34] J. W, Structure of fibrin: Impact on clot stability, Journal of Thrombosis and Haemostasis 5(SUPPL. 1) (2007) 116-124.
[35] I.N. Chernysh, C. Nagaswami, S. Kosolapova, A.D. Peshkova, A. Cuker, D.B. Cines, C.L. Cambor, R.I. Litvinov, J.W. Weisel, The distinctive structure and composition of arterial and venous thrombi and pulmonary emboli, Scientific Reports 10(1) (2020) 1-12.
[36] D.A. Gabriel, K. Muga, E.M. Boothroyd, The Effect of Fibrin Structure on Fibrinolysis *, (1992) 24259-24263.
[37] K. Fatah, A. Hamsten, B. Blomback, M. Blomback, Fibrin gel network characteristics and coronary heart disease: Relations to plasma fibrinogen concentration, acute phase protein, serum lipoproteins and coronary atherosclerosis, Thrombosis and Haemostasis 68(2) (1992) 130-135.
[38] J.M. Van Gelder, C.H. Nair, D.P. Dhall, Erythrocyte aggregation and erythrocyte deformability modify the permeability of erythrocyte enriched fibrin network, Thrombosis Research 82(1) (1996) 33-42.
[39] W.A. Lam, O. Chaudhuri, A. Crow, K.D. Webster, T.D. Li, A. Kita, J. Huang, D.A. Fletcher, Mechanics and contraction dynamics of single platelets and implications for clot stiffening, Nature Materials 10(1) (2011) 61-66.
[40] B.J. Potter van Loon, D.C. Rijken, E.J. Brommer, A.P. van der Maas, The amount of plasminogen, tissue-type plasminogen activator and plasminogen activator inhibitor type 1 in human thrombi and the relation to ex-vivo lysibility, Thrombosis and haemostasis 67(1) (1992) 101-5.
[41] L. Robbie, S. Young, B. Bennett, N. Booth, Thrombi Formed in a Chandler Loop Mimic Human Arterial Thrombi in Structure and PAI-1 Content and Distribution, Thrombosis and Haemostasis 77(03) (1997) 510-515.
[42] H.A. Stringer, P. van Swieten, H.F. Heijnen, J.J. Sixma, H. Pannekoek, Plasminogen activator inhibitor-1 released from activated platelets plays a key role in thrombolysis resistance. Studies with thrombi generated in the Chandler loop, Arteriosclerosis and Thrombosis: A Journal of Vascular Biology 14(9) (1994) 1452-1458.

[43] K.B. Neeves, D.A.R. Illing, S.L. Diamond, Thrombin flux and wall shear rate regulate fibrin fiber deposition state during polymerization under flow, Biophysical Journal 98(7) (2010) 1344-1352.
[44] J. Silvain, J.P. Collet, C. Nagaswami, F. Beygui, K.E. Edmondson, A. Bellemain-Appaix, G. Cayla, A. Pena, D. Brugier, O. Barthelemy, G. Montalescot, J.W. Weisel, Composition of coronary thrombus in acute myocardial infarction, Journal of the American College of Cardiology 57(12) (2011) 1359-1367.
[45] E. Mfoumou, J. Tripette, M. Blostein, G. Cloutier, Time-dependent hardening of blood clots quantitatively measured in vivo with shear-wave ultrasound imaging in a rabbit model of venous thrombosis, Thrombosis Research 133(2) (2014) 265-271.
[46] P.J. Garber, A.L. Mathieson, J. Ducas, J.N. Patton, J.S. Geddes, R.M. Prewitt, Thrombolytic therapy in cardiogenic shock: effect of increased aortic pressure and rapid tPA administration, The Canadian journal of cardiology 11(1) (1995) 30-6.
[47] H. Hess, H. Ingrisch, A. Mietaschk, H. Rath, Local Low-Dose Thrombolytic Therapy of Peripheral Arterial Occlusions, New England Journal of Medicine 307(26) (1982) 1627-1630.
[48] K. Kolev, K. Tenekedjiev, E. Komorowicz, R. Machovich, Functional evaluation of the structural features of proteases and their substrate in fibrin surface degradation, Journal of Biological Chemistry 272(21) (1997) 13666-13675.
[49] M. Anand, K. Rajagopal, K.R. Rajagopal, A Model Incorporating Some of the Mechanical and Biochemical Factors Underlying Clot Formation and Dissolution in Flowing Blood, Journal of Theoretical Medicine 5(3-4) (2003) 183-218.
[50] D.M. Wootton, D.N. Ku, Fluid mechanics of vascular systems, diseases, and thrombosis, Annual Review of Biomedical Engineering (1) (1999) 299-329.
[51] A. Dadarlat-Pop, I. Burian, L. Cadis, R. Tomoaia, A. Oprea, Diagnostic Dilemma of Recurrent Pulmonary Embolism, Diagnostics 10(2) (2020) 96-96.
[52] F. Ghalichi, X. Deng, A. De Champlain, Y. Douville, M. King, R. Guidoin, Low Reynolds number turbulence modeling of blood flow in arterial stenoses, Biorheology 35(4-5) (1998) 281-294.
[53] R.J. Leadley, L. Chi, S.S. Rebello, A. Gagnon, Contribution of in vivo models of thrombosis to the discovery and development of novel antithrombotic agents, Journal of Pharmacological and Toxicological Methods 43(2) (2000) 101-116.

[54] H. Peng, E.M. Schlaich, S. Row, S.T. Andreadis, D.D. Swartz, A Novel Ovine ex vivo Arteriovenous Shunt Model to Test Vascular Implantability, Cells Tissues Organs 195(1-2) (2012) 108-121.
[55] J.L. Romson, D.W. Haack, B.R. Lucchesi, Electrical induction of coronary artery thrombosis in the ambulatory canine: A model for evaluation of anti-thrombotic agents, Thrombosis Research 17(6) (1980) 841-853.
[56] B.S. Coller, L.E. Scudder, Inhibition of dog platelet function by in vivo infusion of F(ab')2 fragments of a monoclonal antibody to the platelet glycoprotein IIb/IIIa receptor BS Coller and LE Scudder, Blood 66(6) (1985) 1456-1459.
[57] S.A. Mousa, J.M. Bozarth, M.S. Forsythe, S.M. Jackson, A. Leamy, M.M. Diemer, R.P. Kapil, R.M. Knabb, M.C. Mayo, S.K. Pierce, W.F. De Grado, M.J. Thoolen, T.M. Reilly, Antiplatelet and antithrombotic efficacy of DMP 728, a novel platelet GPIIb/IIIa receptor antagonist, Circulation 89(1) (1994) 3-12.
[58] Y.X. Wang, J. Vincelette, V. da Cunha, B. Martin-McNulty, C. Mallari, R.M. Fitch, S. Alexander, I. Islam, B.O. Buckman, S. Yuan, J.M. Post, B. Subramanyam, R. Vergona, M.E. Sullivan, W.P. Dole, J. Morser, J. Bryant, A novel P2Y(12) adenosine diphosphate receptor antagonist that inhibits platelet aggregation and thrombus formation in rat and dog models, Thrombosis and haemostasis 97(5) (2007) 847-55.
[59] M. Chintala, J. Strony, B. Yang, S. Kurowski, Q. Li, SCH 602539, a protease-activated receptor-1 antagonist, inhibits thrombosis alone and in combination with cangrelor in a Folts model of arterial thrombosis in cynomolgus monkeys, Arteriosclerosis, Thrombosis, and Vascular Biology 30(11) (2010) 2143-2149.
[60] J.F. Eidt, P. Allison, S. Noble, J. Ashton, P. Golino, J. McNatt, L.M. Buja, J.T. Willerson, Thrombin is an important mediator of cyclic coronary blood flow variations due to platelet aggregation in stenosed canine coronary arteries, Transactions of the Association of American Physicians 101(July) (1988) 18-27.
[61] R.J. Leadley, C.J. Kasiewski, J.S. Bostwick, R. Bentley, C.T. Dunwiddie, M.H. Perrone, Inhibition of repetitive thrombus formation in the stenosed canine coronary artery by enoxaparin, but not by unfractionated heparin, Arteriosclerosis, Thrombosis, and Vascular Biology 18(6) (1998) 908-914.

[62] B. Bierbach, G. Horstick, O. Berg, A. Heimann, T. Münzel, C.-F. Vahl, O. Kempski, H. Darius, Potent low dose platelet inhibitory effects of clopidogrel and aspirin on coronary thrombus formation in an animal model of acute unstable angina, Thrombosis and Haemostasis 95(4) (2006) 715-9.

[63] M. Cohen, C. Demers, E.P. Gurfinkel, A.G.G. Turpie, G.J. Fromell, S. Goodman, A. Langer, R.M. Califf, K.A.A. Fox, J. Premmereur, F. Bigonzi, J. Stephens, B. Weatherley, A Comparison of Low-Molecular-Weight Heparin with Unfractionated Heparin for Unstable Coronary Artery Disease, New England Journal of Medicine 337(7) (1997) 447-452.

[64] D.F. Kong, R.M. Califf, D.P. Miller, D.J. Moliterno, H.D. White, R.A. Harrington, J.E. Tcheng, A.M. Lincoff, V. Hasselblad, E.J. Topol, Clinical outcomes of therapeutic agents that block the platelet glycoprotein IIb/IIIa integrin in ischemic heart disease, Circulation 98(25) (1998) 2829-35.

[65] P.R.I.i.I.S.M.i.P.L.b.U.S. Investigators, S. Symptoms, Inhibition of the Platelet Glycoprotein IIb/IIIa Receptor with Tirofiban in Unstable Angina and Non–Q-Wave Myocardial Infarction, New England Journal of Medicine 338(21) (1998) 1488-1497.

[66] J. Lefkovits, J.L. Malycky, J.S. Rao, C.E. Hart, E.F. Plow, E.J. Topol, F.A. Nicolini, Selective inhibition of factor Xa is more efficient than factor VIIa-tissue factor complex blockade at facilitating coronary thrombolysis in the canine model, Journal of the American College of Cardiology 28(7) (1997) 1858-1865.

[67] J.J. Lynch, G.R. Sitko, M.J. Mellott, E.M. Nutt, E.D. Lehman, P.A. Friedman, C.T. Dunwiddie, G.P. Vlasuk, Maintenance of canine coronary artery patency following thrombolysis with front loaded plus low dose maintenance conjunctive therapy. A comparison of factor Xa versus thrombin inhibition, Cardiovascular Research 28(1) (1994) 78-85.

[68] D.G. Hackam, D.A. Redelmeier, Translation of Research Evidence From Animals to Humans, JAMA 296(14) (2006) 1727-1727.

[69] M. Levi, J. Dörffler-Melly, G.J. Johnson, L. Drouet, L. Badimon, Usefulness and limitations of animal models of venous thrombosis: On behalf of the Subcommittee on Animal, Cellular, and Molecular Models of Thrombosis and Haemostasis of the Scientific and Standardization Committee of the International Society on Thrombo, Thrombosis and Haemostasis 86(5) (2001) 1331-1333.

[70] J.P. Clozel, L. Banken, S. Roux, Aprotinin: An antidote for recombinant tissue-type plasminogen activator (rt-PA) active in vivo, Journal of the American College of Cardiology 16(2) (1990) 507-510.
[71] D. Collen, J.M. Stassen, M. Verstraete, Thrombolysis with human extrinsic (tissue-type) plasminogen activator in rabbits with experimental jugular vein thrombosis. Effect of molecular form and dose of activator, age of the thrombus, and route of administration, Journal of Clinical Investigation 71(2) (1983) 368-376.
[72] P. Bacher, D. Welzel, O. Iqbal, D. Hoppensteadt, D. Callas, J.M. Walenga, J. Fareed, The thrombolytic potency of LMW-heparin compared to urokinase in a rabbit jugular vein clot lysis model, Thrombosis Research 66(2-3) (1992) 151-158.
[73] L. Bara, M.F. Bloch, M.M. Samama, A comparative study of recombinant hirudin and standard heparin in the Wessler model, Thrombosis research 68(2) (1992) 167-74.
[74] B. Kaiser, J. Fareed, Recombinant Full-length Tissue Factor Pathway Inhibitor (TFPI) Prevents Thrombus Formation and Rethrombosis after Lysis in a Rabbit Model of Jugular Vein Thrombosis, Thrombosis and Haemostasis 76(04) (1996) 615-620.
[75] E. Perzborn, J. Strassburger, A. Wilmen, J. Pohlmann, S. Roehrig, K.H. Schlemmer, A. Straub, In vitro and in vivo studies of the novel antithrombotic agent BAY 59-7939--an oral, direct Factor Xa inhibitor, Journal of thrombosis and haemostasis : JTH 3(3) (2005) 514-521.
[76] K. Sato, Y. Taniuchi, T. Kawasaki, F. Hirayama, H. Koshio, Y. Matsumoto, R.A. Shand, J.R. Smith, R.B. Wallis, A.B. Kelly, U.M. Marzec, W. Krupski, A. Bass, Y. Cadroy, S.R. Hanson, L.A. Harker, L.W. Schaffer, J.T. Davidson, G.P. Vlasuk, K.S. Siegl, K. Sato, Y. Taniuchi, T. Kawasaki, F. Hirayama, H. Koshio, Y. Matsumoto, B.I. Eriksson, P. Wille-Jørgensen, P. Kälebo, P. Mouret, N. Rosencher, P. Bösch, M. Baur, S. Ekman, D. Bach, S. Lindbratt, P. Close, A. Straub, Relationship between the antithrombotic effect of YM-75466, a novel factor Xa inhibitor, and coagulation parameters in rats, European Journal of Pharmacology 347(2-3) (1998) 231-236.
[77] W. Wienen, J.M. Stassen, H. Priepke, U.J. Ries, N. Hauel, Effects of the direct thrombin inhibitor dabigatran and its orally active prodrug, dabigatran etexilate, on thrombus formation and bleeding time in rats, Thrombosis and haemostasis 98(2) (2007) 333-8.
[78] H.j. Jin, H. Zhang, M.l. Sun, B.g. Zhang, J.w. Zhang, Urokinase-coated chitosan nanoparticles for thrombolytic therapy: preparation and pharmacodynamics in vivo, Journal of Thrombosis and Thrombolysis 36(4) (2013) 458-468.

[79] S. Hollenbach, U. Sinha, P.-H. Lin, K. Needham, L. Frey, T. Hancock, A. Wong, D. Wolf, A Comparative Study of Prothrombinase and Thrombin Inhibitors in a Novel Rabbit Model of Non-Occlusive Deep Vein Thrombosis, Thrombosis and Haemostasis 71(03) (1994) 357-362.
[80] P.C. Wong, E.J. Crain, B. Xin, R.R. Wexler, P.Y.S. Lam, D.J. Pinto, J.M. Luettgen, R.M. Knabb, Apixaban, an oral, direct and highly selective factor Xa inhibitor: In vitro, antithrombotic and antihemostatic studies, Journal of Thrombosis and Haemostasis 6(5) (2008) 820-829.
[81] T. Umetsu, K. Sanai, Effect of 1-Methyl-2-Mercapto-5-(3-Pyridyl)-Imidazole (KC-6141), an Anti-Aggregating Compound, on Experimental Thrombosis in Rats, Thrombosis and Haemostasis 39(01) (1978) 074-083.
[82] R. Létienne, A. Leparq-Panissié, Y. Calmettes, F. Nadal-Wollbold, M. Perez, B. Le Grand, Antithrombotic activity of F 16618, a new PAR1 antagonist evaluated in extracorporeal arterio-venous shunt in the rat, Biochemical Pharmacology 79(11) (2010) 1616-1621.
[83] L.W. Schaffer, J.T. Davidson, G.P. Vlasuk, K.S. Siegl, Antithrombotic Efficacy of Recombinant Tick Anticoagulant Paptide A Potenet Inhibitor of Coagulation Factor Xa in a Primate Model of Arterial Thrombosis, Circulation 84 (1991) 1741-1748.
[84] J. Eikelboom, N.C. Chan, V. Bhagirath, Profile of betrixaban and its potential in the prevention and treatment of venous thromboembolism, Vascular Health and Risk Management 10(1) (2015) 343-343.
[85] S.W. Jordan, C.A. Haller, R.E. Sallach, R.P. Apkarian, S.R. Hanson, E.L. Chaikof, The effect of a recombinant elastin-mimetic coating of an ePTFE prosthesis on acute thrombogenicity in a baboon arteriovenous shunt, Biomaterials 28(6) (2007) 1191-1197.
[86] A.B. Kelly, U.M. Marzec, W. Krupski, A. Bass, Y. Cadroy, S.R. Hanson, L.A. Harker, Hirudin interruption of heparin-resistant arterial thrombus formation in baboons, Blood 77(5) (1991) 1006-1012.
[87] M. Sperzel, J. Huetter, Evaluation of aprotinin and tranexamic acid in different in vitro and in vivo models of fibrinolysis, coagulation and thrombus formation, J Thromb Haemost 5(10) (2007) 2113-2118.
[88] J.M. Herbert, A. Bernat, F. Dol, J.P. Herault, B. Crepon, J.C. Lormeau, DX 9065A a novel, synthetic, selective and orally active inhibitor of factor Xa: in vitro and in vivo studies, J Pharmacol Exp Ther 276(3) (1996) 1030-8.

[89] B.R. Gudmundsdottir, C.W. Francis, A.M. Bjornsdottir, M. Nellbring, P.T. Onundarson, Critical role of factors II and X during coumarin anticoagulation and their combined measurement with a new Fiix-prothrombin time, Thrombosis Research 130(4) (2012) 674-681.
[90] S.M. Donahue, C.M. Otto, Thromboelastography: a tool for measuring hypercoagulability, hypocoagulability, and fibrinolysis, Journal of Veterinary Emergency and Critical Care 15(1) (2005) 9-16.
[91] N. Salooja, D.J. Perry, Thrombelastography, Blood coagulation & fibrinolysis 12(5) (2001) 327-337.
[92] L. Zuckerman, E. Cohen, J. Vagher, E. Woodward, J. Caprini, Comparison of Thrombelastography with Common Coagulation Tests, Thrombosis and Haemostasis 46(04) (1981) 752-756.
[93] S.A. Mousa, J.M. Bozarth, D. Seiffert, G.Z. Feuerstein, Using thrombelastography to determine the efficacy of the platelet glycoprotein IIb/IIIa antagonist, roxifiban, on platelet/fibrin-mediated clot dynamics in humans, Blood Coagulation and Fibrinolysis 16(3) (2005) 165-171.
[94] Y.H. Jeong, K.P. Bliden, M.J. Antonino, U.S. Tantry, P.A. Gurbel, Usefulness of thrombelastography platelet mapping assay to measure the antiplatelet effect of P2Y12 receptor inhibitors and high on-treatment platelet reactivity, Platelets 24(2) (2013) 166-169.
[95] E. Barabas, E. Szell, S. Bajusz, Screening for fibrinolysis inhibitory effect of synthetic thrombin inhibitors, Blood coagulation & fibrinolysis : an international journal in haemostasis and thrombosis 4(2) (1993) 243-8.
[96] R.G. Macfarlane, R. Biggs, Fibrinolysis. Its mechanism and significance, Blood 10(3) (1948) 1167-1187.
[97] T. Urano, K. Sakakibara, A. Rydzewski, S. Urano, Y. Takada, A. Takada, Relationships between Euglobulin Clot Lysis Time and the Plasma Levels of Tissue Plasminogen Activator and Plasminogen Activator Inhibitor 1, Thrombosis and Haemostasis 63(01) (1990) 082-086.
[98] O. Tóth, C. Szabó, M. Kecskés, L. Pótó, Á. Nagy, H. Losonczy, In vitro effect of the potent poly(ADP-ribose) polymerase (PARP) inhibitor INO-1001 alone and in combination with aspirin, eptifibatide, tirofiban, enoxaparin or alteplase on haemostatic parameters, Life Sciences 79(4) (2006) 317-323.

[99] G.J.A.J.M. Kuiper, M.-C.F. Kleinegris, R. van Oerle, H.M.H. Spronk, M.D. Lancé, H. ten Cate, Y.M.C. Henskens, Validation of a modified thromboelastometry approach to detect changes in fibrinolytic activity, Thrombosis Journal 14(1) (2016) 1-1.
[100] A.J. Jones, A.M. Meunier, A precise and rapid microtitre plate clot lysis assay: methodology, kinetic modeling and measurement of catalytic constants for plasminogen activation during fibrinolysis, Thrombosis and haemostasis 64(3) (1990) 455-63.
[101] G.V.R. Born, Aggregation of blood platelets by adenosine diphosphate and its reversal, Nature 194(4832) (1962) 927-929.
[102] O. Bruno, C. Brullo, S. Schenone, A. Ranise, F. Bondavalli, E. Barocelli, M. Tognolini, F. Magnanini, V. Ballabeni, Progress in 5H[1]benzopyrano[4,3-d]pyrimidin-5-amine series: 2-methoxy derivatives effective as antiplatelet agents with analgesic activity, Il Farmaco 57(9) (2002) 753-758.
[103] M. Cattaneo, Aspirin and clopidogrel: Efficacy, safety, and the issue of drug resistance, Arteriosclerosis, Thrombosis, and Vascular Biology 24(11) (2004) 1980-1987.
[104] B. Giusti, A.M. Gori, R. Marcucci, C. Saracini, I. Sestini, R. Paniccia, S. Valente, D. Antoniucci, R. Abbate, G.F. Gensini, Cytochrome P4502C19 loss-of-function polymorphism, but not CYP3A4 IVS10+12G/A and P2Y12 T744C poymorphism, is associated with response variability to dual antiplatelet treatment in high-risk vascular patients, Pharmacogenetics and Genomics 17(12) (2007) 1057-1064.
[105] M.D. Lancé, A general review of major global coagulation assays: Thrombelastography, thrombin generation test and clot waveform analysis, Thrombosis Journal 13(1) (2015) 1-6.
[106] J. Fareed, J. Walenga, A. Kumar, A. Rock, A Modified Stasis Thrombosis Model to Study the Antithrombotic Actions of Heparin and Its Fractions, Seminars in Thrombosis and Hemostasis 11(02) (1985) 155-175.
[107] A.J. Reininger, I. Bernlochner, S.M. Penz, C. Ravanat, P. Smethurst, R.W. Farndale, C. Gachet, R. Brandl, W. Siess, A 2-Step Mechanism of Arterial Thrombus Formation Induced by Human Atherosclerotic Plaques, Journal of the American College of Cardiology 55(11) (2010) 1147-1158.

[108] I.C.A. Munnix, M.J.E. Kuijpers, J. Auger, C.M.L.G.D. Thomassen, P. Panizzi, M.A.M. van Zandvoort, J. Rosing, P.E. Bock, S.P. Watson, J.W.M. Heemskerk, Segregation of Platelet Aggregatory and Procoagulant Microdomains in Thrombus Formation: Regulation by Transient Integrin Activation, Arteriosclerosis, Thrombosis, and Vascular Biology 27(11) (2007) 2484-2490.
[109] M.A. Berny, I.C.A. Munnix, J.M. Auger, S.E.M. Schols, J.M.E.M. Cosemans, P. Panizzi, P.E. Bock, S.P. Watson, O.J.T. McCarty, J.W.M. Heemskerk, Spatial distribution of factor xa, thrombin, and fibrin(ogen) on thrombi at venous shear, PLoS ONE 5(4) (2010).
[110] A. Jain, A. Graveline, A. Waterhouse, A. Vernet, R. Flaumenhaft, D.E. Ingber, A shear gradient-activated microfluidic device for automated monitoring of whole blood haemostasis and platelet function, Nat Commun 7 (2016) 10176.
[111] R.W. Muthard, S.L. Diamond, Side view thrombosis microfluidic device with controllable wall shear rate and transthrombus pressure gradient, Lab on a Chip 13(10) (2013) 1883-1883.
[112] T.V. Colace, R.W. Muthard, S.L. Diamond, Thrombus Growth and Embolism on Tissue Factor-Bearing Collagen Surfaces Under Flow: Role of Thrombin With and Without Fibrin, Arteriosclerosis, Thrombosis, and Vascular Biology 32(6) (2012) 1466-1476.
[113] T.V. Colace, G.W. Tormoen, O.J.T. McCarty, S.L. Diamond, Microfluidics and Coagulation Biology, Annual Review of Biomedical Engineering 15(1) (2013) 283-303.
[114] J.P. Bossavy, C. Thalamas, L. Sagnard, a. Barret, K. Sakariassen, B. Boneu, Y. Cadroy, A double-blind randomized comparison of combined aspirin and ticlopidine therapy versus aspirin or ticlopidine alone on experimental arterial thrombogenesis in humans, Blood 92(5) (1998) 1518-1525.
[115] H. Sugihara, Y. Idemoto, T. Kuwano, Y. Nagata, J. Morii, M. Sugihara, M. Ogawa, S.-i. Miura, K. Saku, Evaluation of the Antithrombotic Effects of Rivaroxaban and Apixaban Using the Total Thrombus-Formation Analysis System ® : In Vitro and Ex Vivo Studies, Journal of Clinical Medicine Research 8(12) (2016) 899-907.
[116] F. Swieringa, M.J.E. Kuijpers, M.M.E. Lamers, P.E.J. van der Meijden, J.W.M. Heemskerk, Rate-limiting roles of the tenase complex of factors VIII and IX in platelet procoagulant activity and formation of platelet-fibrin thrombi under flow, Haematologica 100(6) (2015) 748-756.
[117] K. Hosokawa, T. Ohnishi, H. Sameshima, N. Miura, T. Koide, I. Maruyama, K.A. Tanaka, Comparative evaluation of direct thrombin and factor Xa inhibitors with antiplatelet agents under flow and static conditions: An in vitro flow chamber model, PLoS ONE 9(1) (2014).

[118] L. Di Meglio, J.P. Desilles, V. Ollivier, M.S. Nomenjanahary, S. Di Meglio, C. Deschildre, S. Loyau, J.M. Olivot, R. Blanc, M. Piotin, M.C. Bouton, J.B. Michel, M. Jandrot-Perrus, B. Ho-Tin-Noe, M. Mazighi, Acute ischemic stroke thrombi have an outer shell that impairs fibrinolysis, Neurology 93(18) (2019) e1686-e1698.
[119] A.B. Chandler, In vitro thrombotic coagulation of the blood; a method for producing a thrombus, Laboratory investigation; a journal of technical methods and pathology 7(2) (1958) 110-4.
[120] L.A. Robbie, S.P. Young, B. Bennett, N.A. Booth, Thrombi Formed in a Chandler Loop Mimic Human Arterial Thrombi in Structure and PAI-1 Content and Distribution, Thrombosis and Haemostasis 77(03) (1997) 510-515.
[121] M. Berndt, S. Prothmann, C. Maegerlein, P. Oberdieck, C. Zimmer, B. Hegge, J. Pelisek, L. Schirmer, H. Poppert, T. Boeckh-Behrens, Artificial Stroke Clots: How Wide is the Gap to the Real World?, World Neurosurg 110 (2018) e90-e99.
[122] S. Krajewski, R. Prucek, A. Panacek, M. Avci-Adali, A. Nolte, A. Straub, R. Zboril, H.P. Wendel, L. Kvitek, Hemocompatibility evaluation of different silver nanoparticle concentrations employing a modified Chandler-loop in vitro assay on human blood, Acta Biomaterialia 9(7) (2013) 7460-7468.
[123] K. Christensen, R. Larsson, H. Emanuelsson, G. Elgue, A. Larsson, Effects on blood compatibility in vitro by combining a direct P2Y 12 receptor inhibitor and heparin coating of stents, Platelets 17(5) (2006) 318-327.
[124] R.A. Gardner, An examination of the fluid mechanics and thrombus formation time parameters in a Chandler rotating loop system, The Journal of laboratory and clinical medicine 84(4) (1974) 494-508.
[125] N.J. Mutch, N.R. Moore, C. Mattsson, H. Jonasson, A.R. Green, N.A. Booth, The use of the Chandler loop to examine the interaction potential of NXY-059 on the thrombolytic properties of rtPA on human thrombi in vitro, British Journal of Pharmacology 153(1) (2008) 124-131.
[126] J. John, W. Garabon, Impact of Thrombomodulin and Thrombin- Activatable Fibrinolysis Inhibitor on the Anticoagulant and Profibrinolytic Effects of Rivaroxaban Justin, 2016.
[127] V. Binder, B. Bergum, S. Jaisson, P. Gillery, C. Scavenius, E. Spriet, A.K. Nyhaug, H.M. Roberts, I.L.C. Chapple, A. Hellvard, N. Delaleu, P. Mydel, Impact of fibrinogen carbamylation on fibrin clot formation and stability, Thromb Haemost 117(5) (2017) 899-910.

3. CHARACTERIZATION OF FIBRIN UNDER VARIOUS CLOTTING CONDITIONS

One version of this chapter was published in Thrombosis Research entitled "Fibrin clot formation under diverse clotting conditions: Comparing turbidimetry and thromboelastography", Volume 187, Page 48-55, (2020), access via https://doi.org/10.1016/j.thromres.2020.01.001

Endogenous plasma variables impact fibrin polymerization affecting ultimate clot structure and stability. Understanding the role of individual variables in clot formation can help build a tunable *in-vitro* synthetic clot substrate for drug evaluation. The introduced tunability also potentiates the fabrication of a patient-specific clot substrate to aid in the development of personalized medicine. Therefore, studying fibrin formation under very controlled conditions and across a diverse range of clotting circumstances is crucial. TEG and turbidity assays are two methods that can monitor fibrin formation in progress along with offering physical properties such as clot strength and clot turbidity. In some clinical instances, TEG and turbidity assay have been used interchangeably while the feasibility is not assessed. This chapter will thoroughly explore the synergistic use of TEG and turbidity assays to create a reliable fibrin characterization system.

3.1 Abstract

Thrombosis is a leading cause of death around the world. Fibrin, the protein primarily responsible for clot formation, is formed via cleaving soluble fibrinogen by thrombin with resulting properties varying under different clot forming conditions. This study sought to compare trends across thromboelastography (TEG) and turbidimetry utilizing a simplified fibrinogen/thrombin clot model. Turbidimetry is an optical measure (550 nm) of fibrin clot formation and is widely utilized due to its laboratory accessibility and ease of use. Thromboelastography (TEG) is a specialized viscoelastic technique that directly measures clot strength and is primarily utilized in the clinical setting to assess patients' hemostasis. In these experiments, human and bovine fibrin clots were formed *in-vitro* by mixing fibrinogen and thrombin under diverse clotting conditions. Increasing thrombin concentration (0 to 10 U/mL), ionic strength (0.05 to 0.3 M), pH (5.5 to 8.1), and lowering albumin concentration (100 to 0 mg/mL) resulted in decreased clot turbidity and increased clot strength using species-matched

bovine and human fibrinogen and thrombin. Whereas, increasing fibrinogen concentration (1 to 5 mg/mL) resulted in increased clot turbidity and increased clot strength for both species-matched and cross-species fibrinogen and thrombin. Clotting times with both techniques followed a similar trend and were observed to be unchanged when varying albumin concentration, elongated with increasing fibrinogen, and shortened with increasing pH, ionic strength, and thrombin. TEG and turbidimetry track clot formation via two distinct methods and when utilized together provide complementary clot strength and fiber structural information across diverse clotting conditions.

3.2 Introduction

Blood coagulation is a complex cascade of multiple activators and inhibitors working in concert with each other to maintain hemostasis. Thrombosis is the pathological formation of a thrombus, or blood clot, in the body that partially or completely restricts blood flow, limits perfusion, and can result in tissue death. Fibrin, a protein that is primarily responsible for clot formation, is a critical component in thrombosis. Fibrin monomers are formed via the cleavage of soluble fibrinogen by thrombin. These monomers spontaneously polymerize and aggregate laterally to form fibrin fibers.[1] In the final step of the coagulation cascade the fibers are crosslinked by coagulation factor FXIIIa forming a hemostatic fibrous clot in a calcium dependent process.[2] The conditions that fibrin polymerization occurs under determines the fibrin clot structure in addition to mechanical and fibrinolytic properties of the clot.[3] A number of critical factors that affect the kinetics of fibrin polymerization and the resulting fiber thickness/morphology include fibrinogen and thrombin concentrations, ionic strength, pH, and total protein concentration.[4-6]

To better understand fibrin formation in pathological thrombosis, it is necessary to study fibrin formation under very controlled conditions and across a diverse range of clotting circumstances. In literature, multiple assays and specialized equipment have been utilized to measure blood clot formation characteristics that include electron microscopy, clot permeability tests, clot turbidity assays, prothrombin time (PT and normalized INR), activated partial thromboplastin time (aPTT), rotational thromboelastogram (ROTEM), and thromboelastography (TEG) assays, to list a few.[7-9] These clot analysis tools vary based on their utilization for research purposes and as clinical diagnostic tools. PT and aPTT are two common clinical assays that measure the integrity of specific coagulation pathways to assist in diagnosis and monitoring

of patient coagulation disorders and is commonly utilized for therapeutic dosage decision making. These assays monitor time as the only variable and give little indication of physical characteristics like clot structure, mechanical strength, and fibrinolytic properties. While there are many clot formation analysis tools this study will focus on thromboelastography and turbidity measurements to track dynamic fibrin clot formation characteristics over a range of different clot formation conditions.

Turbidity assays (turbidimetry) are widely used for research and clinical applications due to their simplistic implementation and utilization of commonly accessible equipment found in research laboratories. Turbidimetry measures light transmittance through a clot and is carried out utilizing a spectrophotometer looking at a defined wavelength, typically 405nm (or in the range of 350-700 nm).[10, 11] Turbidity measurements of a clot can be tracked over time to monitor formation dynamics (**Figure 3.1A**). It is not surprising that turbidity is a popular measure of clot formation as it can easily be adapted to a multi-well plate format for multiplexing to allow for high through-put sample screening. A turbidity tracing (or absorbance over time plot) allows determination of a number of clot-forming parameters that include maximum turbidity, time to maximum turbidity, time to clot onset, and clot formation rate (V_{max}). Prior studies have developed correlations to convert raw turbidity tracings to fibrin fiber mass/length ratio for use as a relative estimate of fiber thickness.[4, 11-13] Turbidity is limited; however, in that it does not directly measure clot strength or fibrin structure and it is incapable of use in whole blood clot formation assays as red blood cells absorb significantly at the wavelengths that are typically utilized.[14]

As previously mentioned, thromboelastography is another method for characterizing clot formation that has received widespread attention dating back to the 1980s.[15, 16] In recent years, TEG has been primarily utilized in the clinic for testing clot formation and digestion dynamics to assess a patient's hemostatic status in trauma and during surgery. TEG®6s, TEG®5000 and ROTEM® represent three commercially available thromboelastography tools that have gained significant popularity. Although they may differ slightly in instrument design and functionality, their ability to monitor clot formation and digestion significantly overlap. Since TEG is a viscoelastic technique that directly measures clot strength, it can be utilized for both whole blood and fibrin analysis. The TEG®5000 instrument, employed in this study, monitors blood coagulation in a TEG cup as it is rotated at a 4º 45' arc back and forth against a pin and an electromechanical torsion sensor measures the increasing viscoelastic strength of an evolving clot

(**Figure 3.1B**). The accompanying TEG software interprets the raw TEG tracing (clot strength over time) and presents multiple parameters that include maximum amplitude (MA), reaction rate (R), kinetics time (K), α angle (Angle), and time to maximum amplitude (TMA) compared to an acceptable clinical normal range to assess coagulation state. While this level of analytical capability is desirable, TEG is a less commonly utilized technique in research laboratories as it requires specialized equipment to carry out the assays. TEG also suffers from its inability to multiplex without purchasing multiple instruments as each TEG instrument only has two-channels which significantly reduces throughput. This study sought to compare TEG and turbidimetry to determine under what conditions they provide similar or different experimental trends for clot characterization.

Utilizing a simplified fibrinogen and thrombin model clot system, this study monitored thrombin-mediated fibrin clot formation under various clotting conditions to determine their unique influence on clot strength and fibrin structure that included: fibrinogen and thrombin concentrations, ionic strength, and pH.[11, 12, 17, 18] Albumin, the most abundant protein found in blood plasma, was also varied in solution to determine if overall protein concentration affects clot formation dynamics in both TEG and turbidity assays. While FXIIIa is required to crosslink the fibrin fibers and does contribute significantly to overall clot strength, FXIIIa is not required for fibrin polymerization and lateral aggregation of protofibrils.[1, 19] Clinically, patients that exhibit a significant FXIII deficiency with nearly no residual FXIII activity still produce a TEG tracing, albeit at a significantly reduced MA than that of normal blood.[20] To prevent confounding results from residual FXIII activity in this simplified clot model all fibrin formation assays were conducted in the absence of calcium to mitigate FXIII activation.

In some research and clinical settings bovine clotting factors are utilized as a substitute to human clotting factors and for this reason both human and bovine fibrinogen and thrombin were compared throughout this study. It is interesting to note that bovine thrombin was the first FDA-approved thrombin and is easily obtainable at a relatively low cost compared to human thrombin.[21] An example of cross-species fibrinogen / thrombin utilization can also be found in some clinical fibrin-based sealants used for wound closure applications that combine human fibrinogen with bovine thrombin. Vitagel (Orthovita ®, Malvern, PA), one of the commercially available fibrin sealant kits that contains bovine thrombin, is used as labeled for anastomotic bleeding, cancellous bone bleeding, and capillary bed bleeding which is widely used in hospitals

in the US.[22] This study also compared human and bovine cross-species fibrin clot formation (human fibrinogen / bovine thrombin, or bovine fibrinogen / human thrombin) via both TEG and turbidity assays.

3.3 Material and Methods

3.3.1 Materials

Human plasminogen-depleted fibrinogen (> 90% clottable protein, lyophilized at 44 mg/ml in 20 mM sodium citrate-HCl), human thrombin (lyophilized at 7,571 U/ml in 50 mM sodium citrate and 0.2 M NaCl), bovine fibrinogen (> 95% clottable protein, lyophilized at 49 mg/ml in 20 mM sodium citrate-HCl), and bovine thrombin (lyophilized at 10,223 U/ml in 50 mM sodium citrate and 0.2 M NaCl), bovine serum albumin, human serum albumin, and additional reagents for buffer preparation were purchased from Millipore Sigma (St. Louis, MO). The fibrinogen and thrombin used in this study cannot be used for clinical applications. Technochrom® factor XIII kit and Technochrom® coagulation reference was purchased from Diapharma (West Chester, Ohio). Slide-A-Lyzer® dialysis cassettes (20 kDa cutoff) were purchased from Thermo Scientific (Waltham, MA). UV transparent flat bottom 96-wells plates were purchased from Corning® (Kennebunk, ME). Thromboelastography clear disposable pins and cups were purchased from Haemonetics® (Braintree, MA).

3.3.2 Sample Preparation

Lyophilized human and bovine fibrinogen were reconstituted in PBS 20 min prior to use. PBS (0.01 M, pH 7.4, ionic strength 0.165 M) was used in all clotting experiments unless otherwise specified. Lyophilized human and bovine thrombin were reconstituted in deionized water, aliquoted, and kept at -20 °C. All thrombin aliquots were thawed at room temperature (RT) and diluted 15 min prior to use. In all experiments, protein concentrations were determined via extinction coefficients (513,400 L mol-1 cm-1 for fibrinogen and 43,800 L mol-1 cm-1 for albumin at 280 nm) on a spectrometer (SpectraMax M5, Molecular Devices; Sunnyvale, CA). Bovine fibrinogen was clotted by bovine thrombin (with or without bovine albumin) and human fibrinogen was clotted by human thrombin (with or without human albumin), unless otherwise specified.

Fibrin clotting was performed at 37 °C for TEG and at room temperature in turbidimetry assays as these are the most utilized experimental conditions for each technique. Turbidity Assays

Before clotting, 10 µL thrombin (20 U/mL unless specified) solution was added into 140 µL of PBS in 96-well plates. Clotting was initiated by mixing 50 µL fibrinogen (12 mg/mL unless otherwise specified) in the well. For clotting with albumin, albumin solutions were mixed in wells before the addition of fibrinogen. Clot turbidity was monitored by kinetic reads of absorbance at 550 nm at RT using the spectrometer directly following clot initiation for 60 minutes. Maximum turbidity ($Turb^{max}$) and time from the end of the clot lag period to 90% maximum turbidity ($Turb^{Time}$) were determined. All data represents means (±SD) of triplicates.

3.3.3 Thromboelastography Assays

Fibrin clots in TEG assays were initiated by mixing 340 µL fibrinogen (3.2 mg/mL unless specified) solution with 20 µL thrombin solution (18 U/mL unless specified) in a clear uncoated TEG cup. For clotting with albumin, albumin solutions were mixed with fibrinogen prior to being added into the cup. Thromboelastography was measured using TEG®5000 Thromboelastograph Hemostasis Analyzer at 37 °C with TEG Analytical Software® Version 4 (Haemonetics Corporation, Braintree, MA). TEG tracings were monitored immediately following clot initiations for 60 minutes. Maximum amplitude (TEG^{Max}) and time to maximum amplitude (TEG^{Time}) were collected for further analysis. TEG assays were performed in duplicate with clot strength measurements averaged at 12 reads/min for each sample (data plotted as means). A TEG reproducibility test was performed to verify TEG accuracy in assessing purified fibrinogen and thrombin clot formation characteristics in addition to determining instrument variability.

3.3.4 Varying Ionic Strength

For clotting at different ionic strengths PBS solutions (0.01 M) were made by dissolving individual buffer components and their ionic strengths were adjusted by varying the concentration of sodium chloride (21, 101, 111, 121, 131, 141, and 271 mM) along with 1.8 mM potassium phosphate monobasic, 10 mM sodium phosphate dibasic and 2.7 mM potassium chloride to get final ionic strengths of 0.05, 0.13, 0.14, 0.15, 0.16, 0.17 and 0.3 M. Due to significant dilution

factors residual buffer salts from the lyophilized fibrinogen and thrombin contributed < 3% to the final ionic strength of the clotting solution.

3.3.5 Varying pH

For clotting at different pH values, PBS solutions (0.01 M) were made by varying the concentration of sodium phosphate dibasic (0.7, 3.2, 7.7, 8.1, 8.4, 9.5 mM) and potassium phosphate monobasic (8.2, 6.0, 2.0, 1.7, 1.4, 0.5 mM) to achieve pH values of (5.8, 6.6, 7.3, 7.4, 7.5, 8) along with 2.7 mM potassium chloride and sodium chloride (153, 147, 138, 137, 136, 134 mM) to keep the final ionic strength at 0.165 M. Solution pH values were verified via pH probe (Mettler Toledo, OH). The lyophilized buffer present in the stock protein products do not significantly affect the pH of the final clotting solution. pH values were directly measured for each sample to ensure the desired pH was attained prior to analysis.

3.3.6 Statistical Analysis

$Turb^{max}$, $Turb^{Time}$, TEG^{Max} and TEG^{Time} were collected and analyzed in each assay. Summary data are presented in text using descriptive statistics with normally distributed data described as mean ± standard deviation. Means were compared using Student's t-test (equal sample size) or Welch's t-test (unequal sample size).[23] All tests were two-sided and P-values < 0.05 were considered significant. For assessing statistically significant of data comparing TEG, instrument error was included in the significance calculations as determined by the TEG reproducibility assays (**Table 3.1**). The reproducibility of TEG was examined by monitoring both bovine and human fibrin formation by mixing 1, 2, 3 mg/mL fibrinogen with 1 U/mL thrombin. TEG^{Max} (or MA) and TEG^{Time} (or TMA) showed less than 1.5 mm and 1.6 min standard deviations for sample repeats on different days using at least three different aliquots and two different TEG machines. TEG showed a high level of reproducibility for both TEG^{Max} and TEG^{Time} values for both human and bovine fibrin formation under these very challenging testing conditions. Technical replicates demonstrated TEG^{Max} and TEG^{Time} standard deviations of <0.5 mm and <0.7 min, respectively.

Table 3.1. Reproducibility test of TEG varying fibrinogen concentration in fibrin

	TEG^{Max} (mm)		**TEG^{Time} (min)**	
	Bovine biological replicates	Human biological replicates	Bovine biological replicates	Human biological Replicates
1 mg/ml	8.8 ± 0.6	6.9 ± 1.0	3.2 ± 0.8	3.4 ± 0.8
2 mg/ml	21.5 ± 0.9	17.5 ± 0.9	5.6 ± 0.8	6.4 ± 1.6
3 mg/ml	33.3 ± 1.5	24.0 ± 1.2	7.9 ± 1.1	10.2 ± 0.8

3.4 Results and Discussion

Due to the extensive complexity of whole blood and potential significant confounders from donor sample to donor sample, a simplified model clot that utilizes only fibrinogen and thrombin was used in this study to accurately compare turbidity and TEG assays. While both TEG and turbidity are relatively continuous measures of clot formation over time, we selected two parameters (**Figure 3.1**) that are representative of maximum clot formation and time to achieve the maximum clot formation. For turbidity assays, maximum turbidity ($Turb^{max}$) and time to 90% maximum turbidity ($Turb^{Time}$), were extracted from the absorbance tracings at 550nm. While fibrin fiber thickness was not directly measured, maximum turbidity is directly related to the average size of the fibers or fiber bundles at fixed fibrinogen concentrations and thus, turbidity can be considered a surrogate marker of fibrin fiber thickness under the highly controlled clotting conditions in this model.[5] For TEG assays, maximum amplitude (TEG^{Max}), which is a measure of maximum clot strength, and time to maximum amplitude (TEG^{Time}), were determined by the TEG software. Both assays exhibit a preliminary lag time typically resulting from a clot initiation period in which activation of the clotting cascade, through external stimulus, causes the slow formation of fibrin fibers as the system builds in clotting intensity. In this study, however, purified thrombin was used directly resulting in shorter lag periods, particularly in turbidity measurements, as activation of the clotting cascade was not necessary.

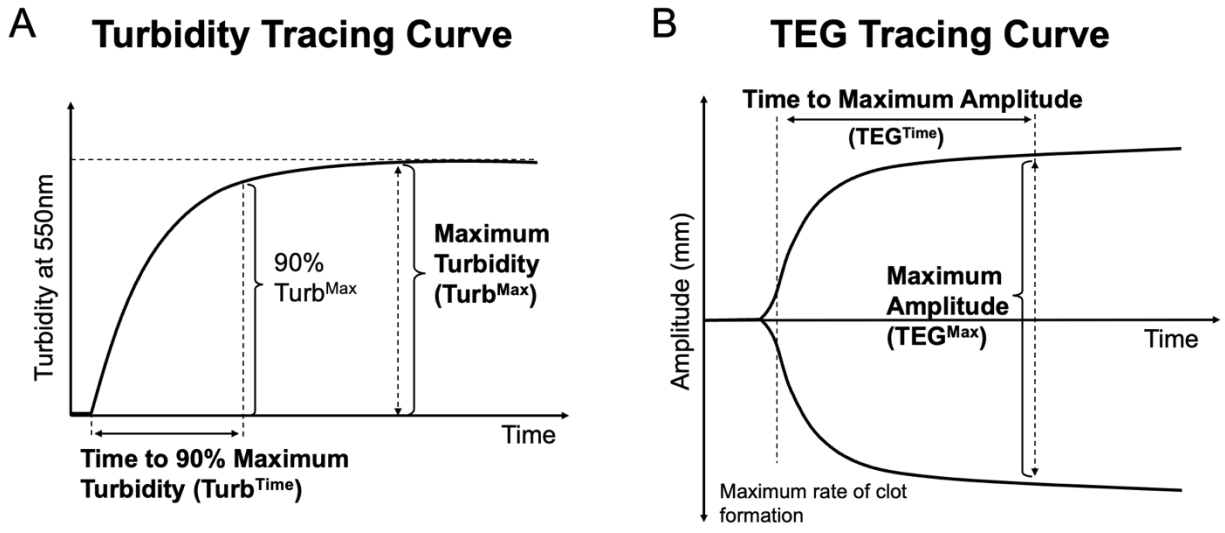

Figure 3.1. (A) Turbidity and (B) TEG tracing curves. After a lag period following the clot initiation, clot absorbance (turbidity assay) and clot amplitude (TEG assay) increase over time and level off at the end of clot formation. The symmetrical shaped trajectory in the TEG assay is a result of the dual-direction rotation and sensing by the pin.

3.4.1 Factor Contamination Study

Factor contamination is common in commercially available purified blood proteins. The direct addition of active thrombin to highly clottable fibrinogen mitigates the impact of most coagulation factor contaminants as the fibrin formation in this system does not rely on activation of multiple components throughout the blood coagulation cascade.[24] Factor XIII, a common factor contaminant in fibrinogen, was quantified using the Technochrom® FXIII assay under saturating calcium conditions in both the bovine and human fibrinogen samples demonstrating 9.3 ± 1.6% (bovine) and 35.4 ± 5.7% (human) FXIIIa activity at a 3 mg/mL fibrinogen stock concentration (100% representing the average normal FXIIIa activity level in pooled plasma). Depleting calcium in the Technochrom® testing reagents by the addition of citrate resulted in a FXIIIa activity decrease to 2.6 ± 0.1% (bovine) and 2.7 ± 4.2% (human), below the lower detection limit of the assay (**Figure 3.2**).

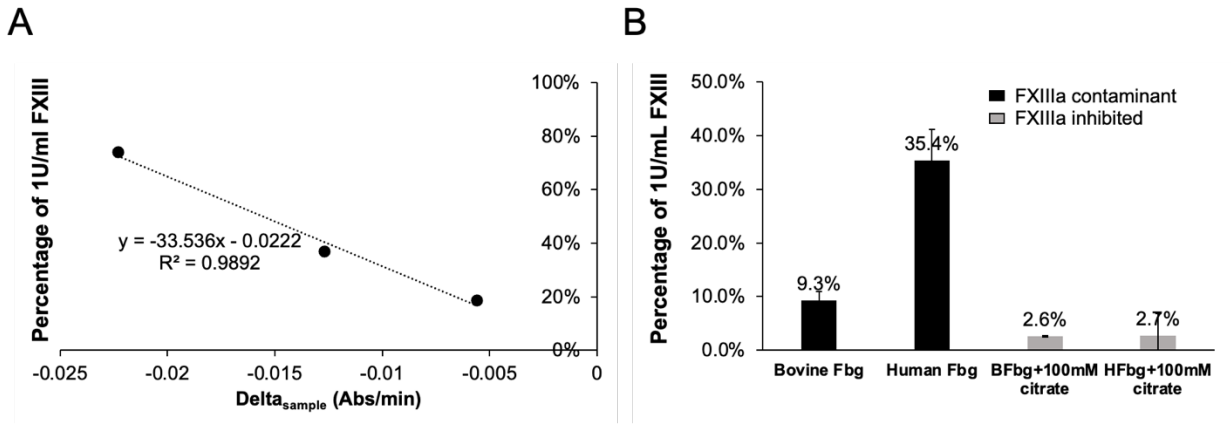

Figure 3.2. Standard curve of Technochrom® FXIII kit (A) and Factor XIII activity in bovine and human 3 mg/mL fibrinogen stock (B). Triplicates were performed using different aliquots on different days with data represented as means ± std.

To explore FXIIIa activity in fibrinogen, 3 mg/mL fibrinogen concentration was selected as it is the concentration of fibrinogen utilized throughout this manuscript, except in the varied fibrinogen assays. FXIIIa activity percent values are relative to a purchased known control FXIIIa with 100% representing the average of normal pooled plasma. In the absence of calcium, the FXIIIa activity was significantly suppressed below the limit of detection for this assay (< 3%). Since calcium cannot be readily removed from the assay kit the supplier recommended addition of 100 mM citrate to sequester the added calcium providing a means for running the assay in the presence and absence of calcium. As suspected, these results indicate that FXIII contaminants in the stock fibrinogen are inactive in the absence of calcium as FXIII is known to require calcium to be converted into FXIIIa. All clotting assays were carried out in the absence of calcium rendering residual FXIII in the fibrinogen preparations inactive. A comparison test on fibrin clot formation by dialyzed fibrinogen in the presence and absence of calcium was also carried out (**Figure 3.3**). Bovine and human fibrinogen were reconstituted using 0.01 M PBS and 0.5 mL of each solution was dialyzed against 1L 0.01 M PBS using a 20 kDa cutoff Slide-A-Lyzer® Dialysis Cassette (Thermo Scientific). After 24 hours of dialysis, bovine and human species-matched fibrin were examined via TEG at 3 mg/ml fibrinogen and 1 U/mL thrombin.

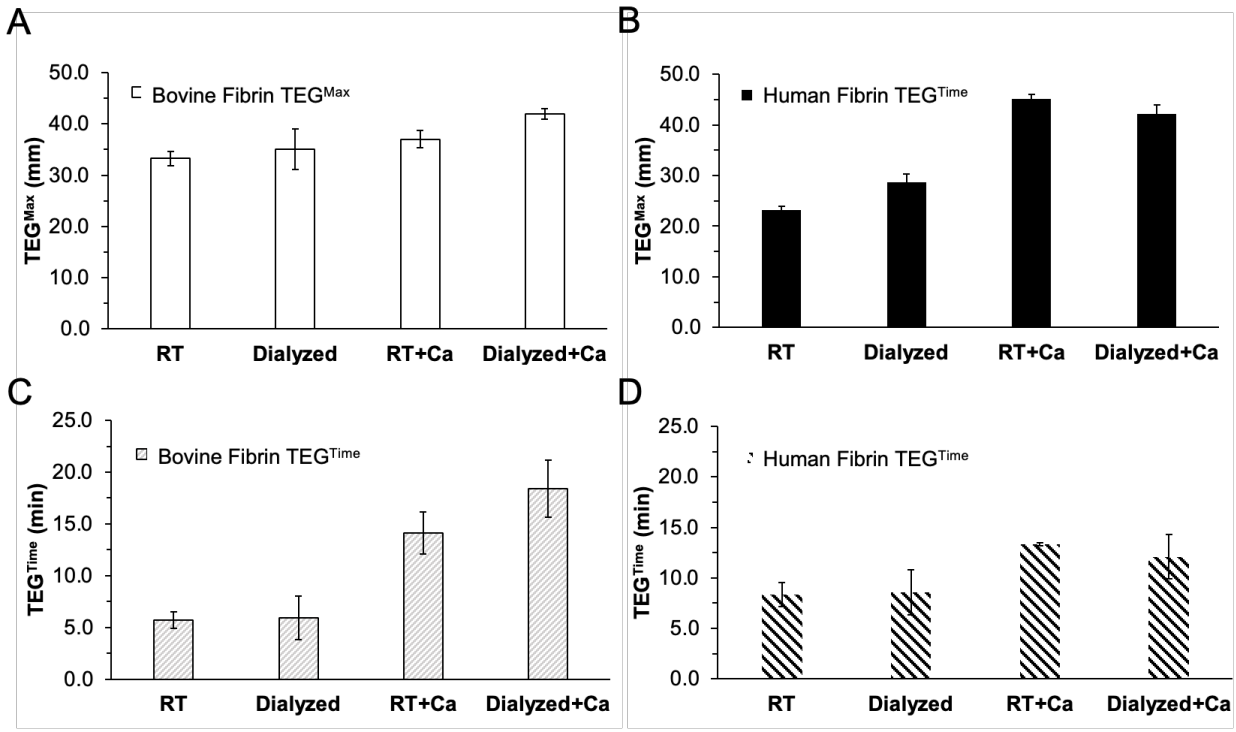

Figure 3.3. Comparison of RT (non-dialyzed), dialyzed, RT+Ca and Dialyzied+Ca groups for bovine fibrin TEG^{Max} (A) and TEG^{Time} (C) and human fibrin TEG^{Max} (B) and TEG^{Time} (D). RT and dialyzed groups showed little difference in TEG^{Max} and TEG^{Time} for both bovine and human. Experiments were performed in triplicates using different aliquots and dialysis cassettes on different days.

After the addition of calcium (2 mM final concentration), the human TEG^{Max} demonstrated a larger increase in MA than bovine TEG^{Max}. This result was expected since there was significantly more FXIII contamination present in the human fibrinogen than the bovine fibrinogen and with the addition of calcium a crosslinked fibrin network is expected to produce a stronger clot (**Figure 3.3B**). Student t-tests were performed across RT and dialyzed groups, p values were compared to 0.05, to determine significance. This test sought to compare dialyzed vs non-dialyzed fibrinogen. When comparing non-dialyzed (RT) with dialyzed groups in the presence and absence of calcium only two groups demonstrated a significant difference ($P<0.05$): human TEG^{Max} vs dialyzed TEG^{Max} and bovine RT+Ca TEG^{Max} vs bovine dialyzed+Ca TEG^{Max}. While statistical significance was observed with both sample comparisons, they exhibited only small absolute MA deviations.

In summary, results in this section showed a consistency across assays and demonstrate that FXIIIa activity in the absence of calcium and dialysis are not significant contributors to fibrin

formation under these tightly controlled clotting conditions. Additionally, by keeping the concentrations for all components held constant across both TEG and turbidity assays they exhibit identical factor contamination levels allowing for accurate comparisons to be drawn across assays.

3.4.2 Effects of Fibrinogen Concentration on Clot Formation

While there are many clotting factors and platelets that are attributed to the overall clot formation process *in-vivo*, fibrinogen is the primary clot forming protein contributing to bulk clot structure and stability. Fibrin formation, or cleavage of fibrinogen by thrombin, occurs at the end of the clotting cascade. The physiological range of fibrinogen in human plasma is 1.5 to 4 mg/mL (3 to 7 mg/mL in bovine). Resting fibrinogen concentrations above or below this physiologic range would be indicative of a coagulation disorder causing either increased bleeding or hypercoagulability. To experimentally test the effects of fibrinogen concentration on clot formation, thrombin was held at a fixed concentration of 1 U/mL and fibrinogen was varied from 1 to 5 mg/mL while maintaining a constant total clotting volume.

Turbidity and TEG assays were carried out with species matched bovine or human fibrinogen and thrombin. Maximum amplitude (TEG^{Max}), time to maximum amplitude (TEG^{Time}), maximum turbidity ($Turb^{max}$), and time to 90% maximum turbidity ($Turb^{Time}$) were compared. With increasing fibrinogen concentration, both bovine and human fibrin clots demonstrated increased clot turbidity and clot strength (**Figure 3.4**). This was in agreement with previous scanning electron microscopy (SEM) and rheology studies that showed at higher fibrinogen substrate concentrations, clots were composed of thinner fibers which resulted in tighter fibrous networks that exhibited higher clot strength.[4, 12] Since more fibrinogen at a constant volume results in more fiber formation, an increase in turbidity is anticipated as a denser fibrous blockage increases light scatter and limits light transmission. A tighter fibrin fiber network also provides for a stronger clot structure as evidenced by the increased clot strength in the TEG assays. Comparing clot formation times across both assays, $Turb^{Time}$ and TEG^{Time} lengthened at elevated fibrinogen concentrations. This elongation in time was expected since high levels of fibrinogen can exhibit inhibitory effects on fibrin monomer polymerization through a competitive inhibition interaction between fibrin monomers and non-cleaved fibrinogen [30]. While both clot formation times ($Turb^{Time}$ and TEG^{Time}) are calculated differently they both revealed a similar increasing trend with no significant differences ($P > 0.05$). TEG^{Time} is calculated from the end of the lag period to the

maximum amplitude and the $Turb^{Time}$ is calculated from the end of the lag period to 90% of the maximum turbidity. The lag periods for these two assays differ in sensitivity as the initial lag period in turbidimetry probes for the change in optical density as protofibrils form and lateral aggregation occurs in solution, while TEG probes for the time necessary for clot gelation to occur where mechanical strength is detectable by the sensor.

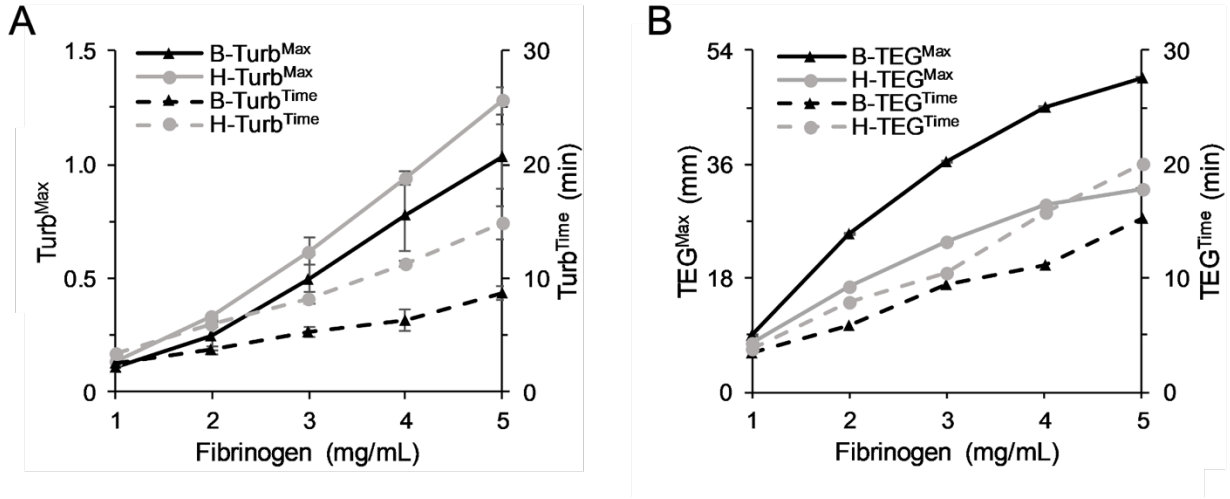

Figure 3.4. Turbidity (A) and TEG assays (B) on bovine and human fibrin clots with different fibrinogen concentrations (1, 2, 3, 4, 5 mg/mL) at constant 1U/mL thrombin. $Turb^{max}$ and TEG^{Max} on primary axis; $Turb^{Time}$ and TEG^{Time} on secondary axis. All comparisons were made using averages. Raw tracing curves of turbidity and TEG shown in Figure A.1 and Figure A.2 with V_{max}, Lag time, α angle and R included in Table A.1.

In comparison to bovine fibrin clots, human fibrin clots showed 26 ± 5% higher $Turb^{max}$ ($P < 0.05$), 61 ± 15% longer $Turb^{Time}$ ($P < 0.05$), and 53 ± 1% lower TEG^{Max} above 2 mg/mL fibrinogen concentrations ($P < 0.05$). Since TEG is a direct measurement of clot strength and turbidity is an optical measurement, the human fibrin clot can be interpreted to be mechanically weaker and optically more turbid than the bovine fibrin clot. In all, TEG and turbidity assays tracked similarly on clot formation with varying fibrinogen concentrations demonstrating higher turbidity and higher clot strength at increasing fibrinogen levels.

3.4.3 Effects of Thrombin Concentration on Clot Formation

The concentration of thrombin in plasma has a steady state of 1 U/mL of thrombin in its prothrombin form in adult plasma but can vary greatly locally depending upon the coagulation

state.[25] In some instances, prothrombin is activated through the coagulation cascade and thrombin levels reach as high as 20 U/mL when associated with a clot.[26] To test the effects of thrombin concentration on clot formation, fibrinogen was held constant at 3 mg/mL and thrombin was varied from 0.1 to 10 U/mL. An upper limit of 10 U/mL of thrombin was selected based on preliminary results that had shown that higher thrombin levels did not significantly affect clot formation kinetics as fibrinogen rapidly became the limiting reagent.

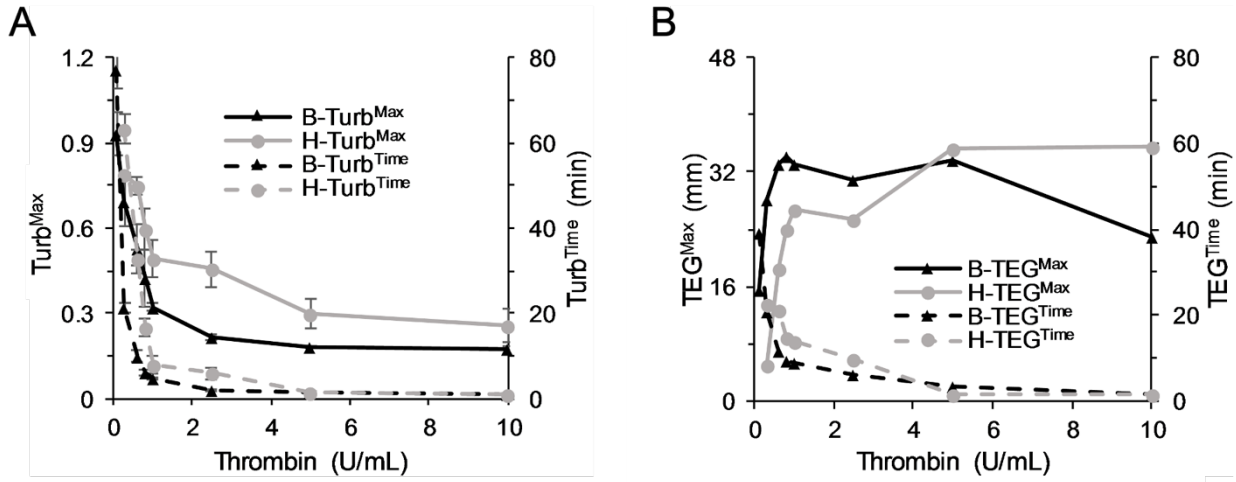

Figure 3.5. Turbidity (A) and TEG assays (B) on bovine and human fibrin clots at 3 mg/mL fibrinogen with different thrombin concentrations (0.1, 0.3, 0.6, 0.8, 1, 2.5, 5, 10 U/mL). $Turb^{max}$ and TEG^{Max} on primary axis; $Turb^{Time}$ and TEG^{Time} on secondary axis. All comparisons were made using averages. Raw tracing curves of turbidity and TEG shown in Figure A.3 and Figure A.4 with V_{max}, Lag time, α angle and R included in Table A.2.

For both bovine and human fibrin clots the increase in thrombin concentration resulted in decreased clot formation times across both TEG and turbidity assays (**Figure 3.5**). This result was expected since the presence of more enzyme provided for an increased rate of overall fibrinogen conversion. Interestingly, increasing thrombin resulted in a decreased $Turb^{max}$ and an increased TEG^{Max}. At elevated thrombin levels, thinner fibrin fibers and a tighter fibrous network were previously observed both under SEM and by permeability assays.[5, 7] By combining these observations, it can be explained that at a fixed amount of fibrinogen, the thinner fibers impart more strength to the overall fiber network which results in an increased TEG^{Max} while simultaneously having less optical density, lowering the observed $Turb^{max}$. No previous study has directly compared species across both TEG and turbidity and as observed here the combination of

the assays provide insight into clot strength and clot structure without the need for SEM.[4, 5] Comparing species is important as much of the preclinical work on blood coagulation, fibrinolysis, and pharmaceutical development are performed in animals often with limited regard to species based variations as assays and pharmaceuticals transition into interventions and diagnostics for human use.

Increasing thrombin from 0 to 1 U/mL resulted in a sharp decline in turbidity and a sharp increase in TEG^{Max} which leveled off at thrombin levels above 1 U/mL. This indicates that at thrombin levels above 1 U/mL at 3 mg/mL fibrinogen, the clot formation time and resulting clot strength and turbidity remain largely unaffected ($P > 0.05$). This effect became more prominent as thrombin concentrations were elevated for both assays as the reaction becomes substrate limited. Similar to the varying fibrinogen concentration experiment detailed previously, bovine and human fibrin clots shared a similar overall trend for all four parameters across both assays with human fibrin showing higher turbidity at thrombin levels above 0.8 U/mL ($P < 0.05$) and lower clot strength at thrombin levels below 5 U/mL ($P < 0.05$) compared to bovine.

3.4.4 Effects of Ionic Strength on Clot Formation

Ionic strength plays an important role in regulating the kinetics of fibrin polymerization.[17] For these experiments, fibrinogen and thrombin were held constant at 3 mg/mL and 1 U/mL, respectively, while the ionic strength of the clotting solution was varied from 0.05 to 0.3 M by adjusting the concentration of sodium chloride in 0.01 M PBS (pH = 7.4). Since the physiological ionic strength of human blood plasma is tightly regulated around 0.15 M, the bulk of ionic strengths tested were between 0.13 M and 0.17 M to attain a more detailed physiologically relevant clot formation condition.

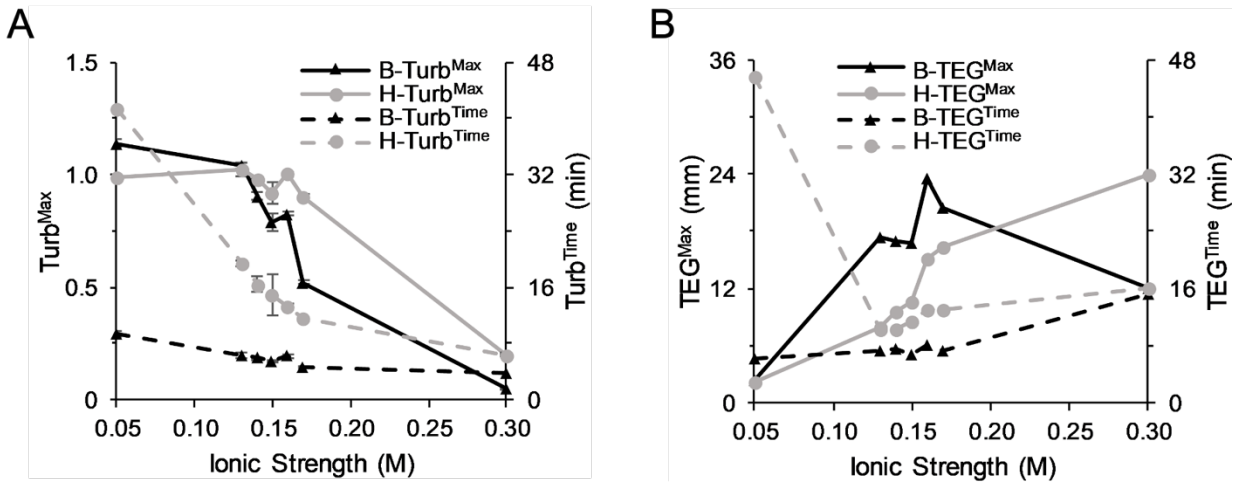

Figure 3.6. Turbidity assays (A) and TEG assays (B) on bovine and human fibrin clots at 3 mg/mL fibrinogen with 1U/mL thrombin at different ionic strength in PBS (0.05, 0.13, 0.14, 0.15, 0.16, 0.17, 0.3M). $Turb^{max}$ and TEG^{Max} on primary axis; $Turb^{Time}$ and TEG^{Time} on secondary axis. All comparisons were made using averages. Raw tracing curves of turbidity and TEG shown in Figure A.5 and Figure A.6 with V_{max}, Lag time, α angle and R included in Table A.3.

By increasing ionic strength, both bovine and human fibrin showed decreased $Turb^{max}$ and increased TEG^{Max} (**Figure 3.6**). These trends are similar to the previous thrombin experiment in that at higher ionic strength there was lower turbidity, or higher light transmittance, and higher clot strength, indicative of the formation of a tighter fibrous network. Human and bovine fibrin showed an overall similar trend in $Turb^{max}$ and TEG^{Max} compared to bovine fibrin. The maximum clot strength of bovine fibrin occurred at 0.16 M which was very close to physiological ionic strength. At an ultrahigh ionic strength of 0.3 M, bovine fibrin TEG^{Max} showed a large decline while human fibrin TEG^{Max} maintained an upward trend.

Regarding clot formation kinetics, increasing ionic strength resulted in a shortened clot formation time for human fibrin. At the lowest ionic strength (0.05 M), human fibrin showed extremely long clot formation times in both assays: $Turb^{Time}$ (41.4 minutes, $P < 0.05$) and TEG^{Time} (45.6 minutes, $P < 0.05$) compared to all other ionic strengths tested. Interestingly, the $Turb^{Time}$ and TEG^{Time} of bovine fibrin were unaffected by increasing ionic strength compared to human fibrin ($P > 0.05$). Varying salt concentration more significantly affects the formation of human fibrin than that of bovine fibrin. Overall, with increasing ionic strength, clotting times across both assays showed similar overall trends and $Turb^{max}$ and TEG^{Max} showed generally opposite trends.

3.4.5 Effects of pH on Clot Formation

Similar to ionic strength blood pH is also tightly regulated around 7.4 (7.35 to 7.45) for both human and bovine. However, in some pathological conditions local blood pH far outside of the normal range have been observed. An example of this phenomena occurs in solid tumors which can exhibit local pH values as low as 5.8 due to elevated production of lactic acid by cancer cells with insufficient blood flow.[27-29] This significantly lower pH can negatively affect hemostasis and result in dysfunctional coagulation. Despite the generally tight control over *in-vivo* pH we sought to explore how pH affects clotting *in-vitro* across a much wider range. For these experiments, fibrinogen and thrombin were held constant at 3 mg/mL and 1 U/mL, respectively, while pH was varied from 5.8 to 8.0 in PBS.

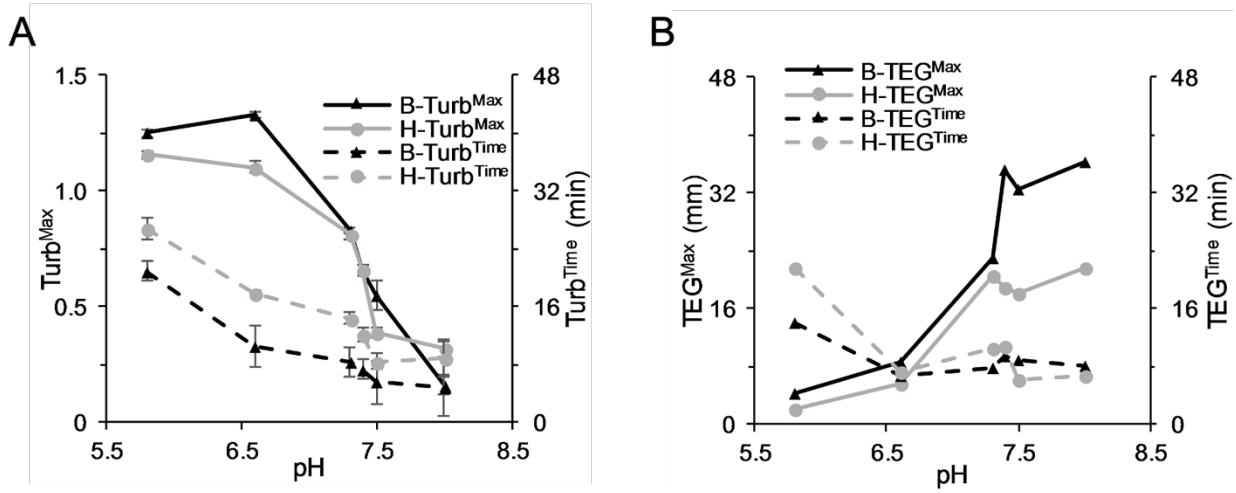

Figure 3.7. Turbidity assays (A) and TEG assays (B) on bovine and human fibrin clots at 3 mg/mL fibrinogen with 1U/mL thrombin in PBS at different pH (5.8-8.0). $Turb^{max}$ and TEG^{Max} on primary axis; $Turb^{Time}$ and TEG^{Time} on secondary axis. All comparisons were made using averages. Raw tracing curves of turbidity and TEG shown in Figure A.6 and Figure A.7 with V_{max}, Lag time, α angle and R included in Table A.4.

For both human and bovine fibrin, an increase in clotting solution pH resulted in decreased clot turbidity and increased clot strength (**Figure 3.7)**. A previous SEM study in human fibrin reported that increased solution pH resulted in the formation of thinner fibers which is confirmed here by decreased clot turbidity and increased clot strength [6]. Bovine and human fibrin showed similar trends across all four parameters. Additionally, the TEG^{Max} for bovine fibrin was larger than those of human fibrin at pH > 7.3 ($P < 0.05$), whereas $Turb^{max}$ showed no significant

differences ($P > 0.05$). Both assays showed downward trends on clot formation times. Lower pH (< 7.3) proved to impact fibrin formation than higher pH (> 7.3) more significantly. In this experiment with varying pH in the clotting solution, $Turb^{max}$ and TEG^{Max} showed opposite trends. Near physiological pH, TEG was more effective than turbidity in elucidating differences between bovine and human fibrin clots.

3.4.6 Effects of Albumin Concentration on Clot Formation

Albumin is the most abundant protein in blood plasma with a normal range of 35-55 mg/mL in human and an average of 33 mg/mL in bovine.[30] To study the effects of albumin on clot formation, a wide concentration range was selected from 0 to 100 mg/mL. For these experiments, fibrinogen and thrombin were held constant at 3 mg/mL and 1 U/mL with albumin (0, 20, 40, 50, 60, 80, 100 mg/mL) being varied in the solution prior to clot initiation (**Figure 3.8**). Increasing the concentration of albumin resulted in increased clot turbidity ($Turb^{max}$) and decreased clot strength (TEG^{Max}). The influences on $Turb^{max}$ and TEG^{Max} were quite prominent at low albumin concentrations but less significant at higher albumin concentrations with no significant differences observed in TEG^{Max} above 40 mg/mL ($P > 0.05$). The addition of albumin; however, did not alter clot formation times in either of the assays ($P < 0.05$). This could be attributed to the fact that albumin does not participate directly in the fibrinogen cleavage reaction. While it does not contribute to the clot formation kinetics its presence in the clot, due to bystander incorporation, may affect the fibrin fiber packing which in turn affects both clot turbidity and clot strength. The presence of albumin likely resulted in the formation of thicker fibers and a less dense fibrin network ultimately contributing to weaker clot formation. At low albumin/fibrin molar ratios, < 5:1, albumin has been shown to modulate lateral assembly of fibrin polymers resulting in a finer fiber structure that is associated with decreased turbidity.[31] At higher albumin to fibrin ratios, representative of the albumin levels used in this study (≥20 mg/mL, albumin: fibrin of ≥ 30:1), this effect is diminished and the maximum turbidity showed a dramatic increase as the albumin level in the clotting solution increased. Bovine and human fibrin tracked similarly in both assays.

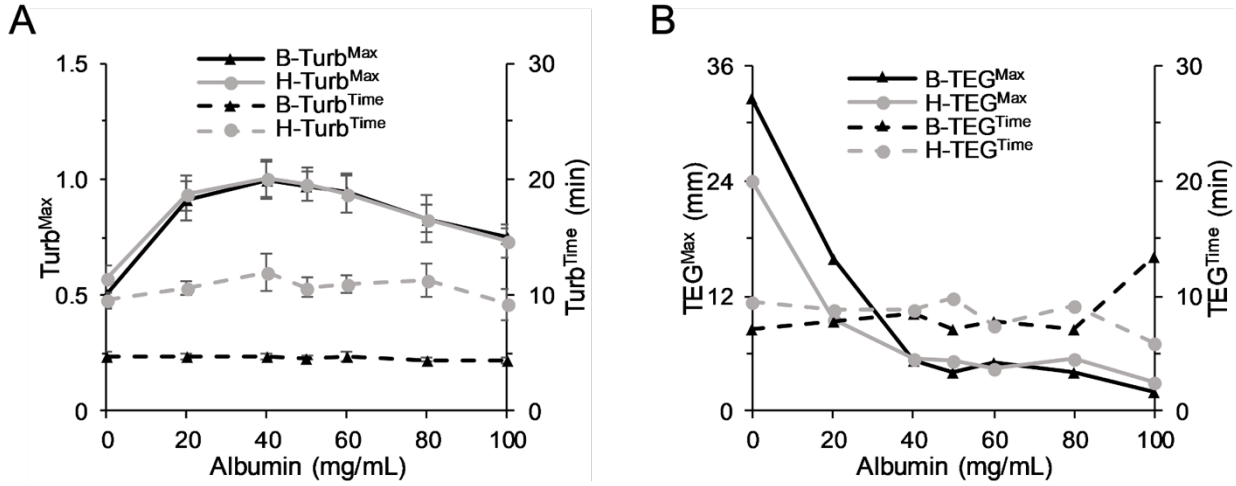

Figure 3.8. Turbidity assays (A) and TEG assays (B) on bovine and human fibrin clots at 3 mg/mL fibrinogen with 1 U/mL thrombin with the addition of different amount of albumin (0, 20, 40, 50, 60, 80, 100 mg/mL in final solution). $Turb^{max}$ and TEG^{Max} on primary axis; $Turb^{Time}$ and TEG^{Time} on secondary axis. All comparisons were made using averages. Raw tracing curves of turbidity and TEG shown in Figure A.8 and Figure A.9 with V_{max}, Lag time, α angle and R included in Table A.5.

3.4.7 Cross-Species Fibrin Deposition

As previously mentioned, there are some instances where non-species matched fibrinogen and thrombin are utilized to either take advantage of faster enzymatic rates or lower associated reagent cost. It is fairly common for proteins that perform a similar task from different species to have significant sequence homology and human and bovine fibrinogen and thrombin follow this trend with over 64% and 81% cross-species amino acid sequence homology, respectively.[32, 33] To test the effects of utilizing cross-species clotting proteins the following experiment was carried out with mismatched human / bovine thrombin and fibrinogen. In all instances, thrombin was held constant at 1 U/mL in PBS pH 7.4 while fibrinogen was varied from 1 to 5 mg/mL.

With increasing fibrinogen, clot turbidity, clot strength, and clot formation times increased in all four groups as previously observed with the species matched thrombin / fibrinogen (**Figure 3.4**). Regarding $Turb^{max}$, all thrombin and fibrinogen pairs were clustered at increasing fibrinogen concentrations (**Figure 3.9A**). TEG^{Max} values; however, were observed in two distinct groups associated around each fibrinogen species which indicated that fibrinogen species more significantly determined fibrin clot strength compared to thrombin species (**Figure 3.9B**; $P < 0.05$). This result suggests that bovine and human thrombin can potentially be used interchangeably to

achieve a similar clot strength if the fibrinogen species is held constant. When looking at clot formation times, all groups shared similar values across both assays except that in human fibrinogen with bovine thrombin. In bovine thrombin with human fibrinogen, $Turb^{Time}$ was nearly twice as long compared to the other groups (**Figure 3.9C**; $P < 0.05$) while the observed TEG^{Time} remained similar (**Figure 3.9D**; $P > 0.05$). It is unclear why there was such a slow catalytic effect of bovine thrombin on human fibrinogen in the turbidity assay that was not observed in the TEG assay other than the presence of gentle mixing and slightly elevated temperature (37 °C) associated with the TEG assay. As demonstrated throughout this manuscript study other variables such as: thrombin concentration, ionic strength, and pH, can all be altered to achieve desired kinetics or control over resulting clot strength and fiber structure in both species matched and cross-species fibrin clot formation.

Clot formation times have been used to assess blood coagulation potential in a large range of diseases and good overall correlations between $Turb^{Time}$ and TEG^{Time} were found in this study. For this reason, clot formation time measurements in both TEG and turbidity assays can assess coagulation dynamics over physiological and most pathological conditions. Kinetic parameters to assess the rate of clot strengthening in TEG (α angle) and the maximum rate of turbidity increase (V_{max}, milliunit per min) were also determined.[34] It is worth noting that the α-angle in this study did not correlate well with the TEG^{Time} but showed a similar trend to TEG^{Max} (**Table A.1-6)**. This may indicate that a more rapid clot strengthening results in a stronger fibrin clot. Due to the rapid increase in turbidity at the concentrations of fibrinogen and thrombin used in this study resulting from the direct addition of active thrombin, there was a high level of variability in calculated V_{max}. Despite this, V_{max} showed a similar trend to the α-angle in TEG across most of the tested experimental conditions conducted in this study (**Table A.1-6**).

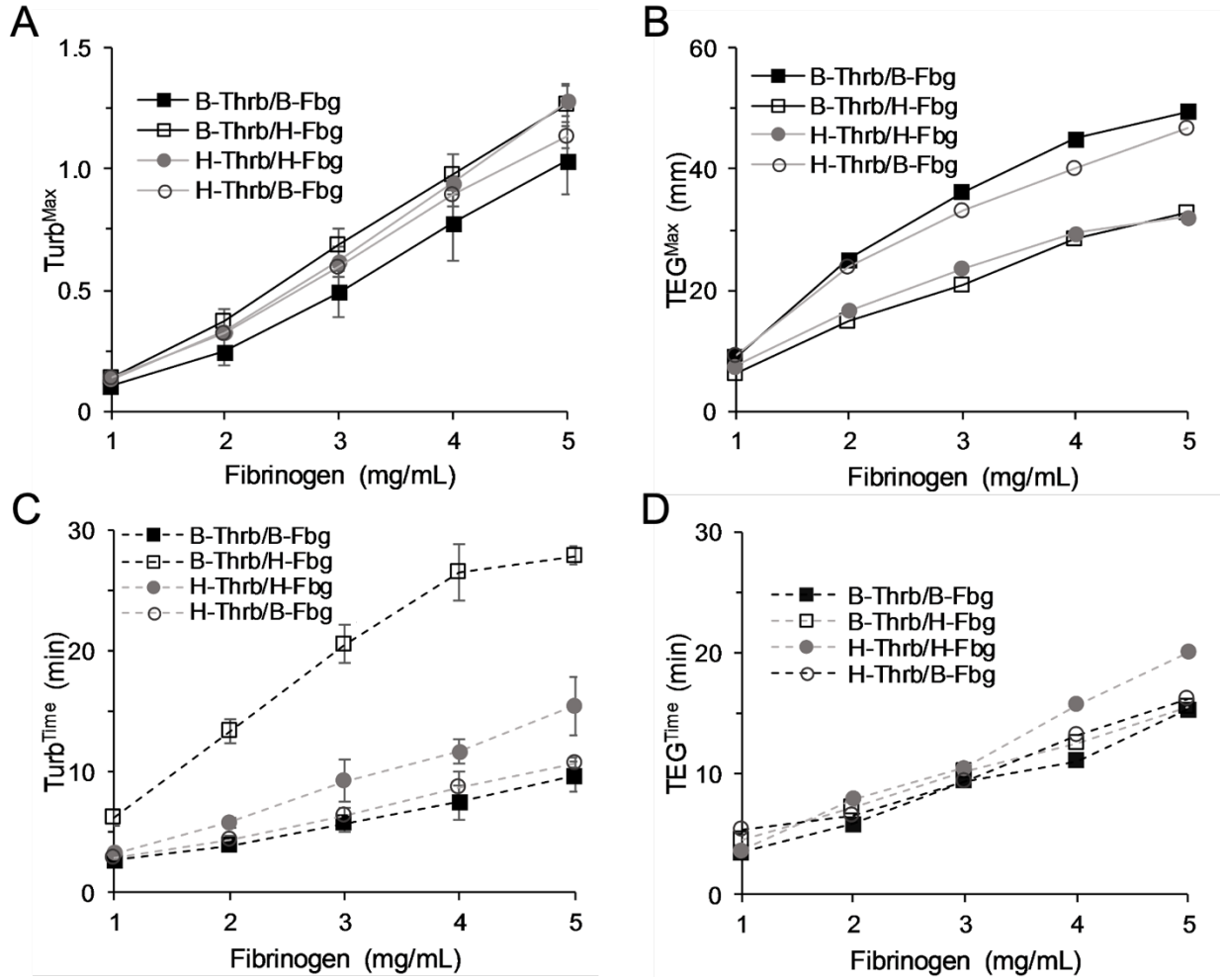

Figure 3.9. Turbidity assays (A, C) and TEG assays (B, D) on clots formed by four different thrombin and fibrinogen combinations: bovine thrombin and fibrinogen, bovine thrombin with human fibrinogen, human thrombin and fibrinogen, and human thrombin with bovine fibrinogen ($Turb^{max}$ (A), TEG^{Max} (B), $Turb^{Time}$ (C) and TEG^{Time} (D)). In all groups, 1 U/mL thrombin and 1, 2, 3, 4, 5 mg/mL fibrinogen concentrations were used. All comparisons were made using averages. Tracing curves of turbidity and TEG for this experiment were shown in Figure A.11 and Figure A.12 with V_{max}, Lag time, α angle and R included in Table A.6.

3.5 Conclusions

By utilizing a simplified clot model of purified thrombin and fibrinogen, we were able to compare TEG and turbidity assays across a wide range of clot forming conditions such as: varying fibrinogen, thrombin and albumin concentrations, ionic strength, and pH. Clot strength by TEG and maximum turbidity showed similar increasing trends for increasing fibrinogen concentration and opposite trends for increasing thrombin concentration, ionic strength, pH, and albumin. This

opposite trend is related to the fibrin fiber thickness which directly impacts resulting clot strength and optical turbidity. TEG^{Max} and $Turb^{max}$ showed opposite trends in some experiments and similar trends in other experiments throughout this study and are best utilized together as complementary tools to directly assess clot strength through TEG and the optical fiber thickness properties of a fibrin clot through turbidity measurements. The TEG and turbidity assays performed in this study expand on the previous findings that thinner fibers result in lower turbidity ($Turb^{max}$) and higher clot strength (TEG^{Max}) at a fixed fibrinogen concentration. Under *in-vitro* human physiological blood conditions, human fibrin clots are optically more turbid and mechanically weaker than bovine fibrin clots. This study demonstrates that both TEG and turbidity have different strengths and weakness and to perform a comprehensive clot characterization under diverse clotting conditions that includes clot strength, time to attain maximum clot strength, and fiber thickness analysis both assays are necessary.

3.6 References

[1] J.W. Weisel, R.I. Litvinov, Mechanisms of fibrin polymerization and clinical implications, Blood 121(10) (2013) 1712-1719.

[2] C.G. Curtis, K.L. Brown, R.B. Credo, R.A. Domanik, A. Gray, P. Stenberg, L. Lorand, Calcium-Dependent Unmasking of Active Center Cysteine During Activation of Fibrin Stabilizing Factor, Biochemistry 13(18) (1974) 3774-3780.

[3] J. W, Structure of fibrin: Impact on clot stability, Journal of Thrombosis and Haemostasis 5(SUPPL. 1) (2007) 116-124.

[4] E.A. Ryan, L.F. Mockros, J.W. Weisel, L. Lorand, Structural origins of fibrin clot rheology, Biophysical Journal 77(5) (1999) 2813-2826.

[5] J.W. Weisel, C. Nagaswami, Computer modeling of fibrin polymerization kinetics correlated with electron microscope and turbidity observations: clot structure and assembly are kinetically controlled, Biophysical Journal 63(1) (1992) 111-128.

[6] A.S. Wolberg, Thrombin generation and fibrin clot structure, Blood Reviews 21(3) (2007) 131-142.

[7] B. Blombäck, K. Carlsson, B. Hessel, A. Liljeborg, R. Procyk, N. Åslund, Native fibrin gel networks observed by 3D microscopy, permeation and turbidity, Biochimica et Biophysica Acta (BBA)/Protein Structure and Molecular 997(1-2) (1989) 96-110.

[8] T. Lang, V. Depka, Possibilities and limitations of thromboelastometry/thromboelastography, Hämostaseologie 26(S 02) (2006) S21-S29.
[9] M.M. Tripathi, S. Egawa, A.G. Wirth, D.M. Tshikudi, E.M. Van Cott, S.K. Nadkarni, Clinical evaluation of whole blood prothrombin time (PT) and international normalized ratio (INR) using a Laser Speckle Rheology sensor, Scientific Reports 7(1) (2017) 1-8.
[10] M.E. Carr, J. Hermans, Size and Density of Fibrin Fibers from Turbidity, Macromolecules 11(1) (1978) 46-50.
[11] A.S. Wolberg, D.A. Gabriel, M. Hoffman, Analyzing fibrin clot structure using a microplate reader, Blood Coagulation and Fibrinolysis 13(6) (2002) 533-539.
[12] M.E. Carr, L.L. Shen, J. Hermans, Mass–length ratio of fibrin fibers from gel permeation and light scattering, Biopolymers 16(1) (1977) 1-15.
[13] D.A. Gabriel, K. Muga, E.M. Boothroyd, The Effect of Fibrin Structure on Fibrinolysis *, (1992) 24259-24263.
[14] A. Roggan, M. Friebel, K. Dörschel, A. Hahn, G. Müller, Optical Properties of Circulating Human Blood in the Wavelength Range 400–2500 nm, Journal of Biomedical Optics 4(1) (1999) 36-36.
[15] C.W. Whitten, P.E. Greilich, Thromboelastography®: past, present, and future, Anesthesiology: The Journal of the American Society of Anesthesiologists 92(5) (2000) 1223-1225.
[16] S.V. Mallett, D.J. Cox, Thrombelastography, British journal of anaesthesia 69(3) (1992) 307-13.
[17] J.W. Weisel, Fibrin assembly. Lateral aggregation and the role of the two pairs of fibrinopeptides, Biophysical Journal 50(6) (1986) 1079-1093.
[18] C.H. Nair, G.A. Shah, D.P. Dhall, Effect of temperature, ph and ionic strength and composition on fibrin network structure and its development, Thrombosis Research 42(6) (1986) 809-816.
[19] R.A.S. Ariens, T.-S. Lai, J.W. Weisel, C.S. Greenberg, P.J. Grant, Role of factor XIII in fibrin clot formation and effects of genetic polymorphisms, Blood 100(3) (2002) 743-754.

[20] M.E. Martinuzzo, Effects of factor XIII deficiency on thromboelastography. Thrombelastography with calcium and lysis by addition of streptokinase is more sensitive than solubility tests, Mediterranean Journal of Hematology and Infectious Diseases 8 (2016) e2016037-e2016037.
[21] W.K. Lew, F.A. Weaver, Clinical use of topical thrombin as a surgical hemostat, Biologics: Targets and Therapy 2(4) (2008) 593-599.
[22] W.D. Spotnitz, R. Prabhu, Fibrin Sealant Tissue Adhesive - Review and Update, Journal of Long-Term Effects of Medical Implants 15(3) (2005) 245-270.
[23] J.C.F. de Winter, Using the student's t-test with extremely small sample sizes, Practical Assessment, Research and Evaluation 18(10) (2013) 1-12.
[24] E.L. Smith, B. Cardinali, L. Ping, R.A.S. Ariëns, H. Philippou, Elimination of coagulation factor XIII from fibrinogen preparations, Journal of Thrombosis and Haemostasis 11(5) (2013) 993-995.
[25] M. Andrew, B. Paes, R. Milner, M. Johnston, L. Mitchell, D.M. Tollefsen, P. Powers, Development of the human coagulation system in the full-term infant, Blood 70(1) (1987) 165-72.
[26] H.C. Hemker, P.L.A. Giesen, M. Ramjee, R. Wagenvoord, S. Béguin, The Thrombogram : Monitoring Thrombin Generation in Platelet Rich Plasma, (4) (2000) 589-591.
[27] I.F. Tannock, D. Rotin, Acid pH in Tumors and Its Potential for Therapeutic Exploitation PerspectivesinCancerResearch Acid pH in Tumors and Its Potential for Therapeutic Exploitation1, Cancer Research 49 (1989) 4373-4384.
[28] F. Graus, L.R. Rogers, J.B. Posner, Cerebrovascular complications in patients with cancer, Medicine 64(1) (1985) 16-35.
[29] S. Kvolik, M. Jukic, M. Matijevic, K. Marjanovic, L. Glavas-Obrovac, An overview of coagulation disorders in cancer patients, Surgical Oncology 19(1) (2010).
[30] D. Alberghina, C. Giannetto, I. Vazzana, V. Ferrantelli, G. Piccione, Reference intervals for total protein concentration, serum protein fractions, and albumin/globulin ratios in clinically healthy dairy cows, Journal of Veterinary Diagnostic Investigation 23(1) (2011) 111-114.
[31] D.K. Galanakis, B.P. Lane, S.R. Simon, Albumin modulates lateral assembly of fibrin polymers: evidence of enhanced fine fibril formation and of unique synergism with fibrinogen, Biochemistry 26(8) (1987) 2389-2400.

[32] T. Cartwright, R.G.O. Kekwick, A comparative study of human, cow, pig and sheep fibrinogen, Biochimica et Biophysica Acta (BBA) - Protein Structure 236(3) (1971) 550-562.
[33] P.D. Martin, W. Robertson, D. Turk, R. Huber, W. Bode, B.F. Edwards, The structure of residues 7-16 of the A alpha-chain of human fibrinogen bound to bovine thrombin at 2.3-A resolution, The Journal of biological chemistry 267(11) (1992) 7911-20.
[34] M. Zucker, U. Seligsohn, O. Salomon, A.S. Wolberg, Abnormal plasma clot structure and stability distinguish bleeding risk in patients with severe factor XI deficiency, Journal of Thrombosis and Haemostasis 12(7) (2014) 1121-1130.

4. FLUORESCENTLY CONJUGATED ANNULAR FIBRIN CLOT FOR MULTIPLEXED REAL-TIME DIGESTION ANALYSIS

One version of this chapter was published in *Journal of Materials Chemistry B* entitled "Fluorescently conjugated annular fibrin clot for multiplexed real-time digestion analysis", Volume 9, Page 9233-9424, (2021), access via https://doi.org/10.1039/D1TB02088A

Monitoring *in-vitro* thrombolysis can be achieved through a variety of methods ranging from the estimation of complete clot disappearance time to a tracking of a real-time clot lysis. To directly assess the thrombolytic efficacy of a drug agent, fibrin degradation is primarily tracked as fibrin is the main therapeutic target of thrombolytic agents. D-dimer is a fibrin degradation product that is generated during native thrombolysis process and an increased D-dimer level in plasma can be indicative of ongoing thrombolysis in patients.[1, 2] However, monitoring a D-dimer level requires a time-consuming preparation and a use of expensive immunological products. Clot turbidity refers to the absorbance of a clot. Whereas turbidity assesses the bulk clot structure and lacks molecular level interpretation capabilities. The measurement also requires a fixed path length and a clear background which is hard to maintain in a thrombolysis model perfused with whole blood. Thromboelastography (TEG), as discussed in previous chapter, is a specialized instrument that is commonly used to assess patient hemostasis in clinical settings. Although the clot lysis monitoring under TEG offers clinical relevance, the measurement cannot be easily multiplexed or adapted for flow conditions or the addition of therapeutic agents. Another promising strategy is through labeling fibrin clot with reporter molecules and monitoring accumulated reporter signal levels to track clot lysis. While both isotopic iodine and fluorescein isothiocyanate (FITC) labeled fibrin clot have been previously used to monitor thrombolysis, FITC molecules are much easier and safer to use.[3, 4] The labeled clot substrate can be adapted into any flow models as those reporters usually covalently bond to the clot which prevents an easy wash-away by the shear flow. More importantly, reporters commonly conjugate fibrinogen non-specifically at primary amines of lysine residuals. These conjugations are irreversible and could dramatically affect the fibrin polymerization and crosslinking process resulting in impaired fibrin structures. When conjugations block C-terminal lysine residuals or potential fibrin digestion sites on fibrin, fibrinolysis becomes disturbed as a constant exposure of these residuals is crucial.[5, 6] An accurate interpretation of the molecular interplays of fibrinolytic factors and inhibitors relies on the precise molecular

tracking of clot digestion, which is affected by the homogeneity of fluorescence labeling in fibrin. Fluorescence aggregates could contribute to a big variation in fluorescence release upon digestion. Beyond fluorescence aggregation, heavy labeling can result in fluorescence quenching causing an over estimation of fluorescence molecular release while lightly labeled clot substrates could exhibit poor analytical sensitivity and poor limit of detection (LOD).[7] Thus, labeling homogeneity and intensity levels of FITC-fibrin clots should be examined to guarantee a reliable interpretation of clot lysis data.

Thus, the optimization of fibrin tagging level is the primary step to develop a physiologically relevant fluorescently labeled fibrin-based clot. This chapter explores the impact of fluorescent conjugation on fibrin properties and introduces an innovated setup of a high throughput thrombolytic drug evaluation assay.

4.1 Abstract

Impaired fibrinolysis has long been considered as a risk factor for venous thromboembolism. Fibrin clots formed at physiological concentrations are promising substrates for monitoring fibrinolytic performance as they offer clot microstructures resembling *in-vivo*. Here we introduce a fluorescently labeled fibrin clot lysis assay which leverages a unique annular clot geometry assayed using a microplate reader. A physiologically relevant fibrin clotting formulation was explored to achieve high assay sensitivity while minimizing labeling impact as fluorescence isothiocyanate (FITC)-fibrin(ogen) conjugations significantly affect both fibrin polymerization and fibrinolysis. Clot characteristics were examined using thromboelastography (TEG), turbidity, scanning electron microscopy, and confocal microscopy. Sample fibrinolytic activities at varying plasmin, plasminogen, and tissue plasminogen activator (tPA) concentrations were assessed in the present study and results were compared to an S2251 chromogenic assay. The optimized physiologically relevant clot substrate showed minimal reporter-conjugation impact with nearly physiological clot properties. The assay demonstrated good reproducibility, wide working range, kinetic read ability, low limit of detection, and the capability to distinguish fibrin binding-related lytic performance. In combination with its ease for multiplexing, it also has applications as a convenient platform for assessing patient fibrinolytic potential and screening thrombolytic drug activities in personalized medical applications.

4.2 Introduction

Impaired fibrinolysis has long been considered a risk factor for venous thromboembolism (VTE). Although efforts have been made over the years, no existing fibrinolytic assessment assays appears to genuinely aid in thrombosis diagnosis or offer a reliable testing platform for therapeutic development.[8-10] In response to blood vessel injury, the human body initiates a hemostasis process which is an innate series of actions ultimately resulting in clot formation. Fibrin is a protein that is primarily responsible for clotting and degrades through a fibrinolysis process that following hemostasis. A typical fibrinolysis process involves the activation of plasminogen by tissue plasminogen activator (tPA) to produce plasmin, which is the enzyme that is responsible for fibrin digestion. The five kringle domains present on the surface of plasmin bind to C (carboxy)-terminal lysine residues on fibrin to facilitate local clot binding and subsequent digestion via its catalytic domain. The fibrinolytic system is carefully regulated by inhibitors including type 1 plasminogen activator inhibitor (PAI-1) which regulates tPA activity in addition to α2-antiplasmin and α2-macroglobulin which regulate plasmin activity.[11-13] In acute thrombosis patients, thrombolytic drugs known as recombinant plasminogen activators can be administered to accelerate plasmin conversion and clot digestion to offer a fast relief from life-threatening clotting events such as pulmonary embolism and ischemic stroke.[14-16] Despite the development of novel drug agents, the clinical translation success rate remains very low in part due to a lack of representative drug testing platforms. Due to the complexity of the fibrinolytic system, an ideal fibrinolytic testing platform for diagnosis and drug development applications should use a standardized substrate and be capable of dynamically monitoring the fibrinolytic process at a physiologically relevant scale and offer reproducible and translatable results.

Numerous assays have been developed to meet this challenge, but all exhibit a variety of benefits and drawbacks limiting their overall utility. Chromogenic or antigenic assays are frequently used to measure individual clotting factor levels or activities. These assays, however; do not directly yield clinically representative results as they are unable to assess processes that involve native fibrinolytic events such as protein adsorption, multi-factor interactions, or plasmin-fibrin binding. Assays such as euglobulin clot lysis time (ECLT) and dilute whole-blood clot lysis time (DWBCLT), have been extensively used since the 1980s.[8, 17, 18] While these assays more globally represent *in-vivo* clotting conditions they are inherently difficult to measure an accurate plasma fibrinolytic activity as they either test only a small sub-fraction of plasma or ignore the

presence of varying amounts of fibrinogen in the test system. More recently, a plasma clot lysis assay was developed that tracks clot turbidity, an optical measure of bulk clot structure, over time. It has rapidly gained popularity for use in clinical studies due to its ease of implementation.[19-21] Using tissue factor and tPA-treated patient plasma, a change in clot turbidity is monitored throughout the clot formation and lysis processes. However, this assay utilizes the patient's own plasma and results are often difficult to compare across samples due to variations from patient-to-patient. For example, clot lysis time is influenced by fibrinogen levels due to its impact on fibrin clot formation density and fiber thickness making interpretation of therapeutic effect by turbidity difficult.[9] More importantly, the turbidity reading lacks microstructural or molecular interpretation capabilities. Although a fibrin fiber mass-length ratio can be extracted from turbidity measurements, the calculation relies on a number of assumptions that are sometimes difficult to determine.[22] None of these assays allows for a physiologically relevant clot lysis determination that provides results than can directly be compared across patients in the presence and absence of a variety of therapeutic interventions.

Additional assays utilize exogenous fibrin as the substrate to assess fibrinolytic activity with the ability to offer physiologically relevant microstructures including binding moieties, cleavage sites and clot digestion depths. The fibrin plate method measures fibrinolytic potential by quantifying the lysed area of preformed fibrin in a petri-dish following incubation with a drop of patient plasma to its center. The assay is difficult to multiplex, and quantification methods require standardization to allow for comparison across groups.[23] Radioactively or fluorescently labeled fibrin clot lysis assays have also been developed to measure plasmin activity or plasma fibrinolytic potential.[3, 4] These assays incorporate molecular reporters such as ^{125}I or fluorescein isothiocyanate (FITC) labels in preformed fibrin clots to track clot digestion activity. Fibrinolysis is monitored by tracking the reporter signal released into the clot supernatant during digestion. The monitored fibrinolytic activity is independent of fibrinogen concentration in patient samples.[24] A common setup of such assays requires the frequent transfer of clot supernatant to a clean well for signal acquisition throughout the digestion process making these assays intensive and lacking the ability for dynamic reads over time without disturbing the assay. This procedure largely interferes with the ongoing fibrinolytic reaction, introducing artifacts and making it difficult for multiplexing, standardization, and utilization under fast-responding clinical interventions. More importantly, both isotopic iodine and FITC molecules conjugate fibrinogen none-specifically at

primary amines of lysine residuals. These conjugations are irreversible and can negatively impact the fibrin polymerization process resulting in disrupted fibrin structures.[25] When conjugations block C-terminal lysine residuals, or alternate digestion sites on fibrin, fibrinolysis becomes less representative as a constant exposure of these residuals is critical.[5, 6] Therefore, results of these assays may not have good clinical relevance unless a characterization of reporter-labeled fibrin clots is thoroughly addressed.

This study describes a highly reproducible *in-vitro* clot lysis assay that offers a physiologically relevant assessment of sample fibrinolytic activity through a controlled fibrin substrate and easily multiplexed design. The assay utilizes a FITC-labeled fibrin-based clot forming at physiological fibrinogen and thrombin concentrations. The clot substrate was engineered to be an annular shape and pre-formed in a 96-well plate with the help of a 3D-printed molding insert. Specifically, the unique clot geometry provides for a clear light path for fluorescence excitation and emission by taking advantage of the centrally located signal acquisition mechanism of a commercial spectrometer (**Figure 4.1**). With the addition of fibrinolytic sample solution to the center of the annular clot, increasing amounts of soluble fluorescently tagged fibrin degradation products are released and measured dynamically over time. These fragments disperse into the solution and fluorescence signal is monitored by the detector. This setup enables a real-time measurement of clot lysis with no disturbance during the reading process. To reduce FITC-fibrin(ogen) conjugation impact on clot formation/digestion and to establish a physiologically relevant FITC labeled clot, clotting mixtures using different FITC per fibrinogen and different ratios of FITC-fibrinogen to unmodified fibrinogen were explored. Multiple tools were used to assess fibrin clot characteristics. Clot formation, bulk structure and viscoelastic property were examined by clot turbidity and thromboelastography (TEG) assays. Clot microstructure, including fiber thickness and pore size, was examined via scanning electron microscopy (SEM). Fluorescence labeling homogeneity and signal density were compared via confocal microscopy. This information was combined to guide an optimized FITC labeling strategy in fibrin to achieve a physiologically relevant FITC labeled fibrin clot that is structurally indistinct from an unmodified *in-vitro* statically formed fibrin clot. The FITC-fibrin clots were further tested for fibrinolysis using samples that contain plasmin, or a mixture of exogenous tPA and plasminogen, to demonstrate the assay's capacity of differentiating sample fibrinolytic potential or examining drug dose-response.

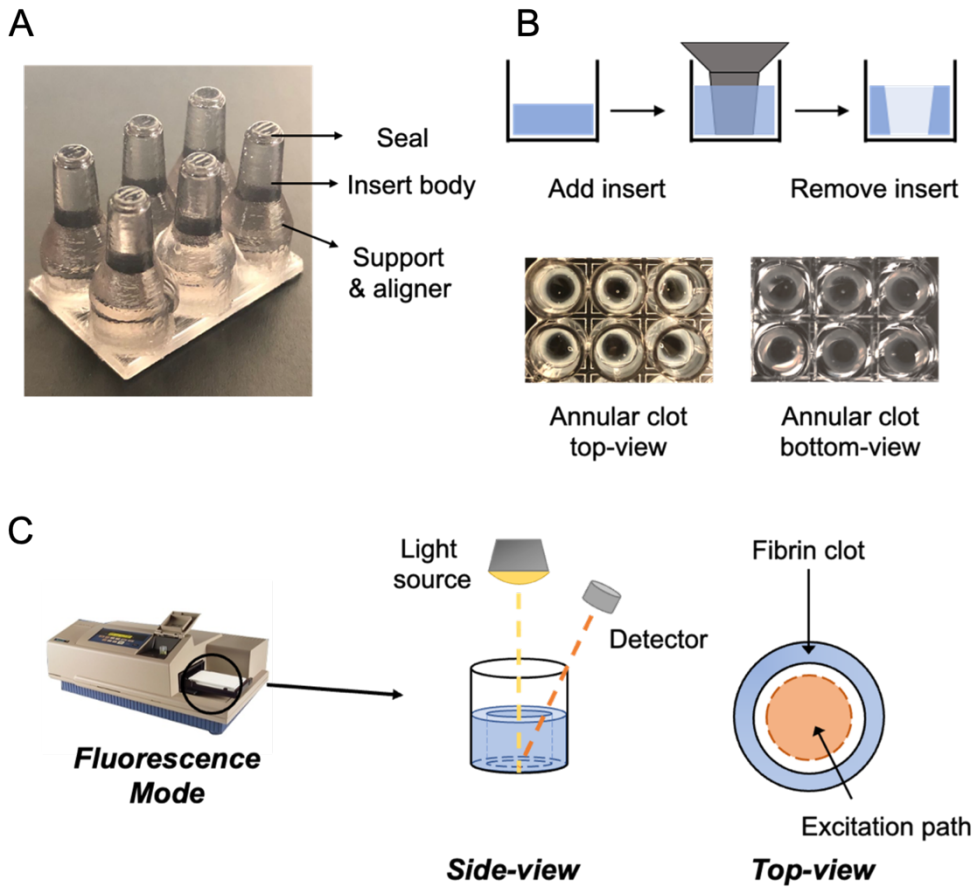

Figure 4.1. (A) The schematic of the 3D molding 3 X 2 insert and the printed product. (B) The schematic of annular clot formation in the well and the actual annular clot prepared by the 3 X 2 insert in the 96-well plate (C) Side and top views of the setup in the well.

4.3 Materials and Methods

4.3.1 FITC-Fibrinogen Conjugation

Human fibrinogen and thrombin lyophilized powder (Sigma Aldrich, St. Louis, MO) were reconstituted in phosphate buffer saline (PBS) and deionized water (DI), respectively. FITC (Sigma Aldrich, St. Louis, MO) was reconstituted in PBS with 10% dimethyl sulfoxide (DMSO) to improve solubility. FITC labeled human fibrinogen (FhF) is made by mixing 200-fold excess FITC to fibrinogen at room temperature (RT) in PBS for 10, 120 minutes, and overnight to attain three different FITC per fibrinogen labeling levels (<8% DMSO in reaction solution) (**Figure 4.2A**). Following conjugation, tagged fibrinogen was purified from unreacted FITC using serial dilutions in 4mL 100 kDa molecular weight cutoff centrifugal filters following manufacturer

recommendations (Amicon®, Millipore, Burlington, MA). An example of such purification setting is by running the 4 mL cutoff tubes at 4000 rcf in a swing bucket for 30 min on a Legend XTR centrifuge (Thermo Scientific, Waltham, MA). Depending on the concentration of the protein, a total of 6 or more runs should be expected (**Figure 4.2B**).

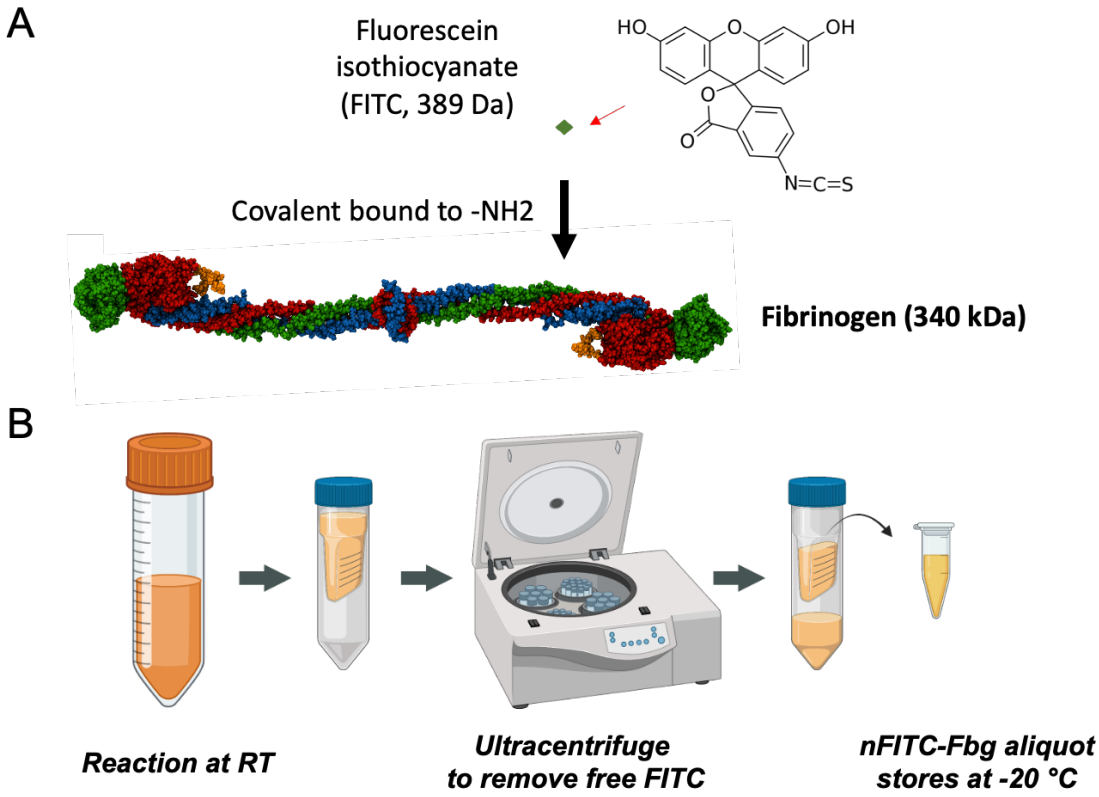

Figure 4.2. (A) Comparison of relative size of FITC and fibrinogen molecule (B) FITC-Fibrinogen conjugation reaction and standard procedure for ultra-filtration.

The number of FITC per fibrinogen were determined to be 3, 7, and 12- FITC per human fibrinogen comparing 280 and 494 nm absorptivity via a spectrometer (Molecular Device® SpectraMax M5, San Jose, CA), calculated through Beer's law and molar extinction coefficients, ε = 513, 400 L mol^{-1} cm^{-1} (at 280 nm) for fibrinogen and ε = 75,855 L mol^{-1} cm^{-1} (at 494 nm) for FITC. FITC absorbance contribution at 280 nm was subtracted. FhFs were aliquoted and stored at -20 °C and thawed directly before experiments. These FhF products were experimentally found to be active for clot formation and stable with no change in absorbance (280 nm and 494 nm) or fluorescence intensity for four consecutive freeze-thaw cycles and over a period of four weeks of storage (**Figure 4.3**).

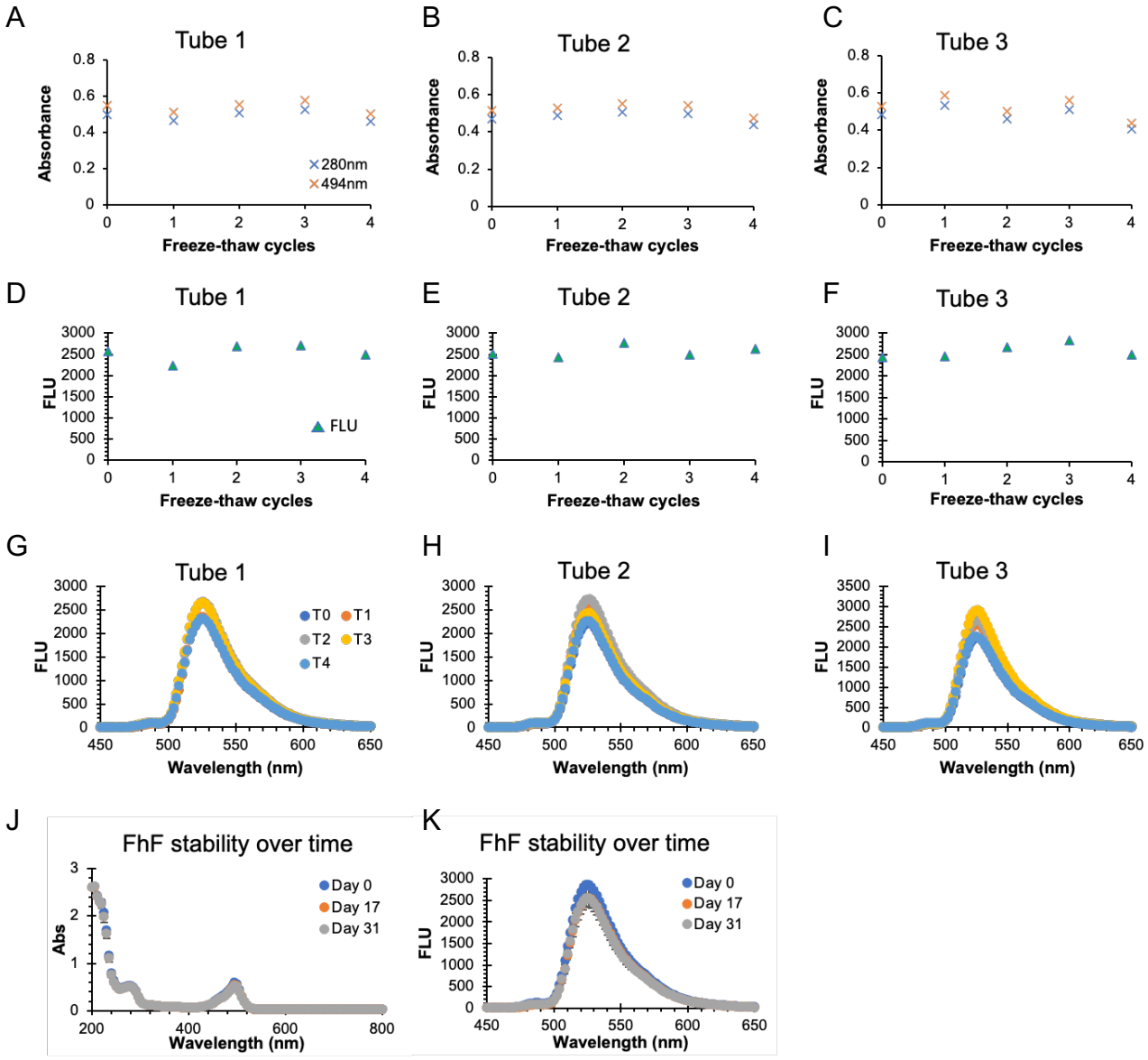

Figure 4.3. 12FITC-Fibrinogen (FhF) molecular and fluorescent stability after 4 freeze-thaw cycles. Three tubes of product were examined at (A, B, C) absorbance 280nm and 494 nm of stock aliquots at 20-fold dilution, (D, E, F) fluorescence endpoint Ex 495nm and Em 519 nm of stock aliquots at 400-fold dilution, and (G, H, I) additional fluorescent emission spectrum (Ex 495 nm, Em 450 - 650 nm, 400-fold dilution). No significant difference was found for product absorbance after 3 cycles (n=3, p_280 nm=0.1089, p_494nm=0.0897) and no significant difference were observed for emission spectrum as well as fluorescence endpoint after 4 cycles (n=3, p=0.2312). In addition, FhF aliquots were examined over storage time using the same metric. Both (J) absorbance spectrum and (K) fluorescence (Ex 495 nm, Em 450 - 650 nm, 400-fold dilution) showed consistent values over 31 days. This result indicates fluorescence intensity of FITC-Fbg product is stable after vigorous freeze-thaw cycles and storage.

Importantly, DMSO percentage as well as its adding sequence largely affects the solubility of FITC and FhFs. In most experiments performed in our lab, FITC and fibrinogen were reacted at 7.2% DMSO with a reaction yield of 50% after recovery. By tunning the DMSO down to 4%, the yield went above 90% (the overnight incubation for making 14FhF). The listed experimental procedures should be followed as a guide to achieve good solubility and high yield of the conjugated product: 1) Dissolve 4 mg of FITC in 400 μL DMSO and transferred into 3600 μL PBS to obtain FITC 10% DMSO stock solution. 2) Dissolve 20 mg human fibrinogen aliquot in 610 μL PBS to obtain fibrinogen stock solution. 3) Determine FITC and fibrinogen stock solutions concentrations at 200-fold and 20-fold, respectively. 4) Mix FITC and fibrinogen at a molar ratio of 200:1 and add more PBS to dilute DMSO to 4% when necessary.

4.3.2 Clotting Solution Preparation

Unmodified fibrinogen was mixed with 3, 7, 12-FhF at fibrinogen to FhF ratios of 1:0 (unmodified fibrinogen control), 5:1, 10:1, 30:1, 50:1, and 0:1 (neat FhF). All fibrin clots were formed at a final concentration of 3 mg/mL fibrinogen and 1U/mL thrombin in PBS.

4.3.3 FITC-Fibrin Turbidity and TEG Assays

Clot characterization via clot turbidity and TEG assays were described previously.[26, 27] Clot turbidity assays were initiated by mixing thrombin with fibrinogen in a 96-well plate (Corning®, Corning, NY) and monitored at 550 nm absorbance for 30 min via a spectrometer. $Turb^{max}$ (maximum turbidity) was derived from the turbidity tracing curve. TEG assays were initiated by mixing thrombin with fibrinogen in a clear TEG cup and monitored for 30 min in a TEG 5000 Analyzer (Haemonetics®, Braintree, MA). TEG^{Max} (maximum amplitude or MA) was derived by the TEG software (Haemonetics®, Braintree, MA).

4.3.4 Scanning Electron Microscopy

Fibrin clots (80 μL) were fixed by 2.5% glutaraldehyde (Electron Microscopy Sciences Supplier, Hatfield, PA) in PBS solution overnight and washed with DI water five times. Clot samples were then fully dehydrated via overnight lyophilization (FreezeZone 2.5, Labconco). It is important to note that the fibrin dehydration process was critical to preserve its micro-morphology

under SEM since clots formed in this study were at a concentration of only 0.3% (w/v). Additional dehydration methods were also assessed (**Figure A.12**). Dehydrated samples were further sputter coated with gold (Denton Vacuum Desktop V) for 30 seconds at $3*10^{-4}$ Torr to obtain a ~ 10 nm gold coating for SEM. Fibrin micro-structural images were taken using a field emission scanning electron microscopy (JSM-7800F, JEOL) at an acceleration voltage of 5 kV. Fiber diameters, pore size, pore counts, and total pore area were quantified using an open-source Image J software.

4.3.5 Confocal Microscopy

Selected fibrin clots were prepared in a 35 mm glass-bottom dish (MaTek Corporation) microscope dish at a volume of 40 µL. Images were acquired using LSM 800 confocal microscope (Zeiss, Germany) equipped with a C-Apochromat 40X/1.20W Korr objective. FITC was excited at 488 nm and collected at 519 nm (maximum emission). Confocal fluorescence images were analyzed using Image J.

4.3.6 Fibrin Clot Stability After Storage

FITC-Fibrin clots and unmodified fibrin clots were formed in a 96-well plate at 150 µL and stored at RT and 4 °C for comparison. Longitudinal fibrin clot stability was tested by tracking turbidity at 550 nm over 56 days.

4.3.7 Annular Clot Fabrication

The annular clot molding insert was designed and drafted using an open-source CAD software based on dimensions of a UV transparent 96-well plate (Corning® 3635). The insert was 3D printed at the IU Health 3D Innovations Lab using a Stratsys® Connex 3 printer (**Figure 4.1A**) providing for high precision with a build layer as fine as 16 µm. The body of the insert used an acrylic-based material (VeroClear® RGD810) to ensure a smooth surface. The elastomeric end cap (TangoPlus® FLX930) was later cured at the end of the insert to prevent unwanted clot formation in the light path at the base of the well. Annular clots were formed by directly adding clotting solution to the plate at 80 µL and immediately placing the DI water rinsed 3D printed insert into the well. The insert was gently pressed during the first 2 min to ensure a good bottom

seal. After 30 min clotting at RT the insert was carefully removed, and the annular clots were gently washed with 0.01 M PBS twice and stored in 120 µL PBS before use.

4.3.8 Dose Response Experiment

Lyophilized plasmin, plasminogen (Athens Biotech, Athens, GA) and tPA (Alteplase® Genentech, San Francisco, CA) were reconstituted in DI water. Sample solutions were made by diluting stock to targeted concentrations with PBS. Plasmin dose-response experiments were conducted at 0.01 to 1.5 U/mL unless otherwise specified. For experiments with varying plasminogen and fixed tPA level (500 ng/mL), 0 to 87.2 µg/mL plasminogen were examined. For experiments with varying tPA and fixed plasminogen level (58.1 µg/mL), 0 to 1000 ng/mL tPA were examined.

4.3.9 Annular Clot Lysis Assay

In all experiments, 120 µL sample solution was well mixed and added to the center of the annular clot to initiate clot lysis. Fluorescence (Ext 495, Em 519) was monitored for 60 min at a 30 sec interval without pre- or post- shaking. All clot lysis experiments were performed at 37 °C in triplicate. The Limit of Detection (LoD) is defined as the lowest analyte concentration reliably distinguished from the blank. Thus, LoDs of annular clot lysis assay were determined based on the measured Limit of Blank (LoB) and the lowest concentration of plasmin that has a significantly different fluorescence release rate compared to the blank. Analytical sensitivity was determined by the slope of a linear fitted line at lower plasmin concentrations (<0.05 U/mL).[28]

4.3.10 S2251 Chromogenic Assay

S2251 assays were performed in non-binding 96-well plates (Corning® 3641). Sample solutions were pipetted into the well containing 500 µM S2251 chromogenic substrate (Diapharma, West Chester, OH) at a final volume of 100 µL. p-Nitroaniline (pNA) absorbance (405 nm) was monitored for 10 min at a 30 sec interval. All experiments were performed at 37 °C with experimental groups in triplicates. V0 (Initial velocity) was derived using the initial linear region of the absorbance tracing curve.

4.3.11 Statistical Analysis

All results were reported as mean ± standard deviation. Two tailed student t-tests were performed, and significant statistical differences were reported at P values < 0.05. P values lower than 0.01 and 0.001 were also indicated as appropriate in plots and tables. Linear regressions were fitted in some plots and corresponding R^2 values were reported. The detailed protocols were specified in corresponding figure legends.

4.4 Results and Discussion

4.4.1 Effect of Fibrinogen Tagging on Clot Formation

The clinical relevance of an *in-vitro* fibrin clot lysis assay relies on a representative clot substrate that has non-disrupted physical and biological properties. Since the FITC-fibrinogen conjugation is mediated through a covalent bond, it is necessary to examine the fibrinogen tagging effect on clot properties. In this study, FITC labeled human fibrinogen (FhF) was made by incubating human fibrinogen with FITC at a 200-fold excess. Although a single fibrinogen molecule has around 200 lysine residues, we can only achieve a maximum of 16 FITC per fibrinogen. FITC conjugation sites on fibrinogen were also identified and detailed (**Figure A.13 and A.14**). By increasing the incubation time from 10 min to 2 hours to overnight, 3, 7, and 12-FITC per fibrinogen were fabricated and these numbers were determined via spectrometer using 494 nm to 280 nm absorbance conversion derived from the FITC absorbance spectrum. To assess the effects of fibrinogen tagging on fibrin clot formation, FhF were mixed with unmodified fibrinogen prior to thrombin initiated fibrin formation. Bulk clot strength and fibrin fiber packing were examined by TEG and turbidity assays. Turbidity and amplitude were tracked over time for clots formed at increasing levels of FITC-fibrinogen (**Figure 4.4C and 4.4D**). $Turb^{max}$ and TEG^{Max} were obtained for analysis and data were normalized to that of unmodified human fibrinogen to eliminate batch-to-batch variation (± 9% for $Turb^{max}$ and ± 5% for TEG^{Max}) and allow for direct comparisons of percent change across samples. All tested sample turbidities were within the detection limit of the spectrometer and were baseline-subtracted before data normalization. FITC absorbance at 550 nm at the concentrations used in this study are negligible. As was expected, FITC-fibrin(ogen) conjugation rendered a significant impact to both clot strength and macroscopic clot structure as determined by turbidity. Overall, increasing FhF levels (FhF to fibrinogen ratio)

in the clot contributed to higher $Turb^{max}$ (maximum turbidity) and lower TEG^{Max} (clot strength) which was consistently observed in all three groups (3, 7 and 12-FhF) (**Figure 4.4E and 4.4F**).

Specifically, neat 3, 7 and 12-FhF clot samples showed 45, 74 and 92% reduction in clot strength and 35, 65, and 69% increase in clot turbidity compared to unmodified fibrinogen, respectively. 12-FhF showed very low TEG^{Max} and high $Turb^{max}$ amidst all neat samples indicating a larger disruption of fibrin polymerization due to an increase of FITC-conjugations per fibrinogen. At lower FhF ratios, clot strength and clot turbidity values leveled off and matched values of the unmodified fibrinogen sample. The inverse tracking of clot strength and clot turbidity at increased FhF ratios in fibrin resembled what was observed in experiments on varying multiple other clotting variables published previously.[26] Importantly, this combination of high turbidity and low clot strength at a constant fibrinogen level demonstrates formation of thick fibers and a loose fibrous fibrin network. Time to maximum clot strength was also determined to assess the impact of fibrinogen tagging on the dynamic process of clotting (**Figure 4.4G and 4.4H**). Under both assays, most samples showed a similar time to maximum clot formation with a difference less than 20% indicating similar clotting performance across groups. However, neat 12-FhF sample showed three times longer time to achieve maximum clot strength compared to all other samples due to its slow clotting progression and low ultimate clot strength.

From this analysis, physiologically relevant fibrin clotting mixtures for each of the modified fibrinogen levels were determined through matching clot properties of a sample to that of the unmodified fibrin clot. Therefore, 7FhF (30:1) and 12FhF (50:1) groups were determined to be physiologically relevant as their $Turb^{max}$ and TEG^{Max} showed no statistical difference ($P < 0.05$) above 30:1 and 50:1, respectively. 3FhF (10:1) was also selected as a physiologically relevant mixture as TEG^{Max} showed no statistical difference while $Turb^{max}$ showed less than 10% difference.

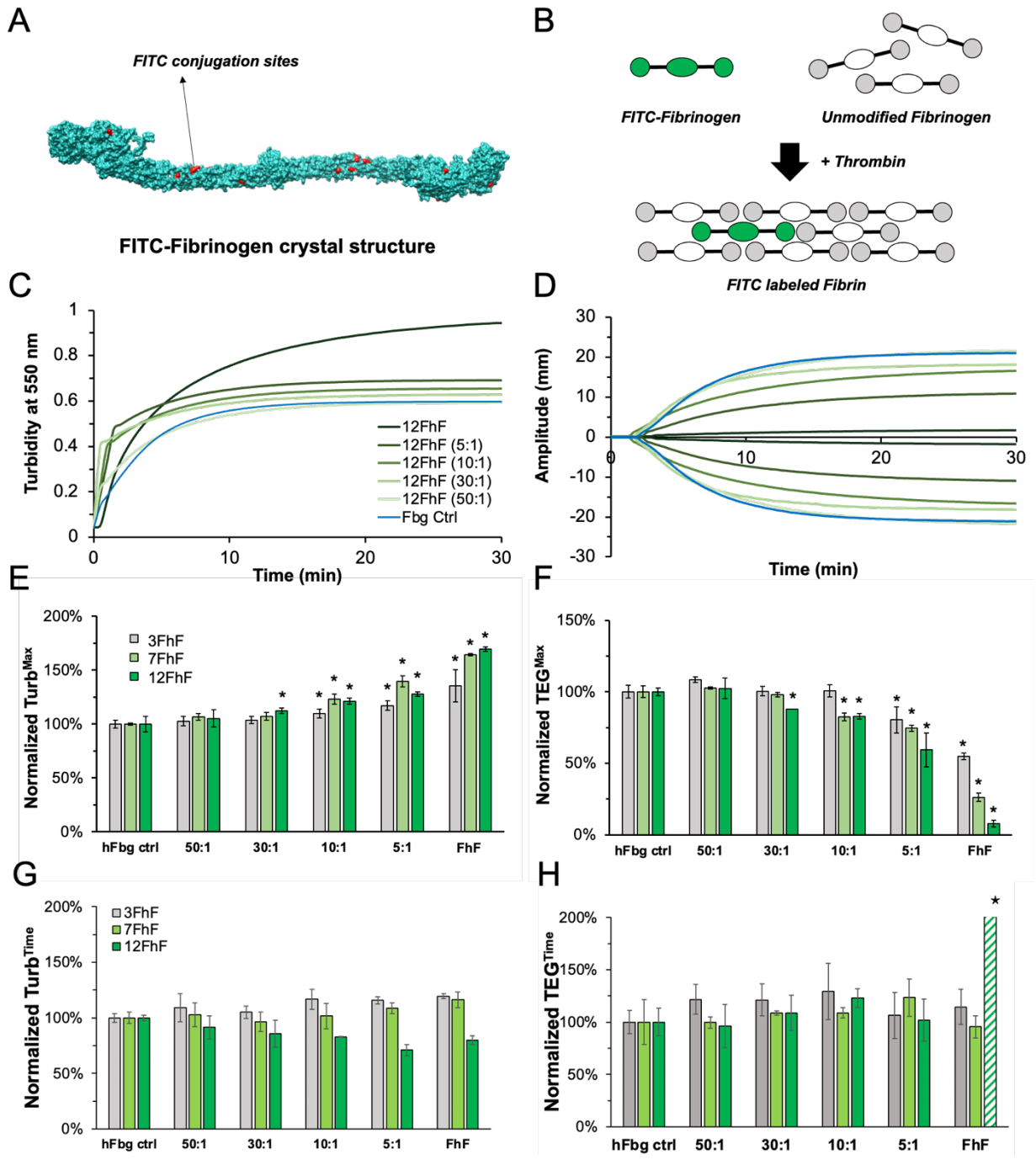

Figure 4.4. (A) Representative FITC conjugation sites on fibrinogen crystal structure displaying widespread FITC labels across the surface of fibrinogen. (B) Forming FITC labeled fibrin clot using thrombin-cleaved unmodified fibrinogen and FITC-fibrinogen mixture. Representative tracing curves of (C) turbidity assay and (D) TEG assay for varying 12FITC labeled human fibrinogen (FhF) levels in 12FITC-fibrin clot. (E) $Turb^{max}$, (F) TEG^{Max} (Maximum amplitude), (G) $Turb^{Time}$, and (H) TEG^{Time} of 3, 7 and 12- FITC-fibrin clots at different FhF levels were compared. Data were normalized by values of human fibrinogen control groups. * denotes significant differences (P value < 0.05) between FhF groups and hFbg ctrl group.

4.4.2 Fibrin clot Morphology via SEM

To directly assess clot morphology at varying ratios of tagged and untagged fibrinogen, SEM was carried out on an array of fibrin clot mixtures. These clots include neat FhF, unmodified fibrin clots, and three physiologically relevant FhF clot samples--3FhF (10:1), 7FhF (30:1) and 12FhF (50:1). Clots were formed, crosslinked, lyophilized and gold coated prior to SEM analysis. Clot microstructures were compared at 4,000X and 35,000X magnifications (**Figure 4.5A and 4.5B**). Neat FhF clot samples exhibited scale-like patterns and fused fibrin fiber morphology. These clots were further categorized as having larger fiber diameter, smaller pore size and smaller total pore area percentage compared to the other groups (**Figure 4.5C**). A quantitative analysis was conducted using Image J. Pore size and total pore area were measured using a thresholding method where the same threshold level was applied across all the samples throughout the analysis. Based on the quantitative results, the neat 12FhF clot sample showed the most unique and dissimilar SEM morphology, i.e., thickest fiber and lowest pore area. These direct morphological measurements are consistent with the bulk clot structure as assessed by clot turbidity. The physiologically relevant clot groups showed much cleaner fibrin morphology more similar to that of neat unmodified fibrinogen clots.

Despite having similar TEG and turbidity values as unmodified fibrinogen, not all physiologically relevant groups exhibited a native fibrin structure under SEM. 3FhF (10:1) and 7FhF (30:1) clots showed similar fiber diameters compared to unmodified fibrin clots but both groups were found to have significantly smaller pore size and a moderate level of fused fibrin fiber morphology. Only the 12FhF (50:1) sample showed minimal differences, both qualitatively and through defined characteristics, compared to the unmodified fibrin control. This suggests that the ratio of fibrinogen to FhF rather than the amount of FITC per fibrinogen exerts a larger ultimate impact on fibrin structure upon clotting. To further explore this, the effect of fibrinogen to FhF ratio on clot micro-morphology was further examined under SEM. In this experiment, clots were formed by decreasing 12FhF ratios (fibrinogen to FhF = 0:1, 10:1, 30:1, 50:1, 1:0) in the fibrin (**Figure 4.6** and **Table 4.1**). Results showed that the presence of more FhF contributed to clots with significantly larger fiber diameters, reduced pore size and total pore area. This confirmed that increasing FITC-fibrin(ogen) levels in fibrin clots disrupt clot properties resulting in less physiologically relevant fibrin clots. In summary, the clotting solution that mixes unmodified

fibrinogen with 12 FITC per human fibrinogen at 50:1 ratio produces the most physiologically relevant fibrin clot as determined by TEG, Turbidity, and SEM.

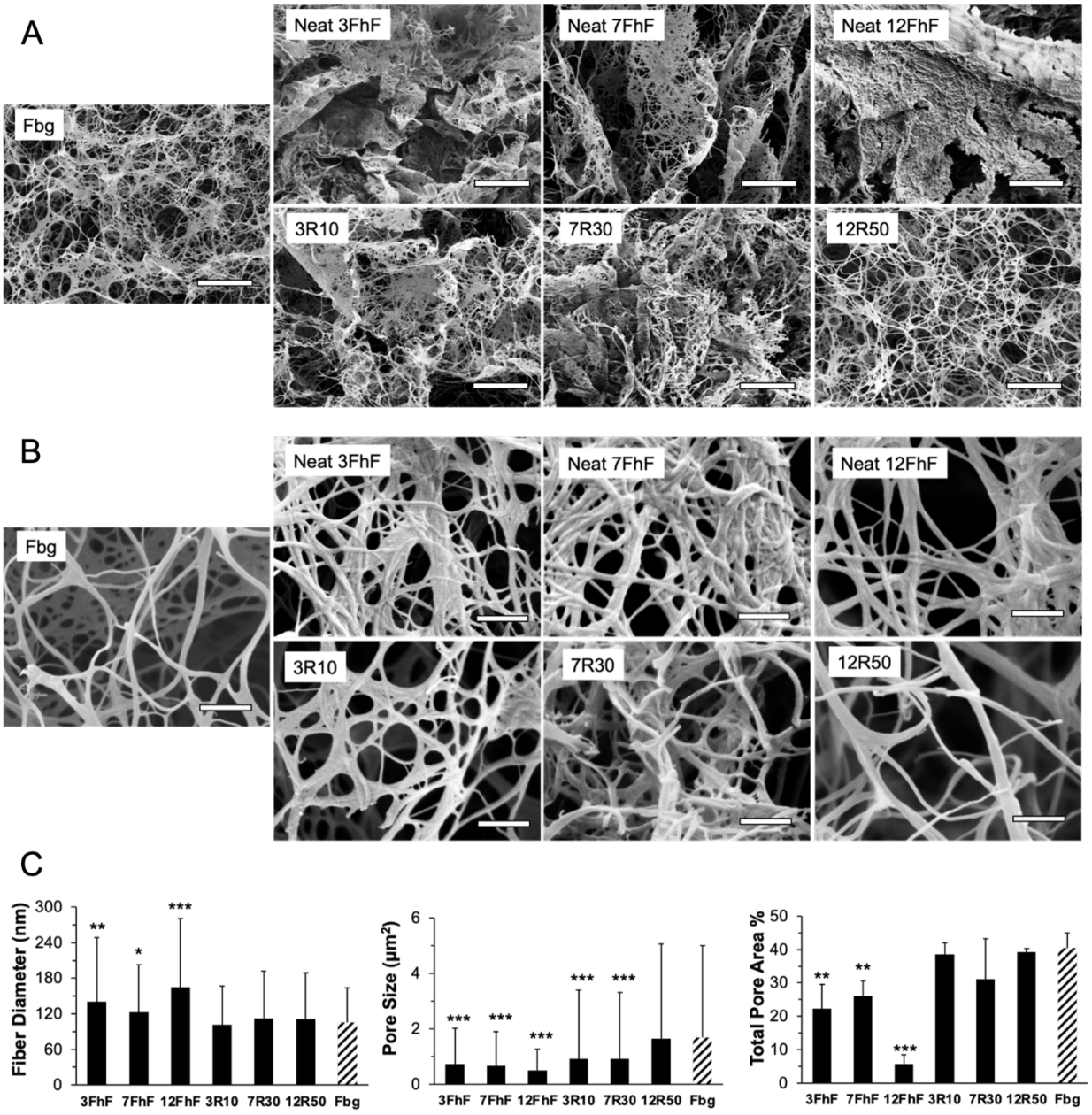

Figure 4.5. Representative SEM Images of FITC labeled human fibrin formed by neat and unmodified fibrinogen mixed 3, 7, 12- FITC-Fibrinogen at (A) 4,000X and (B) 35,000X. Scale bars were shown as 5 μm and 500 nm, respectively. Average fiber diameter (nm), average pore size (μm^2) and total pore area (%) were reported as bar plots and data were compared with unmodified fibrin controls using *, ** and *** denoting p values < 0.05, 0.001, and 0.0001.

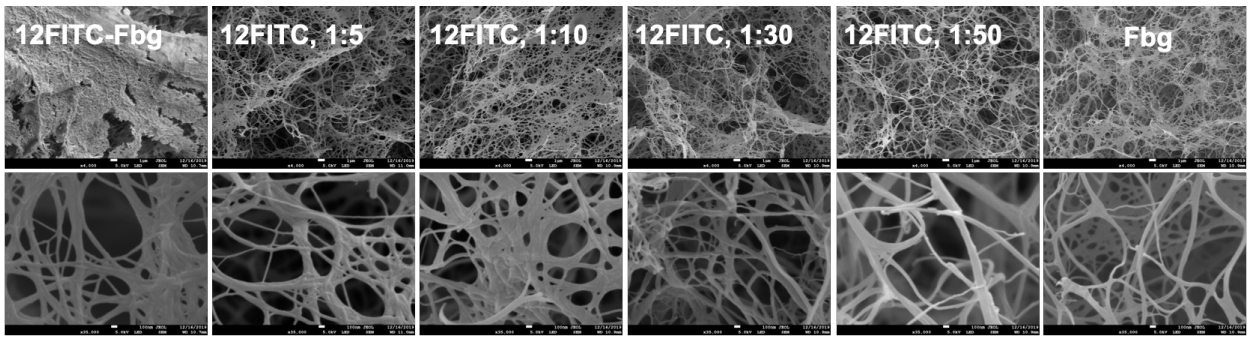

Figure 4.6. Representative SEM images of varying 12 FhF in fibrin. 4,000X (first row) and 35,000X (second row). Scale bars shown as 1 μm (first row) and 100 nm (second row).

Table 4.1. Total pore area and fiber diameter of clot at different fibrinogen to 12FhF ratios

Clot formula	Neat 12FhF	12FhF R5	12FhF R10	12FhF R30	12FhF R50	Fibrinogen
Fiber diameter (nm)	***165 ± 115	***153 ± 83	***157 ± 114	*125 ± 79	111 ± 78	105 ± 59
Pore size (μm^2)	***0.5 ± 0.8	***0.9 ± 1.6	***1.1 ± 2.1	*1.3 ± 3.0	1.6 ± 3.4	1.7 ± 3.3
Total pore area	***5.7% ± 2.7%	*24.5% ± 7.5%	**28.0% ± 1.7%	39.2% ± 6.3%	39.3% ± 0.9%	40.4% ± 4.5%

Note: P values of groups comparing to the fibrinogen control group were determined by two-tailed unpaired t test, *** denotes P value <0.0001, ** denotes P value <0.001, * denotes P value <0.05.

4.4.3 Tagging Consistency via Confocal Microscopy

Homogeneity of FITC incorporated into the final fibrin clot structure is critical to ensure that release of FITC during clot digestion is consistent throughout the entirety of the clot digestion process. To assess FITC labeling homogeneity, z-stack confocal images of neat and physiologically relevant 3, 7, 12FhF formed fibrin samples were taken at three different locations with five slices at an interval of 10 μm. Three slices at locations that are 30 μm below the surface were used for comparison and quantitative analysis. Neat FhF clot samples exhibit bright images with significant fluorescent aggregates at higher FITC per fibrinogen whereas the three physiologically relevant FhF clots showed homogeneous FITC labeling throughout their fibrin structures (**Figure 4.7A and 4.7C**). Unmodified fibrin clots could not be imaged utilizing this technique as they did not exhibit endogenous fluorescence in the absence of FITC tagging.

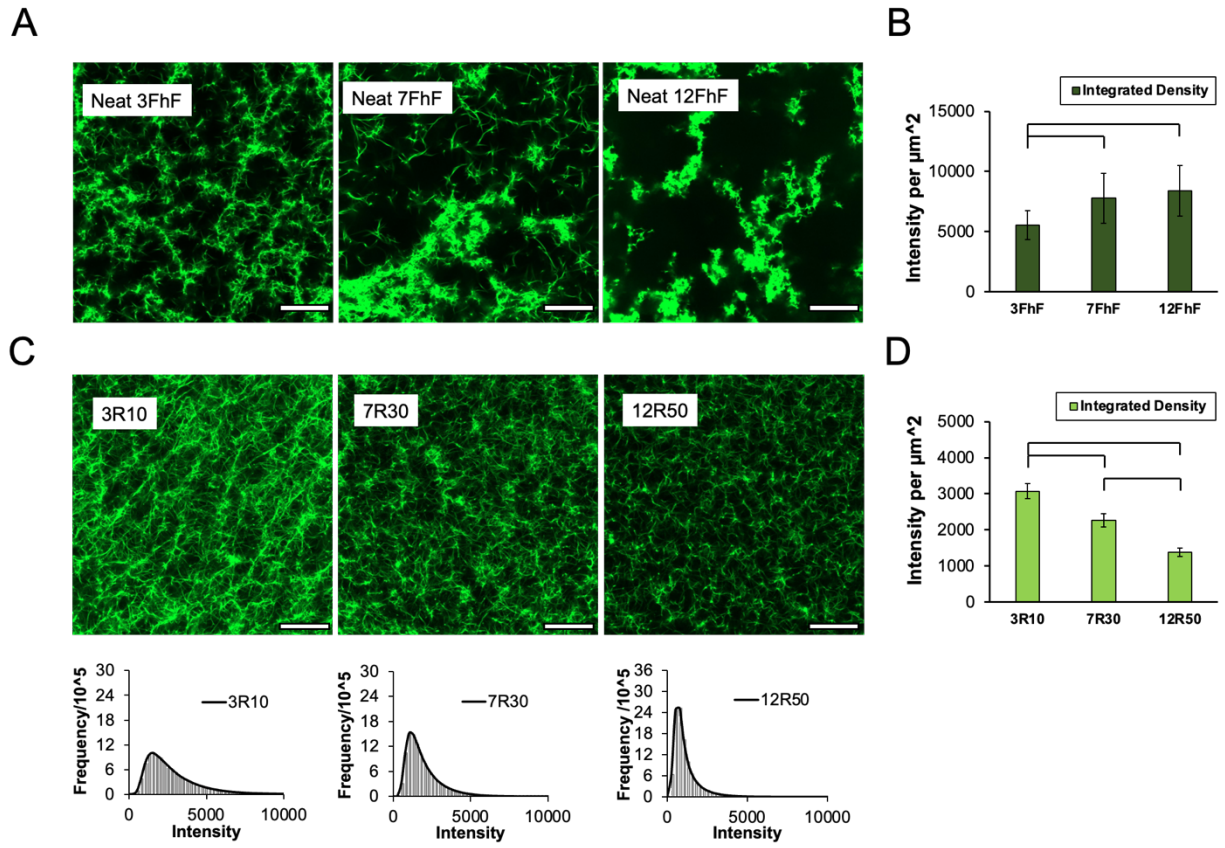

Figure 4.7. Representative confocal microscope images (40X objective with 1.5X digital zoom, excitation energy at 1%) of clots formed by (A) neat 3, 7, 12 - FhF, and (B) 3FhF (10:1), 7FhF (30:1) and 12FhF (50:1). Fluorescence intensity distribution were shown for physiologically relevant FhF clots. Integrated density was shown for (C) neat FhF and (D) physiologically relevant clots in bar plots with brackets denoting pairs of groups that exhibit significant differences ($P < 0.05$). Image brightness of 12FhF (50:1) clots were adjusted to enhance structure visualization. Scale bar = 20 µm.

Neat and physiologically relevant FhF clot samples were excited at 0.2% and 1% energy levels to avoid signal underexposure or saturation, respectively. Images were taken immediately after excitation to avoid photobleaching over time. Integrated intensities were reported in fluorescence units (RFU, or arbitrary units) per µm2 by averaging multiple images at different depths for each sample in bar plots (**Figure 4.7B and 4.7D**). It was not surprising that neat FhF clots showed higher integrated intensity at increased FITC per fibrinogen. However, the value of the neat 12FhF sample is only 1.5 times as that of the neat 3FhF sample while the FITC concentration ratio of these two samples is 4 times higher. This represents a reduction in intensity per FITC of 62% indicative of local fluorescence quenching due to increasing FITC proximity on

fibrinogen which has been reported previously.[3, 29] Comparing 12FhF (50:1) to 3FhF (10:1) samples, integrated intensity ratios and FITC concentration ratios were also mismatched contributing to a 64% reduction of integrated intensity per FITC in the former group. 7FhF neat and 7FhF (30:1) samples also showed 39.6% and 42.7% reductions in integrated intensity per FITC compared to 3FhF neat and physiologically relevant samples, respectively. Since similar levels of reduction in integrated intensity per FITC were observed for neat and physiological relevant samples, fluorescence quenching was dominated by intra-fibrinogen quenching effects rather than inter-fibrinogen quenching. This quenching effect is largely due to the use of FITC as a fluorescent probe and can be mitigated by selecting a probe that is less prone to self-quenching.

The labeling homogeneity was quantitatively assessed by looking at the integrated intensity fluctuation across a set of five image locations. All neat FhF samples showed > 20% fluctuation in fluorescence intensity with obvious fluorescence aggregation while physiologically relevant FhF samples exhibit less than 10% variation. This confirmed that physiologically relevant FhF samples have a more consistent labeling homogeneity throughout the clot. Additionally, the unlabeled area between the fluorescently labeled fibers were also quantified using a thresholding method in Image J. The unlabeled area is a function of both empty space in the clot, and fluorescent labeling density. While the physiologically relevant clot samples shared similar clot structure under SEM, the 3FhF (10:1) showed 63.0% ± 1.1% unlabeled area which is significantly lower than 76.2% ± 6.7% ($P < 0.001$) for 7FhF (30:1) and 80.9% ± 7.2% ($P < 0.001$) for 12FhF (50:1). This result was expected due to physiologically relevant 3FhF clot sample having the highest labeling ratio of 10:1, representing the most total FITC in the clot of any of the physiological ratios. Based on clot characterization results from clot turbidity, TEG, and SEM, 12FhF (50:1) showed the best match to unmodified fibrin. Although its fluorescence labeling signal intensity was not the highest via confocal microscopy among all three physiological relevant formula, the 12FhF (50:1) clotting mixture demonstrates good labeling homogeneity which potentiates a uniform tracking of fluorescence signal during subsequent clot lysis experiments in the annular clot digestion assay.

4.4.4 Annular Clot Formation

Fluorescently labeled fibrin digestion cannot be monitored directly through the labeled clot substrate to track clot digestion due to the saturating level of fluorescent tag present in the

excitation path. A common solution to this saturation problem is to allow digestion to proceed for a short period of time before removing, or sampling, the digestion supernatant to take static reads throughout the digestion process. This procedure prevents real-time clot digestion tracking and removing of clot supernatant disrupts the clot digestion process negatively impacting assay reproducibility and limiting the capability to multiplex the assay.

The annular clot geometry described herein is a simple and unique solution to the problem of real-time clot lysis monitoring. Through utilizing commonly available 3D printing technology, a small plastic insert can be fabricated for use in a 96-well plate assay format (**Figure 4.1**). This design not only enables real-time signal tracking through measuring soluble digestion fragments that enter the vacant interior of the annular clot, but it also increases assay-multiplexing potential and largely eliminates experimental artifacts commonly associated with repeat sampling type assays. As determined from the characterization experiments in the previous sections, the 12FhF (fibrinogen to FhF=50:1) was selected as the clotting mixture to form the physiologically relevant FITC-fibrin clots. The annular clots were made by placing the insert into the clotting mixture directly following clot initiation through mixing thrombin with neat or physiologically relevant 12FhF solutions. Following 30 minutes the molding insert can be removed and due to the smooth walls of the insert no visible interruption to the annular clot surfaces can be seen following removal. The inserts can be reused indefinitely. The annular clot showed an average volume of 60.5 ± 0.8 µL and an averaged background value of 798 ± 319 RFU (n = 114). With the addition of PBS into the center of the annular clot, no degradation of fibrin was observed throughout the duration of the experiments as determined by monitoring absorbance at 280 nm. Overall, the described annular clot method is a highly reproducible elegant solution to a common problem with far reaching potential to have an impact in the field of drug development and as a diagnostic tool in the areas of coagulation and fibrinolysis.

4.4.5 Effects of Fibrinogen Tagging on Plasmin Clot Digestion

Plasminogen is the protease present in the blood plasma primarily responsible for fibrinolysis following activation into its active plasmin form. Its activity directly contributes to the fibrinolytic potential of a plasma sample. Maximal inducible plasmin activity in plasma is about 1 U/mL following full activation of endogenous plasminogen and exhaustion of plasmin inhibitors.[30] To examine the fibrinogen tagging effect on fluorescently labeled fibrin clot

digestion, increasing amounts of active plasmin were tested comparing S2251 chromogenic substrate to neat 12FhF and 12FhF (50:1) annular clots. In the S2251 assay, the plasmin dose-response result was reported by plotting the initial velocity V0 (Abs/min) over plasmin concentrations (**Figure 4.8A**). A linear relationship was observed between V0 and plasmin concentration. At plasmin levels above 1 U/mL the substrate digestion rate occurs too rapidly to get an accurate initial velocity by the spectrometer. In all, the S2251 assay showed good linearity with increasing plasmin levels from 0.01 to 1 U/mL.

Unlike digesting evenly mixed, small soluble peptide substrates like S2251, plasmin digestion of thick and insoluble physiologically relevant fibrin, such as is present in the annular clot format, involves solid-liquid phase interactions and molecular transport. Initial velocity measurements that are commonly utilized for monitoring chromogenic assays need to be modified when applied to the annular fibrin clot lysis assay. Contrary to initial linear signal tracing monitored for S2251 digestion, annular clot lysis assays demonstrate an initial lag phase followed by a linear phase and an ultimate plateau phase (**Figure 4.9A**). The lag phase is associated with plasmin diffusion due to the static nature of the assay and the discrete liquid-solid separation. The diffusion of plasmin is not solely based on its relative hydrodynamic size compared to the fibrin pore size but rather it is also dependent on plasmin-fibrin binding which is achieved through binding of plasmin's kringle domains to fibrin.[31] Recent *in-vitro* experiments have confirmed that diffusion of plasmin(ogen) is restricted within a thin fibrin layer (5-8 μm) due to fibrin bindings.[32] A potential co-contributor to the lag phase is the gradual exposure of more binding sites, i.e., C-terminal lysine residues, by plasmin accumulation to the digestion front.[33] The exposing rate can be easily affected by protease concentration and the presence of protease inhibitors. In the annular clot lysis assay, the lag phase is useful to examine the initial interactions of the protease and fibrin. Taking this into account a new digestion parameter was developed, FLU200, defined as the time it takes to digest enough FhF to reach 200 fluorescence units. At increasing plasmin levels, FLU200 times showed a decreasing trend (**Figure 4.9B**). In the linear phase where fibrin binding moieties are relatively abundant, digestion rate better reflects the maximal fibrinolytic activity of the sample. Therefore, V_{FR} (fluorescence release rate, RFU/min) was derived by taking the maximum velocity (10 min period) to represent clot digestion rate in this assay. Fluorescence signal was tracked over time at a 30 second interval exhibiting an overall faster fluorescence release at a higher plasmin concentration. At lower plasmin concentrations (<1

U/mL plasmin), although lag and linear phases can hardly be distinguished since C-terminal lysine residuals are constantly larger than plasmin amount, digestion rates were still determined at the fastest 10-min linear period. The coefficients of variance were 9.4% for V_{FR} and 10.6% for FLU200 of physiologically relevant 12FhF annular clot digested by 1 U/mL plasmin through experiments performed two weeks apart. Despite the relatively small coefficient of variance for V_{FR} and FLU200, a standard plasmin calibration curve is recommended prior to testing samples to mitigate clot formation variations.

Neat and physiologically relevant 12FhF mixtures were compared in the annular clot lysis assay to determine the fibrinogen tagging effects on fibrinolysis. Overall, both annular clot lysis assays showed that V_{FR} increased and leveled off at higher plasmin concentrations, which agreed with clot digestion at increased plasmin as previously described by the fibrin plate method.[34] To derive simple calibration equations to determine plasmin activity in unknown samples, the V_{FR} and plasmin concentrations were plotted in a double-logarithmic scale (**Figure 4.8B**). Data points of both groups showed good linear regressions with $R^2 > 0.95$. Neat and physiologically relevant 12FhF groups shared similar slopes indicating a comparable dose-response performance across tested plasmin concentrations. The analytical sensitivity of the neat 12FhF substrate is 19 times higher than its physiologically relevant counterpart (**Figure 4.8C**). Its LoD was also slightly lower giving a 0.0015 U/mL comparing to 0.0069 U/mL for the physiologically relevant 12FhF clot. The digestion performance of both substrates was further compared using equivalent fibrin degradation rates (V_{FDR}). V_{FDR} of physiologically relevant and neat 12FhF were normalized to absolute FITC quantity by multiplying their V_{FR} values by 50 and 1, respectively. It was anticipated that neat FhF clots would have larger V_{FDR} at these plasmin concentrations since fibrin composed of thick and loose fibers usually exhibit faster clot digestion. Contrary to this prediction, V_{FDR} of physiologically relevant 12FhF clots were 16 to 22 times faster than those of neat 12FhF clots at the tested plasmin concentrations (**Figure 4.8D**). The increased FhF levels impaired fibrinolysis to a large extent. In all, despite the higher levels of signal associated with the neat 12FhF, its digestion was considerably slower than the physiologically relevant 12FhF clots. This reduced digestion rate can be attributed to the tagged fibrin impairing plasmin's ability to bind and facilitate fibrin digestion. For applications in which the highest clot digestion signal is necessary, the neat 12FhF can be utilized. For applications requiring a physiologically relevant clot substrate, preparing a 12FhF (50:1) mixture is necessary.

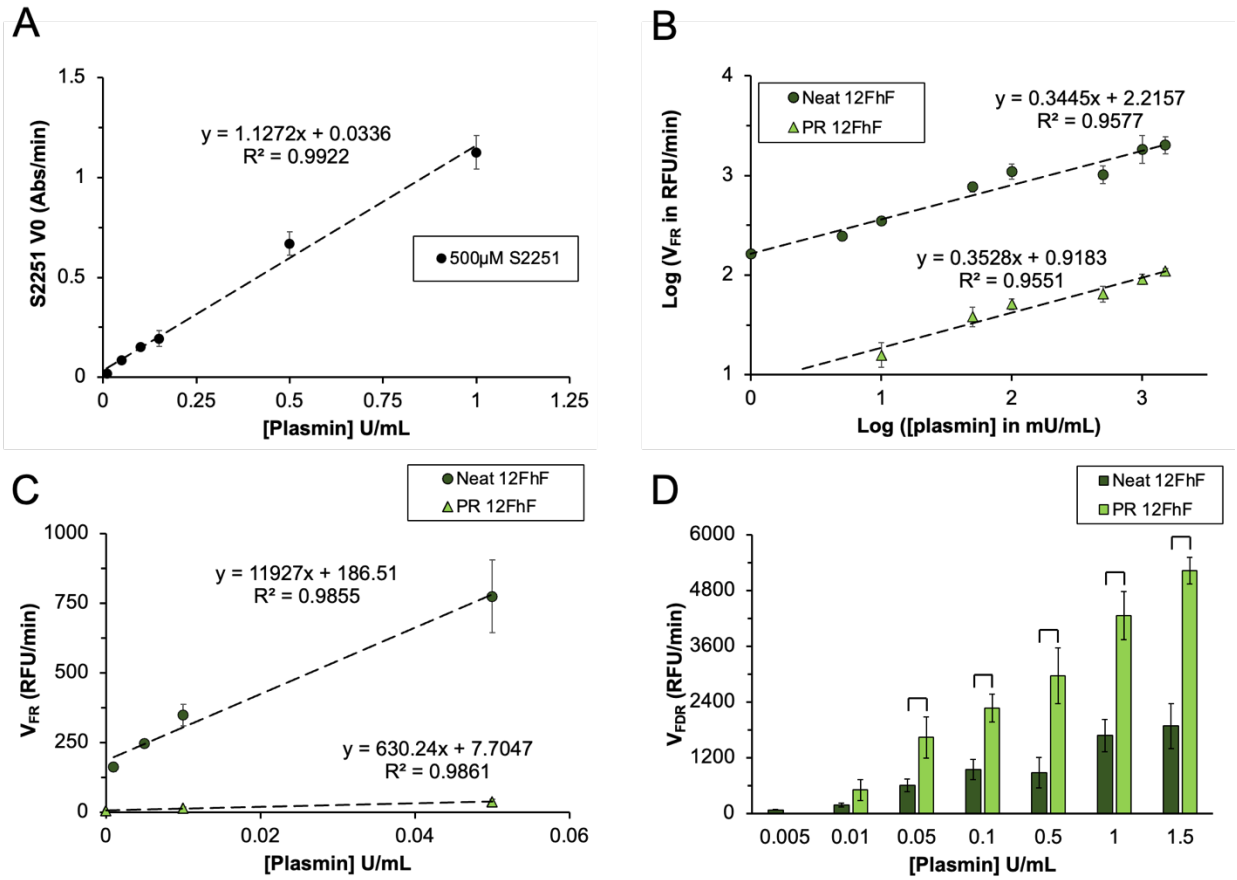

Figure 4.8. Plasmin dose-response curve by (A) initial velocity (V_0) in S2251 assay and (B) fluorescence release rate (V_{FR}) in neat and physiologically relevant (PR)- 12FhF annular clot lysis assay where data were shown at the double-logarithmic scale. (C) Analytical sensitivity determination curves of annular clot lysis assay by plotting data points below 0.05 U/mL plasmin. Analytical sensitivity of neat 12FhF and PR12FhF annular clots were 11927 and 630. (D) Fibrin degradation rate (V_{FDR}) at increasing [plasmin]. V_{FDR} of PR- and neat 12FhF were converted via multiplying their fluorescence release rates (RFU/min) by 50/12 and 1/12, respectively. All fluorescence tracing curves were shown in Figure A.15 and A.16.

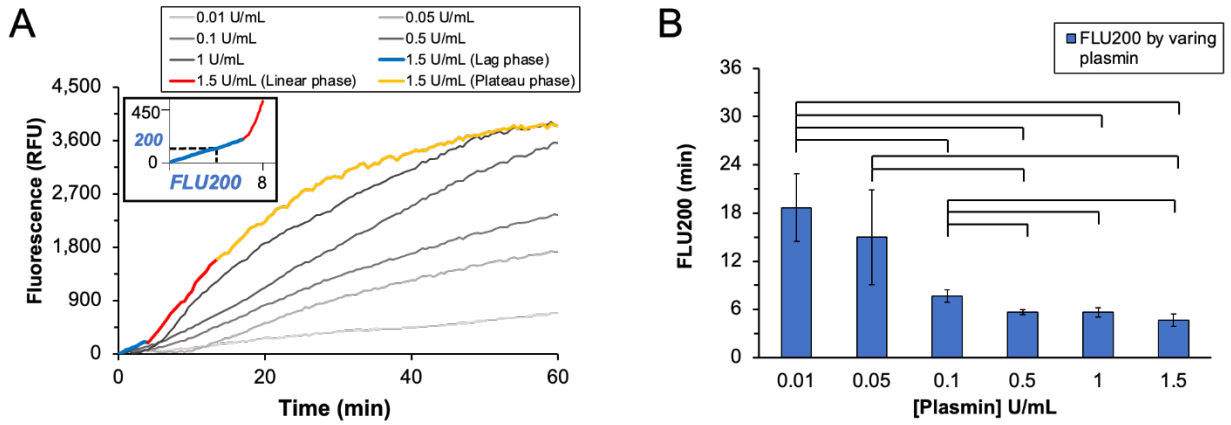

Figure 4.9. (A) Representative fluorescence release tracing curves of physiologically relevant (PR)-12FhF at varying [plasmin] and the derivation of FLU200 for PR-12FhF at 1.5 U/mL. (B) FLU200 for PR-12FhF over varying [plasmin]. Brackets denoting pairs of groups that exhibit significant differences ($P < 0.05$).

4.4.6 Varying Plasminogen and tPA levels on Annular Clot Digestion

In plasma, tPA cleaves plasminogen into plasmin to initiate fibrinolysis. The baseline concentration of plasma tPA is less than 10 ng/mL for healthy individuals.[35] A typical thrombolytic therapy for a pulmonary embolism patient is a regimen of 100 mg Alteplase over 2 hours of intravenous infusion.[36] The catalytic efficiency of plasminogen activation by tPA has been reported to be orders of magnitude higher in the presence of fibrin than in its absence. The S2251 assay has commonly been used to assess urokinase and streptokinase-initiated plasminogen activation but lacks the ability to examine plasminogen activation by tPA due to the absence of fibrin in the assay. To demonstrate a benefit of using the annular clot lysis assay over this chromogenic substrate, digestion solutions made by combining tPA and plasminogen were tested in the physiologically relevant 12FhF annular clot and S2251 assay. Varying plasminogen at fixed tPA and varying tPA at fixed plasminogen dose-response experiments were performed. V0 (in S2251) and V_{FR} (in annular clot lysis assay) over component concentration were plotted using the primary axis. Equivalent plasmin activities were computed using equations derived from plasmin dose-response plots and were reported in U/mL in plots on the secondary axis (**Figure 4.10A, 4.10B, 4.10C and 4.10D**). At increasing plasminogen levels and a fixed 500 ng/mL tPA, S2251 assay reached its detection limit at ~29 µg/mL plasminogen. Conversely, V_{FR} from the annular clot lysis assay showed a clear increasing trend leveling-off at concentrations above 58.1 µg/mL.

This indicates that the annular clot lysis assay is a more sensitive candidate to determine plasminogen activity in plasma in the presence of endogenous or exogenous tPA.

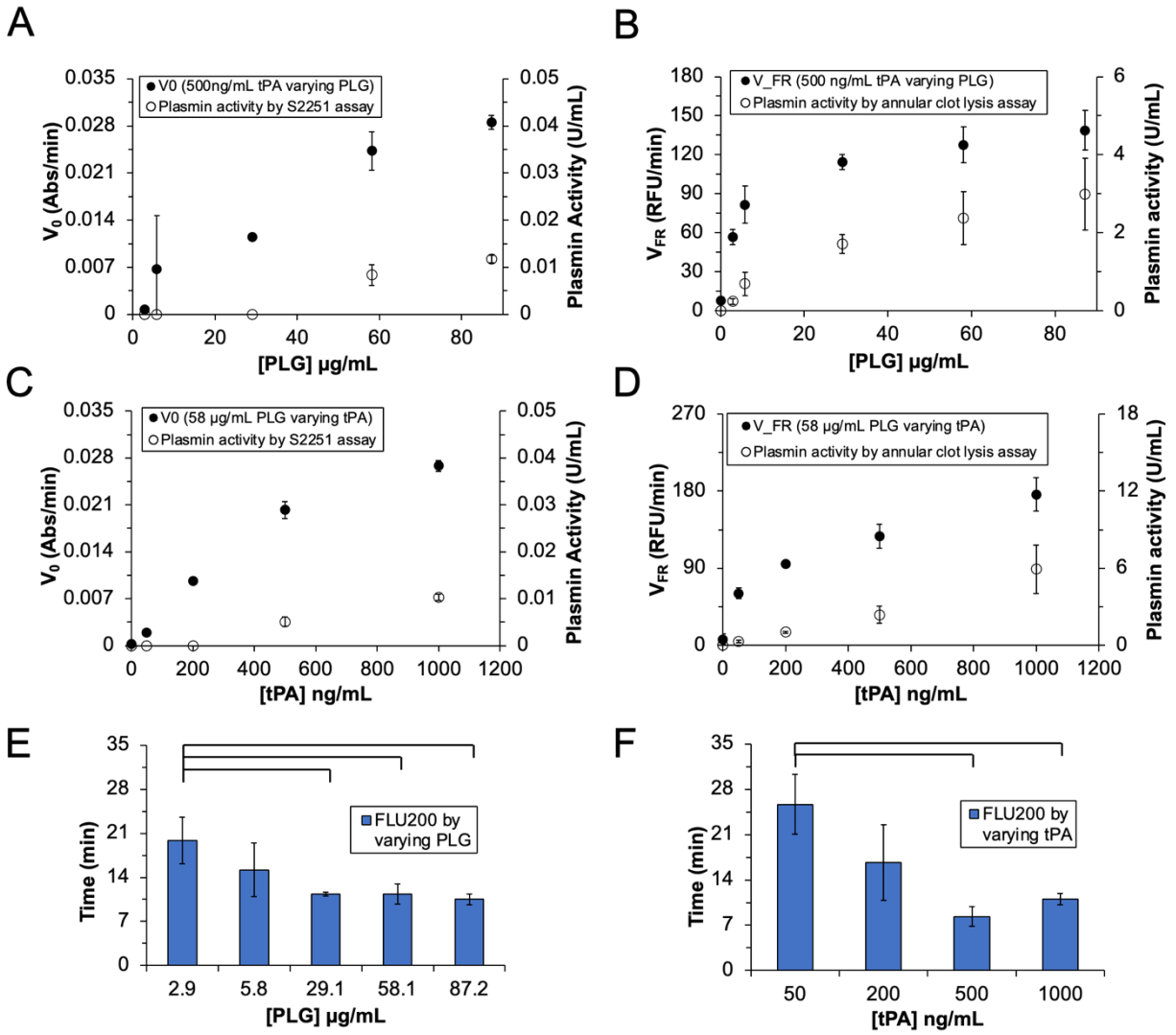

Figure 4.10. Digestion rates (primary axis, Abs/min or RFU/min) and plasmin activity (secondary axis, U/mL) by (A) fixed tPA and varying PLG in S2251 assay, (B) fixed tPA and varying PLG in PR-12FhF annular clot lysis assay (C) fixed PLG and varying tPA in S2251 assay and (D) fixed PLG and varying tPA in PR-12 FhF annular clot lysis assay. FLU200 by PR-12FhF were shown in bar plots at (E) varying PLG and (F) varying tPA experiments with brackets denoting pairs that have significant differences. Plasmin activities were converted by plugging the digestion rate values in linear regression equations derived in Figure 4.8. Plasmin activities were of two orders of magnitude faster in annular clot lysis assay compared to S2251 assay. Fluorescence tracing curves were shown in Figure A.17 and A.18.

At increased tPA levels and a fixed 58.1 µg/mL plasminogen, both V0 and V_{FR} increased and showed a tendency to level off at higher tPA concentrations. Plasmin activities were compared across and within assays. As expected, in the absence of fibrin, the S2251 assay showed extremely low plasmin activity values converted using the standard curve and the equation derived in the plasmin dose-response experiment. The annular clot lysis assay showed two orders of magnitude larger ($P < 0.05$) plasmin activity values than those of S2251 at all tested groups for both varying tPA and varying plasminogen experiments. Within the annular clot lysis assay, plasmin activities showed significant differences across all groups ($P < 0.05$) when varying tPA. In experiments varying plasminogen, all groups showed significantly different plasmin activities compared to 2.9 µg/mL ($P < 0.05$) and all groups except 29.1 µg/mL showed significant differences compared to 5.8 µg/mL ($P < 0.05$). These results confirmed that the annular clot lysis assay could differentiate digestion rate or plasmin activities at a wide range of plasminogen or tPA levels. Overall, FLU200 decreased and leveled off at higher plasminogen or tPA levels (**Figure 4.10E and 4.10F**). Importantly, the FLU200 of groups in these experiments were almost 3 times longer than groups with an equivalent V_{FR} in the plasmin dose-response experiment ($P < 0.05$). The extended lag phases in these samples were expected since the activation of plasminogen by tPA and the molecular interaction involving fibrin binding can contribute to elongated activation time prior digestion. These findings also demonstrated the capability of the annular clot lysis assay at picking up interplays between different fibrinolytic factors.

The tPA activation of plasminogen with S2251 was also run in the presence of soluble fibrinogen and a similarly low activation of plasminogen was observed (**Figure 4.11**). In general, tPA and plasmin(ogen) are key enzymes in the fibrinolytic pathway. Being capable of differentiating tPA and plasminogen levels in an unknown sample is an important assay feature. The annular clot lysis assay provides for a more versatile assessment of sample fibrinolytic potential compared to the S2251 assay. In addition, since tPA or alteplase is commonly used as a thrombolytic therapy for treating acute thrombosis events, the annular clot lysis assay could be conducted as a clinical pilot test to predict patient response to the thrombolytic therapy. With a proper modification of the fibrin clot, for example, by including patient own plasma protein, red blood cells and platelets to form labeled platelet-free, platelet-rich plasma clots and whole blood clots, annular clot lysis assay can potentially optimize the dosing strategy prior to administering a treatment clinically.

The FITC-labeled annular clot lysis assay is a convenient method for a reliable assessment of sample fibrinolytic activity. The assay offers a real-time tracking of clot digestion where both a lag phase and a clot digestion rate can be identified and quantitatively compared. Based on these metrics, the present study has demonstrated the assay's capabilities of differentiating multiple fibrinolytic factors at physiological concentrations. In addition, the tagged clot substrate has long-lasting stability when stored at 4 °C for up to 8 weeks (**Figure 4.12**). Clot structures were monitored every week over 56 days through clot turbidity reads at 550 nm. Turbidity values tracked similarly across all groups. At RT, turbidity values started to decrease after 35 days and reached 30-50% of their starting turbidity at the end of the tested period. While 4 °C turbidity values showed no overall changes ($P < 0.05$) for 3, 7, 12 Physiologically relevant (PR) FhF clots and no more than 8% overall changes ($P < 0.05$) for control clots throughout indicating a stable clot structure in all groups over 56-days. As there were no stabilizer agents specifically added to these samples, it is likely that the reduced turbidity over time observed at RT is due to bacterial growth. To test this, an additional untagged fibrin clot was stored in 0.05% sodium azide and no reduction in turbidity was observed over 56-days (**Figure 4.12E**). Long-lasting stability of a tagged clot substrate greatly expands its utility especially under the fast-responding clinical setting as it does not need to be formed directly prior to use.

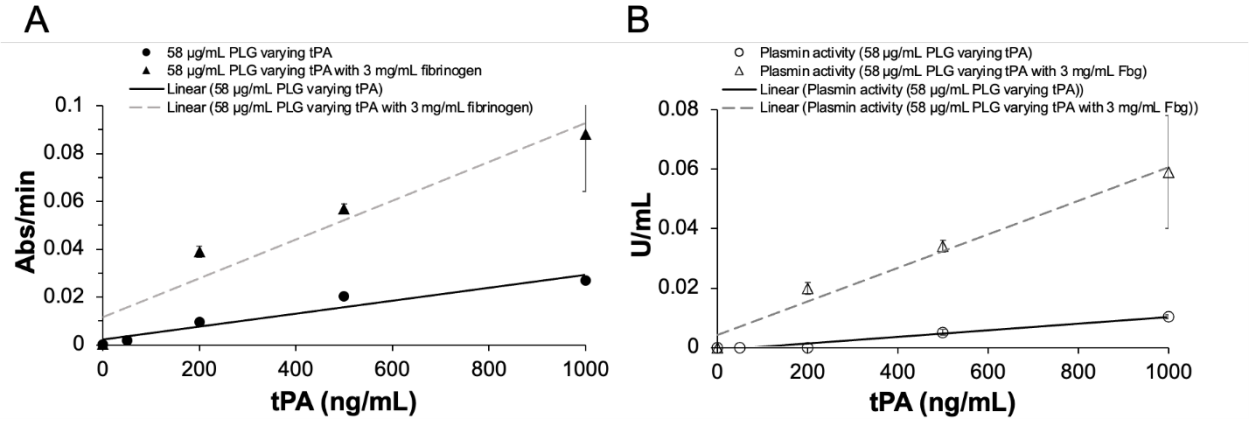

Figure 4.11. Comparing (A) digestion rates (initial velocity, abs/min) at 405 nm by S2251 assay and (B) converted plasmin activity at varying [tPA] (0, 200, 500, 1000 ng/mL) with or without 3 mg/mL fibrinogen at 37 °C.

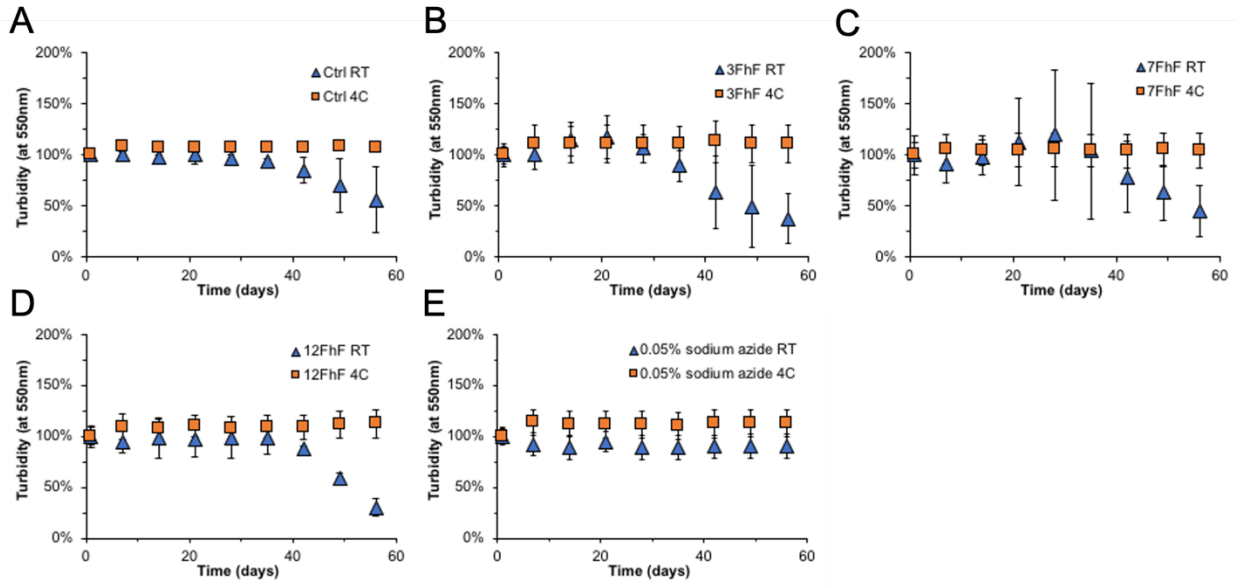

Figure 4.12. FITC-fibrin structural stability by clot turbidity (at 550 nm) over 8 weeks. Turbidity values were normalized by starting turbidity values of each sample. (A) Unmodified and (B, C, D) physiologically relevant 3, 7, and 12 FhF FITC-fibrin clots were formed in 96 well plates and stored at both RT and 4 °C to determine the long-term stability of the formed clots. Additional untagged fibrin clot was stored in (E) 0.05% sodium azide.

4.5 Conclusion

The annular clot lysis assay approaches a representative fibrinolytic process by utilizing a physiological relevant fibrin substrate with a concentration gradient-driven sample digestion. Formation of fibrin substrates at a known concentration enables the inter and intra test comparison of sample fibrinolytic potential. FITC labeling in the fibrin clot with a unique annular shape in the 96-well plate facilitate an easy-to-multiplex design to acquire fibrinolytic information of samples via a spectrometer (or fluorometer). By optimizing the fibrinogen: FhF ratio in the clotting mixture, the impact of FITC to fibrinogen conjugation on bulk fibrin properties such as clot strength and clot turbidity were minimized. Results demonstrated that the fibrinogen to FITC-fibrinogen ratios that mitigate deleterious effects associated with FITC tagging were at 10:1 for 3FhF, 30:1 for 7FhF, and 50:1 for 12FhF. SEM imaging results validated the similarity between 12FhF (50:1) and unmodified fibrinogen. Fibrinolytic activities of solutions containing different levels of plasmin were tested, both neat and physiologically relevant 12 FhF annular clot showed good limits of detection while neat 12FhF annular clots showed 19 times better sensitivity than its physiologically

relevant counterpart. It is also important to be aware that without additional modification, the annular clot lysis assay described here is not designed to diagnose sample fibrinolytic activities that is contributed by upper stream coagulant factors.

Fibrinolytic activities of solutions containing plasminogen and tPA were further examined, the physiological relevant 12 FhF annular clot lysis assay could differentiate digestion at varying fibrinolytic component levels or varying fibrin-binding affinity. Based on experimental results, the addition of > = 500 ng/mL external plasminogen activators is recommended to derive an expedient result for patient fibrinolytic potential diagnosis. In addition, the physiological relevant clotting formulation exhibits clots with properties akin to native clots that make it feasible to test clot structure under alternate diverse clotting conditions. For example, clotting conditions can be adjusted to mimic pathological conditions and FITC labeled fibrin can be utilized as a reporter to determine effects on coagulation and fibrinolysis stemming from the pathologic conditions. The tunable fibrin clot substrate itself or as a base of a tunable synthetic blood clot can be used to mimic clinical clot or thrombi structures to provide insights into the treatment for thrombosis at specific patient conditions. For instance, annular clots can be made at varying fibrinogen levels to help predict therapeutic dosage for patient with fibrinogen deficiency or hyper-fibrinogen levels as were seen in COVID-19 patients.[37, 38] The optimized FITC labeling fibrin(ogen) formula is also worth being introduced to studies that monitor FITC-fibrin digestion under a confocal microscopy because of its modest intensity and labeling homogeneity. Thrombolytic drug efficacy is usually examined in a 125I-fibrinogen contained plasma clot.[39, 40] The present assay is a better alternative for this type of study as FITC is a more accessible and less hazardous reporter compared to isotopic iodine.

4.6 References

[1] W. Lim, G. Le Gal, S.M. Bates, M. Righini, L.B. Haramati, E. Lang, J.A. Kline, S. Chasteen, M. Snyder, P. Patel, M. Bhatt, P. Patel, C. Braun, H. Begum, W. Wiercioch, H.J. Schünemann, R.A. Mustafa, American Society of Hematology 2018 guidelines for management of venous thromboembolism: Diagnosis of venous thromboembolism, Blood Advances 2(22) (2018) 3226-3256.

[2] P.S. Wells, D.R. Anderson, M. Rodger, M. Forgie, C. Kearon, J. Dreyer, G. Kovacs, M. Mitchell, B. Lewandowski, M.J. Kovacs, Evaluation of D-dimer in the diagnosis of suspected deep-vein thrombosis, New England Journal of Medicine 349(13) (2003) 1227-1235.
[3] E. Genton, A.P. Fletcher, N. Alkjaersig, S. Sherry, Assay of plasma thrombolytic activity with fluorescein-labeled clots, The Journal of laboratory and Clinical Medicine 64(2) (1964) 313-320.
[4] N.J.G. L A Moroz, A Rapid and Sensitive 125I-fibrin Solid-Phase Fibrinolytic Assay for Plasmin, Blood 46(4) (1975).
[5] G. Cesarman-Maus, K.A. Hajjar, Molecular mechanisms of fibrinolysis, British Journal of Haematology 129(3) (2005) 307-321.
[6] J.J. Wang, M.L. Baker, P.J. Hand, G.J. Hankey, R.I. Lindley, E. Rochtchina, T.Y. Wong, G. Liew, P. Mitchell, Transient ischemic attack and acute ischemic stroke: Associations with retinal microvascular signs, Stroke 42(2) (2011) 404-408.
[7] J.H. Wu, S.L. Diamond, A fluorescence quench and dequench assay of fibrinogen polymerization, fibrinogenolysis, or fibrinolysis, Anal Biochem 224(1) (1995) 83-91.
[8] M.H. Prins, J. Hirsh, A Critical Review of the Evidence Supporting a Relationship Between Impaired Fibrinolytic Activity and Venous Thromboembolism, Archives of Internal Medicine 151(9) (1991) 1721-1721.
[9] C.P.M. Hayward, How I investigate for bleeding disorders, International Journal of Laboratory Hematology 40(January) (2018) 6-14.
[10] C. Korninger, K. Lechner, H. Niessner, H. Gössinger, M. Kundi, Impaired Fibrinolytic Capacity Predisposes for Recurrence of Venous Thrombosis, Thrombosis and Haemostasis 52(02) (1984) 127-130.
[11] P. Toulon, Developmental hemostasis: laboratory and clinical implications, International Journal of Laboratory Hematology 38 (2016) 66-77.
[12] N. Mackman, R.E. Tilley, N.S. Key, Role of the Extrinsic Pathway of Blood Coagulation in Hemostasis and Thrombosis, Arteriosclerosis, Thrombosis, and Vascular Biology 27(8) (2007) 1687-1693.
[13] M.W. Mosesson, Fibrinogen and fibrin structure and functions, Journal of thrombosis and haemostasis : JTH 3(8) (2005) 1894-1904.
[14] Q. Hao, B.R. Dong, J. Yue, T. Wu, G.J. Liu, Thrombolytic therapy for pulmonary embolism, Cochrane Database of Systematic Reviews (12) (2018).

[15] G.A. Donnan, S.M. Davis, M.W. Parsons, H. Ma, H.M. Dewey, D.W. Howells, How to make better use of thrombolytic therapy in acute ischemic stroke, Nature Reviews Neurology 7(7) (2011) 400-409.
[16] V.F. Tapson, K. Sterling, N. Jones, M. Elder, U. Tripathy, J. Brower, R.L. Maholic, C.B. Ross, K. Natarajan, P. Fong, L. Greenspon, H. Tamaddon, A.R. Piracha, T. Engelhardt, J. Katopodis, V. Marques, A.S.P. Sharp, G. Piazza, S.Z. Goldhaber, A Randomized Trial of the Optimum Duration of Acoustic Pulse Thrombolysis Procedure in Acute Intermediate-Risk Pulmonary Embolism: The OPTALYSE PE Trial, JACC: Cardiovascular Interventions 11(14) (2018) 1401-1410.
[17] T. Urano, K. Sakakibara, A. Rydzewski, S. Urano, Y. Takada, A. Takada, Relationships between Euglobulin Clot Lysis Time and the Plasma Levels of Tissue Plasminogen Activator and Plasminogen Activator Inhibitor 1, Thrombosis and Haemostasis 63(01) (1990) 082-086.
[18] A. Ilich, I. Bokarev, N.S. Key, Global assays of fibrinolysis, International Journal of Laboratory Hematology 39(5) (2017) 441-447.
[19] T. Lisman, P.G. De Groot, J.C.M. Meijers, F.R. Rosendaal, Reduced plasma fibrinolytic potential is a risk factor for venous thrombosis, Blood 105(3) (2005) 1102-1105.
[20] W.B. Stubblefield, N.J. Alves, M.T. Rondina, J.A. Kline, Variable Resistance to Plasminogen Activator Initiated Fibrinolysis for Intermediate-Risk Pulmonary Embolism, PLOS ONE 11(2) (2016) e0148747-e0148747.
[21] J. Siudut, M. Grela, E. Wypasek, K. Plens, A. Undas, Reduced plasma fibrin clot permeability and susceptibility to lysis are associated with increased risk of postthrombotic syndrome, Journal of Thrombosis and Haemostasis 14(4) (2016) 784-793.
[22] M.E. Carr, L.L. Shen, J. Hermans, Mass–length ratio of fibrin fibers from gel permeation and light scattering, Biopolymers 16(1) (1977) 1-15.
[23] J. Jespersen, T. Astrup, A Study of the Fibrin Plate Assay of Fibrinolytic Agents, Pathophysiology of Haemostasis and Thrombosis 13(5) (1983) 301-315.
[24] N.J. Mutch, L. Thomas, N.R. Moore, K.M. Lisiak, N.A. Booth, TAFIa, PAI-1 and α2-antiplasmin: Complementary roles in regulating lysis of thrombi and plasma clots, Journal of Thrombosis and Haemostasis 5(4) (2007) 812-817.
[25] V. Binder, B. Bergum, S. Jaisson, P. Gillery, C. Scavenius, E. Spriet, A.K. Nyhaug, H.M. Roberts, I.L.C. Chapple, A. Hellvard, N. Delaleu, P. Mydel, Impact of fibrinogen carbamylation on fibrin clot formation and stability, Thromb Haemost 117(5) (2017) 899-910.

[26] Z. Zeng, M. Fagnon, T. Nallan Chakravarthula, N.J. Alves, Fibrin clot formation under diverse clotting conditions: Comparing turbidimetry and thromboelastography, Thrombosis Research 187(January) (2020) 48-55.
[27] Z. Zeng, T.N. Chakravarthula, N.J. Alves, Leveraging turbidity and thromboelastography for complementary clot characterization, Journal of Visualized Experiments 2020(160) (2020) 1-7.
[28] D.A. Armbruster, T. Pry, Limit of blank, limit of detection and limit of quantitation, The Clinical biochemist. Reviews 29 Suppl 1(August) (2008) S49-52.
[29] J.-H. Wu, S.L. Diamond, Fluorogenic Fibrinogen and Fibrin Facilitate Macromolecular Assembly and Dynamic Assay of Picomolar Levels of Plasminogen Activators under Well Mixed Conditions, Thrombosis and Haemostasis 74(02) (1995) 711-717.
[30] T.W. Stief, R. Bünder, A. Richter, B. Maisch, H. Renz, J. Fareed, In vitro simulation of therapeutic plasmatic fibrinolysis, Clinical and Applied Thrombosis/Hemostasis 9(3) (2003) 211-220.
[31] S.L. Diamond, Engineering design of optimal strategies for blood clot dissolution, Annual Review of Biomedical Engineering (1) (1999) 427-461.
[32] D.V. Sakharov, J.F. Nagelkerkel, D.C. Rijken, Rearrangements of the fibrin network and spatial distribution of fibrinolytic components during plasma clot lysis: Study with confocal microscopy, Journal of Biological Chemistry 271(4) (1996) 2133-2138.
[33] S.L. Diamond, S. Anand, Inner clot diffusion and permeation during fibrinolysis, Biophysical Journal 65(6) (1993) 2622-2643.
[34] T. Astrup, S. Müllertz, The fibrin plate method for estimating fibrinolytic activity, Archives of Biochemistry and Biophysics 40(2) (1952) 346-351.
[35] J. Giedrojć, A. Stankiewicz, M. Walkowiak, M. Galar, M. Bielawiec, Tissue plasminogen activator and plasminogen activator inhibitor in aqueous humor, Klinika oczna 98(4) (1996) 283-285.
[36] S.M. Arcasoy, J.W. Kreit, Thrombolytic Therapy of Pulmonary Embolism, Chest 115(6) (1999) 1695-1707.
[37] M. Panigada, N. Bottino, P. Tagliabue, G. Grasselli, C. Novembrino, V. Chantarangkul, A. Pesenti, F. Peyvandi, A. Tripodi, Hypercoagulability of COVID-19 patients in intensive care unit: A report of thromboelastography findings and other parameters of hemostasis, Journal of Thrombosis and Haemostasis 18(7) (2020) 1738-1742.

[38] J.M. Connors, J.H. Levy, COVID-19 and its implications for thrombosis and anticoagulation, Blood 135(23) (2020) 2033-2040.
[39] P.J. Burck, D.H. Berg, M.W. Warrick, D.T. Berg, J.D. Walls, S.R. Jaskunas, R.M. Crisel, B. Weigel, C.J. Vlahos, D.B. McClure, B.W. Grinnell, Characterization of a modified human tissue plasminogen activator comprising a kringle-2 and a protease domain, Journal of Biological Chemistry 265(9) (1990) 5170-5177.
[40] J.-C. Murciano, A.A.-R. Higazi, D.B. Cines, V.R. Muzykantov, Soluble urokinase receptor conjugated to carrier red blood cells binds latent pro-urokinase and alters its functional profile, Journal of Controlled Release 139(3) (2009) 190-196.

5. EFFECT OF CHANDLER LOOP SHEAR AND TUBING SIZE ON CLOT ARCHITECTURE

One version of this chapter was currently under review at a peer-reviewed journal as a publication entitled “Effect of Chandler Loop Shear and Tubing Size on Thrombus Architecture”.

Native thrombi comprise different levels of fibrin, RBCs and platelets due to variations in hemodynamics, pathologies and patient-specific blood conditions. The diversity of thrombus structure has resulted in the clinical use of thrombolytic agents at different therapeutic dosage and through distinctive delivery methods.[1] This fact enlightens the modeling of clot substrates that have varying component composition and distribution. The Chandler loop is an *in-vitro* clot formation device, which has been extensively used to examine thrombogenicity of prosthetic materials.[2-4] Clots formed in the Chandler loop have shown good resemblance to native thrombi.[4, 5] A Chandler loop apparatus is made by joining and sealing open ends of a tube, in which non-anticoagulated whole blood is partially filled. Vertically rotating the loop in a 37 °C water bath, the internal liquid flows relative to the tubing to mimic a physiological shear flow. An array of clot structures can be achieved by mixing blood components at different levels and under different wall shear rates in the loop. The flow dynamics in this model have been previously defined and a shear rate can be easily derived using the rotating velocity and tube geometry.[6, 7] Thus, this chapter explores conditions in a Chandler loop to fabricate diversified arterial or venous clot substrate with good physiological relevance.

5.1 Abstract

Thrombosis is the pathological formation of blood clots that can lead to a wide variety of life-threatening circumstances. Thrombolytic drugs that offer direct clot dissolution can be prescribed to patients who have ischemic strokes and pulmonary embolisms. As current drug screening models often poorly predict drug profiles, leading to failure of thrombolytic therapy or clinical translation, more representative clot substrates and systems are necessary for evaluating novel thrombolytic candidates. Utilizing a Chandler loop device to form clot analogs has gained popularity in stroke societies in recent years. However, clot analogs are commonly formed at high shear to resemble stroke thrombi while low shear conditions are often overlooked. Additionally,

clot micro-structure as it relates to shear conditions have not been fully addressed. In this study, we characterized the impact of shear (126 to 951 s^{-1}) on clot properties in the Chandler loop. Tubing loops were partially filled (50%) with recalcified citrated blood and spined at 20-60 revolutions per minute for 40 min. To expand the utility of the Chandler loop for various thrombosis applications, multiple tubing sizes (3.2 to 7.9 mm) were employed facilitating creation of different sized clots. Formed clot samples were further characterized by histology and scanning electron microscopy (SEM). In summary, clot properties showed shear-dependent variations. Increased shear resulted in unaffected WBC counts, decreased RBC counts (76.9 ± 4.3% to 17.6 ± 0.9%) and increased total fibrin (10 to 60%) based on clot histology. Increased fibrin sheet morphology and platelet aggregates were also observed at a higher shear under SEM. In addition, using larger diameter tubing resulted in larger clots with smaller tubing occlusion (63.5% to 34.6%). These results show the significant impact of shear rate and tubing size on resulting clot properties and demonstrate the capability of forming a variety of *in-vivo*-like clot analogs in the Chandler loop device.

5.2 Introduction

Varying shear conditions in blood circulation can result in the formation of thrombi with diversified clot compositions. Components of these thrombi comprise heterogenous fibrin morphology and packed cellular networks such as polyhedral red blood cells (RBCs) and platelet aggregates that often result from patient-specific physiology.[8] Formation of such structures can challenge the efficacy of a standard thrombolytic therapy leading to high risk-benefit ratios in circumstances such as deep venous thrombosis (DVT).[9] This calls on evaluating novel drug candidates, or therapeutic regimens, using a representative drug target or system that can incorporate these properties. While animal blood clot models have enhanced the understanding of thrombosis, the cost for use of human comparable large animal models are significant and small animals, such as rodents, are not optimal for drug development as their hematological composition deviates considerably from that of humans.[10] Utilizing artificial human blood clots to study thrombolysis has attracted growing research interests in recent years.[11-13] These clot substrates formed at physiologically relevant flow conditions are believed to better capture the dynamic nature of the *in-vivo* thrombi and offer more accessible and representative results for use in thrombolytic drug screening.

A Chandler loop apparatus is a validated tool that has previously demonstrated its capability of forming artificial clots that resemble native thrombi.[4, 14, 15] The apparatus consists of a hollow tube with ends joined to form a continuous loop, wherein the tubing is typically filled with 30% to 70% fluid (**Figure 5.1**). Rotating the tubing about its center creates a torsion gradient that drives internal fluid flow against the rotational direction allowing for control over shear by adjusting tubing geometry and rotational rate. Clots formed in this device are commonly subjected to high shear yielding a structure that consists of a platelet-rich head and fibrin-rich tail, resembling the morphology of thrombi in stroke patients.[4, 16] Although shear has a known effect on clot composition within native blood, it has not yet been thoroughly characterized in the Chandler loop apparatus under low shear conditions (< 500 s^{-1}) where venous thrombi are commonly formed. Tubing size is another important device parameter that is often overlooked despite the knowledge that lumen size-dependent flow effects, such as platelet margination and cell-free layer thickness, can contribute to clot diversity.[17, 18] Characterizing these device conditions for making artificial clots can extend the usage of the Chandler loop in preclinical drug development applications and improve the reproducibility of clots formed utilizing the device.

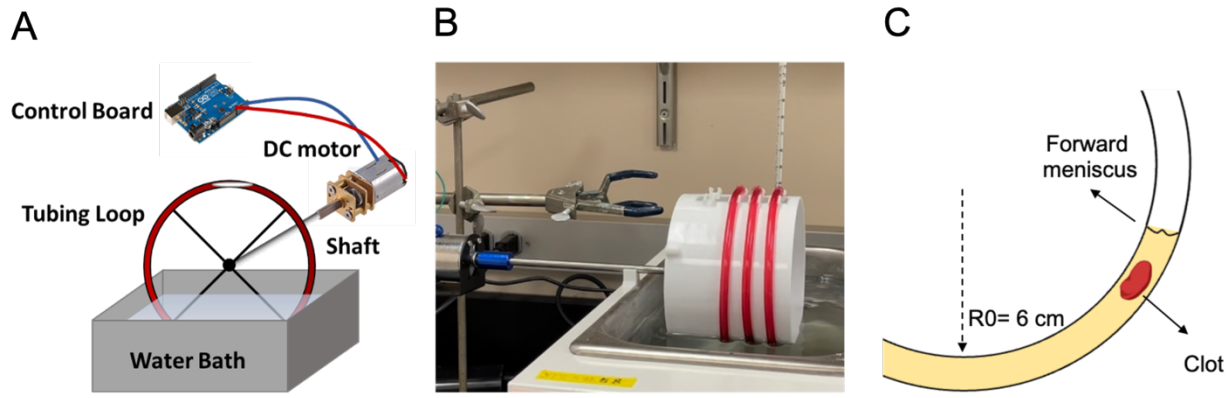

Figure 5.1. (A) Schematic representation of the Chandler loop setup. (B) A photo of the assembled Chandler loop apparatus with blood running in the device. (C) Illustration depicting clot formation within the Chandler loop at the forward meniscus.

In this study, we explored how tubing size and shear rate, affect clot formation in the Chandler loop device. We compared clot weight, size, histological composition, and component distribution across nine groups comprising three tubing inner diameters (3.2, 4.8, and 7.9 mm) and

three rotational rates (20, 40, and 60 RPM), whose corresponding shear rates are from 126 to 951 s^{-1} (6 groups <500 s^{-1}). In addition, scanning electron microscopy (SEM) was utilized to examine clot micro-architecture and identified shear-dependent morphology of clot components. These results reveal a significant impact of tubing size and shear rates on resulting clot properties - demonstrating the capability of forming a wide variety of *in-vivo-like* clot analogs by modulating very simple and highly controllable clot forming parameters using the Chandler loop device. This level of control over resulting clot characteristics is not possible when utilizing purely animal thrombosis models which often makes pharmaceutical drug optimization more complicated.

5.3 Materials and Methods

5.3.1 Materials

Sodium citrate, calcium chloride, and 10% Neutral Buffered Formalin (NBF) were purchased from Sigma (St. Louis, MO). Glutaraldehyde was purchased from Fisher Scientific (Hampton, NH). Tygon® ND 100-65 medical tubing was purchased from U.S. Plastic Corp (Lima, OH). Martius Scarlett Blue (MSB) staining kit was purchased from Avantik (Pine Brook, NJ). Animal use and care in this study was approved by the IACUC at the Indiana University School of Medicine. Ossabow swine was kept on anesthesia and mechanical ventilation during blood draw using a protocol described previously.[19] Venous blood with a 33% hematocrit was collected through the jugular vein using an 18-gauge needle into a syringe that was prefilled with 3.2% sodium citrate at a 1:9 anticoagulant to blood ratio.

5.3.2 Chandler Loop Clot Formation

A vertical Chandler loop apparatus was assembled using a DC motor (100 RPM Max) and a 3D printed spool (Creality 3D printer). A potentiometer and 12 V power supply were connected into the circuit to adjust the motor speed to provide for varying rotational rates. Clots were formed in three tubing sizes at three rotational rates each. Tubing inner diameters (R) are S = 4/32” (3.2 mm), M = 6/32” (4.8 mm), L = 10/32” (7.9 mm). Rotational rates (ω) are 20, 40, and 60 RPM. In these experiments, all tubing lumens were filled to 50% volume of blood which are 1.5, 3.4 and 5.4 mL corresponding to the three tubing sizes. To initiate clot formation, fresh citrated blood was recalcified with 11 mM calcium chloride and transferred into the tubing. Tubing was immediately

end-joined and fixed by an inner diameter to outer diameter fitted tubing segment to form a loop with a 6 cm radius of curvature (R_0). Tubing loops were then put on the spool and rotated for 40 minutes partially submerged in a 37 °C water bath. All clot formation variations were completed in a single day within three hours of blood collection. Shear rates ($\dot{\gamma}$) were calculated by an equation shown below derived using a straight tube laminar approximation.[20]

$$\dot{\gamma} = \frac{2\pi R_0 \omega}{15R}$$

5.3.3 Clot Properties and Histology

Resulting clots were gently blotted, weighed and their dimensions were measured for comparison. One clot from each group was placed in 1.5 mL of 10% NBF at RT overnight. Paraffin embedment, sectioning, and hematoxylin and eosin (H&E) staining were performed by the Indiana University School of Medicine histology core using a standard tissue-processing protocol.[21] Clot samples were cut into sections of 2 μm thickness. One slide of each group was further stained with MSB staining kit to identify platelet-rich regions of thrombi in addition to RBCs, white blood cells (WBCs), and fibrin. Images of the samples were scanned at 40X on a Zeiss Axio Scan microscope. Higher definition photos at spots of interests were taken at 40X for detailed comparison on a Leica CME microscope. Clot compositions were quantitatively analyzed using ImageJ.

5.3.4 Scanning Electron Microscopy

SEM samples were prepared and processed as described previously.[22] Clots from each group were treated in 2.5% glutaraldehyde followed by an overnight lyophilization (FreezeZone 2.5, Labconco). Dehydrated samples were subsequently sputter coated with gold (Denton Vacuum Desktop V) for 30 seconds at $3*10^{-4}$ Torr to obtain a ~10 nm gold coating for SEM. Clot micro-structural images were taken using a field emission scanning electron microscopy (JSM-7800F, JEOL) at the Integrated Nanosystems Development Institute at Indiana University Purdue University Indianapolis. An acceleration voltage of 5 kV was applied for all samples.

5.3.5 Statistical Analysis

Data is described as mean ± standard deviation. Means were compared using Student's t-test (equal sample size) or Welch's t-test (unequal sample size) and statistical significance was reported at P-values < 0.05.

5.4 Results

5.4.1 Clot Formation

Nine conditions were tested to form 3 to 4 replicates of clot analog for each condition on two identical Chandler loop apparatuses using venous blood from a single donor (Ossabow swine). In all groups, blood was able to spontaneously flow against the direction of the rotating tubing throughout the duration of the clotting process with clot formation occurring at the forward meniscus. After clotting, the remaining serum volume was measured, revealing a range of 75 - 86% of the starting blood volume across all groups. In addition, no apparent hemolysis was found by comparing the morphology of RBCs in the remaining liquid with those in the fresh blood (**Figure 5.2**).

5.4.2 Clot Appearance and Weight

To examine clot appearance, clot samples were collected, gently blotted, weighed, and transferred into petri-dishes. At higher rotational rates and smaller diameter tubing (higher shear), clots appeared to be smaller, paler, and more uniform in color. At lower rotational rates and larger diameter tubing (lower shear), clots were larger, darker, and heterogenous. The smallest clots were formed at S60 while the largest clots were at L20 (**Figure 5.3**). To quantitatively analyze morphological differences, clot dimensions were measured using ImageJ, clot volume and cross-sectional areas were measured utilizing calipers. The resulting clot diameter was more significantly impacted by tubing size than rotational rate (RPM). Specifically, tubing occlusion was calculated by taking a ratio of the cross-sectional area of the clot to the cross-sectional area of tubing lumen. Occlusion percentages showed significant differences ($P < 0.05$) which were 63.5 ± 13.1% in the small sized, 46.5 ± 13% in the medium sized, and 34.6 ± 15.9% in the large sized tubing. Although larger diameter tubing often led to clots with larger radii, our results indicated that clot radius is not linearly proportional to the lumen size. Clot weights were further compared, indicating a large

range from 50 to 800 mg with the most massive clot formed at the slowest RPM inside the largest tubing. The variation in clot mass may also be in part due to the different blood volumes prefilled into the tubing. For example, clots formed at M60 were 1.8 times heavier ($P < 0.05$) than those formed at S40 despite these two conditions having the same calculated shear rate. Importantly, 50% lumen fill was selected in each group since using one volume may result in flow inconsistency across the wide tubing size range used in this study. However, in tubing sizes where identical blood volumes were employed, clot weight showed a significant reduction at an increased RPM ($P < 0.05$) demonstrating that high RPM, or high shear, can cause the reduction of clot weight.

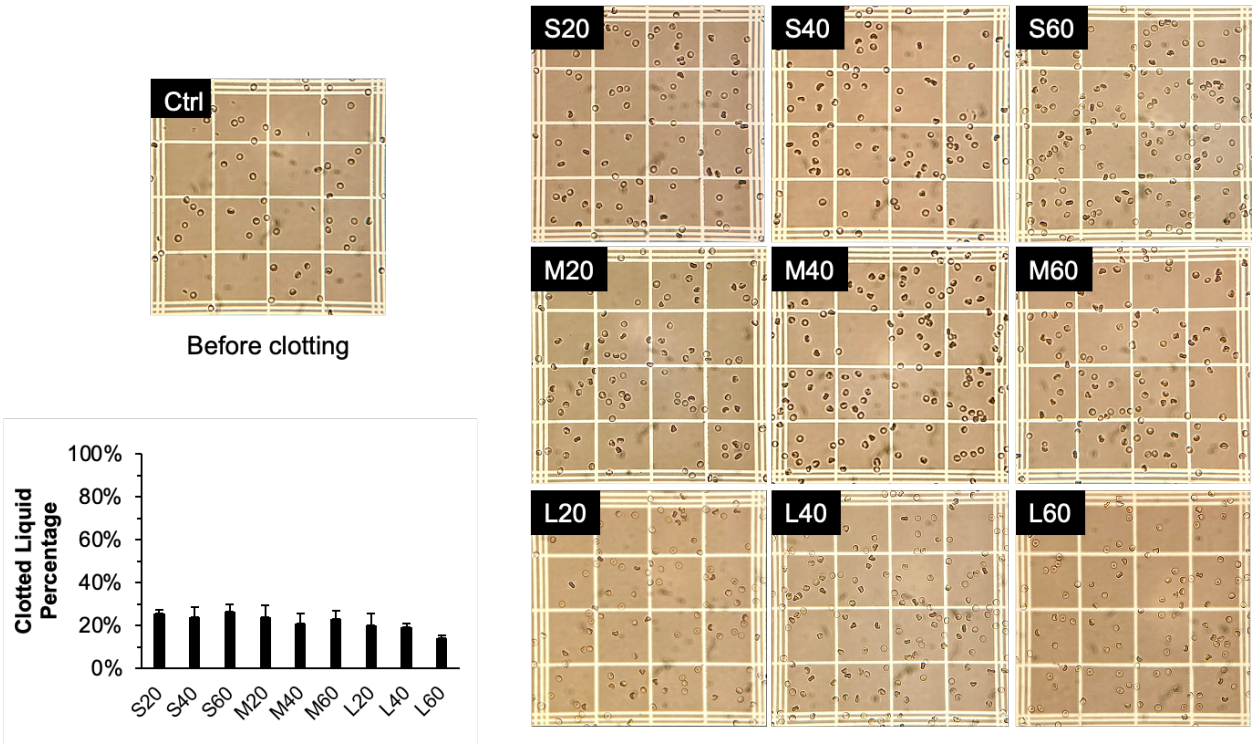

Figure 5.2. Images showing RBC morphology before and after clot formation in a hemacytometer (Bright-Line™ Hemacytometer). For RBC images after clot formation, remainder clot-free solution samples were 1:200 diluted in formalin citrate, which is an isotonic solution to preserve RBC morphology. In addition, clotted liquid volume was measured and showed an overall consistent volume ratio with respect to total solution before solution.

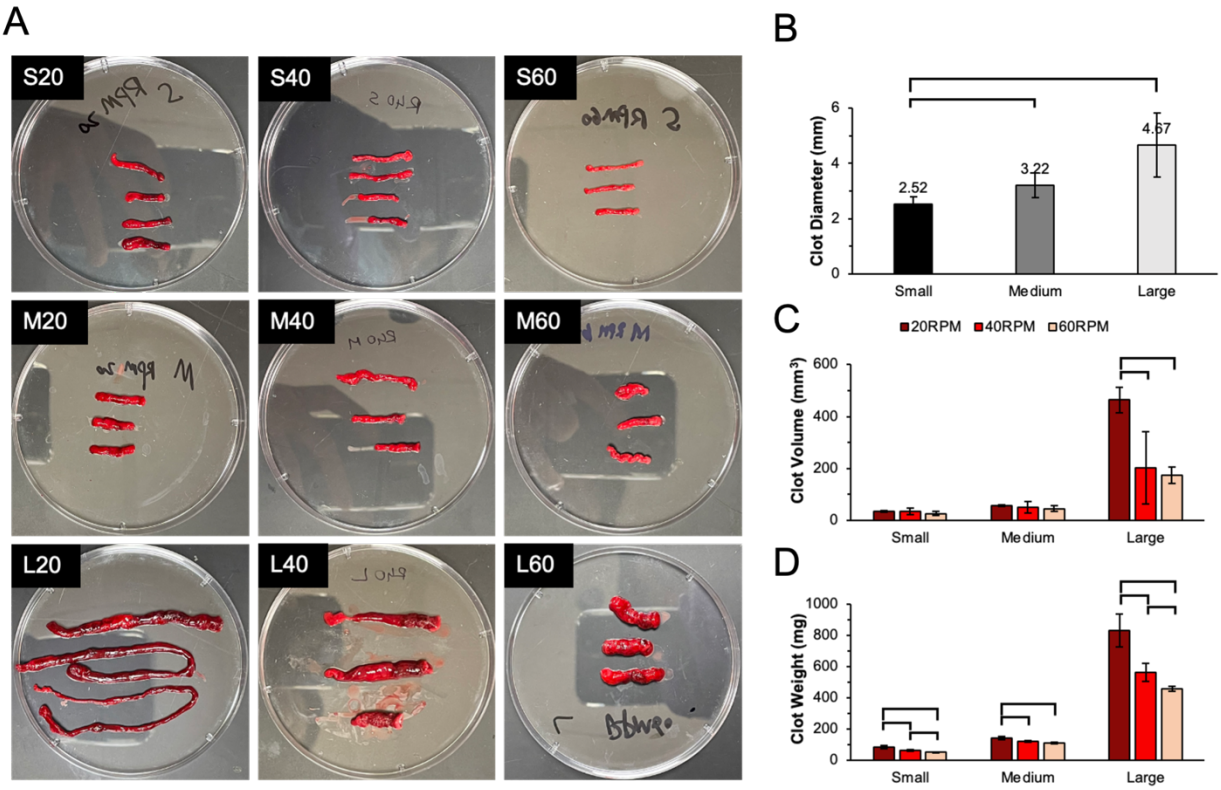

Figure 5.3. (A) Comparison of clot samples across nine groups. Clots formed at S-small, M-medium, and L-large tubing (top to bottom) at 20, 40 and 60 RPM (left to right). (B) Comparison of the average clot diameters formed in different diameter tubing. Comparison of (C) clot volume estimated through clot appearance using ImageJ and (D) clot weight across groups. Brackets denote significant differences between groups.

5.4.3 Histologic Composition

Clots made in the Chandler loop were better than statically formed clots in capturing *in-vivo* thrombi composition and component distribution as the latter clots formed in the absence of shear provide only homogenous structures.[23] One clot sample was selected from each group to be paraffin-embedded, sectioned, and stained with both H&E and MSB for subsequent analysis of clot composition as it is affected by shear and tubing size. Under H&E staining, WBCs (stained in blue), RBCs (stained in red), and fibrin (stained in pink) were differentiated (**Figure 5.4A**). WBCs resided mostly in the fibrin (stained in pink) regions accounting for less than 3% of clot volume in all clot samples made in this study, which was consistent with the percentage found in native thrombi.[24, 25] To better compare RBCs and fibrin distribution, three related structural patterns were identified which comprise stacked RBC regions, fibrin-rich regions, and RBC-infiltrated

fibrin regions (**Figure 5.4B, 5.4C and 5.4D**). Due to the employment of different blood volumes at different tubing diameters, the presence of these patterns was primarily compared across different shear rates within the same tubing size. Stacked RBC regions showed a reduction at higher RPM in all tubing groups. Fibrin-rich regions (light pink) defines a specific clot structure composed of high-density fibrin. They were seen most in clot heads and tails as was reported by other studies.[4, 26] In all tubing sizes, more fibrin-rich regions were observed at higher RPM. RBC infiltrated fibrin regions did not show a deviation in small and medium tubing groups while a significantly lower RBC infiltrated fibrin region was observed in L20 than L40 or L60 ($P < 0.05$), which was attributed to the low wall shear condition (126 s^{-1}). In summary, an increased rotational rate results in increased fibrin-rich regions and decreased stacked RBCs.

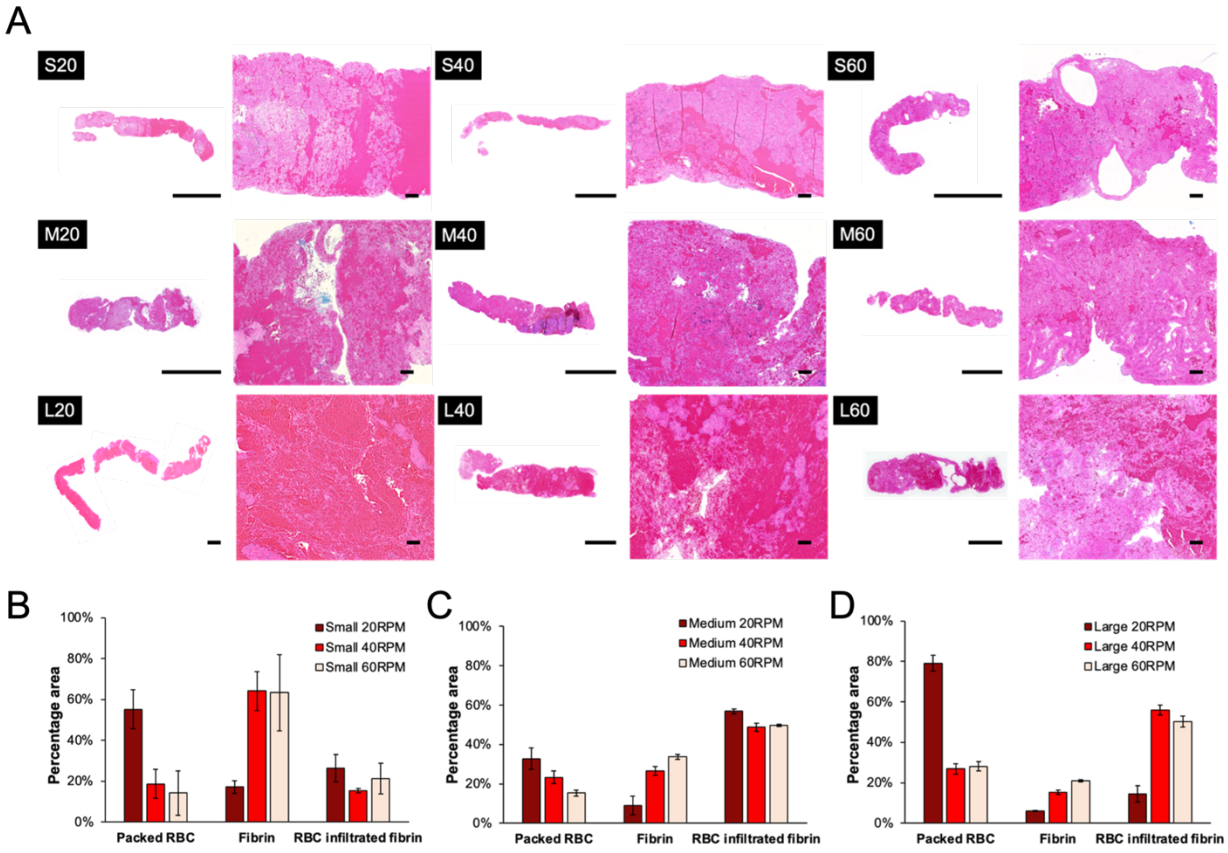

Figure 5.4. (A) Gross and 5X H&E photos of representative clots. WBCs (blue), RBCs (red), fibrin (pink). Scale bars are 5 mm in gross photos and 200 µm in 5X images. Comparing the percent area of packed RBC, fibrin-rich, and RBC infiltrated fibrin in clot samples formed at different RPMs in (B) small, (C) medium, and (D) large diameter tubing. Detailed measurements highlighting these regions of interests were included in Figure A.19.

5.4.4 Shear Effects on Clot Composition

Apart from the analysis of three defined clot structural patterns, individual components in clots were further compared based on clot forming shear rates. Therefore, data was combined and reorganized into three categories to better illustrate the effect of shear on overall clot compositions. Three shear bins were created, representing low (0 – 300 s^{-1}; composed of L20, L40 and M20 tubing), medium (300 – 500 s^{-1}; composed of L60, M40 and S20) and high shear (> 500 s^{-1}; composed of M60, S40, and S60) (**Figure 5.5**).

Fibrin and platelets were examined using H&E and MSB staining. Fibrous fibrin network and porous fibrin were able to be differentiated using light microscopy. Porous fibrin was more frequently present at higher shear conditions. MSB staining has been regarded as the standard criterion for assessing platelet-rich regions.[11] Platelets were shown as gray granules in MSB images (**Figure 5.5**). At low shear rates (**Figure 5.5A**), platelets were uniformly sized and shaped, densely packed, and restricted in islands of fibrin. At high shear (**Figure 5.5C**), platelets tended to be heterogeneous in size and mainly resided near the fibrin bundle junctions or near the edge of fibrin pores. The increased prevalence of these fibrin structures in clots formed at high shear provides for incorporation of a large number of platelets resulting in a generally fibrin and platelet-rich clot. At medium shear (**Figure 5.5B**), the distribution of platelets comprised an equal mix of same-sized platelets found in densely packed fibrin sheets and highly contracted platelets found in the fibrous-fibrin structures. These observations could be directly attributed to platelet conformational changes in response to different shear conditions.[27]

A quantitative analysis of WBC and RBC occupied area in these clots was also performed. Comparing to the weak trend of WBC percentage, area occupied by RBC showed an explicit negative correlation against the shear rate ($R^2 = 0.9298$). Specifically, RBC percent area ranged from 17.6 ± 0.9% in S60 (highest shear) to 76.9 ± 4.3% in L20 (lowest shear, $P < 0.05$) (**Figure 5.6)**. Similar to the fact that different shear rates lead to RBC-poor or RBC-rich native thrombi formation, varying shear in the Chandler loop device also resulted in clots with different amounts of RBCs.

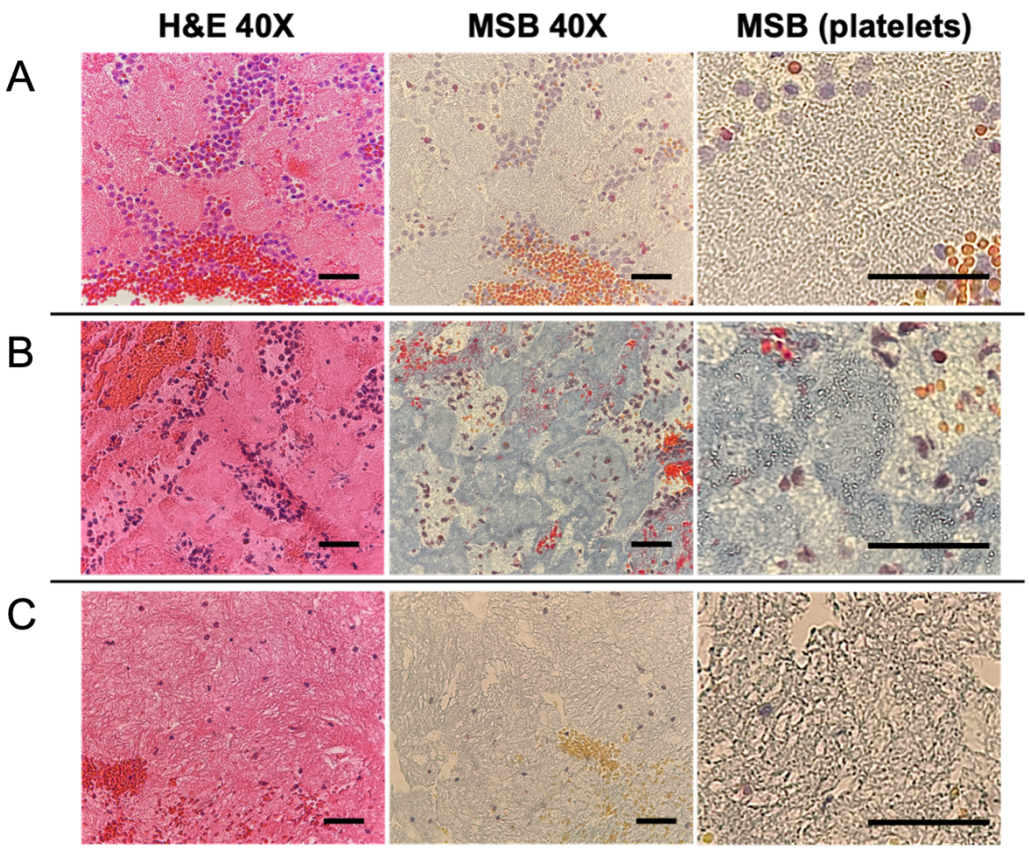

Figure 5.5. Histology photos of representative clot samples at (A) low, (B) medium, and (C) high shear rates. From left to right: photos of identical spots in the fibrin-rich region under H&E versus MSB at 40X and zoomed MSB platelet-specific regions. H&E stains: WBCs (blue), RBCs (red), fibrin (pink). MSB stains: WBCs (purple), RBCs (yellow or red), fibrin (blue or red), platelets (gray). Red arrows indicate platelets in MSB (platelets) photos. Scale bars are 5 mm for photos in the first column, 200 µm for the second column and 50 µm for the rest. Remainder clot sample photos are listed in Figure A.20.

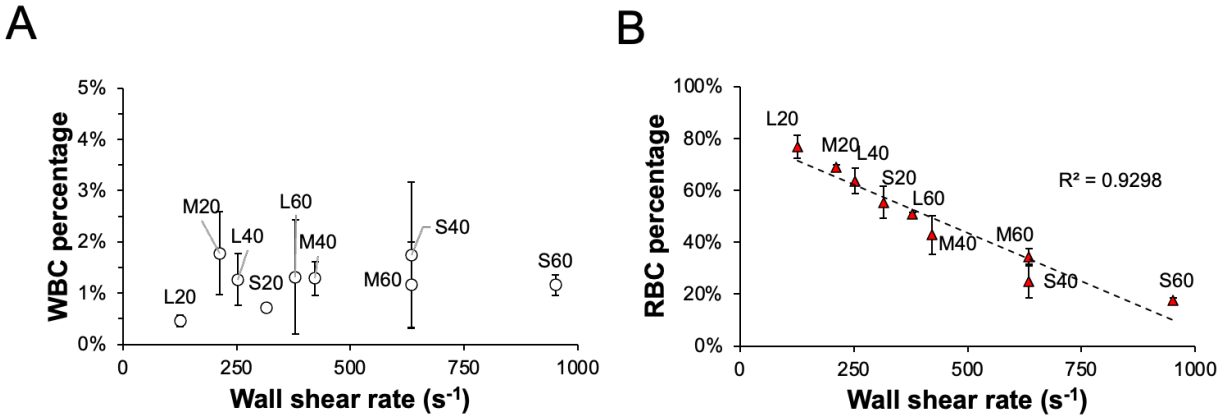

Figure 5.6. (A) WBC and (B) RBC percentage area in clots are shown over shear rates. Linear regression was plotted by RBC percentage area over increased shear rates.

5.4.5 Scanning Electron Microscopy

Native thrombi micro-structures are affected largely by thrombosis pathogenesis. A recent SEM study has reported varying compositions of micro-structures in arterial, venous, and pulmonary thrombi/emboli.[8] To further demonstrate the resemblance of clots formed in the Chandler loop device to those described clinically, SEM images of clot samples were taken to provide for a complimentary structural analysis in addition to clot histology.

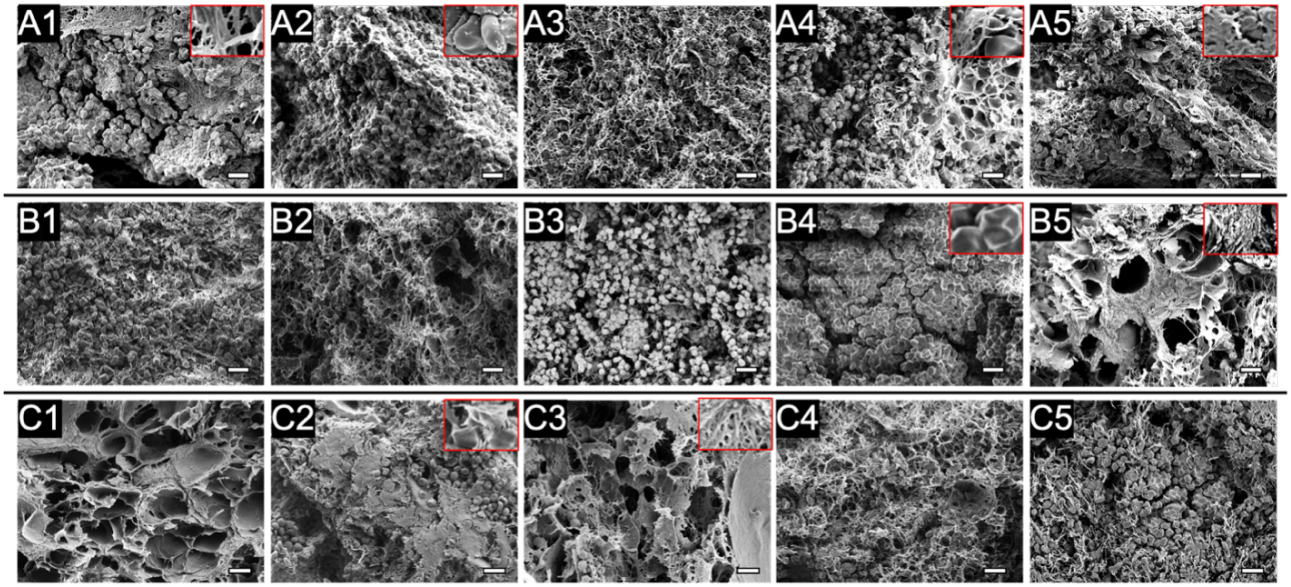

Figure 5.7. Representative SEM images of clots formed at (A1-A5) low, (B1-B5) medium, and (C1-C5) high shear in each row. In each row, structures were ranked based on their high-to-low presence frequency in the sample groups, for example, A1 is the most common structure in the low shear group. Images were taken at 1000 X and spots of interests were shown at 2000X in selected images. Scale bars are 10 μm in these graphs.

Clot samples processed for SEM were sliced in the longitudinal direction to better visualize underlying clot structure.[28] This was necessary as the clot surface was covered with a thin fibrin film preventing direct visualization of internal clot morphology using intact clots. Samples were grouped into three shear levels and representative SEM images were ranked based on their presence frequency and shown accordingly (**Figure 5.7**). Fibrin in these clots revealed a large variety of shear-dependent morphologies. Fibrin sponge (**Figure 5.7-C1,** taken at S60 clots), sheet (**Figure 5.7-C3**, taken at M60 clots), and bundles (**Figure 5.7-C4**, taken at S40 clots) are the

dominant motifs present at high shear compared to fibrin fibers at low (**Figure 5.7-A3**, taken at M20 clots) and medium (**Figure 5.7-B2**, taken at S20 clots) shear.

RBCs also showed shear-dependent morphology variations at select shear levels. Packed RBCs were observed at all shear levels under histology with these aggregating structures more clearly resolved under SEM. Importantly, RBCs were shown to be associated with minimal fibrin at low shear (**Figure 5.7-A1 and A2**, taken at L20 clots) but were largely infiltrated with fibrin fibers at medium (**Figure 5.7-B1 and B3**, taken at L20 and M40 clots) and high (**Figure 5.7-C5**, taken at M60 clots) shears. Within the packed structure, RBCs were further identified as biconcave-like (**Figure 5.7-A2**, taken at L20 clots) and polyhedral shapes (**Figure 5.7-B4 and C5**, taken at S20 and M60 clots) and quantified using a similar method published previously (1). The predominant RBC shape was determined in a 10X 10 μm grid in 8 to 12 SEM photos that contains RBCs for each sample. Area fractions of the predominant shape to total RBCs occupied area were derived and compared across samples. Significantly more biconcave-like RBCs (28.6% ± 14.9% of total RBCs) were observed at shear rates below 500 s^{-1} compared to only 10.2% ± 1.6% at shear rates above 500 s^{-1} ($P < 0.05$). Platelets are another clot component that was identified. More platelet aggregates (**Figure 5.7-C1**, taken at S60 clots) were resolved at high shear showing their preferrable residence in between the fibrin sheet layers. On the other hand, at low shear, very few platelets were found - most of which were surrounded by abundant RBCs (**Figure 5.7-A5**, taken at L20 clots). In all, micro-structures and compositions of the formed clot analogs showed good resemblance to *in-vivo* thrombi, making them good candidates for use in thrombolytic drug testing.

5.5 Discussion

Presented here is a study that examines a wide range of shear impacts on clotting and formation of diversified clot analogs using the Chandler loop device incorporating both tubing size and rotational rate variations in the analysis. Through adjusting the tubing size and rotational rate, clot size, weight, morphology, and component distribution can be precisely tuned with a high level of reproducibility, which has not been significantly addressed thus far in the literature. Formed clot samples were significantly different across experimental groups; however, properties of in-group replicates were highly consistent showing only minor variation. This was confirmed by small standard deviations demonstrating the Chandler loop's high reproducibility in fabricating *in-vivo*-like clot analogs (**Figure 5.3**). Shear rates used for this study were not sufficiently high as we

did not see significant disruption of the RBC membrane. Importantly, the device curvature radius was carefully selected so that the calculated shear rate values using the laminar approximation are also consistent with results derived using an empirical equation provided by a previously conducted numerical Chandler loop simulation. Shear rates calculated by the two methods are compared (**Figure 5.8**). [29]

	20RPM	40RPM	60RPM	20RPM	40RPM	60RPM
	Laminar flow (Gardner et al. eqn)			Dean flow considered (Touma et al. eqn)		
4/32"	315	634	951	317	617	899
6/32"	212	422	634	212	420	623
10/32"	126	253	379	127	254	379

Laminar flow approximation:

$$\tau_w = \frac{2\pi R_0 w \mu}{15R}$$ *(Gardner et al., 1974)*

R_0: Loop curvature radius R: Tubing inner radius
w: Rotational rate μ: Blood viscosity

Numerical solution:

$$De = \sqrt{\frac{2R}{R_0}} * Re$$

$$\frac{\bar{\varepsilon}\delta}{\omega} = -0.0039\left(\frac{\mathrm{De}^*}{(100\delta)^3}\right)^2 - 0.0208\frac{\mathrm{De}^*}{(100\delta)^3} + 2.6946$$ *(Touma, 2014)*

$$\tau_w = \frac{\bar{\varepsilon}\delta}{\omega} * \frac{\pi R_0}{20R} * w$$

Figure 5.8. Shear rates calculation at nine different Chandler loop conditions (20, 40 and 60 RPMs, and small, medium, and large tubing inner diameters) using an equation derived from laminar flow assumption by Gardner et al.[7] vs an empirical equation derived by computational simulating Chandler loop published by Touma et al.[29]

An increased shear rate resulted in the formation of a clot with decreased RBCs, packed RBC structures and fibrin fibers, increased total fibrin, fibrin sheets and platelets based on both histology and SEM results. WBCs percentage in clots appeared to be unaffected by varying shear conditions. RBC aggregation is a notable phenomenon at low shear, or stasis, that contributes to increased viscosity and hydrodynamic resistance in blood circulation.[30] The formation of stacked RBC structures at low shear flow conditions confirmed that the Chandler loop device can fabricate clots that resemble venous thrombi. While at higher shear, a higher fraction of rigid polyhedral RBC cellular conformation was observed that is indicative of a much tighter clot structure which was also visualized in patient thrombi samples.[8, 30] In addition, high shear promotes the formation of fibrin sheets, bundles, and sponges compared to only fibrin fibers at lower shear conditions. Although this difference in morphology has been previously addressed in

in-vitro fibrin only formation studies, our results confirmed that incorporating other blood components such as platelets and RBCs enhanced the shear impact on fibrin morphology.[31] Tubing size was also found to significantly affect clot properties. Increasing tubing size resulted in a larger clot radius with varying proportions to tubing inner radius. Additionally, shear conditions (126 – 980 s^{-1}) and tubing sizes (3.2 – 7.9 mm) employed in this study captured a wide variety of parameter combinations, which can be easily replicated in research or clinical laboratories.

Pig blood functions as a good analog to human blood and has been demonstrated to predict similar outcomes for human clot research.[15] This study would benefit more if human blood were to be employed although a large fresh blood volume from a single human donor can be problematic. Clot formation experiments were all performed at a fixed shear while native blood flow is a more complicated condition. Although clot analogs observed herein showed good thrombi resemblance, the results should be carefully interpreted to guide for therapies development.

5.6 Conclusions

Ultimately, the exploration of tunable clot formation in this study promises to expand the capability of the Chandler loop device in forming diversified, reproducible, and highly controllable clot substrates, which can have large ranges of properties that include clot weight (50 – 800 mg), cross-sectional diameter (2.5 to over 4.6 mm), clot RBC percentage (20 – 80 %), fibrin-rich component (10 - 60%), and fibrin/cellular morphology - as demonstrated in this study. Blood component storage protocols and diversified clot formation conditions can also be employed for prolonging substrate usable life and expanding the utility to mimic pathological conditions.[32, 33] These clots formed via that Chandler loop can be used directly in *ex-vivo* assays under static or flowing conditions for thrombolytic testing, introduced into animal models via injection as autologous clots for drug screening applications, or to study thromboresistance of medical devices such as blood pumps and artificial heart valves.[34] These diverse applications for Chandler loop formed clots capture a wide spectrum of thrombosis events that can ultimately facilitate the development of personalized treatment regimens for patients.

5.7 References

[1] M.G. Lansberg, M.J. O'Donnell, P. Khatri, E.S. Lang, M.N. Nguyen-Huynh, N.E. Schwartz, F.A. Sonnenberg, S. Schulman, P.O. Vandvik, F.A. Spencer, P. Alonso-Coello, G.H. Guyatt, E.A. Akl, Antithrombotic and thrombolytic therapy for ischemic stroke: Antithrombotic therapy and prevention of thrombosis, 9th ed: American college of chest physicians evidence-based clinical practice guidelines, Chest 141(2 SUPPL.) (2012) 601-636.

[2] T. Lenz-Habijan, M. Brodde, B.E. Kehrel, C. Bannewitz, K. Gromann, P. Bhogal, M. Aguilar Perez, H. Monstadt, H. Henkes, Comparison of the Thrombogenicity of a Bare and Antithrombogenic Coated Flow Diverter in an In Vitro Flow Model, CardioVascular and Interventional Radiology 43(1) (2020) 140-146.

[3] G. Tepe, J. Schmehl, H.P. Wendel, S. Schaffner, S. Heller, M. Gianotti, C.D. Claussen, S.H. Duda, Reduced thrombogenicity of nitinol stents - In vitro evaluation of different surface modifications and coatings, Biomaterials 27(4) (2006) 643-650.

[4] L.A. Robbie, S.P. Young, B. Bennett, N.A. Booth, Thrombi Formed in a Chandler Loop Mimic Human Arterial Thrombi in Structure and PAI-1 Content and Distribution, Thrombosis and Haemostasis 77(03) (1997) 510-515.

[5] H.A. Stringer, P. van Swieten, H.F. Heijnen, J.J. Sixma, H. Pannekoek, Plasminogen activator inhibitor-1 released from activated platelets plays a key role in thrombolysis resistance. Studies with thrombi generated in the Chandler loop, Arteriosclerosis and Thrombosis: A Journal of Vascular Biology 14(9) (1994) 1452-1458.

[6] T. Gaamangwe, S.D. Peterson, M.B. Gorbet, Investigating the Effect of Blood Sample Volume in the Chandler Loop Model: Theoretical and Experimental Analysis, Cardiovascular Engineering and Technology 5(2) (2014) 133-144.

[7] R.A. Gardner, An examination of the fluid mechanics and thrombus formation time parameters in a Chandler rotating loop system, The Journal of laboratory and clinical medicine 84(4) (1974) 494-508.

[8] I.N. Chernysh, C. Nagaswami, S. Kosolapova, A.D. Peshkova, A. Cuker, D.B. Cines, C.L. Cambor, R.I. Litvinov, J.W. Weisel, The distinctive structure and composition of arterial and venous thrombi and pulmonary emboli, Scientific Reports 10(1) (2020) 1-12.

[9] S. Vedantham, G. Piazza, A.K. Sista, N.A. Goldenberg, Guidance for the use of thrombolytic therapy for the treatment of venous thromboembolism, Journal of Thrombosis and Thrombolysis 41(1) (2016) 68-80.
[10] C.R. Benedict, C.J. Refino, B.A. Keyt, R. Pakala, N.F. Paoni, G.R. Thomas, W.F. Bennett, New Variant of Human Tissue Plasminogen Activator (TPA) With Enhanced Efficacy and Lower Incidence of Bleeding Compared With Recombinant Human TPA, Circulation 92(10) (1995) 3032-3040.
[11] S.T. Fitzgerald, Y. Liu, D. Dai, O.M. Mereuta, M. Abbasi, J.L.A. Larco, A.S. Douglas, D.F. Kallmes, L. Savastano, K.M. Doyle, W. Brinjikji, Novel Human Acute Ischemic Stroke Blood Clot Analogs for In Vitro Thrombectomy Testing, American Journal of Neuroradiology (2021) 1-8.
[12] C.S. Whyte, H.A. Mostefai, K.M. Baeten, A.J. Lucking, D.E. Newby, N.A. Booth, N.J. Mutch, Role of shear stress and tpa concentration in the fibrinolytic potential of thrombi, International Journal of Molecular Sciences 22(4) (2021) 1-15.
[13] S.L. Jessen, A.M. Masse, M.D. Carpenter, F.J. Clubb, B.R. Weeks, A method for creating artificial thrombi in vitro using a rotating mechanical surface, ASAIO Journal 62(3) (2016) 252-260.
[14] N.J. Mutch, E. Moir, L.A. Robbie, S.H. Berry, B. Bennett, N.A. Booth, Localization and identification of thrombin and plasminogen activator activities in model human thrombi by in situ zymography, Thrombosis and Haemostasis 88(6) (2002) 996-1002.
[15] M. Berndt, S. Prothmann, C. Maegerlein, P. Oberdieck, C. Zimmer, B. Hegge, J. Pelisek, L. Schirmer, H. Poppert, T. Boeckh-Behrens, Artificial Stroke Clots: How Wide is the Gap to the Real World?, World Neurosurg 110 (2018) e90-e99.
[16] W. Merritt, A.M. Holter, S. Beahm, C. Gonzalez, T.A. Becker, A. Tabor, A.F. Ducruet, L.S. Bonsmann, T.R. Cotter, S. Frenklakh, Quantifying the mechanical and histological properties of thrombus analog made from human blood for the creation of synthetic thrombus for thrombectomy device testing, Journal of NeuroInterventional Surgery 10(12) (2018) 1168-1173.
[17] D.A. Reasor, M. Mehrabadi, D.N. Ku, C.K. Aidun, Determination of critical parameters in platelet margination, Annals of Biomedical Engineering 41(2) (2013) 238-249.
[18] T. Krüger, Effect of tube diameter and capillary number on platelet margination and near-wall dynamics, Rheologica Acta 55(6) (2016) 511-526.

[19] D.M. Beam, E.M. Neto-Neves, W.B. Stubblefield, N.J. Alves, J.D. Tune, J.A. Kline, Comparison of isoflurane and α-chloralose in an anesthetized swine model of acute pulmonary embolism producing right ventricular dysfunction, Comparative Medicine 65(1) (2015) 54-61.
[20] E. Genton, A.P. Fletcher, N. Alkjaersig, S. Sherry, Assay of plasma thrombolytic activity with fluorescein-labeled clots, The Journal of laboratory and Clinical Medicine 64(2) (1964) 313-320.
[21] M. Huang, H.G. Kim, X. Zhong, C. Dong, B. Zhang, Z. Fang, Y. Zhang, X. Lu, R. Saxena, Y. Liu, C. Zhang, S. Liangpunsakul, X.C. Dong, Sestrin 3 Protects Against Diet-Induced Nonalcoholic Steatohepatitis in Mice Through Suppression of Transforming Growth Factor β Signal Transduction, Hepatology 71(1) (2020) 76-92.
[22] Z. Zeng, T. Nallan Chakravarthula, C. Muralidharan, A. Hall, A.K. Linnemann, N. Alves, Fluorescently Conjugated Annular Fibrin Clot for Multiplexed Real-time Digestion Analysis, Journal of Materials Chemistry B (2021).
[23] N. Krasokha, W. Theisen, S. Reese, P. Mordasini, C. Brekenfeld, J. Gralla, J. Slotboom, G. Schrott, H. Monstadt, Mechanical properties of blood clots - A new test method, Materialwissenschaft und Werkstofftechnik 41(12) (2010) 1019-1024.
[24] J. Silvain, J.P. Collet, C. Nagaswami, F. Beygui, K.E. Edmondson, A. Bellemain-Appaix, G. Cayla, A. Pena, D. Brugier, O. Barthelemy, G. Montalescot, J.W. Weisel, Composition of coronary thrombus in acute myocardial infarction, Journal of the American College of Cardiology 57(12) (2011) 1359-1367.
[25] T. Boeckh-Behrens, M. Schubert, A. Förschler, S. Prothmann, K. Kreiser, C. Zimmer, J. Riegger, J. Bauer, F. Neff, V. Kehl, J. Pelisek, L. Schirmer, M. Mehr, H. Poppert, The Impact of Histological Clot Composition in Embolic Stroke, Clinical Neuroradiology 26(2) (2016) 189-197.
[26] N.J. Mutch, J.S. Koikkalainen, S.R. Fraser, K.M. Duthie, M. Griffin, J. Mitchell, H.G. Watson, N.A. Booth, Model thrombi formed under flow reveal the role of factor XIII-mediated cross-linking in resistance to fibrinolysis, Journal of Thrombosis and Haemostasis 8(9) (2010) 2017-2024.
[27] M. Kuwahara, M. Sugimoto, S. Tsuji, H. Matsui, T. Mizuno, S. Miyata, A. Yoshioka, Platelet shape changes and adhesion under high shear flow, Arteriosclerosis, Thrombosis, and Vascular Biology 22(2) (2002) 329-334.

[28] F.L. Macrae, C. Duval, P. Papareddy, S.R. Baker, N. Yuldasheva, K.J. Kearney, H.R. McPherson, N. Asquith, J. Konings, A. Casini, J.L. Degen, S.D. Connell, H. Philippou, A.S. Wolberg, H. Herwald, R.A.S. Ariëns, A fibrin biofilm covers blood clots and protects from microbial invasion, Journal of Clinical Investigation 128(8) (2018) 3356-3368.
[29] H. Touma, I. Sahin, T. Gaamangwe, M.B. Gorbet, S.D. Peterson, Numerical investigation of fluid flow in a chandler loop, Journal of Biomechanical Engineering 136(7) (2014) 1-8.
[30] R.I. Litvinov, J.W. Weisel, Role of red blood cells in haemostasis and thrombosis, ISBT Science Series 12(1) (2017) 176-183.
[31] K.B. Neeves, D.A.R. Illing, S.L. Diamond, Thrombin flux and wall shear rate regulate fibrin fiber deposition state during polymerization under flow, Biophysical Journal 98(7) (2010) 1344-1352.
[32] A. Christodoulides, Z. Zeng, N.J. Alves, In-vitro thromboelastographic characterization of reconstituted whole blood utilizing cryopreserved platelets, Blood Coagulation & Fibrinolysis Publish Ah (2021) 1-8.
[33] Z. Zeng, M. Fagnon, T. Nallan Chakravarthula, N.J. Alves, Fibrin clot formation under diverse clotting conditions: Comparing turbidimetry and thromboelastography, Thrombosis Research 187(January) (2020) 48-55.
[34] M. Selmi, W.C. Chiu, V.K. Chivukula, G. Melisurgo, J.A. Beckman, C. Mahr, A. Aliseda, E. Votta, A. Redaelli, M.J. Slepian, D. Bluestein, F. Pappalardo, F. Consolo, Blood damage in Left Ventricular Assist Devices: Pump thrombosis or system thrombosis?, International Journal of Artificial Organs 42(3) (2019) 113-124.

6. REAL-TIME TRACKING OF FIBRINOLYSIS UNDER PHYSIOLOGIC SHEAR IN AN IN-VITRO THROMBOLYSIS MODEL

One version of this chapter was currently under review at a peer-reviewed journal as a publication entitled “Real-time Tracking of Fibrinolysis under Physiologic Shear in an *in-vitro* Thrombolysis Model”.

Since blood flow largely affect the transport of thrombolytic agent into the clot, it is necessary to mimic these conditions in the *in-vitro* model to study therapeutic agents. Although microfluidic chambers have attracted huge research interests and extensively studied for *in-vitro* flow modeling, these devices have small length scales and highly ordered flow patterns which are incomparable to native conditions. Models with physiological diameter lumens (1 to 30 mm) offer a more representative environment to cultivate biological and hemodynamic interactions. One limitation about physiological scaled models is the requirement of using a large amount of blood to conduct a single experiment. A common and efficient strategy to circumvent this issue is by joining the inlet and outlet into a loop and incorporating a peristaltic pump to offer a flow. The peristaltic pump is largely in favored for blood related applications since it provides for a large, circulative, and non-contact flow output. Similar thrombolysis models using the mentioned components are poorly documented and mostly seen in ultrasound-aided thrombolytic applications which is not primarily intended for thrombolytic drug screening.[1, 2]

Taking the knowledge from previous chapters for fabricating a physiologically relevant FISC, this chapter reports a design, development and characterization of a novel physiologic scale *in-vitro* flow model for fluorescence tagging leveraged thrombolysis monitoring. Developing a well-characterized flow model to molecularly track clot digestion, especially fibrin degradation, in real-time, is to-date the first of its kind, and can be extremely useful to evaluate drug profiles. Acknowledging potential variations and versatility of the setup, this chapter focuses on the primary utilization of this model, which is to establish a continuous shear flow to study the effect of wall shear rate on clot digestion. The laminar flow pattern is developed with a help of dampeners and ensured by pressure sensor readings and a flow entrance length.

6.1 Abstract

A great need exists for the development of an *in-vitro* model to screen for novel thrombolytic therapies more efficiently in a physiologically relevant system without the immediate reliance on animal models that are inefficient, costly, and often have distinct physiology from humans. Thus, we propose here a highly reproducible, physiological scale, flowing clot lysis model with real-time fibrinolysis monitoring to screen thrombolytic therapies utilizing a FITC-labeled clot analog. Using this Real-Time Fluorometric Flowing Fibrinolysis Assay (RT-FluFF Assay) a tPA-dependent degree of thrombolysis was observed both via clot mass loss as well as fluorometrically monitored fluorescence release. Percent clot mass loss ranged from 33.6% to 85.9% with fluorescence release rates of 0.53 to 1.17 RFU/min in 40 and 1,000 ng/mL tPA conditions, respectively. Correlation analysis indicated a strong linear correlation ($r = 0.78$) between percent mass loss and rise in plasma fluorescence. This was similar to other digestion assay standards such as the Chandler loop ($r = 0.81$) and the static clot lysis ($r = 0.91$). The proposed *in-vitro* clot model offers real-time digestion monitoring and represents a versatile testing platform for thrombolytic drug screening.

6.2 Introduction

Thrombosis is the pathologic formation of a blood clot that obstructs flow through veins or arteries. Complications of thrombosis can be life-threatening, such as ischemic stroke, myocardial infarction, and pulmonary embolism. The mainstay thrombosis treatment is either through mechanical thrombectomy, which requires a specialized device and an experienced clot retriever-operator, or by intravenous infusion of thrombolytic drugs.[3, 4] Both approaches do maintain inherent risks, bleeding being the primary.[5] Current evaluation of thrombolytic agents has largely relied on animal models. However, animals do not predict a reliable drug efficacy profile due to their distinct physiology.[6-8] To circumvent the problem, numerous *in-vitro* drug testing methods have been developed to assist in the screening and development of novel thrombolytic agents. A static *in-vitro* clot lysis assay using a statically formed clot is the most common protocol found in the literature.[9, 10] Tests are performed by adding drugs to a preformed clot and tracking changes in clot weight to depict drug efficacy. However, properties of statically formed clots are different from those of native thrombi due to the lack of shear effects

during clotting, for example the promotion of fibrin cross-linking during clotting under shear. [11, 12] Drug-induced static clot digestion also ignores human hemodynamics where parameters like trans-thrombus pressure drop, and turbulent flow can dramatically affect the clot permeation resulting in distinctive drug efficacy profiles.[13, 14] Thus, devices have been engineered to achieve more relevant physiological digestion conditions. Microfluidic related assays are useful in studying thrombosis progression, given their highly ordered flow patterns and ease of imaging. However, clots formed in these devices tend to be dissimilar to native thrombi due to the nature of device lumen size and difference in generated flow dynamics.[15, 16] Utilizing a Chandler loop device to form clot analogs and study clot digestion has gained popularity in thrombosis societies in recent years.[12, 17] Clot analogs formed in the Chandler loop have revealed a good resemblance to native venous thrombi, arterial thrombi, and pulmonary emboli.[11] The Chandler loop also allows for clot digestion under shear; however, its over-simplified nature makes it a less representative model since the setup lacks important physiological circulatory components such as a reservoir and pressurized flow conditions. Given the drawbacks and benefits of existing methods, developing a drug screening platform that combines a physiologically relevant clot and a biomimetic flow setup is essential to a more meaningful drug screening. This model may not eliminate the need for preclinical animal testing but can exclude inefficient agents earlier in the drug development pipeline to expedite the drug evaluation process.

This study reports the design, validation, and characterization of an *in-vitro* thrombolysis model for thrombolytic drug screening. This model is a tubing-based system that offers physiologically relevant shear flows. It incorporates a peristaltic pump, a flow dampener, a heated reservoir, pressure sensors, an in-line fluorometer, and a Chandler loop-formed clot analog (**Figure 6.1**). The clot analog is fluorescently labeled using a previously reported low-impact strategy, to facilitate real-time tracking of fibrinolysis.[18] The entire system will be referred to as Real-Time Fluorometric Flowing Fibrinolysis Assay (RT-FluFF Assay) for the purposes of this manuscript. A series of characterization experiments were conducted to validate flow dynamics, impact-free fluorescent clot labeling, and real-time fluorescence tracking under flow. Digestion experiments were further adopted to demonstrate the capability of differentiating increased thrombolytic drug levels for clot digestion efficacy.

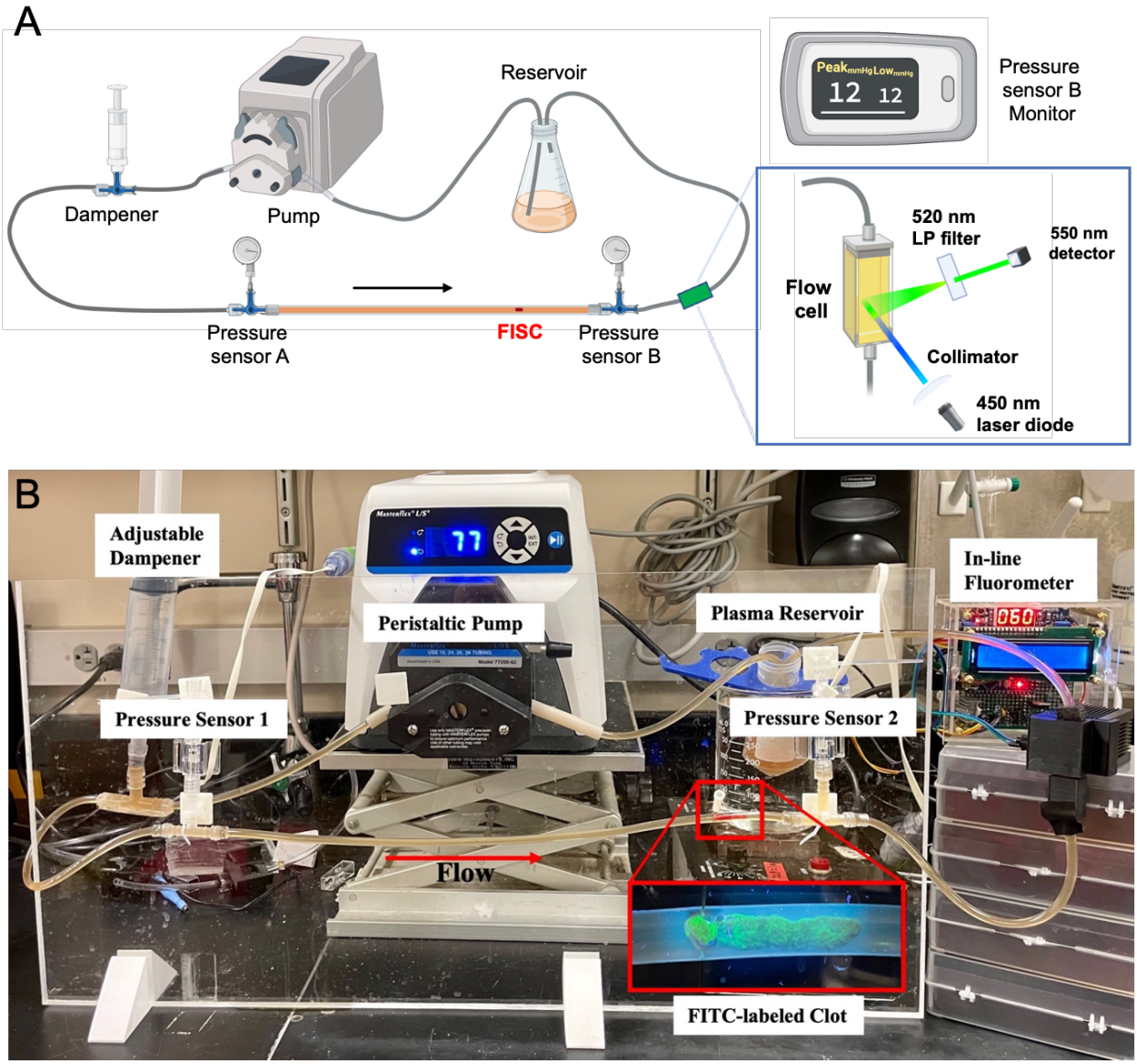

Figure 6.1. (A) Schematic representation and (B) Lab setup of Real-Time Fluorometric Flowing Fibrinolysis Assay (RT-FluFF). Components from left to right are dampener, peristaltic pump, pressure sensors (before clot), reservoir, pressure sensor (after clot), fluorometer.

6.3 Materials and Methods

6.3.1 Whole Blood and Plasma Processing

Venous whole blood was collected from healthy volunteers (n=5) by a trained phlebotomist in accordance with an institutionally approved IRB protocol (1610652271). Volunteers were questioned to ensure they had no clinical diagnoses or medication regimens that might impact clotting behavior. Blood was collected into 3.2% Sodium-Citrate tubes and immediately pooled into 15 mL tubes for use (BD Vacutainer, Franklin Lakes, NJ). Prior to performing any analyses, sample hematocrits were calculated utilizing microhematocrit tubes centrifuged at 2750 xg for 3 minutes (Thermo Fisher, Waltham, MA). The whole blood was stored at 4°C and brought to room temperature over the course of 30 minutes prior to use. Human plasma units were donated on behalf of the Eskenazi Blood Bank for research use and were aliquoted prior to storage at -20°C.

6.3.2 FITC-Fibrinogen Synthesis

Fibrinogen was labeled with FITC to form FITC labeled human fibrinogen (FhF) as previously described.[18] In short, lyophilized human fibrinogen and FITC (Sigma Aldrich, St. Louis, MO) were reconstituted in phosphate buffer saline (PBS) and 10% dimethyl sulfoxide (DMSO) PBS solution, respectively. 200-fold excess FITC was reacted with human fibrinogen at room temperature (RT) for 18 hours to attain 14 FITC per fibrinogen molecule (< 8% DMSO in reaction solution). Tagged fibrinogen was purified using 100 kDa cutoff filters following manufacturer recommendations (Amicon®, Millipore, Burlington, MA). The average amount of FITC per fibrinogen was verified using a previously mentioned method.[18] FhF aliquots were then made to a final concentration of 3 mg/mL and stored at -20 °C.

6.3.3 Thromboelastography

Thromboelastography (TEG) was utilized to capture baseline patient clotting profiles to ensure adequate clotting behavior prior to whole blood clot formation in the Chandler loop (see method below). TEG was run in accordance with manufacture-provided protocols and prior-published protocols utilizing Haemonetics TEG-5000 instruments (Haemonetics, Boston, MA).[19] In brief, 1 mL of citrated whole blood was mixed into 40 µL of Kaolin and followed by introduction of 340 µL of the mixed sample into non-coated TEG cups containing 20 µL of 12

mM $CaCl_2$. Clotting was monitored at 37 °C. Incorporation of FhF into our samples for TEG analysis was performed prior to introducing the whole blood into the kaolin. Ratios of FhF utilized were 50:1, 10:1, and 5:1 which corresponds to 0.18, 0.88, and 1.76 μM, respectively. A vehicle control that contained PBS was also included in analysis to account for potential dilution of the whole blood samples upon addition of the FhF. Samples were run in triplicate.

6.3.4 Whole Blood Clot Analog Formation

Whole blood clots were formed utilizing a Chandler Loop to mimic exposure to physiologic levels of shear during the process of coagulation. The protocol utilized was similar to priorly published protocols. In brief, FhF was added to citrated whole blood at a final ratio of 10:1 (0.88 μM) prior to recalcification. After gentle inversion of the mixture, the whole blood was recalcified utilizing $CaCl_2$ to achieve a final concentration of 11.8 mM. Recalcified whole blood was subsequently loaded, using a syringe, into 5/32" tubing (Tygon 100-65 medical tubing) such that half of the volume of the end-joined loop would remain empty - final volume of whole blood utilized estimated around 2 mL (U.S. Plastics, Lima, OH). The loops of tubing were immediately placed on a rotating semi-submerged drum of 6 cm radius to begin clot formation. The drum was set to rotate at 40 RPM (calculated shear: 506 s^{-1}) for 60 minutes. Partial submersion of the Chandler Loop drum in a water bath ensured clot formation was conducted at a constant 37 °C. Once 60-minutes had passed, the Chandler Loop was stopped, and individual clots were transferred to a petri-dish for subsequent recording of mass and gross imaging under both white light and UV light. Clots were subsequently re-submerged in their residual serum to ensure they remain hydrated during waiting periods.

6.3.5 Hematoxylin & Eosin Staining and Epifluorescence

A single representative clot formed from the Chandler Loop was collected from each subject and stored in 10% Neutral Buffered Formalin for 24 hours prior to being placed in 70% ethanol. Once preserved, clots were submitted to the Indiana University Histology Core for sectioning and staining with Hematoxylin and Eosin. Analysis of H&E slides was performed utilizing threshold analysis in ImageJ to isolate contributions of red blood cells, white blood cells, and fibrin as part of clot composition. Non-stained sections from the same clots were utilized for

imaging under epifluorescence utilizing a LSM 800 confocal microscope (Zeiss, Oberkochen, Germany).

6.3.6 Static Digestion

A subset of the FhF labeled whole blood clots previously described were subjected to fibrinolysis under static conditions. Frozen plasma was thawed at 37°C and aliquoted to subsequently be loaded with Alteplase at concentrations of 0 ng/mL (i.e., no Alteplase added), 40 ng/mL, 200 ng/mL, or 1,000 ng/mL (Genentech, San Francisco, CA). Clots were gently loaded into 1.5 mL centrifuge tubes and filled to the 1.5 mL mark with plasma. Subsequently, tubes were submerged in a 37°C water bath for the duration of the 60-minute digestion. Triplicate samples of the plasma were taken at 0-, 30-, and 60-minute marks of digestion for fluorescence quantification. A spectrophotometer (Molecular Devices, SpectraMax M5, San Jose, CA) was utilized for all readings. Settings for the spectrophotometer were as follows: 495 nm excitation, 519 nm emission, 515 nm auto-filter. Clot weights were also recorded at the end of the digestion period and compared to respective initial clot weights to calculate the percent clot mass lost.

6.3.7 Chandler Loop Digestion

A second modality of digestion explored was utilizing the Chandler Loop configuration to also conduct fibrinolysis under dynamic conditions. Frozen plasma was thawed at 37°C and aliquoted to subsequently be loaded with Alteplase at concentrations of 0, 40, 200, or 1,000 ng/mL. FhF labeled whole blood clots were subsequently submerged, one at a time, in weigh-boats containing 5 mL of plasma with varying tPA concentrations. A syringe attached to a new 5/32” Tygon tube was used to draw in both the plasma and clot into the tubing (U.S. Plastics, Lima, OH). A final volume, including the clot, of 3 mL was drawn into the tubes each time. End-joined tubes were placed onto the Chandler Loop and rotated at 40 RPM for the duration of 60 minutes. Plasma was sampled at 0, 30, and 60 minute and read via spectrophotometer. Clot masses were collected at the end to calculate percent of clot mass lost.

6.3.8 RT-FluFF Assay Construction

A physiological scale *in-vitro* blood flow device was developed to offer laminar flow at an adjustable shear rate for clot analog digestion experiments. The flow device consists of a peristaltic pump system -Masterflex EasyLoad II pump and 1.5 feet #15 peristaltic tubing (Masterflex, Gelsenkirchen, Germany), a 50 mL tube reservoir (Corning Scientific, Corning, NY), and a flow dampener, which are connected by 5/32" Tygon tubing pieces (r = 0.002 m). To offer a non-contact flow at a desired output, a peristaltic pump was used and Q = 138.6 mL/min. The dampener further mitigates the peristalsis by the pump to provide for an approximate laminar flow pattern. Dampener were designed in three different sizes although the largest 60cc was used for this study (**Figure A.21**). Two disposable pressure sensors (A and B) were placed at a distance of L_{AB} = 0.4 m before and after the clot. A monitor (Siemens, Munich, Germany) was employed to supervise a pressure-drop (ΔP) reads to confirm the model is abided by the Navier Stoke equation:

$$\Delta P = \frac{8\mu Q}{\pi r^4 L_{AB}}$$

Since flow conditions can change due to a change in tube dimensions, an entrance length (Xe) should be considered:

$$Xe = 0.113R\overline{Re}$$

Beyond Xe, laminar flow is fully developed which merely depends on radial position than both radial and axial position.[20] The real-time clot digestion monitoring was achieved by incorporating a portable fluorometer positioned directly after the clot. The fluorometer includes a flow chamber cuvette, 450 nm laser diode, 520 nm long pass filter, and a 550 nm sensitive photodetector. Signal was processed by an operational amplifier circuit forwarding to an Arduino micro-chip for record (Arduino, Somerville, MA) (**Figure A.22**). The fluorescence monitoring performance of the device was demonstrated by comparing reads with a commercial spectrometer. Fluorescence reads were obtained every 30 seconds by default unless otherwise specified. To guarantee a fully developed laminar flow pattern, clot analogs were positioned at a calculated entrance length from the last bifurcation.

6.3.9 RT-FluFF Digestion Assay

FhF labeled whole blood clots were employed in the RT-FluFF Assay for digestion study. Each clot was fixed in the tubing using a 31-gauge syringe needle at one-tenth the distance from the clot head. To mimic human pulmonary flow conditions, the reservoir was heated at 37 °C and lifted to 8 cm above the clot level to give an average flow pressure of 12 mmHg, and the pump rate was adjusted to generate a ~ 400 s^{-1} shear flow (no clot). For each experiment, the model was perfused with newly thawed pooled plasma at a premixed Alteplase level of 0, 40, 200, or 1,000 ng/mL. Clot digestion was monitored utilizing the inline fluorimeter. Flow pressure, clot appearance, and clot break-off times were recorded.

6.3.10 Shear-Stretch Analysis

Chandler loop-formed whole blood clots were fixed in the RT-FluFF assay tubing using a 31-gauge syringe needle at one-tenth the distance from the clot head. PBS was flowed through the system at various rates of shear including 0, 300, 600, and 900 s^{-1}. Clots were allowed to stretch and equilibrate at each shear for two minutes prior to video capture. Quantification of the video frames was conducted utilizing ImageJ in which clot length could be accurately measured from clot head to clot tail. Percent change in length could then be calculated based on respective initial lengths - i.e., no shear condition.

6.3.11 Statistical Analysis

All data was collected and processed using Microsoft Excel. ANOVA analysis was used to ascertain statistical differences among groups with three or more conditions, followed by a Tukey test for individual subset comparisons. Student t-tests were utilized to compare two categorical variables between each other. Statistical significance was deemed to be a p-value < 0.05. A single asterisk denotes a p-value < 0.05, double asterisk denotes a p-value < 0.01, and triple asterisk signifies a p-value < 0.001.

6.4 Results

6.4.1 Generating a Physiologically Relevant Clot Analog

A common means of introducing fluorescence into clot analogs is using FITC labeled fibrinogen [17-19]. The selection of FITC as the reporter for fibrinolysis has been thoroughly studied previously; however, no systematic study has been published examining the potential effects on whole blood clotting and clot analog characteristics that addition of exogenous FhF might have. Common concentrations of FhF utilized for clot studies range anywhere from 0.0075 to 0.6 mg/mL using 1 to 15 FITC per fibrinogen with no justifications as to why a particular concentration or labeling density is preferred.[21-23] To create a truly representative thrombolysis system relying on FITC-Fibrinogen (FhF) labeling, it is necessary to optimize the ratio of Native fibrinogen to FhF present in whole blood samples, aiming to obtain the highest level of fluorescence labeling that would not sacrifice clot integrity and architecture. Clotting mixtures were prepared by adding FhF (14-FITC per human fibrinogen) to whole blood at ratios of native fibrinogen to FhF at 1:0 (control), 50:1, 10:1, and 5:1. Thromboelastography (TEG) was elected to compare clotting parameters across groups. Increasing the amount of FhF added to whole blood noticeably led to decreased maximum amplitude (MA or TEG^{Max}), increased time to maximum amplitude (TMA or TEG^{Time}), and decreased angle (**Figure 6.2**).

A statistically significant drop in clot strength was first noted at the 10:1 ratio where TEG^{Max} had fallen from 61.8 mm in the control group to 58.4 mm ($P = 0.0208$) and subsequently reduced to 53.9 mm in the 5:1 group ($P < 0.001$). Significant differences in TEG^{Time} and alpha angle were only seen in the 5:1 group, where TEG^{Time} had increased from 30 minutes in the control group to 35.6 minutes ($P = 0.010$) with angle decrease from 63.7° in the control to 44.5° in the 5:1 group ($P = 0.013$) (**Figure 6.2C**). The proposed RT-FluFF system relies on the use of clot analogs formed under physiologically relevant shear conditions. Thus, a Chandler Loop device was utilized to further characterize labeled clots at the mentioned FhF ratios. Clot masses recorded at the end of 60 minutes of clot formation did not deviate significantly between groups, the 5:1 group (103.6 mg) and the 10:1 group (102.6 mg) had nearly identical masses to clots in the control group (**Figure 2A**; 103.2 mg). Interestingly, subsequent digestion of the clots under shear, with Alteplase (tPA), suggested increased levels of clot digestion in the 10:1 group (50.4% clot mass lost) compared to no FhF control (40.1% clot mass lost) however there was no statistical significance to this difference (**Figure 6.2D**).

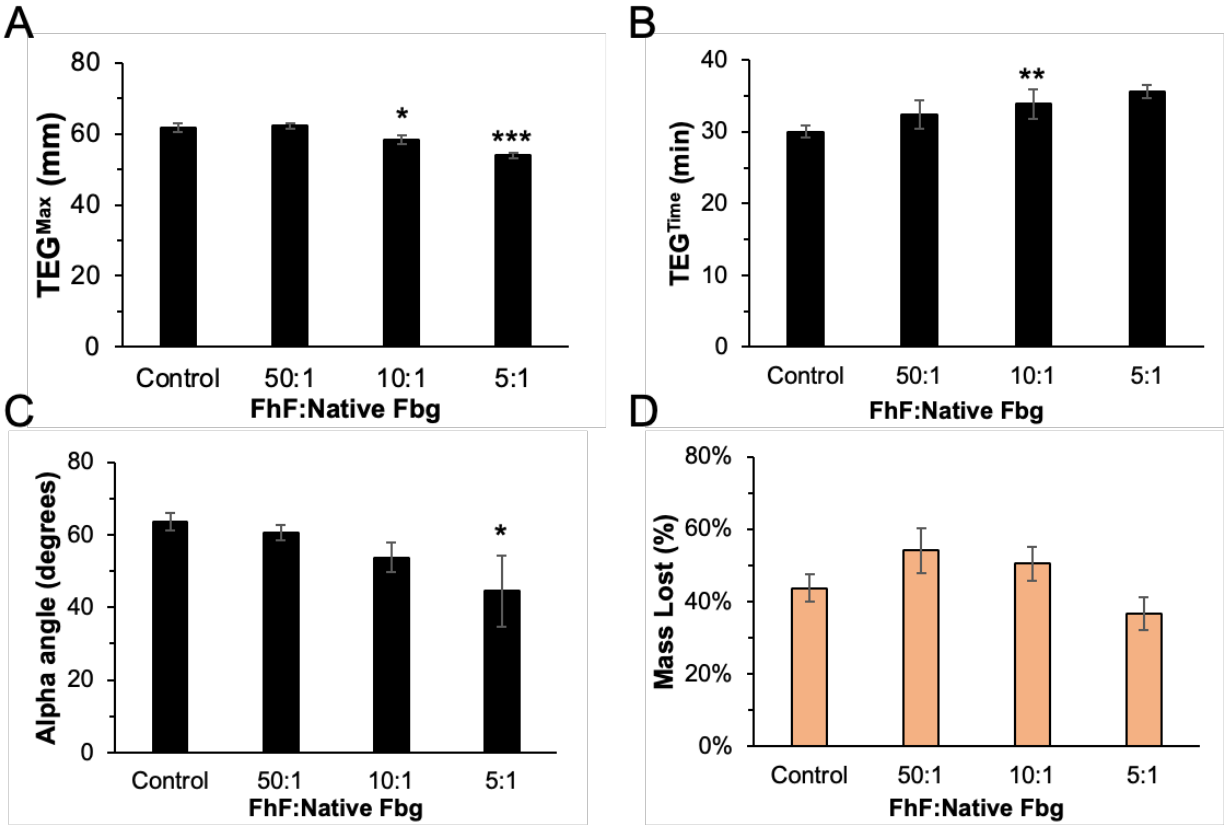

Figure 6.2. Bar plots outlining the TEG parameters (A) TEG^{Max}, (B) TEG^{Time}, and (C) alpha angle in the various FITC-Fg groups explored during optimization. (D) Percent clot mass lost during digestion of Chandler-loop made clots utilizing various ratios of FITC-Fg. Clot digestion conducted over the course of 60-minutes with 600 ng/mL tPA. Single asterisk denotes P-value < 0.05, Double asterisk denotes P-value <0.01, Triple asterisk denotes P-value <0.001.

Grossly, clots between the various FhF ratio groups and control were similar to one another, with exposure to UV light highlighting the increasing fluorescence intensity expected from increasing FhF incorporation at higher ratios (**Figure 6.3B**). H&E staining of the clots revealed the loss of the packed fibrin motif in the 5:1 group's clot region that were seen in all other groups including 10:1 (**Figure 6.3C**). Of note, clots formed utilizing the 5:1 ratio had a more fragile feel during the handling process compared to any other group. Epifluorescence conducted on microtomes of the same clots from H&E staining once again displayed the increasing levels of fluorescence expected with increasing FhF incorporation (**Figure 6.3C**). Both the 10:1 and 5:1 group appeared to have adequate levels of fluorescence at the 150 ms while 50:1 group was too dim. All FhF groups demonstrated relatively uniform FhF incorporation throughout the clots. The

10:1 ratio of FhF was utilized for all subsequent testing as this ratio best balanced increased fluorescence incorporation with minimal deviation of baseline clotting parameters.

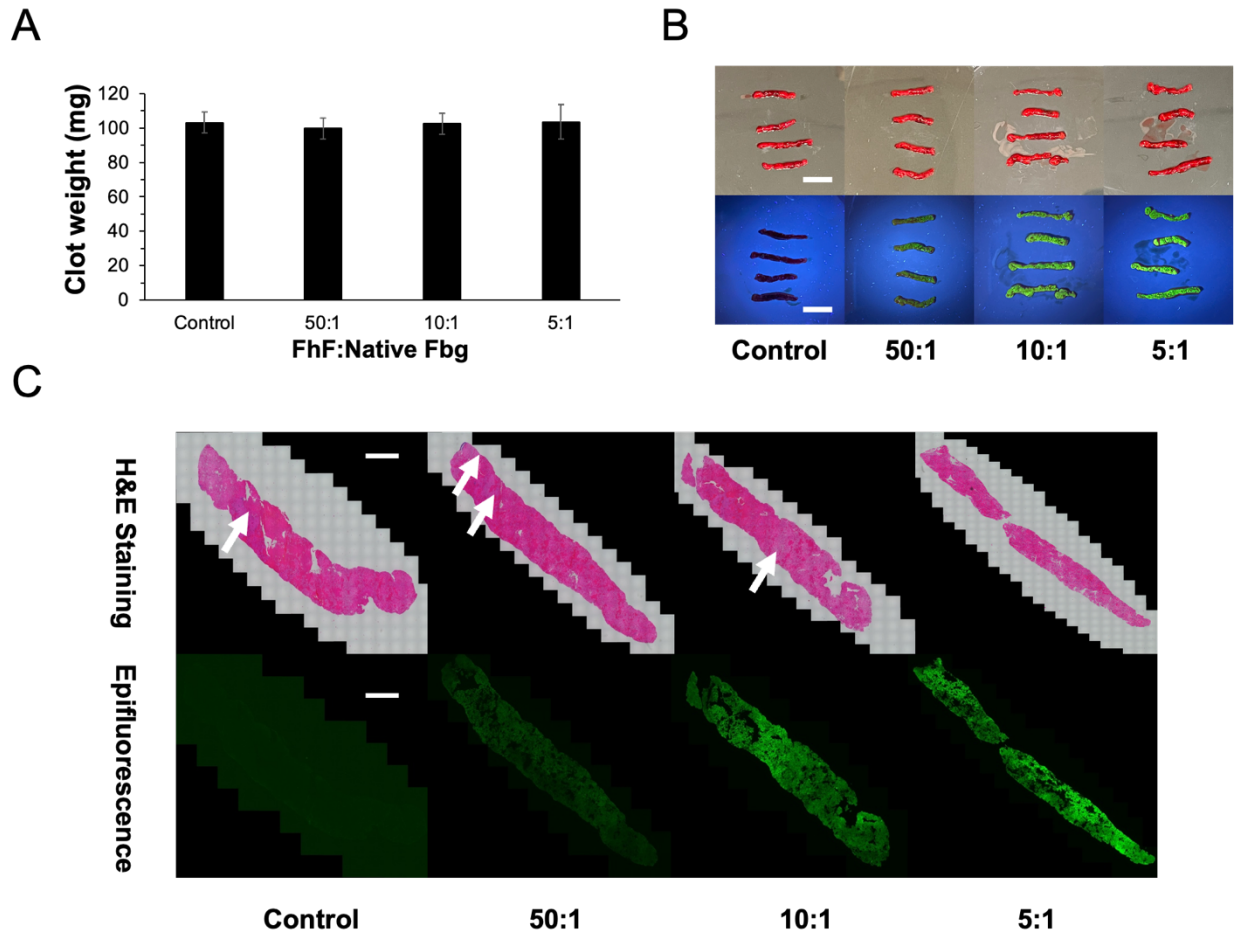

Figure 6.3. (A) Masses of clots formed in the Chandler loop utilizing the control (0:1), 50:1, 10:1, and 10:1 FhF groups. (B) Gross images of clots formed in the Chandler Loop using varying FhF ratios under room light (top row) vs UV light (bottom row). Scale bars represent 20 mm. (C) H&E and epifluorescence images acquired of Chandler loop clots from respective ratios of FhF. White arrow indicates fibrin dense regions. Note the loss of fibrin dense regions in the 5:1 group, indicating significant perturbation of clot architecture. Scales bars represent 2 mm.

6.4.2 RT-FluFF Assay Device Characterization

The overall design of the RT-FluFF assay was pictured (**Figure 6.1B**). Ultimately, the system is a peristaltic pump with a pulsatile-flow dampener that can facilitate physiologic levels of steady shear and pressure in a versatile system that allows for good interchangeability of tubing lumen size and geometry. Pressure sensors were placed before and after the clot location to

quantify flow dynamics. Finally, an in-line fluorometer was incorporated to allow for real-time monitoring of fluorescence in the flowing fluid as it passes through the fluorometer itself.

Utilization of a pulsatile-flow dampener helps reduce pressure fluctuations from peristalsis to ensure the establishment of a laminar flow in the region of the system where clots were loaded and digested. Laminar flow dynamics were first confirmed by matching monitored pressure drop across the two sensors to a theoretical value calculated through the Hagen–Poiseuille equation in the absence of clot. The dampening effect was further demonstrated by having up to a 3-mmHg difference between systolic and diastolic pressures at any given sensor, compared to a ~55 mmHg average fluctuation in un-dampened conditions within ~ 300 – 1,000 s^{-1} shear (**Figure 6.4A and 6.4B**). Importantly, the developed system was able to withstand pressures of up to ~ 140 mmHg at extremes; however, running pressures were generally kept between 8 - 20 mmHg to simulate physiological pressures expected in the pulmonary arteries (**Figure 6.4C and 6.4D**).

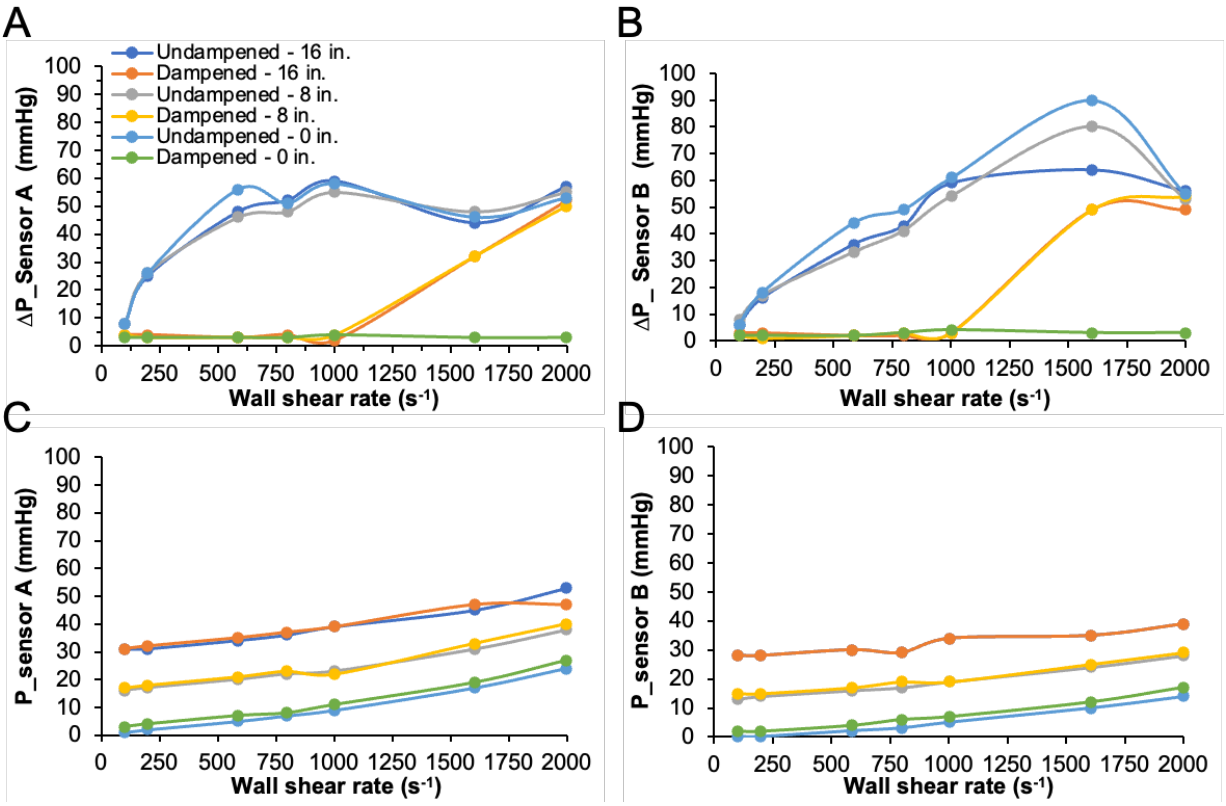

Figure 6.4. Systolic-diastolic pressure difference outlined in (A) pressure sensor A and (B) pressure sensor B in various systemic pressure settings as well as in dampened versus undampened settings. Height (inch) refer to the displacement of output drain from the pressure sensors. Absolute systolic pressure readings at (C) pressure sensor A and (D) pressure sensor B over a wide range of pump shear rates.

Validation of the fluorometer was initially conducted under static conditions and compared against a SpectraMax M5 spectrometer. Sequential dilutions of FhF were carried out in PBS and readings were taken using both the commercially available spectrophotometer and the in-house designed fluorometer. A linear correlation (r = 0.9997) was observed with an R^2 of 0.9987 for the fluorometer and 0.9996 for the spectrometer (**Figure 6.5A**). To test the sensor's ability to capture repeated fluorescent signal introductions and subsequently achieving signal stability, Fluorescein was introduced into the system in a series of 5 µL injections (4.2 mmol) upstream of the fluorometer, allowing for 2 minutes of equilibration after each injection into the ~45 mL total volume of the system. On average, each introduction of Fluorescein led to a rise in fluorescence of 62.8 ± 7.4 RFU (Coefficient of variance = 11.8%; **Figure 6.5B**). Following sensor validation and given the continuous nature of clot digestion *in-vivo*, our focus shifted to perfusion of pooled plasma at 400 s^{-1} with continuous infusions of fluorescein or FhF into flowing plasma (**Figure 6.5C**). Equivalent total fluorescein molecular amounts (0.021 µmol) and infusion rates (1,000 µL/hour) were utilized between both groups to ensure accurate comparisons. Notably, the rise in RFUs was slightly different with 7.16 RFU/minute for fluorescein vs 6.04 RFU/minute for FhF. Additionally, the final plateau reached in the fluorescein group was higher than that of FhF: 441 vs 365 RFU, respectively (**Figure 6.5C**). Calculation of fluorometer RFU contribution from FhF introduction showed that 1 RFU corresponded to a rise in system FhF concentration by approximately 0.1 nM.

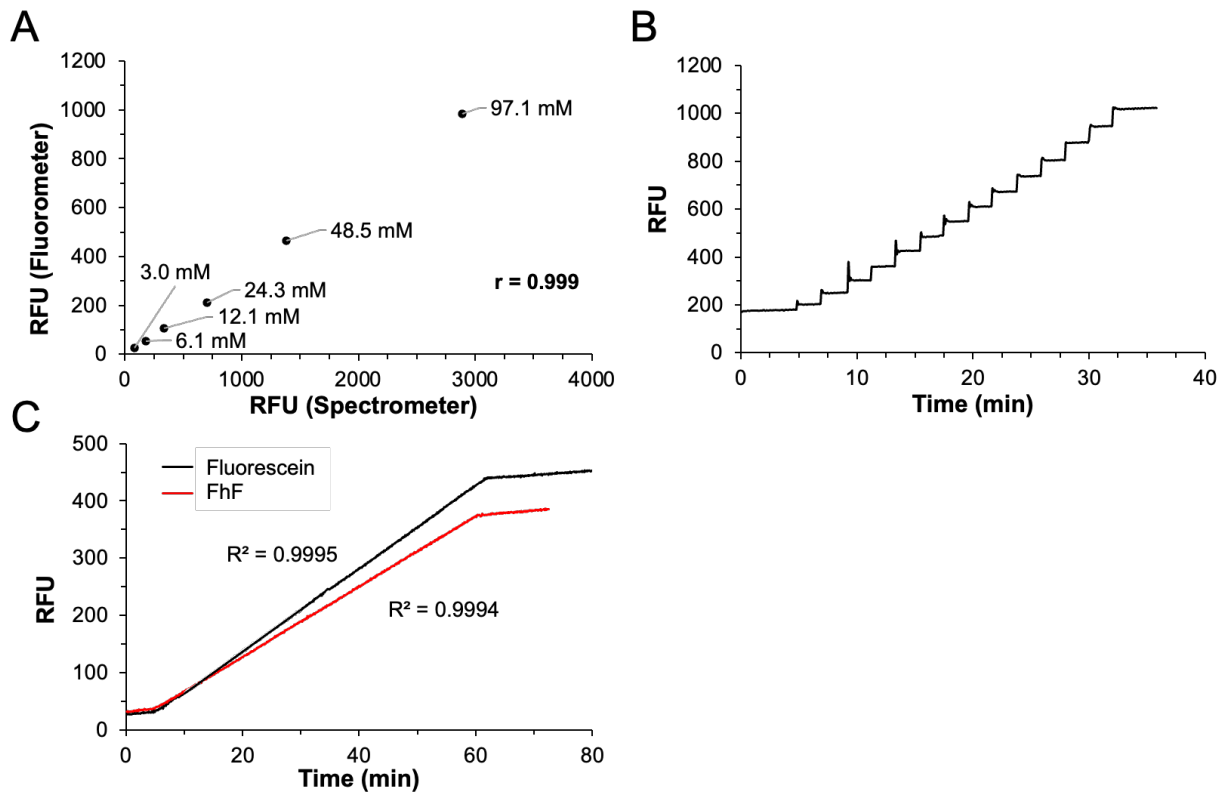

Figure 6.5. (A) Comparison between spectrophotometer and fluorometer in quantifying fluorescence of a serial dilution of FhF. (B) Stepwise injection of Fluorescein into flowing plasma with fluorometer data acquisition. (C) Continuous infusion of either FhF or Fluorescein into plasma with fluorometer data acquisition.

Final system characterization revolved around understanding how a clot would behave under various shear levels prior to the addition of thrombolytic drugs. Chandler loop-formed clots were formed with either no FhF, 5:1, or 50:1 ratio of FhF, i.e., the upper and lower limits explored priorly. Analysis of the percent change in clot length between the groups at various rates of shear, 0 to 900 s^{-1}, showed that clots underwent highly reproducible degrees of elongation with respect to a given shear rate (**Figure 6.6**). The behavior of clots was very consistent between varying levels of shear, ensuring that clots would be exposed to similar mechanical forces if thrombolytic drugs were introduced.

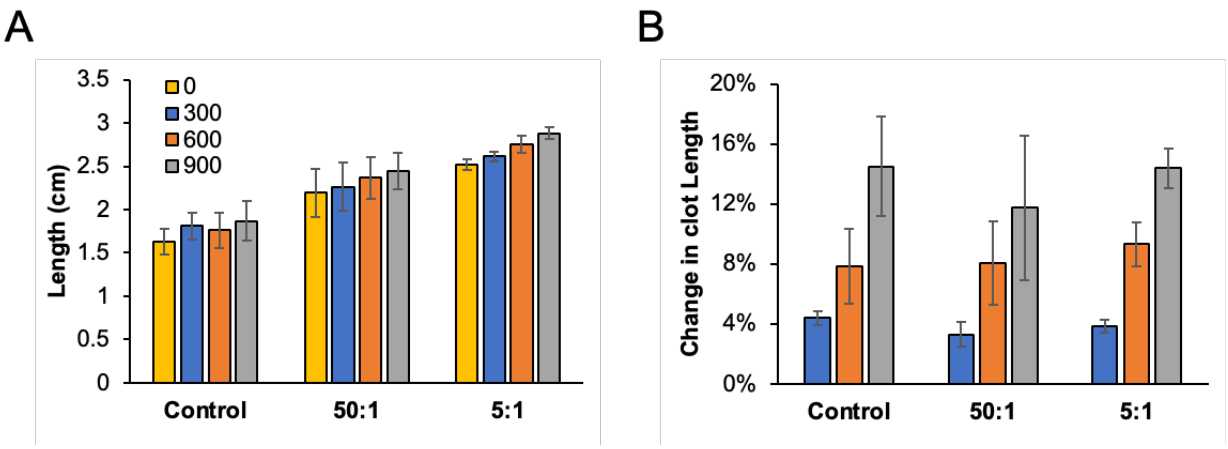

Figure 6.6. (A) Shear-induced clot analog stretching. Individual colored bars represent 0, 300, 600, and 900 s^{-1} wall shear rate. (B) Change in clot length (%) is relative to the clot length under 0 s^{-1} shear. Note the relative uniform stretching of clots in response to varying levels of shear.

6.4.3 Quantifying Fibrinolysis in Real-Time

Noting both the consistency of the in-line fluorometer and the reproducibility of forming FhF incorporated clot analogs, the RT-FluFF assay was ultimately performed. The clot analog was fixed at a 36 cm entrance length away from the first pressure sensor to ensure fully developed laminar flow profile. Clot digestion experiments were conducted using plasma and varying tPA concentrations: 0, 40, 200, and 1,000 ng/mL. Clot dissolutions were observed in all groups although the extent varied based on tPA concentration. Thrombolysis was monitored by a rise in fluorescence within the plasma as FhF was released from the clots themselves, and rates of digestion could be extrapolated from the slopes of the linear phases of the generated scatter plots (**Figure 6.7A and Figure A.23**). Of note, the linear phases generally developed 10-minutes from the time tPA was added and flow was stabilized. In addition to drastic rises in fluorescence, thrombolysis was also readily observable as fibrin degradation led to changes in both clot surface morphology as well as structural stability in response to mechanical shear forces (**Figure 6.7B**). Increasing concentrations of tPA led to consistently noticeable rises in rate of clot digestion - i.e., greater rates of fluorescence release (**Figure 6.7C**). The rate of digestion in the 40 ng/mL tPA (0.53 RFU/min) group did not significantly differ ($P = 0.308$) from the background rise in fluorescence measured from plasma in the 0 ng/mL tPA (0.43 RFU/minute) control group. Addition of 200 ng/mL of tPA led to a statistically significant ($P = 0.008$) rise in the rate of

thrombolysis up to 0.73 RFU/min with 1,000 ng/mL of tPA further raising the slope to 1.17 RFU/min ($P < 0.001$).

We investigated digestion differences associated with pressure driven flow in the RT-FluFF versus non-pressure driven flow in the Chandler loop or static digestion conditions. Similar to the data seen in the pressure-driven flow of RT-FluFF, the rate of fluorescence release increased with increasing tPA concentrations for both static and Chandler loop conditions (**Figure 6.7D and 6.7E**). Rises in the rates of fluorescence release were observed at the 40 ng/mL tPA condition for both static and Chandler loop digestion assays, these differences were both statistically significant compared to their respective control groups. The aforesaid is similar to the 200 ng/mL and 1,000 ng/mL tPA conditions that also reached statistical significance in Chandler loop digestion and static digestion. In addition to collecting fluorescence release as a proxy for thrombolysis, degree of clot digestion was also assessed based on the percentage of mass lost over the duration of the digestion assay. Interestingly, across all the tPA concentrations, digestion in the RT-FluFF assay was consistently slightly higher than in the Chandler loop; however, these differences were minor and statistically not different (Figure 6.7). As an example, percent clot mass lost at the 1,000 ng/mL tPA condition was 79.9% in the Chandler loop versus 85.9% in the RT-FluFF assay ($P = 0.564$). Large reductions in percent clot mass loss were seen when comparing either of the dynamic digestion assays with the respective static condition (**Figure 6.8A**). Comparing the 200 ng/mL tPA condition across all digestion modalities we saw a 26.4% reduction in clot mass for the static condition in contrast to 47.5% and 53.5% in the Chandler loop and RT-FluFF assay respectively (ANOVA $P = 0.003$). Of note, although not statistically significant, a ~10% difference was seen in percent mass lost between both dynamic conditions at 0 ng/mL of tPA and the static condition at 0 ng/mL of tPA.

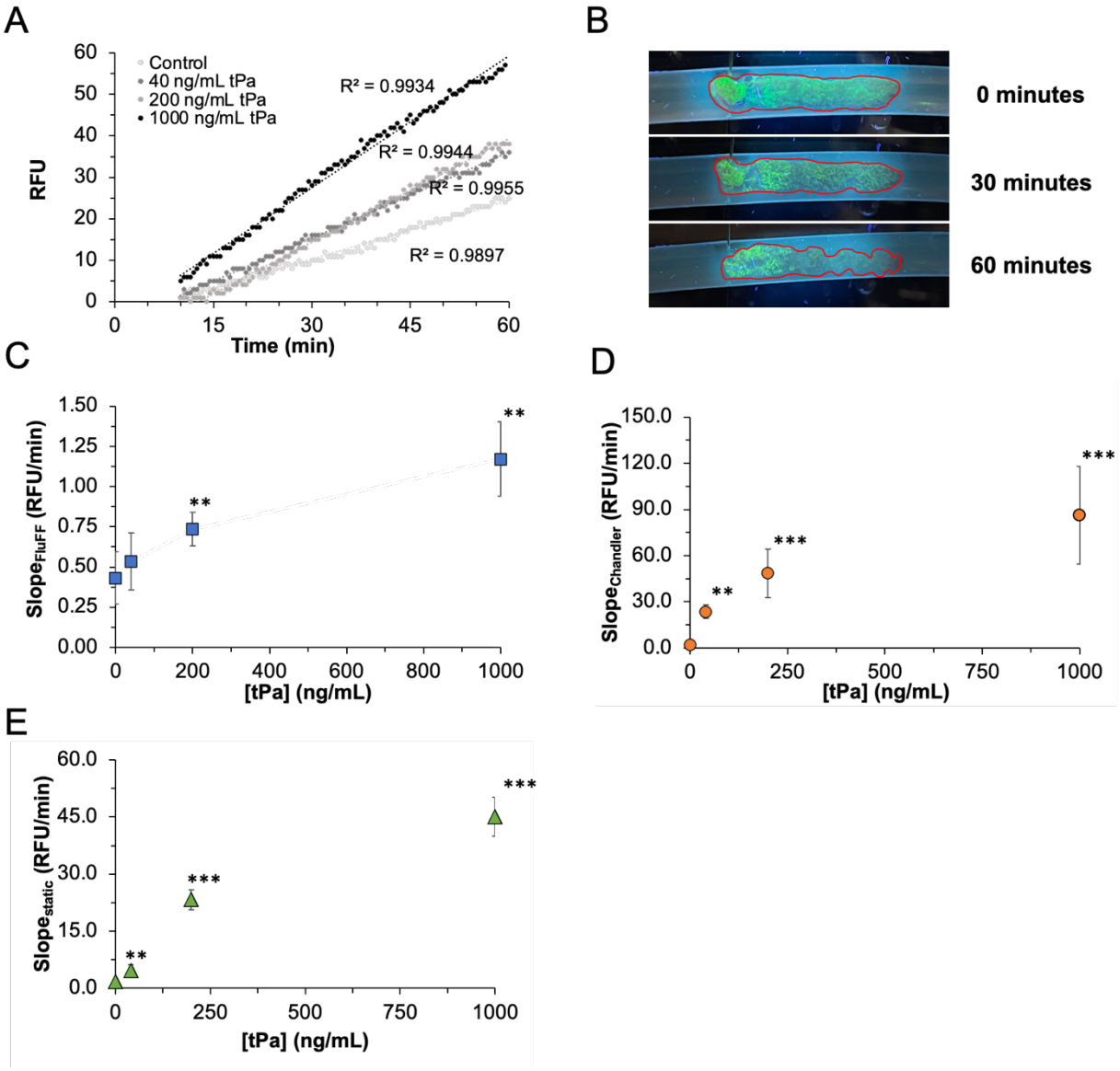

Figure 6.7. (A) Representative scatter plot outlining rise in fluorescence over course of thrombolysis in respective tPA conditions in the RT-FluFF assay. (B) Representative example of gross changes that clots undergo 200 ng/mL tPA digestion illuminated under UV-light. Plot of linear-phase digestion rate by spectrometer captured in (C) RT-FluFF, (D) Chandler loop, and (E) static conditions at varying tPA concentrations.

Lastly, we performed correlation analyses between the percent mass lost during digestion and the rates of digestion as documented by rises in fluorescence from fluorescence release in each respective digestion assay. The strongest correlation was seen in the static digestion assay where a linear correlation coefficient of 0.91 was seen between percent mass loss and the rate of

fluorescence rise during thrombolysis (**Figure 6.8B**). Both dynamic digestion conditions exhibited similarly strong linear correlations to one another albeit less than the static condition. The correlation coefficient for the RT-FluFF assay was 0.78 compared to 0.81 in the Chandler loop (**Figure 6.8C and 6.8D**).

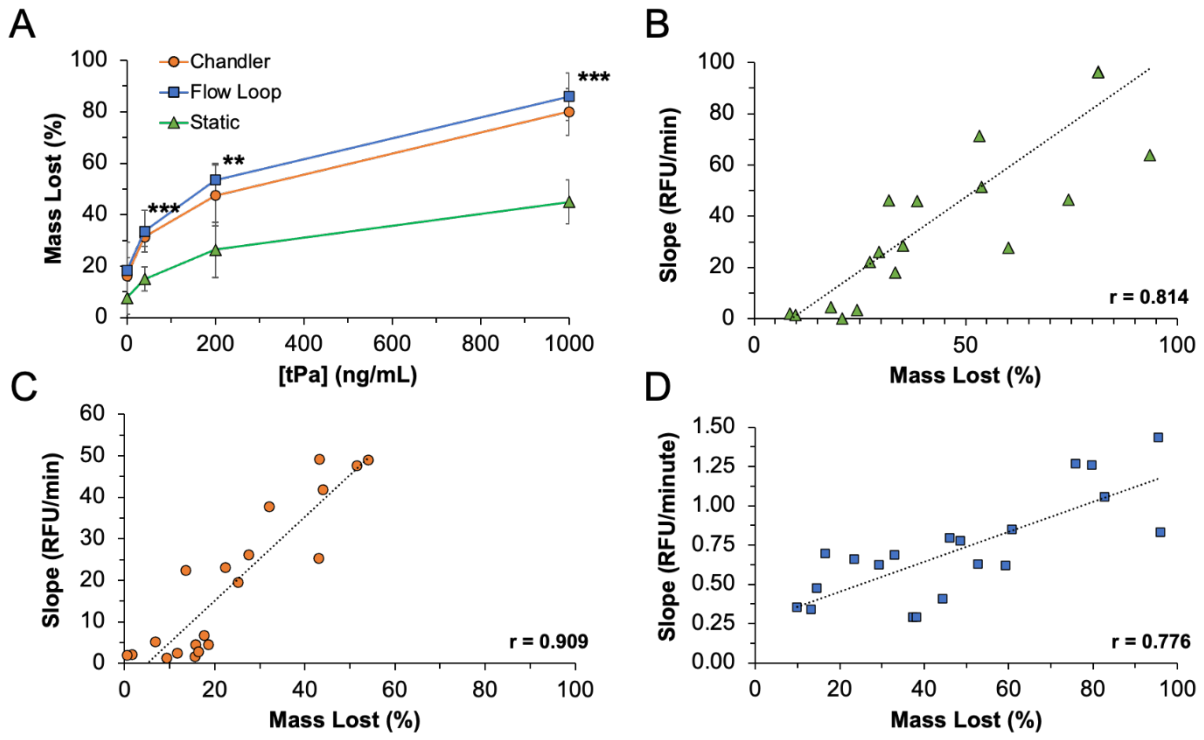

Figure 6.8. A) Percent clot mass lost based on various concentrations of tPA and varying thrombolysis modalities. B) Correlation analysis for static digestion. RFU as tracked by the spectrophotometer. C) Correlation analysis for Chandler loop digestion. RFU as tracked by the spectrophotometer. D) Correlation analysis for the RT-FluFF assay. RFU as tracked by the fluorometer.

6.5 Discussion

6.5.1 Optimization of FITC-labeling

One of the aims of the current study was to characterize and validate the design of a physiologically relevant *in-vitro* model for thrombolytic drug screening. Fibrinolysis is an important step in the dissolution of any thrombus and our study elected to track fibrinolysis via fluorescence release for more informative clot digestion tracking. Ideal clot reporters should have a minimal labeling impact to clot properties whilst maintaining a high fluorescence intensity for

ease of reporting and imaging. In prior studies, we have reported the effect of varying multiple clotting components including reporter conjugated fibrinogen on fibrin clot properties.[18, 24] This study extended the scope and explored the impact of varying FITC conjugated fibrinogen levels on whole blood clots. Based on our TEG results, Chandler loop clot weights/appearances/fibrinolysis behavior, and clot H&E histology our proposed optimal labeling method is to mix whole blood with 14 FITC labels per human fibrinogen to a final concentration of 0.3 mg/mL. This added exogenous FITC-fibrinogen corresponds to one-tenth of the average 3 mg/mL fibrinogen content expected in pooled whole blood from healthy volunteers.[25] Based on our results, this 10:1 ratio of native fibrinogen to FhF corresponds with minimal perturbation of clotting parameters and ultimate clot histology/appearance whilst maximizing fluorescence intensity. Lower fluorescence intensity is to be expected if lower FITC per fibrinogen molecules or lower overall FITC-fibrinogen concentrations are used to achieve a similar impact-free labeling. On the other hand, addition of greater amounts of reporter begin to drastically impact resulting clotting parameters as well as the underlying structure of the clot itself. The above was suggested both through TEG results, particularly the fall in TEG^{Max}, prolongation of TEG^{Time}, and fall in angle, in addition to H&E analysis of the 5:1 FhF group that displayed minor alterations in fibrin organization. H&E analysis of the 5:1 FhF group demonstrated impaired formation of fibrin-rich regions expected within physiologic clots. Lack of such packed fibrin regions likely impacts physical properties of the clot, particularly its mechanical strength, as we experienced during the clot handling process.[26] Interestingly, studies done on the effects of fibrin carbamylation, the same reaction that FITC undergoes with fibrinogen, have shown nearly identical results to ours in terms of perturbations in clotting parameters. Binder et al. were able to show that carbamylation of fibrin led to decreased rates of polymerization, decreased fibrin cross-linking, and even increased propensity to clot lysis.[27, 28]

Our proposition for the ideal ratio of FhF to native fibrinogen should be not viewed as the ultimate standard to be utilized across all assay designs considering that various assays might demand varying levels of reporters. Rather, this data should be used as a guide to others if their aim is to generate physiologically relevant clot analogs for subsequent analysis of fibrinolysis. Additionally, one could easily propose using alternative reporters, labeling strategies, or increasing the utilized FhF concentration at the expense of decreasing the number of FITC molecules per

fibrinogen, a possibility we did not explore in this paper specifically to maintain a higher degree of native fibrinogen in the assay.

6.5.2 Thrombolysis and Fluorometric Monitoring of Fibrinolysis

Thrombolysis, in particular fibrinolysis, was accomplished utilizing tPA introduced into human pooled plasma. Thus, leading to activation of both plasminogen within the plasma itself, in addition to endogenous plasminogen incorporated within the clot analogs during the process of clot formation. We aimed to understand fibrinolysis via two primary means commonly presented in the literature - static and dynamic digestion, with dynamic further subdivided into Chandler loop versus RT-FluFF.

Inherit limits of fibrinolysis detection are reliant on the degree to which FhF is released into solution and the extent to which fluorescence signal is quenched by other particles in the solution – including other FhF molecules themselves. Fibrinolysis was able to be detected at our lowest tPA concentration of 40 ng/mL of tPA in the RT-FluFF assay, as seen by a rise in the rate of fluorescence release compared to baseline; however, this difference was not statistically significant. The blunted rise in fluorescence signal could stems from potential fluorescence quenching triggered by a faster release of loosely incorporated red blood cells (RBCs) from the surface of the clot. The intensity of released FhF quenched as hemoglobin absorbs photons near the wavelength at which FITC emits them upon excitation.[29, 30] We also documented inherit FhF quenching in the experiments comparing rates of fluorescence rise between fluorescein and FhF infusions. This, inherent FhF quenching could also contribute to smaller rises in fluorescence than anticipated as well. The relatively less fluorescence release at the 40 ng/mL of tPA condition are not able to significantly overcome the effects of RBC fluorescence quenching that stem from initial, and continued, RBC wash off from the RBCs loosely coating the clot surface. On the other hand, higher concentrations of tPA lead to drastic rises in FITC labeled fibrin degradation products thus diminishing the impact of the RBCs. Additionally, the inherent rise of baseline plasma fluorescence over the course of 60 minutes of digestion in the RT-FluFF assay also means a decrease in the absolute difference between our control and 40 ng/mL group, thus making statistical significance more difficult. As anticipated, greater concentrations of tPA led to more rapid rises in FITC signal, hence increased fibrinolysis, regardless of the digestion modality.

Although tPA concentrations were conserved between all digestion modalities, mechanical dissolution of the clots stemming from shear forces were not identical. It is these mechanical forces that drive clot mass loss as RBCs get released from the clot upon fibrinolysis.[31] In the static digestion condition, minimal mechanical shear forces are present and thus RBC washout is minimal, leading to smaller degrees of clot mass loss compared to dynamic conditions which were similar in their degree of clot mass loss since the two conditions shared similar shears. Increased RBC release is also suggested by the fact that the RT-FluFF assay does seem to maintain a higher degree of percent clot mass lost during digestion at comparable tPA concentrations. This rise stems not from direct increased fibrinolysis but rather increased RBC release due to mechanical shear forces from pressure-driven flow acting on a degrading fibrin network within the RT-FluFF assay.[32] Additional thrombolysis also stemmed from the mechanical effects of shear in the realm of facilitating dynamic plasminogen interactions with the clot analogs themselves. Prior publications have shown that increasing levels of shear, as well as turbulent flow, allow for greater plasma/plasminogen penetration into the interior fibrin network of clots.[14, 33]

Correlation analyses conducted for each digestion modality indicated that static digestion protocols had the highest correlation of clot mass lost to rate of rise in FhF concentration within plasma. Meanwhile, both dynamic fibrinolysis experimental setups maintained lesser, yet similar, degrees of linear correlation between clot mass loss and a rise in fluorescence. These results are expected when bearing in mind the prior discussion of the importance of mechanical shear forces during thrombolysis. Overall, less linear correlation was seen due to the fact that a given rise in fluorescence release is met by a greater reduction in clot mass than expected based on static digestion, attributable to greater non-fibrinolytic clot mass loss from RBC extrication secondary to mechanical forces induced by shear.[34, 35] Additionally, there is increased potential for FhF to adhere to the tubing within the Chandler loop or RT-FluFF assay compared to simple static digestions, thereby also decreasing the linear correlation coefficients.

6.5.3 Limitations of the *in-vitro* Thrombolysis Model

Although Chandler Loop-formed clots bear good resemblance to native thrombi, the flow conditions generated in the device are not perfect. The circular loop geometry is prone to the formation of Dean flow.[36] This could mean clots formed in the device are a less direct reflection of the effects of shear. Thus, the present *in-vitro* platform can genuinely benefit from the utilization

of clot analog formation techniques ideally incorporating pulsatile flow, or even retrieved patient thrombi labeled with FITC-linked fibrin binding peptides.[37] The portable fluorometer we designed is capable of tracking FITC fluorescence signals in plasma, as plasma has low background fluorescence values with the wavelengths used. However, fluorescence signals can be significantly quenched by RBC release even at levels as low as 0.1% v/v within the system. This is in part due to a 550 nm sensitive photo sensor used for signal acquisition, a wavelength overlapping with RBC absorption at 538 nm.[30] Although experiments were not largely affected, since our digestion medium was plasma, different fluorophores or different photosensors would be recommended for studies that aim to utilize whole blood as a medium. Additionally, reliance on FITC-fibrinogen presents the issue of fluorescence quenching due to FITC residue burial within the protein complex.[38] To ensure stable shear with laminar flow was achieved in the RT-FluFF assay, a dampener was utilized to reduce pressure fluctuations associated with the peristatic pump. While this provides a high degree of digestion control and consistent flow field development, it does not fully encompass the native pulsatile flow in the body.

6.6 Conclusions

Thrombolysis and fibrinolysis are very dynamic processes whose accurate characterization requires numerous repeat observations over a short period of time. Thus, commonly utilized means of quantifying fibrinolysis/thrombolysis such as endpoint reads, whether changes in mass or absolute rises in fluorophore release, may not truly capture the entire process. The RT-FluFF model can help bridge this gap by providing a means of real-time fluorescence monitoring in the context of a flowing system with great fidelity. This allows the user to capture both the instantaneous rates of fibrinolysis in addition to dynamics such as initial lag phases that potentially represent both tPA binding and infiltration, as well as mechanical clot digestion. In addition to mimicking *in-vivo* flow, and allowing for live fluorescence monitoring, our system also maintains numerous other benefits: (a) interchangeable tubing geometries/configurations, (b) real-time pressure monitoring as a means of quantifying degree of lumen occlusion, (c) real-time fluorescence measurements requiring no system intervention, (d) reading duration and frequency flexibility, (e) incorporation of a reservoir to better recapitulate *in-vivo* conditions, (f) flow-patterns generated resemble *in-vivo* conditions since the substrate is stationary with fluid flow-by, in contrast to the Chandler loop, (g) option to include pulsatile flow, (h) live-imaging of substrate

allowing for image analysis. Overall, the RT-FluFF assay serves as a cost-effective and versatile *in-vitro* tool in the development and screening of novel thrombolytic agents.

6.7 References

[1] T. Huang, N. Li, J. Gao, Recent strategies on targeted delivery of thrombolytics, Asian Journal of Pharmaceutical Sciences 14(3) (2019) 233-247.

[2] R.A. Robinson, L.H. Herbertson, S. Sarkar Das, R.A. Malinauskas, W.F. Pritchard, L.W. Grossman, Limitations of using synthetic blood clots for measuring in vitro clot capture efficiency of inferior vena cava filters, Medical Devices: Evidence and Research 6(1) (2013) 49-57.

[3] P. Bhogal, T. Andersson, V. Maus, A. Mpotsaris, L. Yeo, Mechanical Thrombectomy-A Brief Review of a Revolutionary new Treatment for Thromboembolic Stroke, Clin Neuroradiol 28(3) (2018) 313-326.

[4] M.R. Ali, M. Salim Hossain, M.A. Islam, M. Saiful Islam Arman, G. Sarwar Raju, P. Dasgupta, T.F. Noshin, Aspect of thrombolytic therapy: A review, Scientific World Journal 2014(1) (2014).

[5] D.J. Miller, J.R. Simpson, B. Silver, Safety of thrombolysis in acute ischemic stroke: a review of complications, risk factors, and newer technologies, Neurohospitalist 1(3) (2011) 138-47.

[6] F. Fluri, M.K. Schuhmann, C. Kleinschnitz, Animal models of ischemic stroke and their application in clinical research, Drug Des Devel Ther 9 (2015) 3445-54.

[7] E.E. Kaiser, F.D. West, Large animal ischemic stroke models: replicating human stroke pathophysiology, Neural Regen Res 15(8) (2020) 1377-1387.

[8] R. Thiex, W. Kuker, H.D. Muller, I. Rohde, J.M. Schroder, J.M. Gilsbach, V. Rohde, The long-term effect of recombinant tissue-plasminogen-activator (rt-PA) on edema formation in a large-animal model of intracerebral hemorrhage, Neurol Res 25(3) (2003) 254-62.

[9] A. Elnager, W.Z. Abdullah, R. Hassan, Z. Idris, N. Wan Arfah, S.A. Sulaiman, Z. Mustafa, In vitro whole blood clot lysis for fibrinolytic activity study using d-dimer and confocal microscopy, Adv Hematol 2014 (2014) 814684.

[10] S. Prasad, R.S. Kashyap, J.Y. Deopujari, H.J. Purohit, G.M. Taori, H.F. Daginawala, Development of an in vitro model to study clot lysis activity of thrombolytic drugs, Thrombosis Journal 4 (2006) 9-12.

[11] L.A. Robbie, S.P. Young, B. Bennett, N.A. Booth, Thrombi Formed in a Chandler Loop Mimic Human Arterial Thrombi in Structure and PAI-1 Content and Distribution, Thrombosis and Haemostasis 77(03) (1997) 510-515.
[12] N.J. Mutch, N.R. Moore, C. Mattsson, H. Jonasson, A.R. Green, N.A. Booth, The use of the Chandler loop to examine the interaction potential of NXY-059 on the thrombolytic properties of rtPA on human thrombi in vitro, British Journal of Pharmacology 153(1) (2008) 124-131.
[13] A. Blinc, S.D. Kennedy, R.G. Bryant, V.J. Marder, C.W. Francis, Flow through clots determines the rate and pattern of fibrinolysis, Thromb Haemost 71(2) (1994) 230-5.
[14] D.V. Sakharov, D.C. Rijken, The effect of flow on lysis of plasma clots in a plasma environment, Thromb Haemost 83(3) (2000) 469-74.
[15] B.A. Herbig, X. Yu, S.L. Diamond, Using microfluidic devices to study thrombosis in pathological blood flows, Biomicrofluidics 12(4) (2018) 042201.
[16] H. Jigar Panchal, N.J. Kent, A.J.S. Knox, L.F. Harris, Microfluidics in Haemostasis: A Review, Molecules 25(4) (2020).
[17] C.S. Whyte, H.A. Mostefai, K.M. Baeten, A.J. Lucking, D.E. Newby, N.A. Booth, N.J. Mutch, Role of shear stress and tpa concentration in the fibrinolytic potential of thrombi, International Journal of Molecular Sciences 22(4) (2021) 1-15.
[18] Z. Zeng, T. Nallan Chakravarthula, C. Muralidharan, A. Hall, A.K. Linnemann, N. Alves, Fluorescently Conjugated Annular Fibrin Clot for Multiplexed Real-time Digestion Analysis, Journal of Materials Chemistry B (2021).
[19] A. Christodoulides, Z. Zeng, N.J. Alves, In-vitro thromboelastographic characterization of reconstituted whole blood utilizing cryopreserved platelets, Blood Coagulation & Fibrinolysis Publish Ah (2021) 1-8.
[20] G.A. Truskey, F.P.D. Yuan, D.F. Katz, Transport phenomena in biological systems, 2nd , International ed., Pearson, Boston, Mass. ; London, 2010.
[21] N.J. Mutch, J.S. Koikkalainen, S.R. Fraser, K.M. Duthie, M. Griffin, J. Mitchell, H.G. Watson, N.A. Booth, Model thrombi formed under flow reveal the role of factor XIII-mediated cross-linking in resistance to fibrinolysis, Journal of Thrombosis and Haemostasis 8(9) (2010) 2017-2024.
[22] E. Genton, A.P. Fletcher, N. Alkjaersig, S. Sherry, Assay of plasma thrombolytic activity with fluorescein-labeled clots, The Journal of laboratory and Clinical Medicine 64(2) (1964) 313-320.

[23] C.S. Whyte, F. Swieringa, T.G. Mastenbroek, A.S. Lionikiene, M.D. Lancé, P.E.J. Van Der Meijden, J.W.M. Heemskerk, N.J. Mutch, Plasminogen associates with phosphatidylserine-exposing platelets and contributes to thrombus lysis under flow, Blood 125(16) (2015) 2568-2578.
[24] Z. Zeng, M. Fagnon, T. Nallan Chakravarthula, N.J. Alves, Fibrin clot formation under diverse clotting conditions: Comparing turbidimetry and thromboelastography, Thrombosis Research 187(January) (2020) 48-55.
[25] M.W. Oswald, H.H. Hunt, J. Lazarchick, Normal range of plasma fibrinogen, Am J Med Technol 49(1) (1983) 57-9.
[26] K. Gersh, C. Nagaswami, J. Weisel, Fibrin network structure and clot mechanical properties are altered by incorporation of erythrocytes, Thrombosis and Haemostasis 102(12) (2009) 1169-1175.
[27] J.J. de Vries, C.J.M. Snoek, D.C. Rijken, M.P.M. de Maat, Effects of Post-Translational Modifications of Fibrinogen on Clot Formation, Clot Structure, and Fibrinolysis: A Systematic Review, Arterioscler Thromb Vasc Biol 40(3) (2020) 554-569.
[28] V. Binder, B. Bergum, S. Jaisson, P. Gillery, C. Scavenius, E. Spriet, A.K. Nyhaug, H.M. Roberts, I.L.C. Chapple, A. Hellvard, N. Delaleu, P. Mydel, Impact of fibrinogen carbamylation on fibrin clot formation and stability, Thromb Haemost 117(5) (2017) 899-910.
[29] A. Imhof, M. Megens, J.J. Engelberts, D.T.N. de Lang, R. Sprik, W.L. Vos, Spectroscopy of Fluorescein (FITC) Dyed Colloidal Silica Spheres, The Journal of Physical Chemistry B 103(9) (1999) 1408-1415.
[30] M. Wojdyla, S. Raj, D. Petrov, Absorption spectroscopy of single red blood cells in the presence of mechanical deformations induced by optical traps, Journal of Biomedical Optics 17(9) (2012).
[31] F.C. Roessler, M. Ohlrich, J.H. Marxsen, M. Schmieger, P.K. Weber, F. Stellmacher, P. Trillenberg, J. Eggers, G. Seidel, Introduction of a new model for time-continuous and non-contact investigations of in-vitro thrombolysis under physiological flow conditions, BMC Neurol 11 (2011) 58.
[32] R.I. Litvinov, J.W. Weisel, Role of red blood cells in haemostasis and thrombosis, ISBT Sci Ser 12(1) (2017) 176-183.

[33] G. Tratar, A. Blinc, M. Strukelj, U. Mikac, I. Sersa, Turbulent axially directed flow of plasma containing rt-PA promotes thrombolysis of non-occlusive whole blood clots in vitro, Thromb Haemost 91(3) (2004) 487-96.
[34] A.H. Gillespie, A. Doctor, Red Blood Cell Contribution to Hemostasis, Front Pediatr 9 (2021) 629824.
[35] J.R. Byrnes, C. Duval, Y. Wang, C.E. Hansen, B. Ahn, M.J. Mooberry, M.A. Clark, J.M. Johnsen, S.T. Lord, W.A. Lam, J.C.M. Meijers, H. Ni, R.A.S. Ariëns, A.S. Wolberg, Factor XIIIa-dependent retention of red blood cells in clots is mediated by fibrin α-chain crosslinking, Blood 126(16) (2015) 1940-1948.
[36] H. Touma, I. Sahin, T. Gaamangwe, M.B. Gorbet, S.D. Peterson, Numerical investigation of fluid flow in a chandler loop, Journal of Biomechanical Engineering 136(7) (2014) 1-8.
[37] N. Weiss, B. Schenk, M. Bachler, C. Solomon, D. Fries, M. Hermann, FITC-linked Fibrin-Binding Peptide and real-time live confocal microscopy as a novel tool to visualize fibrin(ogen) in coagulation, Journal of Clinical and Translational Research 3(2) (2017) 276-282.
[38] J.H. Wu, S.L. Diamond, A Fluorescence Quench and Dequench Assay of Fibrinogen Polymerization, Fibrinogenolysis, or Fibrinolysis, 1995, pp. 83-91.

7. PULSATILE EFFECT ON THROMBOLYTIC DRUG EFFICACY

Content of this Chapter is being prepared for a journal publication review.

Continued from the previous chapter in developing a representative *in-vitro* flow model for thrombolytic drug evaluations, this chapter describes the modification of the RT-FluFF model to include pulsatile flow dynamic features and study the impact of pulsatile effect on thrombolytic drug efficacy.

7.1 Abstract

Thromboembolism lodged near the main pulmonary artery (MPA) accounts for most of the pulmonary embolism (PE) related mortality. Developing an *in-vitro* model that mimics MPA flow dynamics can benefit the design of novel thrombolytic drugs. Steady shear models such as microfluidic assays have been well-established to study thrombosis and thrombolysis. Models that involve cyclic flows are often overlooked although the effect of pulsatility on drug activities have been widely assumed. We herein report a design of an *in-vitro* flow model for studying the cyclic pressure amplitude on thrombolytic drug induced clot digestion. Fluorescently labeled plasma clots that are formed in a Chandler loop are placed inside an unbranched tubing after which an MPA average pressure is established by elevating the outlet from clot site. 60-, 20- and 6-cc dampeners are used to create pressure amplitudes that are ±2, ± 10, and ± 20 mmHg, respectively. Plasma is perfused at a MPA relevant condition (averaged wall shear rates = 913 s^{-1}) and two slower flows (205 and 523 s^{-1}) with or without the addition of 1000 ng/mL tPA. Increased shear contributes to both larger mechanical digestion and thrombolytic digestion. Increasing pressure amplitude results in an increasing trend of fibrinolysis and clot mass loss. The human heartbeat mimetic setup (523 s^{-1}), which has a 1 Hz pulsatile frequency, also confirmed an increased fibrinolysis compared to its fully dampened counterpart at the same average volumetric flow rate. These findings suggest that the pulsatile flow affects thrombolytic drug activities and increased cyclic pressure amplitude can lead to increased clot digestions.

7.2 Introduction

Thromboembolism lodged near main pulmonary artery (MPA) accounts for most of the pulmonary embolism (PE) related mortality.[1, 2] Developing an *in-vitro* MPA flow condition to study thrombolytic therapy can benefit the design of novel thrombolytic drugs and improve dosage prediction for a thrombolytic therapy. Common methods to study *in-vitro* thrombolysis under flow is through creating an *ex-vivo* wall shear condition where laminar flow and continuous pressure are in use. Lumen dimensions and volumetric input are usually adjusted to get a desired luminal wall shear rate to mimic a blood vessel shear condition. While studying steady-state shear or continuous pressure effects on clot digestion is useful, modeling flow pulsatility generated by the human heart also demands research attention as it more closely represents *in-vivo* hemodynamics. Although pulsatile flow and cyclic wall stress have long been considered to impact *in-vivo* drug or enzyme activities, only a few studies have explored this relation in the past and the information on how pulsatile pressure amplitude affects the thrombolytic efficacy is missing.[3-5] To facilitate a good communication in this manuscript, we refer pulsatile pressure amplitude as the pulsatile pressure difference between systolic and diastolic pressure over a cardiac cycle. Pulsatile pressure amplitude can have a huge variation due to diversified vessel geometry and pathological conditions in human vasculature. For instance, it can be 25 mmHg in the right ventricle and 15 mmHg in the pulmonary artery of a normal patient and as high as 80 mmHg in pulmonary artery hypertension (PAH) patients.[6, 7] In clinical settings, physicians have adopted the pulsatility index, which is a dimensionless adaption of pulsatile pressure amplitude, for diagnosis and treatment monitoring. Pulmonary artery pulsatility index (PAPI) plays an important role in detection of thrombosis related right ventricle failures and correlates with better patient survival rates after treatment. The PAPI is defined as the difference between systolic and diastolic pulmonary artery pressure divided by central venous pressure. [7-9] Therefore, it is important to address the effect of varying pulsatile pressure amplitude on thrombolytic drug efficacy.

Importantly, the increased complexity by involving flow pulsatility demands an *in-vitro* flow model to have as much physiological relevance as possible. Since it is often unpractical to directly perfuse blood at a human heart output level, researchers often adopt a down-scaled *in-vitro* setup to save experimental resources. Matching an averaged wall shear value in a scaled design fails to recapitulate critical components of native flow dynamics. For example, microfluidic assays using a submillimeter lumen could end up having a below unity Reynolds number, which

is indicative of a highly ordered laminar flow that is largely distinct from that of major blood vessels. According to Buckingham-Pi theorem, a better kinematic similarity can potentially be achieved by having identical dimensionless factors. These include ratio of length scales to ensure a dimensional similarity, Reynolds number to have a similar flow pattern, and Fanning friction factor to have a comparable fluid shear effects on lumen surfaces. When the pulsatile flow is relevant, Womersley number should also be matched to that of the target *in-vivo* condition to keep dynamic similarity.[10, 11] Womersley number gives a unique pulsatile flow profile which varies by vessel diameters in human blood at a given heart rate.[12, 13]

In this study, we elected to create an *in-vitro* MPA flow condition to explore the pulsatility impact on thrombolytic drug induced clot digestion.[1] Given that average blood output in MPA is about 5.2 ± 1.0 L/min where average *Re* = 1570 ± 404 with a maximum volumetric flow of 21 L/min, a down-scaled macroscopic *in-vitro* flow model should be adopted.[14] And thus, we modified our previously developed steady flow RT-FluFF, the unbranched tubing loop model, into a setup that can provide for pulsatile flow. To mimic the kinematic dynamics in MPA, parameters in the RT-FluFF model were adjusted to match an averaged *Re* where $\bar{Q}$ is the averaged volumetric flow rate of a pulsatile cycle, D is the lumen diameter and ν is the kinematic viscosity using the following equation:

$$\frac{\bar{Q}_{model}}{D_{model}\nu_{model}} = \frac{\bar{Q}_{MPA}}{D_{MPA}\nu_{MPA}}$$

The fanning friction factor is dependent on *Re*. The Womersley number is also matched using the equation below where f is the pulsatile frequency:

$$D_{model}\sqrt{\frac{f_{model}}{\nu_{model}}} = D_{MPA}\sqrt{\frac{f_{MPA}}{\nu_{MPA}}}$$

Additionally, the diameter of the peristaltic in-pump tubing, which is different from the D_{model}, should be selected based on the calculated volumetric flow output $\bar{Q}_{model}$ of the peristaltic pump. Since model pulsatile frequency f_{model} is dictated by the product of roller numbers and revolution per minute of the pump, which also dictates $\bar{Q}_{model}$, the following equation should also be obeyed.

$$\bar{Q}_{model} = 1\ L/min * \frac{f_{model}}{40}$$

The calculated model condition aims at providing an MPA relevant flow dynamics to study the effect of pulsatile pressure amplitude on thrombolysis. Through further adjusting the dampening efficiency to the oscillation generated by the peristaltic pump, pulsatile pressure amplitude can be further tuned in the RT-FluFF model, where the flow can have different transient *Re* although an average value is still maintained. We used three different dampeners with adjusted air capacity to obtain three levels of pressure amplitude (4, 20, and 40 mmHg) at a calculated MPA relevant condition (**Figure A.21**). To offer a more comprehensive examination on pulsatility impact, we further adopted two extra volumetric flow rates to study thrombolysis at different dampening levels while keeping all other model variables the same. Additionally, given that all model frequency employed thus far were larger than that of the actual human heart, we conduct thrombolysis experiments using a human heart mimetic pulsatile flow (1 Hz). This human heartbeat setup may not give similar MPA flow dynamics but can provide a human relevant pulsatile frequency that benefits the understanding of the impact of pulsatility. Fluorescently labeled clot substrates were formed in a Chandler loop device. These substrates were then placed inside the RT-FluFF model to assess thrombolysis with or without tPA (Alteplase). Both fluorescence release and clot mass loss were recorded to indicate mechanical clot digestion and/or a tPA induced thrombolysis. In all, by incorporating mimetic flow dynamic features, the modified RT-FluFF model can provide a similar MPA flow dynamics and offer a representative platform to study pulsatile flow on thrombolytic therapy.

7.3 Materials and Methods

7.3.1 Pulsatile RT-FluFF Model Setup

The RT-FluFF model was assembled following a protocol mentioned in chapter 6 (**Figure 6.1**). The model includes a peristaltic pump (Masterflex EasyLoad II), in-pump tubing (1.5 feet #6415, Inner Diameter= 3/16 inch; Masterflex, Gelsenkirchen, Germany), two pressure sensors (Disposable IBP transducer), a dampener, a 50 mL reservoir (Corning Scientific, Corning, NY), and an in-line fluorometer, which are connected by 5/32” (Inner diameter = 0.004 m) tubing pieces (Tygon MD 100-65). Two pressure sensors (sensor A and sensor B) were located before and after the clot site in a straight tubing to monitor the pulsatile flow pressures. Dampeners were made via fitting a 5/16” (Inner diameter = 0.008 m) tubing segment to the tip of three different sized plastic

syringes (6 ml, 20 mL, and 60 mL) noted as 6, 20, and 60 cc. A three-way connector was used to incorporate the dampener into the flow loop. Plunger positions of dampeners were adjusted to be spontaneously balanced at a 187 RPM pump rate. This result in 1 mL, 5 mL and 60 mL in 6 mL, 20 mL and 60 mL syringes yielding pressure differences between systolic and diastolic of 4, 20 and 40 mmHg, respectively. In all experiments, liquid only oscillates in the fitted tubing segment without going into the syringe indicating a good retaining of total circulating fluid.

Flow parameters in the *in-vitro* model can be solved using equations mentioned in the introduction. Clinical MPA data were used as a guide while actual *Re* and *alpha* values were calculated based on the basic properties shown in **Table 7.1**. [15] Importantly, we elected to perfuse the *in-vitro* model with platelet-free plasma to create a relatively clear background for real-time fluorescence monitoring. The reservoir is elevated to match average pressure at pressure sensor B (the second pressure sensor) to an average human MPA pressure which is 12 mmHg. A fluorescently labeled clot substrate is fixed immediately before pressure sensor B to match ratio of length scales of the MPA.

The human heartbeat setup, noted as 1Hz on/off, was achieved by modifying peristaltic pump to include an in-house developed fingerbot that pushes the pump on/off button to give a pulsatile flow frequency of 1 Hz. Flow turned on and off at a relatively instant manner generating an approximately sinusoidal wave. The wave form can be confirmed by both pressure sensor A and B in the RT-FluFF. At the largely dampened (± 2 mmHg) 214 RPM pump condition, the pressure curve revealed a smooth oscillation and gives a volumetric output at the same level of the 107 RPM (average wall shear rate = 523 s^{-1}) pump flow.

Table 7.1. Flow Parameters of RT-FluFF model to mimic MPA

	MPA	**RT-FluFF Model**
Viscosity (pa·s)	0.0035	0.0012
Density (kg/m^3)	1060	1025
Frequency (Hz)	1	16.76
Lumen diameter (m)	0.025	0.004
Volumetric flow rate (L/min)	5.2	0.268
Reynolds number	1337	1337
Womersley number	17.2	17.2

Note: MPA data are collected from a clinical study.[15]

7.3.2 Clot Formation and Digestion

Fluorescently labeled plasma clots were formed in a Chandler loop device (**Figure 5.1**) using FITC-human fibrinogens (FhF) mixed pooled plasma at an equivalent fibrinogen ratio, which is plasma: FhF = 10:1. This protocol has been previously demonstrated to have minimal impact to clot properties. A final concentration of 16.5 mM $CaCl_2$ was added to 2 mL plasma to initiate clotting. The rotational rate of Chandler loop was kept at 40 RPM (500 s^{-1}) to mimic pulmonary artery wall shear. Clots were formed for 1.5 hours, and products were gently blotted on papers (Kimtech Science, Fisher Scientific, NH) before weighing.

Clot digestion experiments were conducted by perfusing blood type-matched pooled plasma with or without the addition of 1000 ng/mL tPA in the RT-FluFF model. Thrombolysis was monitored for 30 minutes at three dampening levels and three pump rotational rates: 27, 107 and 187 RPM, corresponding to average wall shear rates of 205, 523, and 913 s^{-1}, respectively. Human heartbeat relevant experiment was performed at 214 RPM with the highly dampened setup (60 cc dampener) and with the pump turning on and off at 1 Hz. With this on/off manner, results at the on/off 214 RPM can be directly compared with those of the 107 RPM steady flow as they share the same volumetric flow rate. All groups were repeated at n = 3 to 6. Readings in the in-line fluorometer (**Figure 6.1A**) were taken with a 450 nm excitation and a 550 nm emission every 30 second. Reminder clots after digestion were collected from the RT-FluFF model, blotted, weighed, and transferred back into the reservoir for an overnight digestion. 1000 ng/mL tPA were added to control groups for digestion. Fluorescence at 0 min, 30 min and time when the clot is complete digested were taken in the spectrometer (excitation 495 nm, emission 519 nm) to calculate digestion%.

7.3.3 Statistical Analysis

ANOVA analysis was used to ascertain statistical differences among groups with three or more conditions, followed by a Tukey test for individual subset comparisons. Student t-tests or Welch's t tests were utilized to compare two categorical variables at equal or unequal sizes. Statistical significance was deemed to be a p-value < 0.05. A single asterisk denotes a p-value < 0.05, double asterisk denotes a p-value < 0.01, and triple asterisk signifies a p-value < 0.001.

7.4 Results

This study explored the impact of pulsatile pressure amplitude on clot digestion with or without thrombolytic drugs. Multiple conditions were mimicked in the RT-FluFF model, among which an MPA relevant flow condition is established through matching dimensionless factors by using selected model components and a peristaltic pump rate of 187 RPM (average wall shear rate = 913 s^{-1}). Three different syringes (60, 20, and 6 cc) were modified to function as dampeners to create three pressure amplitudes at 913 s^{-1} corresponding to 4, 20, and 40 mmHg, respectively. Additional pump rate setups that are 205 s^{-1}, 523 s^{-1}, and a 1 Hz on/off 523 s^{-1}, were also explored at the same dampeners to comprehensively study pulsatile flow impact. Rates of fluorescence release upon digestion were derived from fluorescence tracing curves monitored by the in-line fluorometer to directly indicate clot digestion.

Significant differences were observed across no tPA control and 1000 ng/mL tPA at all flow conditions (**Figure 7.1**). At 913 s^{-1}, the MPA relevant flow dynamic condition, an increasing trend of tPA induced clot digestion rate (19% increase of $Slope_{FluFF}$, P = 0.0013) was observed when pulsatile pressure amplitude increased from 4 to 40 mmHg. Similar trend was also observed at 523 s^{-1} (89% increase) and 205 s^{-1} (51% increase) when comparing clot digestion rates at 4 mmHg (60 cc dampener) and 40 mmHg (6 cc dampener) although no statistical significance (P > 0.05) was noted because of the large variation in these experiment group. No such trend was shown in zero tPA control groups at these flow conditions. This indicated that increasing pressure amplitude at a given flow rate might not increase mechanical digestion but could result in an improved thrombolytic drug efficacy. At any given pressure amplitudes, clot digestion rates were higher at 913 s^{-1} than at 205 s^{-1} in both tPA and no tPA groups. Strong statistical significances were observed in tPA groups at 60 cc (P = 0.0001), 20 mL (P = 0.0107) and 6 cc dampeners (P = 0.006) and no tPA control groups at 60 cc (P = 0.017) and 6 cc dampeners (P = 0.015) demonstrating both increased mechanical digestion and increased drug induced thrombolysis at a higher RPM, or a higher average wall shear stress.

In addition, all pulsatile frequency employed in our model was higher than that of the human heart. To explore the effect of human relevant pulsatility on thrombolysis, an additional experiment was conducted by adding a human heartbeat pulsatile (1 Hz) to the highly dampened (60 cc dampener) the 523 s^{-1} averaged shear condition. The heartbeat setup (523 s^{-1} and 1 Hz on/off) has an equivalent volumetric output as the highly dampened 523 s^{-1}. tPA induced clot digestion

rates were 63% higher (P = 0.0165) in the heartbeat setup than in the highly dampened 523 s^{-1} while an inversed result (P = 0.641) was seen when comparing no tPA groups. These results further confirmed that the addition of pulsatility contributes to an improved fibrinolysis.

Similar results and trends were observed in Mass loss% and clot digestion% as clot digestion rate results in all experiments. (**Figure 7.2**) Clot mass is not used as the primary factor for monitoring thrombolysis in this study due to its limitation in accurately dictating plasma clot digestion. Change in clot mass after digestion can reflect both change in clot dry weights and change in the network's ability in retaining water despite clots were similarly blotted in all experiments. We shifted to use the percent fluorescence release to further document clot digestion percentage. After 30 min clot digestion in RT-FluFF assay, reminder clots were fully digested in tubes. Clot digestion % was calculated based on ratios of sample fluorescence at 30 min release and complete digestion that were both collected using a spectrometer.

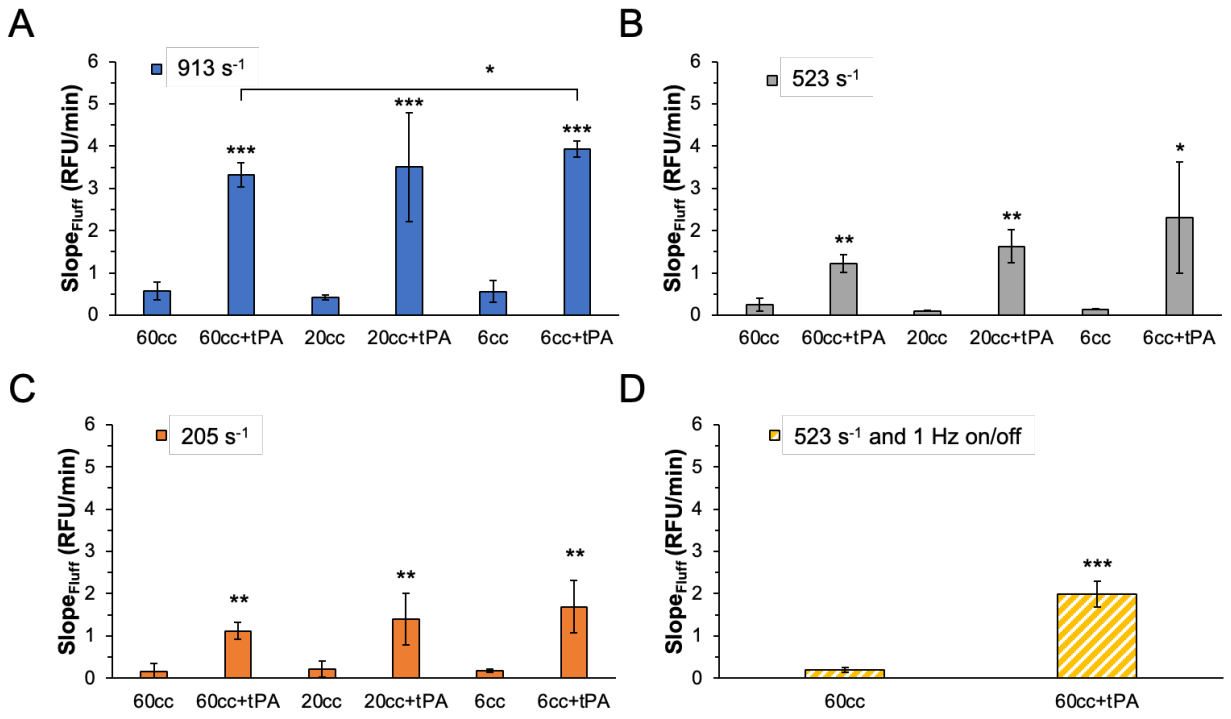

Figure 7.1. Clot digestion slope (RFU/min) by fluorometer in the RT-FluFF model were compared across three dampeners settings at (A) 913 s^{-1}, (B) 523 s^{-1}, (C) 205 s^{-1}, and (D) 523 s^{-1} 1Hz on/off setups. Significant differences between 0 and 1000 ng/mL tPA were shown. Single asterisk denotes P-value < 0.05, double asterisk denotes P-value < 0.01, and triple asterisk denotes P-value < 0.001.

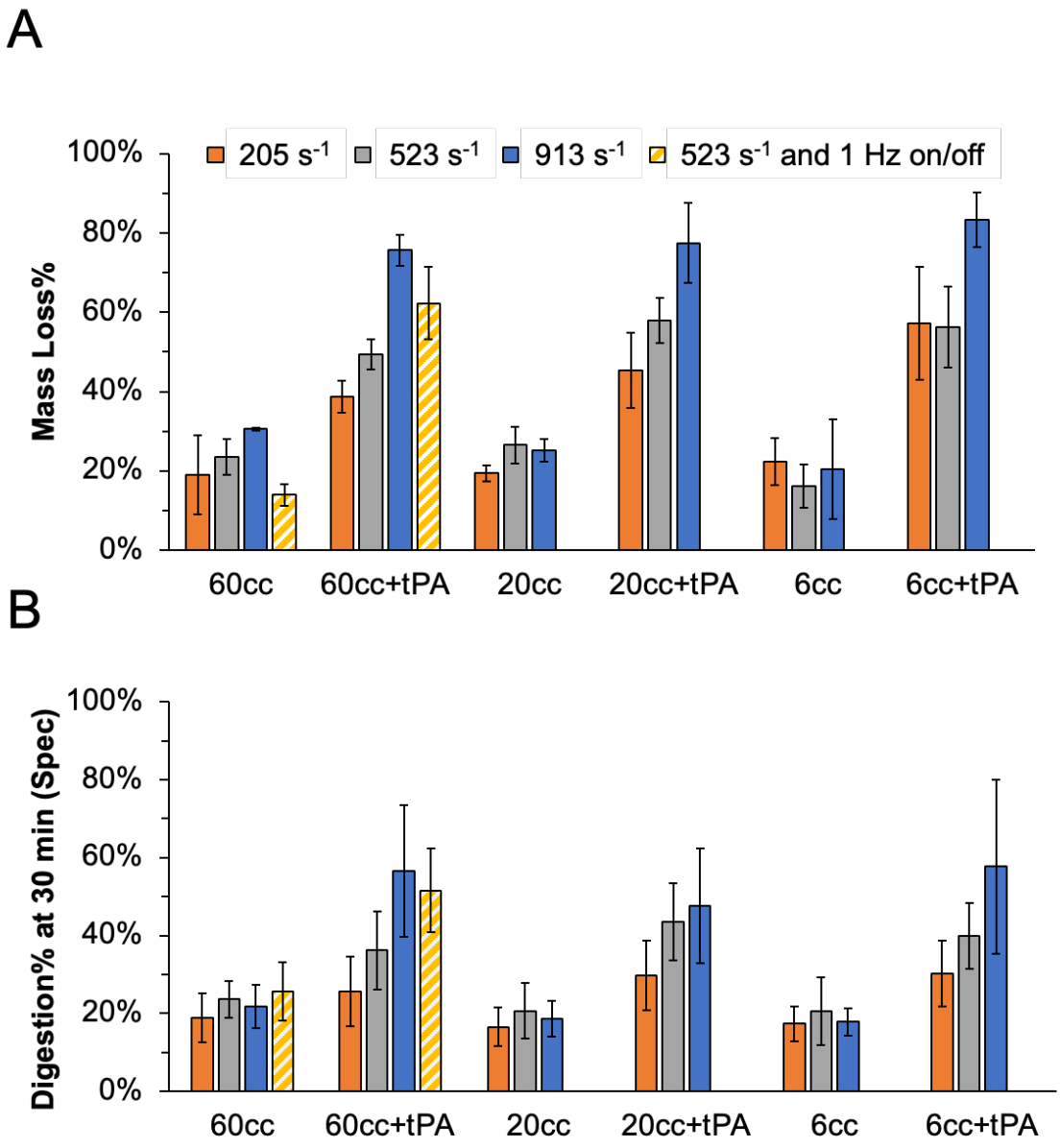

Figure 7.2. (A) Clot mass loss% at 30 min and (B) digestion% at 30 min in the RT-Fluff model were compared across three dampeners (60, 20, and 6 cc) at averaged shear rates of 913 s^{-1}, 523 s^{-1}, 205 s^{-1}, and 523 s^{-1} at 1 Hz on/off.

7.5 Discussion

The effect of pulsatile flow on thrombolytic drug activities has been poorly addressed in the literature. Researchers tend to adopt continuous *in-vitro* flow models to evaluate drugs due to their simplicity. Moreover, left ventricular assist devices (LVADs) are continuous-flow devices that provide hemodynamic supports to patients with heart failure. The great clinical outcome of LVADs also makes people wonder if pulsatile flow is genuinely an essential flow component in humans as the steady flow offered by the pump does not largely affect organ functions. [16, 17] This study explored the impact of pulsatile pressure amplitude on thrombolytic drug induced clot lysis in a variety of pulsatile flow conditions including a human main pulmonary artery (MPA) relevant *in-vitro* condition. In summary to our observation, higher pulsatile pressure amplitude contributes to an increasing trend of tPA induced clot digestion rate. Through adding a human heartbeat pulsatility to a continuous flow, we have also found a faster thrombolysis in the presence 1000 ng/mL tPA compared to that of the continuous-flow-only condition. This improvement in thrombolysis was triggered by a synergistic effect of mechanical and drug-induced digestion. The increase of transient trans-thrombus pressure ultimately contributes to a better drug permeation into the clot and faster exposure of more drug binding and digestion sites.[18] Although a difference in thrombolysis was observed at varying pressure amplitude, they are not as dramatic since the statistics only support an increase of 19% from a pressure amplitude of 4 to 40 mmHg at the MPA averaged shear condition. In addition, higher averaged wall shear stress in the presence of pulsatile flow contributes to increased mechanical and drug induced clot digestion. These findings agreed with results of steady flow models published elsewhere. [19]

This manuscript also introduced a method for creating an *in-vitro* pulsatile flow model using a peristaltic pump with a tubing-based setup. Through matching dimensionless factors including length scale, *Re,* and Womersley numbers of a human MPA, one could establish human MPA relevant pulsatile flow dynamics in the unbranched straight tubing *in-vitro* setup. Importantly, the model version described herein is a simplified demonstration as it focused on getting the same averaged *Re* over a cardiac cycle, however, transient *Re* values dictate a better kinematic similarity of MPA pulsatile flow. Matching the transient *Re* at systolic and diastolic phase constrains the model pressure amplitude, and thus, we elected to match the average value for the purpose of this study. In the MPA relevant model condition (averaged wall shear = 913 s^{-1}), the 20cc dampener which gives 20 mmHg pressure difference is the dampener that more closely captured the native

MPA which has a pressure difference of ~15 mmHg.[20] Furthermore, one could also match *Re* at every moment of the cardiac cycle to improve dynamic similarity. Another limitation of this study is that we only employed platelet-free plasma clots as the digestion substrate. A whole blood clot with components like a platelet contracting fibrin network could end up expressing a much stronger resistance to thrombolytic drugs that might affect our pulsatile flow impact results. On the other hand, native vessel geometry could still contribute to flow variation as well. Thus, incorporating a 3D printed MPA can be a good future direction to continue the study of pulsatile impact on thrombolytic drug activities.

7.6 Conclusions

Varying pulsatile pressure amplitude can affect thrombolytic drug efficacy on clot digestion. Increasing pressure amplitude from 4 to 40 mmHg results in an increased trend of tPA-induced clot digestion at a variety of pulsatile flow conditions including a human MPA mimicked pulsatile flow (average wall shear rate = 913 s^{-1}) as well as slower pulsatile flows (205 and 523 s^{-1}). A human heartbeat mimetic setup further confirmed the impact of pulsatile difference on thrombolysis through a comparison to an approximately equivalent steady flow setup. Knowing the difference in tPA-induced thrombolysis at varying pulsatile pressure difference can help understand the mechanism of thrombolytic therapy in native vessels. The present findings also suggest that incorporating a pulsatile flow in an *in-vitro* model is necessary to provides for a dynamic and potentially more representative platform for evaluating thrombolytic drugs.

7.7 References

[1] M.T. García-Sanz, C. Pena-Álvarez, P. López-Landeiro, A. Bermo-Domínguez, T. Fontúrbel, F.J. González-Barcala, Symptoms, location and prognosis of pulmonary embolism, Revista Portuguesa de Pneumologia 20(4) (2014) 194-199.

[2] C.C. Jain, Y. Chang, C. Kabrhel, J. Giri, R. Channick, J. Rodriguez-Lopez, R.P. Rosovsky, A. Fogerty, K. Rosenfield, M.R. Jaff, I. Weinberg, Impact of Pulmonary Arterial Clot Location on Pulmonary Embolism Treatment and Outcomes (90 Days), American Journal of Cardiology 119(5) (2017) 802-807.

[3] E.F. Grabowski, Thrombolysis, Flow, and Vessel Wall Interactions, Journal of Vascular and Interventional Radiology 6(6) (1995) 25S-29S.
[4] H.D. Hettiarachchi, Y. Hsu, T.J. Harris, Jr., R. Penn, A.A. Linninger, The effect of pulsatile flow on intrathecal drug delivery in the spinal canal, Ann Biomed Eng 39(10) (2011) 2592-602.
[5] K. Spengos, S. Behrens, M. Daffertshofer, C.E. Dempfle, M. Hennerici, Acceleration of thrombolysis with ultrasound through the cranium in a flow model, Ultrasound in Medicine & Biology 26(5) (2000) 889-895.
[6] J.J. Ryan, S.L. Archer, The right ventricle in pulmonary arterial hypertension: disorders of metabolism, angiogenesis and adrenergic signaling in right ventricular failure, Circ Res 115(1) (2014) 176-88.
[7] S. Mazimba, T.S. Welch, H. Mwansa, K.K. Breathett, J.L.W. Kennedy, A.D. Mihalek, W.C. Harding, M.M. Mysore, D.X. Zhuo, K.C. Bilchick, Haemodynamically Derived Pulmonary Artery Pulsatility Index Predicts Mortality in Pulmonary Arterial Hypertension, Heart, Lung and Circulation 28(5) (2019) 752-760.
[8] M. Elder, N. Blank, A. Kaki, M.C. Alraies, C.L. Grines, M. Kajy, R. Hasan, T. Mohamad, T. Schreiber, Mechanical circulatory support for acute right ventricular failure in the setting of pulmonary embolism, Journal of Interventional Cardiology 31(4) (2018) 518-524.
[9] N. Uzuner, O. Ozdemir, G. Tekgol Uzuner, Relationship between pulsatility index and clinical course of acute ischemic stroke after thrombolytic treatment, Biomed Res Int 2013 (2013) 265171.
[10] G.A. Truskey, F.P.D. Yuan, D.F. Katz, Transport phenomena in biological systems, 2nd , International ed., Pearson, Boston, Mass. ; London, 2010.
[11] K.H.K. Wong, J.M. Chan, R.D. Kamm, J. Tien, Microfluidic models of vascular functions, Annual Review of Biomedical Engineering 14 (2012) 205-230.
[12] C.C. O'Brien, V.B. Kolachalama, T.J. Barber, A. Simmons, E.R. Edelman, Impact of flow pulsatility on arterial drug distribution in stent-based therapy, J Control Release 168(2) (2013) 115-24.
[13] J.R. Womersley, Method for the calculation of velocity, rate of flow and viscous drag in arteries when the pressure gradient is known, J Physiol 127(3) (1955) 553-63.
[14] B.T. Tang, S.S. Pickard, F.P. Chan, P.S. Tsao, C.A. Taylor, J.A. Feinstein, Wall Shear Stress is Decreased in the Pulmonary Arteries of Patients with Pulmonary Arterial Hypertension: An Image-Based, Computational Fluid Dynamics Study, Pulmonary Circulation 2(4) (2012) 470-476.

[15] E. Sloth, K.C. Houlind, S. Oyre, W. Yong Kim, E.M. Pedersen, H.S. Jørgensen, J.M. Hasenkam, Three-dimensional visualization of velocity profiles in the human main pulmonary artery with magnetic resonance phase-velocity mapping, American Heart Journal 128(6 PART 1) (1994) 1130-1138.
[16] S.D. Russell, J.G. Rogers, C.A. Milano, D.B. Dyke, F.D. Pagani, J.M. Aranda, C.T. Klodell, Jr., A.J. Boyle, R. John, L. Chen, H.T. Massey, D.J. Farrar, J.V. Conte, I.I.C.I. HeartMate, Renal and hepatic function improve in advanced heart failure patients during continuous-flow support with the HeartMate II left ventricular assist device, Circulation 120(23) (2009) 2352-7.
[17] L.W. Miller, Is Pulsatile Blood Flow No Longer Essential?, Circulation 120(23) (2009) 2313-2314.
[18] R.W. Muthard, S.L. Diamond, Side view thrombosis microfluidic device with controllable wall shear rate and transthrombus pressure gradient, Lab Chip 13(10) (2013) 1883-91.
[19] C.S. Whyte, H.A. Mostefai, K.M. Baeten, A.J. Lucking, D.E. Newby, N.A. Booth, N.J. Mutch, Role of shear stress and tpa concentration in the fibrinolytic potential of thrombi, International Journal of Molecular Sciences 22(4) (2021) 1-15.
[20] G. Kovacs, A. Berghold, S. Scheidl, H. Olschewski, Pulmonary arterial pressure during rest and exercise in healthy subjects: a systematic review, Eur Respir J 34(4) (2009) 888-94.

8. FUTURE DIRECTIONS

Present in this dissertation is the development of *in-vitro* thrombolysis models leveraging fluorescence signals for thrombolytic drug evaluations. We developed a static annular clot lysis assay and a clot analog incorporated real time human relevant flow model with an optional pulsatile variation. These two models can work together to comprehensively examine a thrombolytic drug agent for properties including but not limited to fibrin affinity, blood fibrinolytic potential, drug synergistic effects, drug interplays with blood components, drug permeation, and drug thrombolytic efficacy under stasis, steady shear, pulsatile flow, and more representative hemodynamics. Results can guide the design of novel drug agents, delivery methods, thrombectomy methods, ultrasound aided treatments or offer the prediction of an optimal dosage regimen.

The annular clot lysis assay is a well-characterized high throughput tool for the primary screening of potential thrombolytic agents. Having good limit of detection, inexpensive material components, and better physiological relevance than chromogenic or immunologic assays have extended the assay's feasibility for diagnosing impaired fibrinolytic potential of patient samples.[1] Experiments conducted with the annular clot lysis assay in this dissertation are a proof-of-concept study aiming at exploring the potentials of the assay. Patient trials will be required to further illustrate its merits for both diagnosis of patient fibrinolytic potential and drug screening applications as a tool in a personalized medicine thrombolysis approach for optimal treatment selection. Specifically, patient own blood components can be used to form annular clot substrates for selecting the best thrombolytic drug candidates. The setup can easily be adapted for an automated instrument at a clinical laboratory to provide for faster and more reproducible results. The 96 well plate design can be modified to an even more multiplexed setting like a 384 well to allow for testing of more drug dosages and drug combinations at once, and reducing the minimal requirement of a tested agent, which is extremely helpful for pilot studies.

Human relevant thrombi analogs were formed in an *in-vitro* Chandler loop setup in our studies. Although their structures and compositions were observed to be very similar to those of human thrombi which agreed with results from studies elsewhere, structural differences still existed. These differences are due to two major reasons which are the over-simplified and not representative flow conditions in the loop compared to the actual blood vessel and the

replenishment of blood components.[2] The missing vessel walls in the device gives no lodging site or collagen involvements for clot formation.[3, 4] Further, the absence of endothelial cells also cannot facilitate the inhibition or secretion of factors such as tPA, PAI-1 and Prostaglandin I2 during clotting and lysis. These factors are responsive to shear conditions and can alter ultimate clot properties and lytic resistance.[5, 6] When clots are formed over an extended period, failing to replenish blood components result in a pseudo clot aging. Since the clot aging is quite common in patients that can lead to clot enlargement and clot strengthening.[7] Therefore, it is necessary to address these issues in future studies through modifying the Chandler loop or use a more relevant setup or device for clot formation. Potential setups should not only emphasize the use of mimicked vessel geometry but also incorporate representative initiation methods like focal injury, systemic contraction, or the creation of a hypercoagulative state.[8]

Current *in-vitro* thrombolysis models usually represent native conditions using averaged shear rates, but fail to address the diversified native flow dynamics caused by pulsatility, blood vessel anatomy, and vessel branching, which can largely affect drug pharmacokinetics.[9, 10] The present *in-vitro* flow thrombolysis model is a good starting point as it has matched both wall shear rate and dimensionless factors such as length scale, Reynolds number and Womersley number. This model has also characterized the pulsatility effect on thrombolytic drugs but can definitely be improved by including additional physiological structures such as vessel geometry, branching and valves where thrombi have been reported to be more prone to reside because of these structures. Incorporating a 3D-printed patient-specific *ex-vivo* vascular graft into the flow model provides for the development of more physiologically relevant flow dynamics and clot orientation. This then leads to a complex transport problem, which is inherently difficult to solve by matching dimensionless factors especially when it comes to convoluted blood vessel structure. Computational fluidic dynamics (CFD) is a powerful tool that can predict flow dynamics in a blood vessel.[11] CFD software allows for the creation of a time-varying 3D velocity field within the lumen where spatial distribution of flow velocity, turbulence, and wall shear stress (WSS) can be computed and visualized. Rather than merely matching averaged dimensionless factors, we can leverage the CFD simulation tool to improve the design of the model to achieve a similar time averaged WSS map in the *ex-vivo* vascular graft to those in native blood vessels. More sophisticated thrombolysis situations such as the presence of stents or other in-vessel medical devices, can be tested together with drugs in this model. Furthermore, as the advancement of 3D

printing technology continues, the *ex-vivo* vascular graft may be printed using materials that have similar mechanical properties as native blood vessels. Thus, the enabled vessel dilation or constriction based on patient blood pressure changes can add more values to the evaluation of thrombolytic drug in this model. In all, the proposed model has the potential to serve as a flexible and representative platform for thrombolytic drug development to guide clinical thrombosis treatment and diagnosis.

8.1 Reference

[1] T. Lisman, Decreased Plasma Fibrinolytic Potential As a Risk for Venous and Arterial Thrombosis, Seminars in Thrombosis and Hemostasis 43(02) (2016) 178-184.

[2] H. Touma, I. Sahin, T. Gaamangwe, M.B. Gorbet, S.D. Peterson, Numerical investigation of fluid flow in a chandler loop, Journal of Biomechanical Engineering 136(7) (2014) 1-8.

[3] P.E. van der Meijden, I.C. Munnix, J.M. Auger, J.W. Govers-Riemslag, J.M. Cosemans, M.J. Kuijpers, H.M. Spronk, S.P. Watson, T. Renne, J.W. Heemskerk, Dual role of collagen in factor XII-dependent thrombus formation, Blood 114(4) (2009) 881-90.

[4] A.D. Blann, How a damaged blood vessel wall contibutes to thrombosis and hypertenasion, Pathophysiol Haemost Thromb 33(5-6) (2003) 445-8.

[5] S.L. Diamond, J.B. Sharefkin, C. Dieffenbach, K. Frasier-Scott, L.V. McIntire, S.G. Eskin, Tissue plasminogen activator messenger RNA levels increase in cultured human endothelial cells exposed to laminar shear stress, Journal of Cellular Physiology 143(2) (1990) 364-371.

[6] Z. Yang, J.-m. Wang, L.-c. Wang, L. Chen, C. Tu, C.-f. Luo, A.-l. Tang, S.-M. Wang, J. Tao, In vitro shear stress modulates antithrombogenic potentials of human endothelial progenitor cells, Journal of Thrombosis and Thrombolysis 23(2) (2007) 121-127.

[7] J.M. Rubin, S.R. Aglyamov, T.W. Wakefield, M. O'Donnell, S.Y. Emelianov, Clinical application of sonographic elasticity imaging for aging of deep venous thrombosis: preliminary findings, J Ultrasound Med 22(5) (2003) 443-8.

[8] P.H. Mangin, K.B. Neeves, W.A. Lam, J.M.E.M. Cosemans, N. Korin, S.W. Kerrigan, M.A. Panteleev, In vitro flow-based assay: From simple toward more sophisticated models for mimicking hemostasis and thrombosis, Journal of Thrombosis and Haemostasis 19(2) (2021) 582-587.

[9] N. Nishino, M.F. Scully, M.W. Rampling, V.V. Kakkar, Properties of Thrombolytic Agents in Vitro Using a Perfusion Circuit Attaining Shear Stress at Physiological Levels, Thrombosis and Haemostasis 64(04) (1990) 550-555.
[10] D.A. Graham, T.C. Huang, B.A. Keyt, B.R. Alevriadou, Real-time measurement of lysis of mural platelet deposits by fibrinolytic agents under arterial flow, Annals of Biomedical Engineering 26(4) (1998) 712-724.
[11] V.L. Rayz, L. Boussel, M.T. Lawton, G. Acevedo-Bolton, L. Ge, W.L. Young, R.T. Higashida, D. Saloner, Numerical Modeling of the Flow in Intracranial Aneurysms: Prediction of Regions Prone to Thrombus Formation, Annals of Biomedical Engineering 36(11) (2008) 1793-1804.

APPENDIX

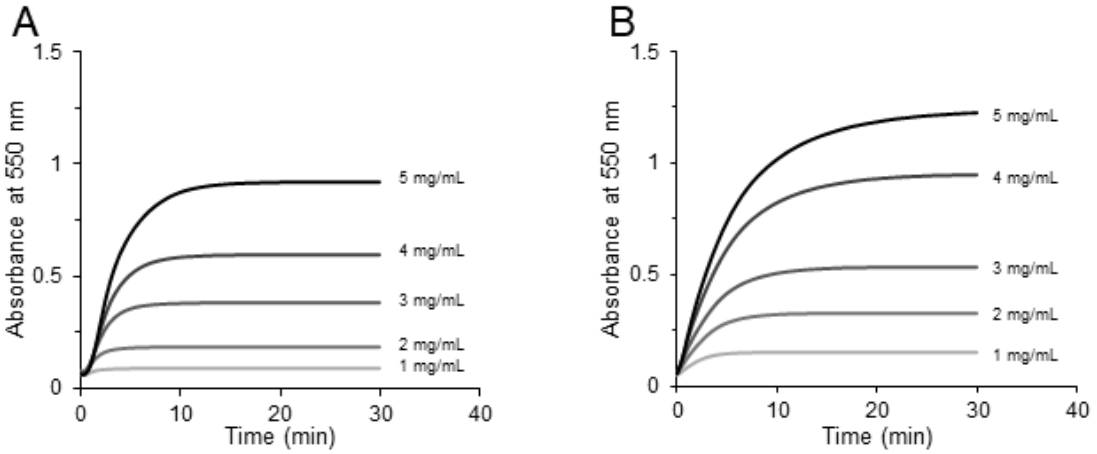

Figure A.1. Turbidity tracings of bovine (A) and human (B) fibrin formation at different fibrinogen concentrations (1, 2, 3, 4, 5 mg/mL) with 1 U/mL species matched thrombin.

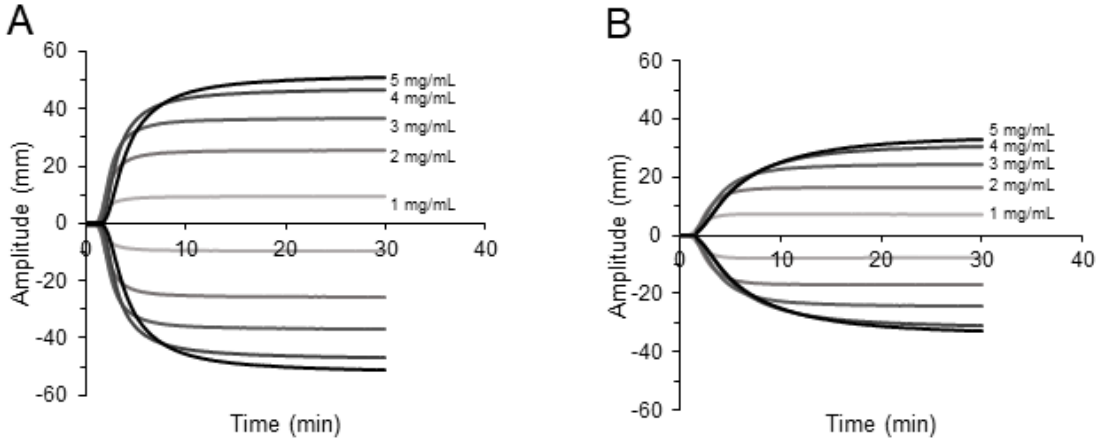

Figure A.2. TEG tracings of bovine (A) and human (B) fibrin formation at different fibrinogen concentrations (1, 2, 3, 4, 5 mg/mL) with 1 U/mL species matched thrombin.

Table A.1. V_{max}, Lag time, α Angle and R in Varying Fibrinogen Concentration on Fibrin Formation

Fibrinogen Concentration	1 mg/ml	2 mg/ml	3 mg/ml	4 mg/ml	5 mg/ml
$V_{max\ Bovine}$ (munit/min)	20.5±4.7	60.5±7.6	115.3±10.4	147.6±6.5	212.9±10.4
$V_{max\ Human}$ (munit/min)	25.2±1.7	53.1±3.4	83.2±3.7	122.9±8.5	158.7±9.2
Lag time $_{Bovine}$ (min)	< 0.5	< 0.5	< 0.5	< 0.5	< 0.5
Lag time $_{Human}$ (min)	< 0.5	< 0.5	< 0.5	< 0.5	< 0.5
α Angle $_{Bovine}$ (deg)	55.9*	70.5	75.6	74.5	70.1
α Angle $_{Human}$ (deg)	39.6*	61.6*	55.7	49.5	47.7
R_{Bovine} (min)	1.2	1.2	1.3	1.6	1.9
R_{Human} (min)	1.4	1.6	1.5	1.8	1.8

Note: * denotes the angle value of the group whose MA does not reach 20 mm

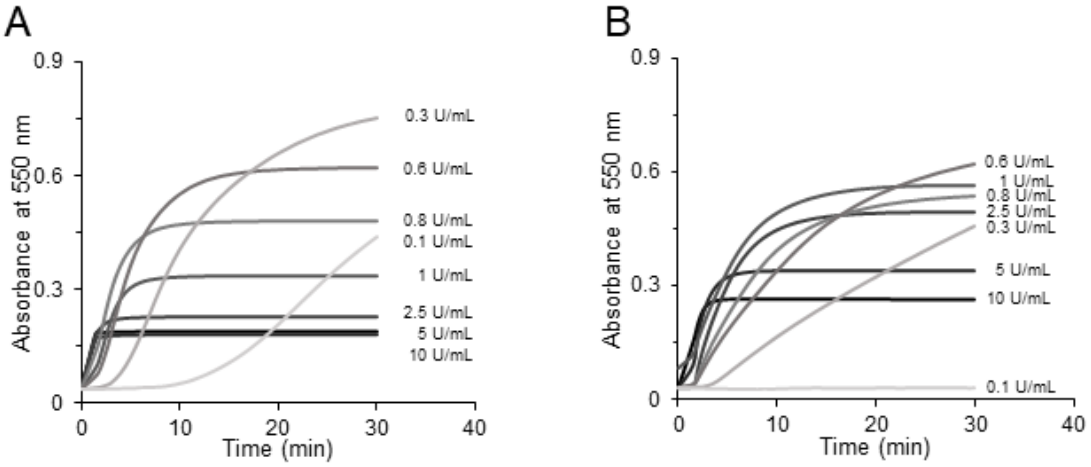

Figure A.3. Turbidity tracings of bovine (A) and human (B) fibrin formation at different thrombin concentrations (0.1, 0.3, 0.6, 0.8, 1, 2.5, 5, 10 U/mL) with 3 mg/mL species matched fibrinogen. These curves are first 30 min of tracings and actual tests may take longer to get desired parameters.

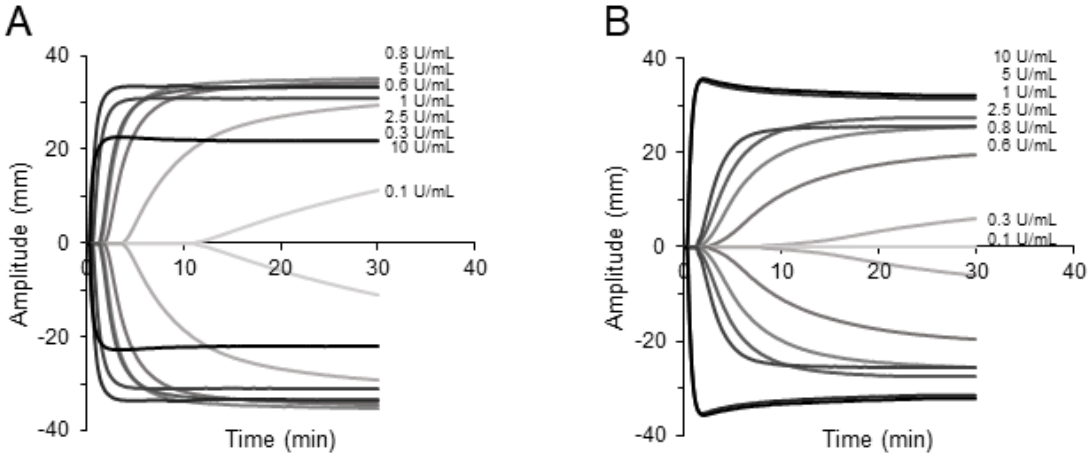

Figure A.4. TEG tracings of bovine (A) and human (B) fibrin formation at different thrombin concentrations (0.1, 0.3, 0.6, 0.8, 1, 2.5, 5, 10 U/mL) with 3 mg/mL species matched fibrinogen. These curves are first 30 min of tracings and actual tests may take longer to get desired parameters.

Table A.2. V_{max}, Lag time, α Angle and R in Varying Thrombin Concentration on Fibrin Formation

Thrombin Concentration	0.1U/ml	0.3U/ml	0.6U/ml	0.8U/ml	1U/ml	2.5U/ml	5U/ml	10U/ml
$V_{max\ Bovine}$ (munit/min)	24.2±2.0	57.7±5.5	91.1±8.2	87.9±21.6	90.1±2.2	94.3±11.0	125±30.8	154.7±62.9
$V_{max\ Human}$ (munit/min)	NA	21.1±1.2	38.5±7.0	58.3±2.1	84.8±14.8	85.7±9.6	147.3±42.0	169.8±17.4
Lag time $_{Bovine}$ (min)	28.8±9.2	1.3±0.4	< 0.5	< 0.5	< 0.5	< 0.5	< 0.5	< 0.5
Lag time $_{Human}$ (min)	3.3±0.1	1.9±1.2	< 0.5	< 0.5	< 0.5	< 0.5	< 0.5	< 0.5
α Angle $_{Bovine}$ (deg)	10.1*	42.2	62.2	73.1	74.3	80.3	82.4	80.4
α Angle $_{Human}$ (deg)	NA	4.3*	21.3*	37.6	50	61.8	84.2	84.1
R $_{Bovine}$ (min)	2	4.3	2.1	1.6	1.3	0.6	0.3	0.2
R $_{Human}$ (min)	NA	15.8	4.2	2.5	1.8	1.5	0.2	0.2

Note: * denotes the angle value of the group whose MA does not reach 20 mm

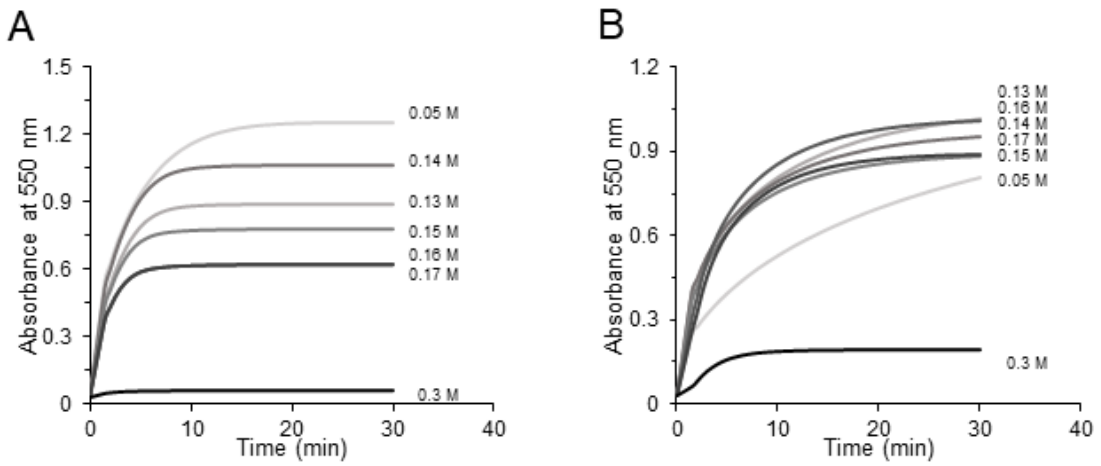

Figure A.5. Turbidity tracings of bovine (A) and human (B) fibrin formation at different ionic strength (0.05, 0.13, 0.14, 0.15, 0.16, 0.17, 0.3 M) with species matched fibrinogen (3 mg/mL) and thrombin (1 U/mL). These curves are first 30 min of tracings and actual tests may take longer to get desired parameters.

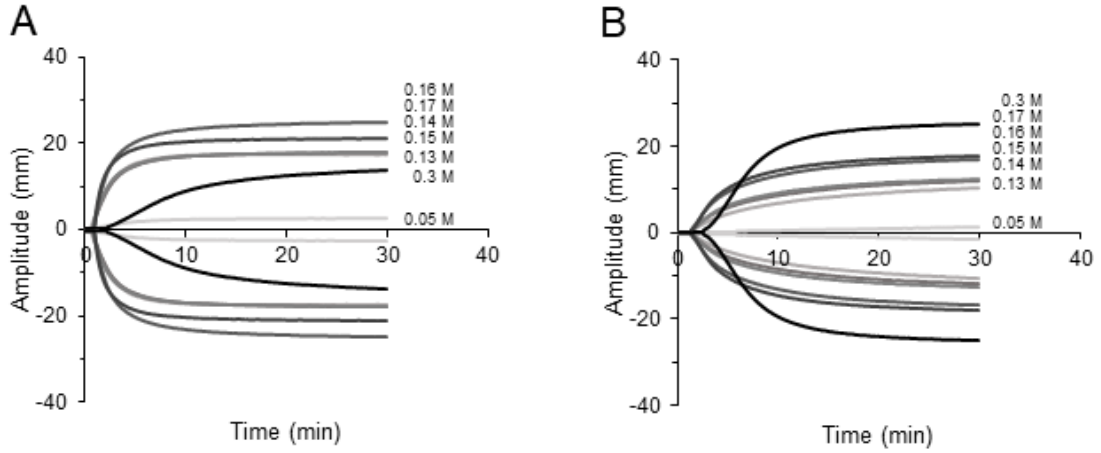

Figure A.6. TEG tracings of bovine (A) and human (B) fibrin formation at different ionic strength (0.05, 0.13, 0.14, 0.15, 0.16, 0.17, 0.3 M) with species matched fibrinogen (3 mg/mL) and thrombin (1 U/mL). These curves are first 30 min of tracings and actual tests may take longer to get desired parameters.

Table A.3. V_{max}, Lag time, α Angle and R in Varying Ionic Strength on Fibrin Formation

Ionic Strength	0.05 M	0.13 M	0.14 M	0.15 M	0.16 M	0.17 M	0.3 M
$V_{max\ Bovine}$ (munit/min)	144.0±23.8	184.3±58.5	183.9±71.9	175.0±63.7	234.5±78.1	155.5±52.1	6.0±1.0
$V_{max\ Human}$ (munit/min)	49±3.7	98.2±15.5	104.7±18.5	108.5±14.7	163.8±20.7	154.0±17.7	43.8±5.4
Lag time $_{Bovine}$ (min)	< 0.5	< 0.5	< 0.5	< 0.5	< 0.5	< 0.5	< 0.5
Lag time $_{Human}$ (min)	< 0.5	< 0.5	< 0.5	< 0.5	< 0.5	< 0.5	< 0.5
α Angle $_{Bovine}$ (deg)	6.2*	55.5*	60.8*	62.9*	68.7	72.1	17.6*
α Angle $_{Human}$ (deg)	0.7*	20.2*	30.8*	31.7*	41.5*	42.5*	37.4
R $_{Bovine}$ (min)	5.2	0.8	0.8	0.8	0.9	0.9	3.6
R $_{Human}$ (min)	44.7	2.3	1.9	1.9	1.7	1.7	3.2

Note: * denotes the angle value of the group whose MA does not reach 20 mm

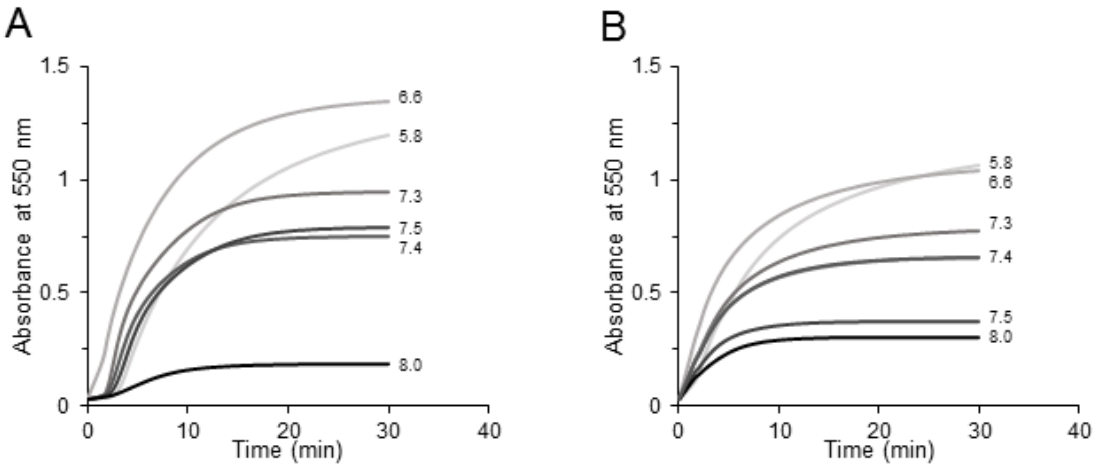

Figure A.6. Turbidity tracings of bovine (A) and human (B) fibrin formation at different pH (5.8, 6.6, 7.3, 7.4, 7.5, 8) with species matched fibrinogen (3 mg/mL) and thrombin (1 U/mL). These curves are first 30 min of tracings and actual tests may take longer to get desired parameters.

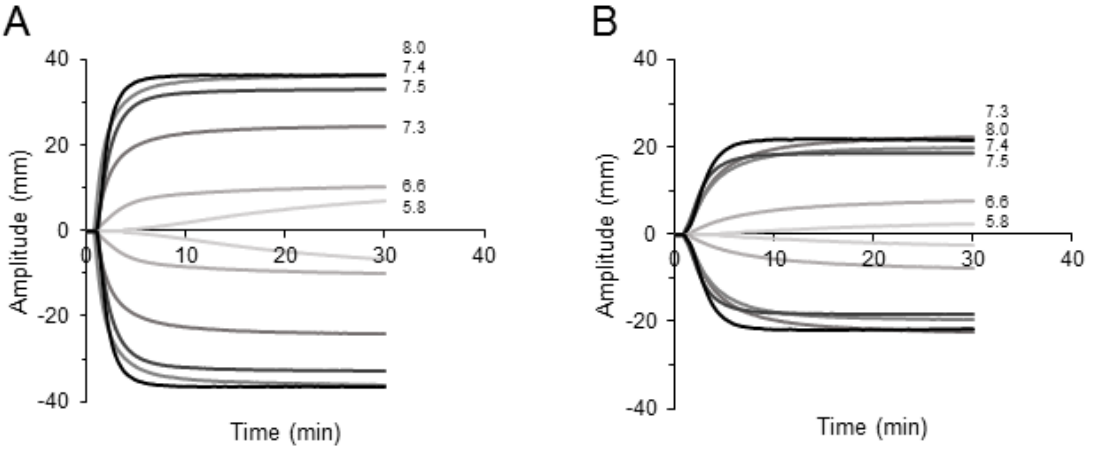

Figure A.7. TEG tracings of bovine (A) and human (B) fibrin formation at different pH (5.8, 6.6, 7.3, 7.4, 7.5, 8) with species matched fibrinogen (3 mg/mL) and thrombin (1 U/mL). These curves are first 30 min of tracings and actual tests may take longer to get desired parameters.

Table A.4. V_{max}, Lag time, α Angle and R in Varying pH on Fibrin Formation

pH	5.8	6.6	7.3	7.4	7.5	8
$V_{max\ Bovine}$ (munit/min)	175.2±7.0	270.4±62.5	227.3±16.3	181.9±5.3	139.8±78.1	33.0±5.8
$V_{max\ Human}$ (munit/min)	134.5±14.9	174.0±31.2	112.1±14.5	98.5±10.2	57.0±9.8	42.2±11.8
Lag time $_{Bovine}$ (min)	3.0±0.5	< 0.5	< 0.5	< 0.5	< 0.5	< 0.5
Lag time $_{Human}$ (min)	< 0.5	< 0.5	< 0.5	< 0.5	< 0.5	< 0.5
α Angle $_{Bovine}$ (deg)	4.7*	32.4*	70.8	78.4	76.1	78.3
α Angle $_{Human}$ (deg)	1.8*	17.8*	51.7	48.3*	56*	56.6
R $_{Bovine}$ (min)	9.9	1.6	1.0	0.8	1.1	1.0
R $_{Human}$ (min)	20.7	2.8	1.2	1.3	1.2	1.3

Note: * denotes the angle value of the group whose MA does not reach 20 mm

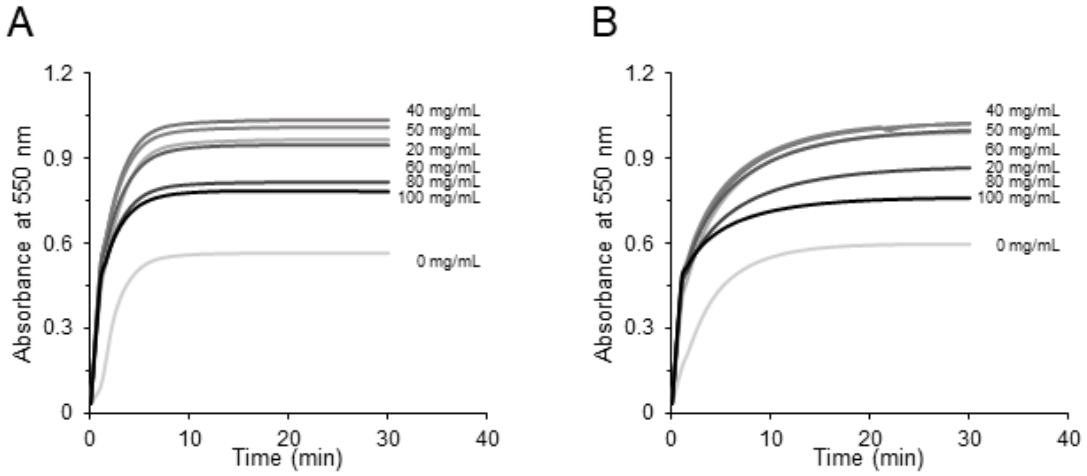

Figure A.8. Turbidity tracings of bovine (A) and human (B) fibrin formation at different albumin concentrations (0, 20, 40, 50, 60, 80, 100 mg/mL) with species matched fibrinogen (3 mg/mL) and thrombin (1 U/mL).

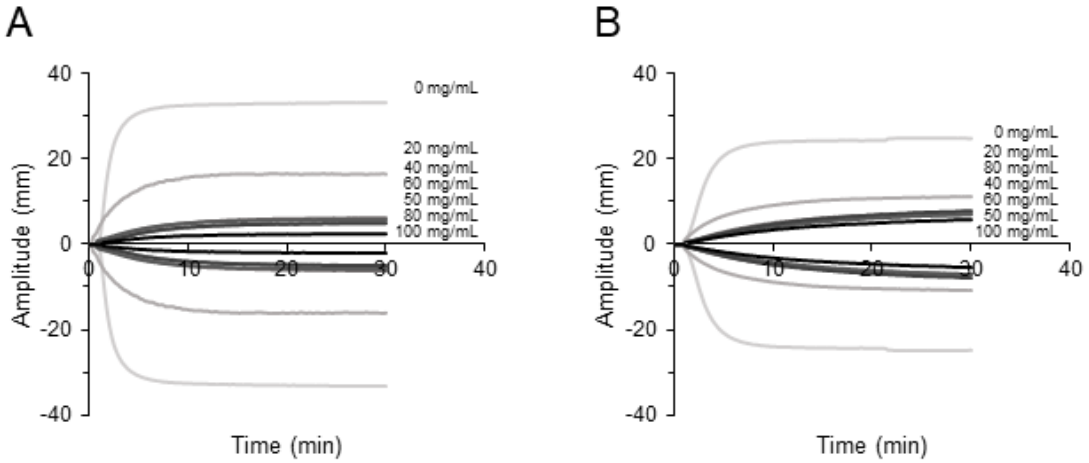

Figure A.9. TEG tracings of bovine (A) and human (B) fibrin formation at different albumin concentrations (0, 20, 40, 50, 60, 80, 100 mg/mL) with species matched fibrinogen (3 mg/mL) and thrombin (1 U/mL).

Table A.5. V_{max}, Lag time, α Angle and R in Varying Albumin on Fibrin Formation

Albumin Concentration	0	20 mg/ml	40 mg/ml	50 mg/ml	60 mg/ml	80 mg/ml	100 mg/ml
$V_{max\ Bovine}$ (munit/min)	161.3±38.8	215.4±64.7	208.7±50.3	196.7±45.5	184.2±51.9	154.6±48.3	128.0±31.7
$V_{max\ Human}$ (munit/min)	103.9±11.3	175.2±49.9	159.2±41.1	149.4±37.6	134.7±32.7	109.2±34.4	92.2±29.3
Lag time $_{Bovine}$ (min)	< 0.5	< 0.5	< 0.5	< 0.5	< 0.5	< 0.5	< 0.5
Lag time $_{Human}$ (min)	< 0.5	< 0.5	< 0.5	< 0.5	< 0.5	< 0.5	< 0.5
α Angle $_{Bovine}$ (deg)	77.9	51.2*	13.7*	10*	14.2*	8.7*	2.4*
α Angle $_{Human}$ (deg)	64.3	49.6*	22.9*	18*	12.5*	17.4*	9*
R $_{Bovine}$ (min)	1.2	0.4	2.8	3.4	2.2	3.8	12.6
R $_{Human}$ (min)	1.2	0.6	1.8	2.0	2.8	1.4	3.9

Note: * denotes the angle value of the group whose MA does not reach 20 mm

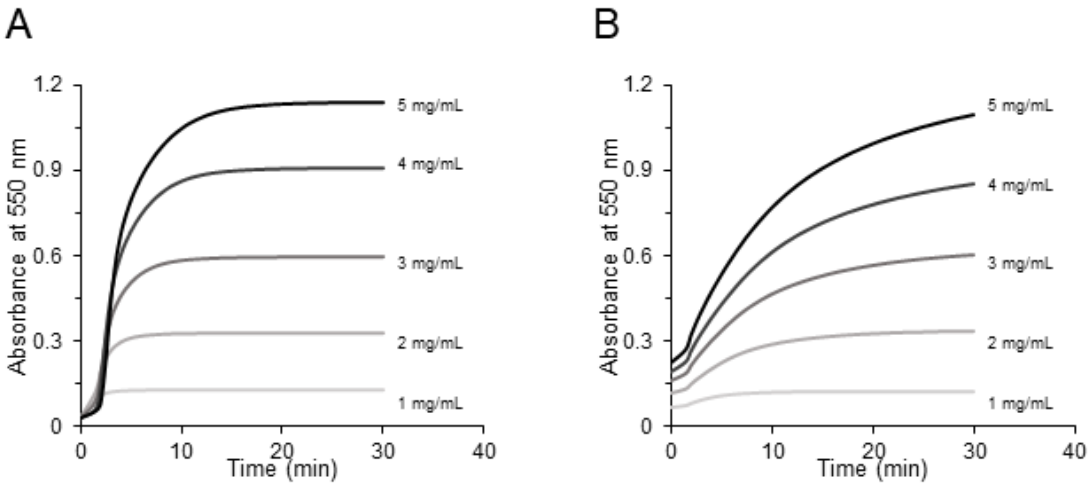

Figure A.10. Turbidity tracings of fibrin formation by bovine fibrinogen / human thrombin (A) and human fibrinogen / bovine thrombin (B) at different fibrinogen concentrations (1, 2, 3, 4, 5 mg/mL) with 1 U/mL thrombin.

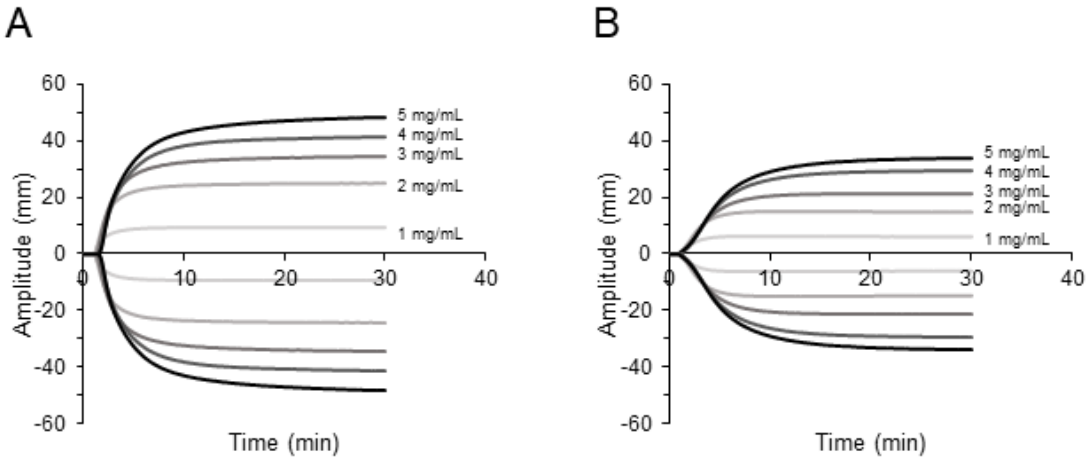

Figure A.11. TEG tracings of fibrin formation by bovine fibrinogen / human thrombin (A) and human fibrinogen / bovine thrombin (B) at different fibrinogen concentrations (1, 2, 3, 4, 5 mg/mL) with 1 U/mL thrombin.

Table A.6. V_{max}, Lag time, α Angle and R in Cross-species Fibrin Formation

	1 mg/ml	2 mg/ml	3 mg/ml	4 mg/ml	5 mg/ml
	Bovine fibrinogen & human thrombin				
V_{max} (munit/min)	58.7±18.9	140.3±15.9	115.3±10.4	147.6±6.5	212.9±10.4
Lag time (min)	< 0.5	< 0.5	< 0.5	< 0.5	< 0.5
α Angle (deg)	57.3	72.0	75.3	73.3	75.2
R (min)	1.2	1.2	1.4	1.7	1.7
	Human fibrinogen & bovine thrombin				
V_{max} (munit/min)	18.5±3.8	42.7±8.4	67.3±13.5	91.2±19.2	121.8±18.9
Lag time (min)	< 0.5	< 0.5	< 0.5	< 0.5	< 0.5
α Angle (deg)	*37	*51	49.4	51.5	50.2
R (min)	1.5	1.3	1.5	1.6	1.4

Note: * denotes the angle value of the group whose MA does not reach 20 mm

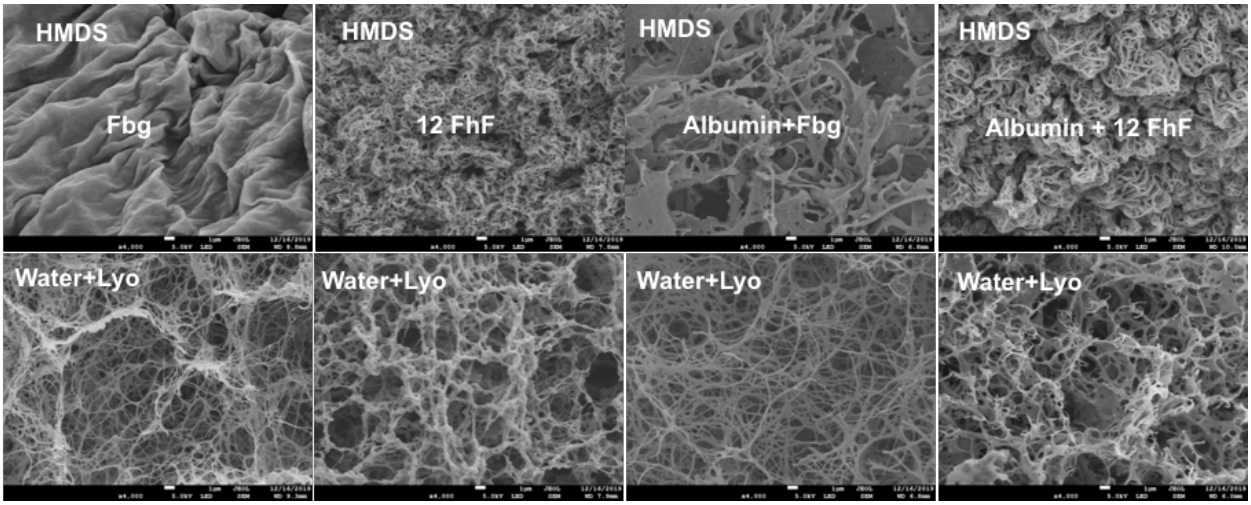

Figure A.12. Representative SEM images (4,000X) were compared for ethanol-Bis(trimethylsilyl)amine (HMDS, Electron Microscopy Sciences Supplier, Hatfield, PA) (first row) and water-lyophilization dehydration methods (second row) of fibrin clots, which were formed by neat fibrinogen, neat 12FhF, Albumin + fibrinogen, and albumin + 12FhF. The HMDS method requires the washing of clot samples using a series of ethanol swaps at 30%, 50%, 70% and 100% (3 times), followed by a 50:50 ethanol to HMDS swap, and an overnight storage in 100% HMDS. However, the HMDS method results in clots that have 95% shrinkage while the lyophilization method offers a puffy dehydrated clot. Scale bar was shown as 1 μm in all images.

Figure A.13. Identification of lysine / FITC conjugation sites on fibrinogen alpha, beta and gamma chains using mass spectrometry. One fibrinogen molecule has a pair of alpha, beta, and gamma chains. Available fibrinogen crystal structures (PDB entity sequence: 3GHG) are derived from the protein data bank for reference. The detailed protocol for fabricating FITC tagged fibrinogen molecules: Reacting human fibrinogen with a 200-fold excess FITC at RT for 24 hours and incubating for another 6 hours with the addition of doubled moles of fresh FITC to maximize the FITC conjugation on fibrinogen. The FITC-fibrinogen was then purified using 100kDa cutoff filter under 6 cycles of centrifugation to remove free FITC molecules. An average of 16 FITC per fibrinogen were identified through absorbance readings using the spectrometer method detailed in the main text. FITC-fibrinogen was then denatured in 8 M urea and digested by 1 µg trypsin/Lys-C protease mix for 4 hours at 37 C before dilution to 2 M urea overnight. Peptide sequences were examined using mass spectrometry. Data were subjected to post-translational modification (PTM) analysis using PEAKS Xpro to find FITC-lysine conjugation sites. Overall, PEAKS Xpro provided ~90% coverage of the fibrinogen protein and peptide sequences were included for analysis at less than 1% false discovery rate. The sum of all lysine residues in each pair are 43+36+34=113; wherein, mass spec covered lysine sites are 38+28+32=98, crystal structure known lysine sites are 16+4+5=25. Mass spec covered FITC sites are 16+6+5=27, and crystal structure known FITC sites are 4+4+5=13. Specifically, locations of these lysine are identified. Alpha chain (81% coverage, 16 sites): K89, K100, K148, K157, K227, K243, K322, K432, K437, K448, K467, K476, K558, K575, K602, K620. K238 is removed (since it had 390, but with a substitution in the peptide); Beta chain (83% coverage, 6 sites): K52, K77, K152, K163, K353, K367. K264 (missing 390 signatures though) and K426 (not full sequencing fragmentation) are removed; Gamma chain (90% coverage, 5 sites): K84, K101, K111, K146, K188. K199 is removed (missing 390, peptide has an AA substitution). Due to the lack of 100% coverage in both mass spec and available crystal structure a comprehensive identification of dominant lysine conjugation sites could not be further characterized. This data is, however; useful in demonstrating the diversity of conjugation sites indicating that there is some degree of conjugation variation even at saturating levels of FITC associated with a lysine conjugation technique of this nature.

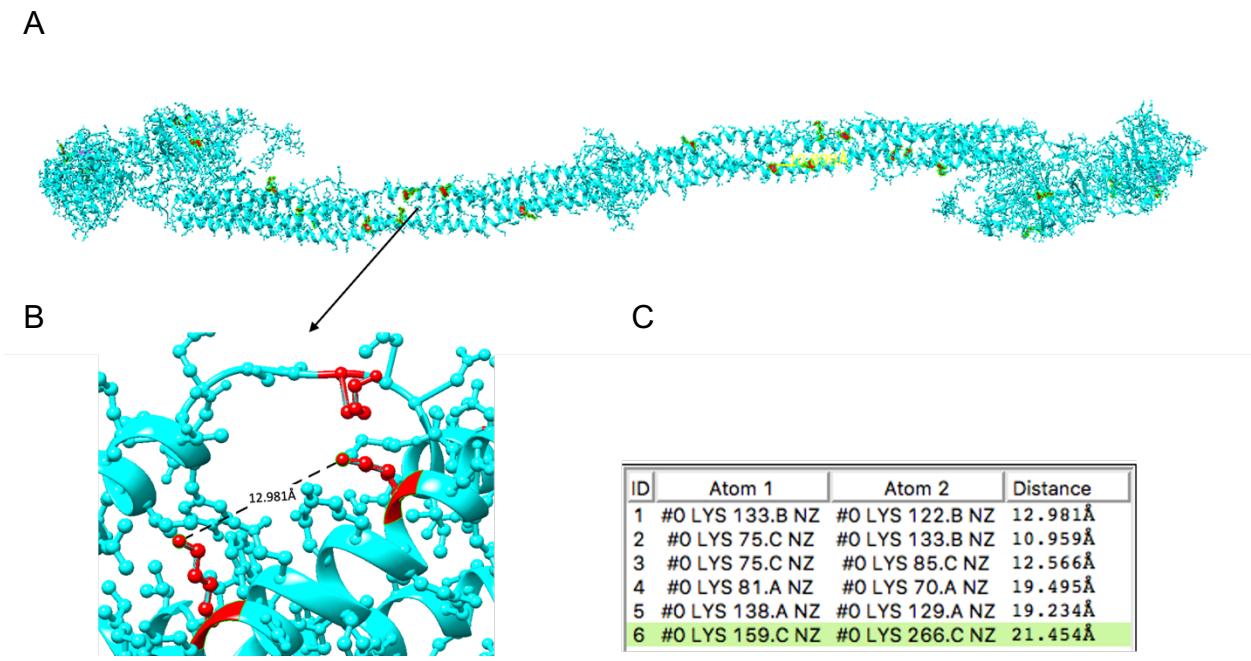

ID	Atom 1	Atom 2	Distance
1	#0 LYS 133.B NZ	#0 LYS 122.B NZ	12.981Å
2	#0 LYS 75.C NZ	#0 LYS 133.B NZ	10.959Å
3	#0 LYS 75.C NZ	#0 LYS 85.C NZ	12.566Å
4	#0 LYS 81.A NZ	#0 LYS 70.A NZ	19.495Å
5	#0 LYS 138.A NZ	#0 LYS 129.A NZ	19.234Å
6	#0 LYS 159.C NZ	#0 LYS 266.C NZ	21.454Å

Figure A.14. (A) Fibrinogen crystal structure (PDB entity sequence: 3GHG, protein data bank) is shown in blue ribbon with identified FITC conjugation sites labeled in red. Despite an average of 16 FITC per fibrinogen calculated via absorbance, 54 lysine sites (27 sites in one set of fibrinogen alpha, beta, and gamma chain) were found to be accessible for FITC conjugation. This indicates that the conjugation reaction yields a heterogeneous FITC-fibrinogen mixture which can have different FITC amounts per fibrinogen or are products that have similar FITC amounts per fibrinogen but possess different combinations of FITC conjugation sites. The average 16 FITC per fibrinogen is most likely contributed by both scenarios. This is typical of non-site-specific conjugation techniques such as lysine-based labeling used here. In addition, only 52.8% of the fibrinogen crystal structure is known with the unknown part mostly belonging to the alpha C domain (representing 28 more possible FITC accessible lysine sites for conjugation). (B) shows a representative example of measuring the distance of adjacent FITC conjugation sites on available fibrinogen crystal structures using Chimera. In the known crystal structure of one set of the fibrinogen chains, 6 pairs (C) totaling 10 non-repeated conjugation sites were found to be within 20 angstroms of one another. Due to the proximity of these sites, the conjugation of one site within a pair likely reduces the probability of FITC subsequently conjugating the other one due to steric effects.

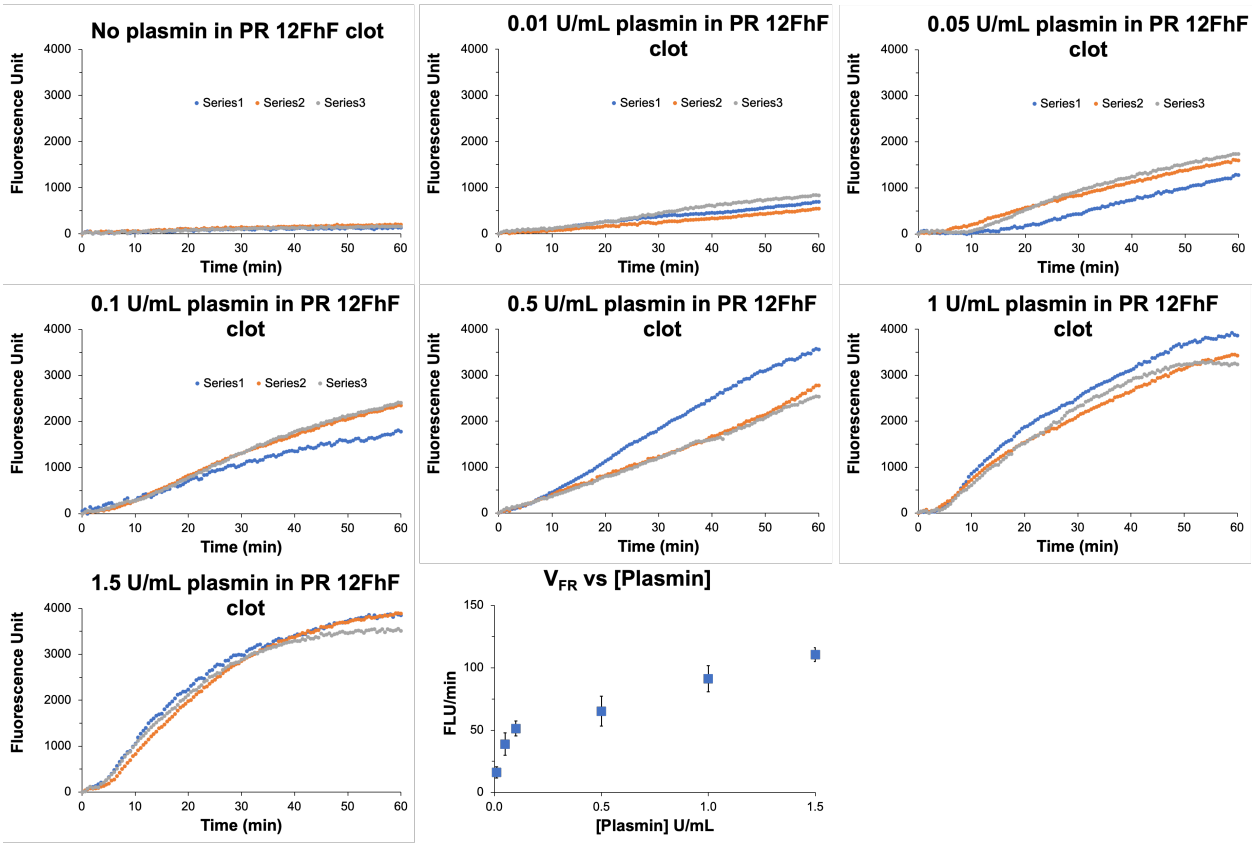

Figure A.15. Fluorescence tracing curves of varying plasmin concentrations for digesting physiologically relevant 12FhF annular clots at 37 °C. The last figure shows V_{FR} (fluorescence release rate) over plasmin concentrations.

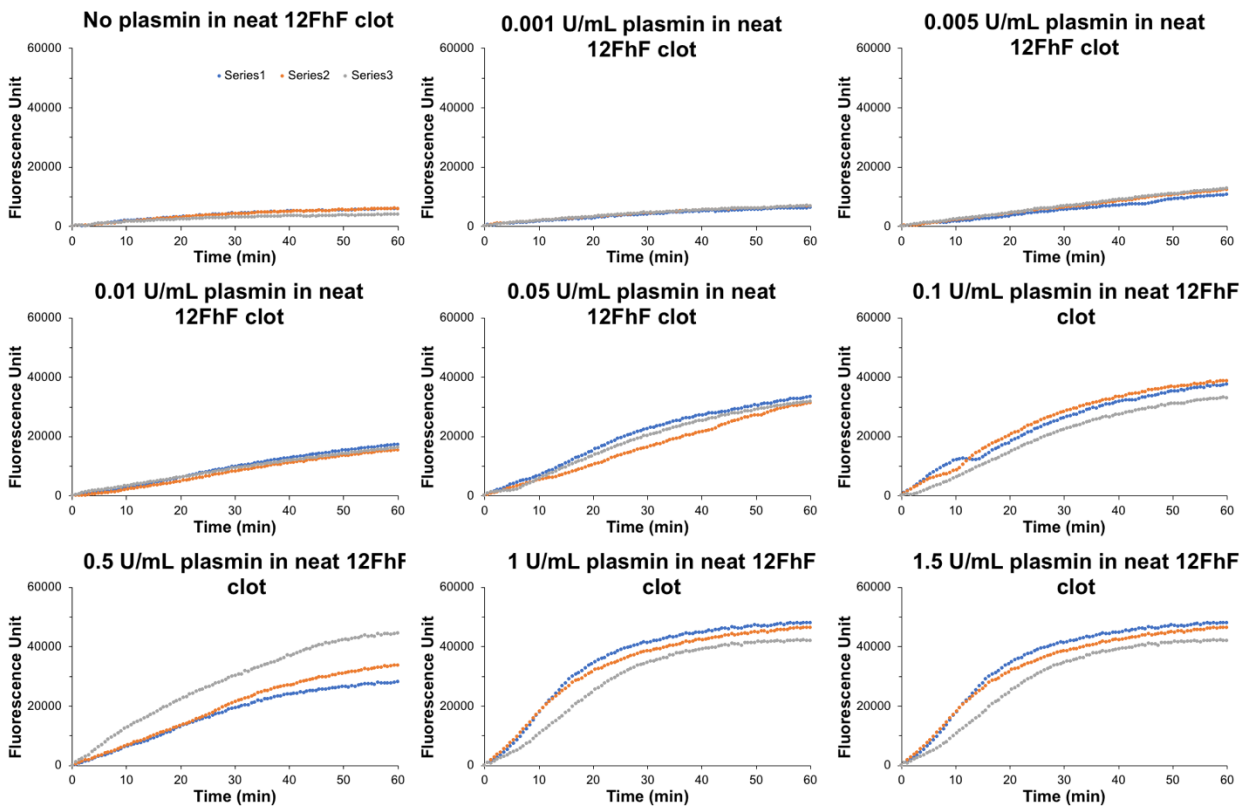

Figure A.16: Fluorescence tracing curves of varying plasmin concentrations for digesting neat 12FhF annular clots at 37 °C.

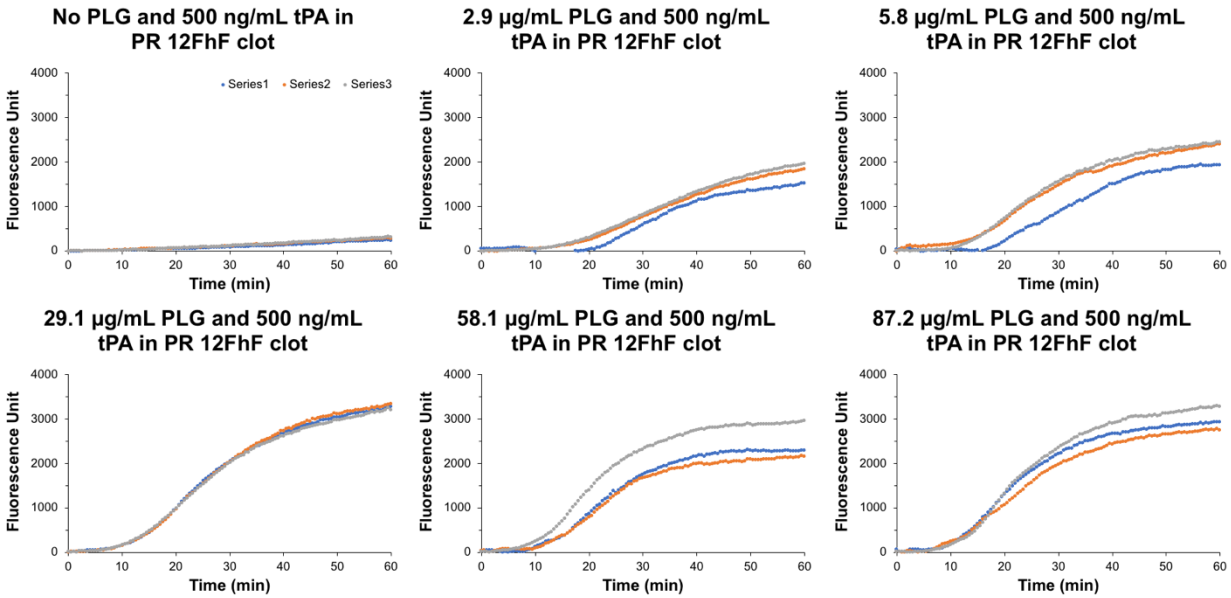

Figure A.17. Fluorescence tracing curves of varying plasminogen concentration at fixed [tPA] for digesting physiologically relevant 12FhF annular clots at 37 °C.

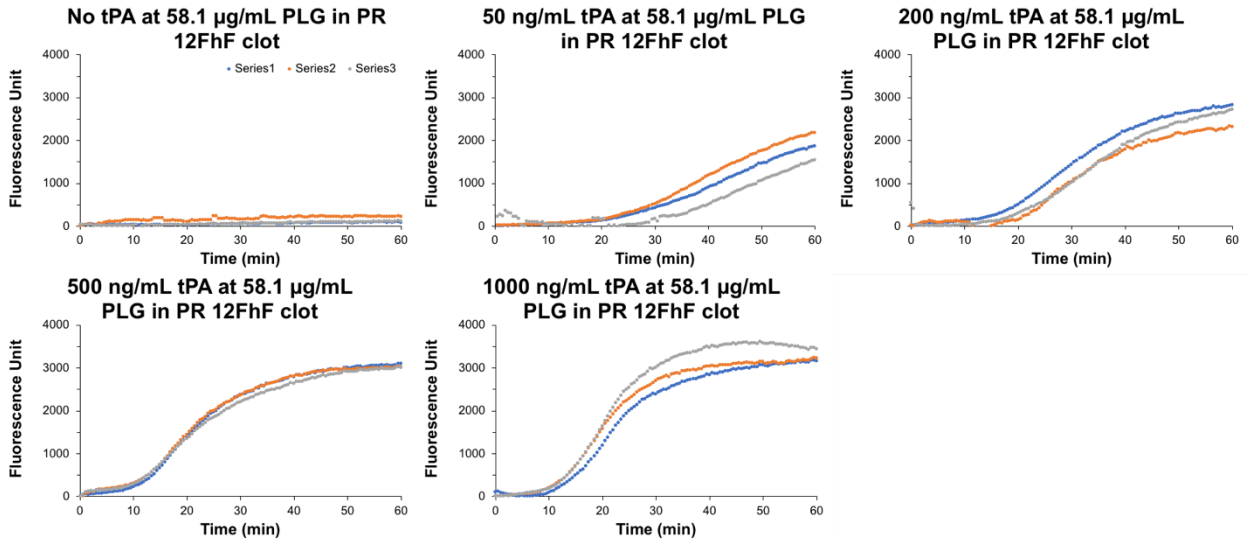

Figure A.18. Fluorescence tracing curves of varying [tPA] at fixed plasminogen concentration for digesting physiologically relevant 12FhF annular clots at 37 °C.

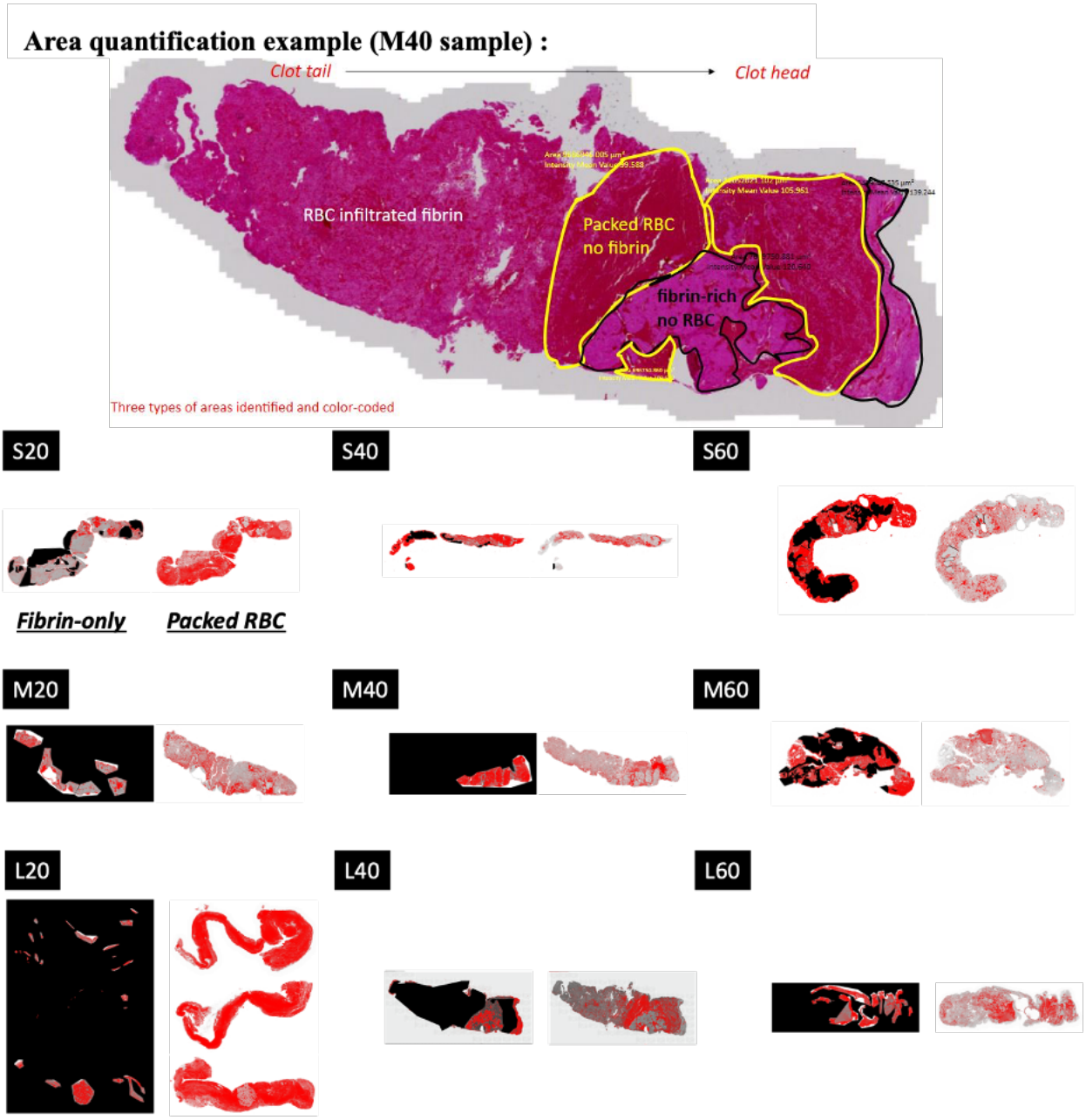

Figure A.19. Quantification of three regions--fibrin-only, packed RBC and RBC-infiltrated fibrin in a clot sample. The demo figure shows representative regions (color coded) and corresponding area in pixel. Representative images processed using ImageJ for the area quantification of fibrin-only region (1st column) and packed RBC region (2nd column) in clots formed at nine different conditions (S, M, L tubing sizes and 20, 40 60 RPMs). RBC infiltrated fibrin areas were indirectly measured by subtracting fibrin-only, packed RBC and WBC areas (not shown in this figure) from total clot areas.

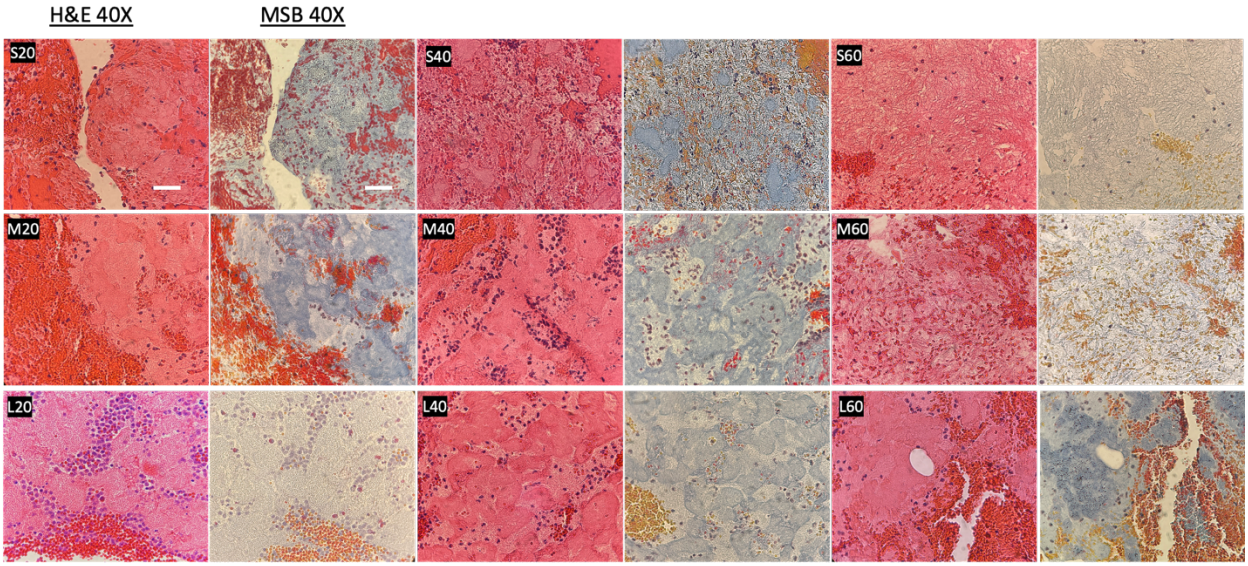

Figure A.20. Histology photos of representative stained clot samples using H&E and MSB at 40X. H&E stains: WBCs (blue), RBCs (red), fibrin (pink). MSB stains: WBCs (purple), RBCs (yellow or red), fibrin (blue or red), platelets (gray). Scale bars are 50 µm.

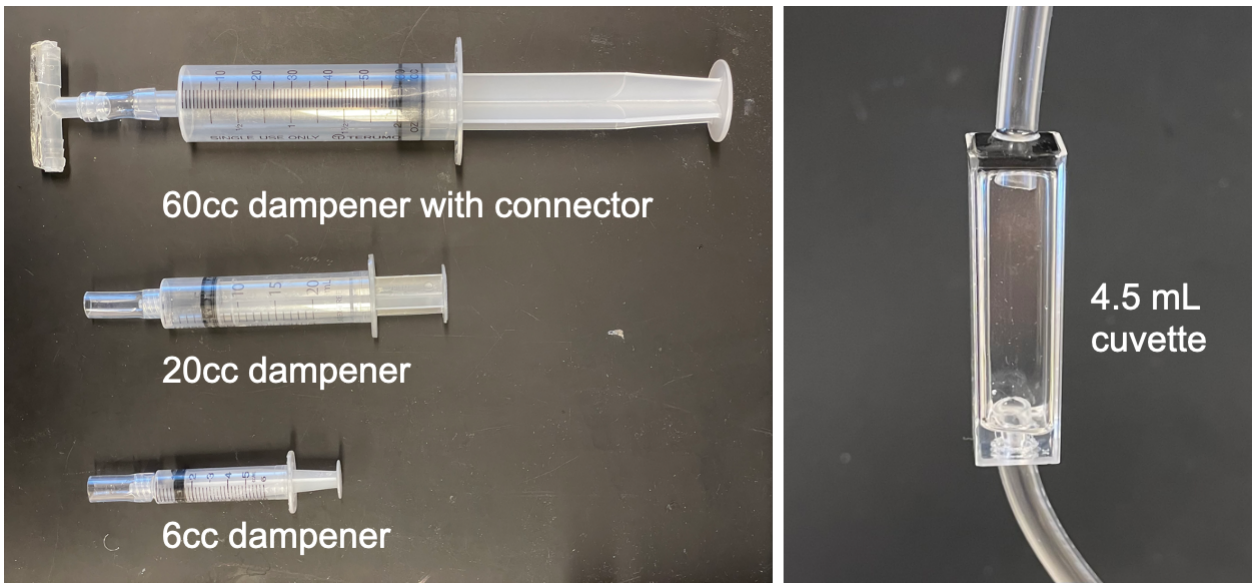

Figure A.21. Three dampeners and a flow cell designed for RT-FluFF setup.

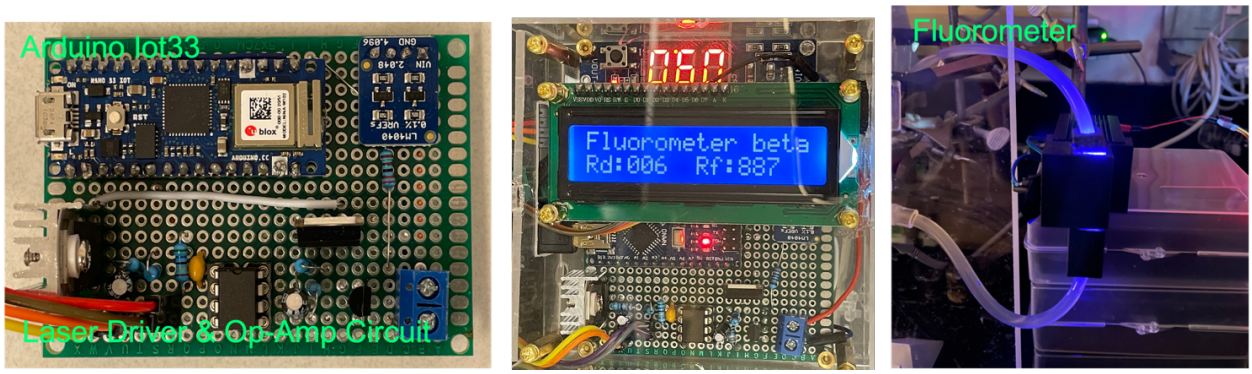

Figure A.22. Operational amplifier circuit with Arduino Iot33 (Left) or Arduino Nano (Nano) for data acquisition. In-line fluorometer work in progress (Right).

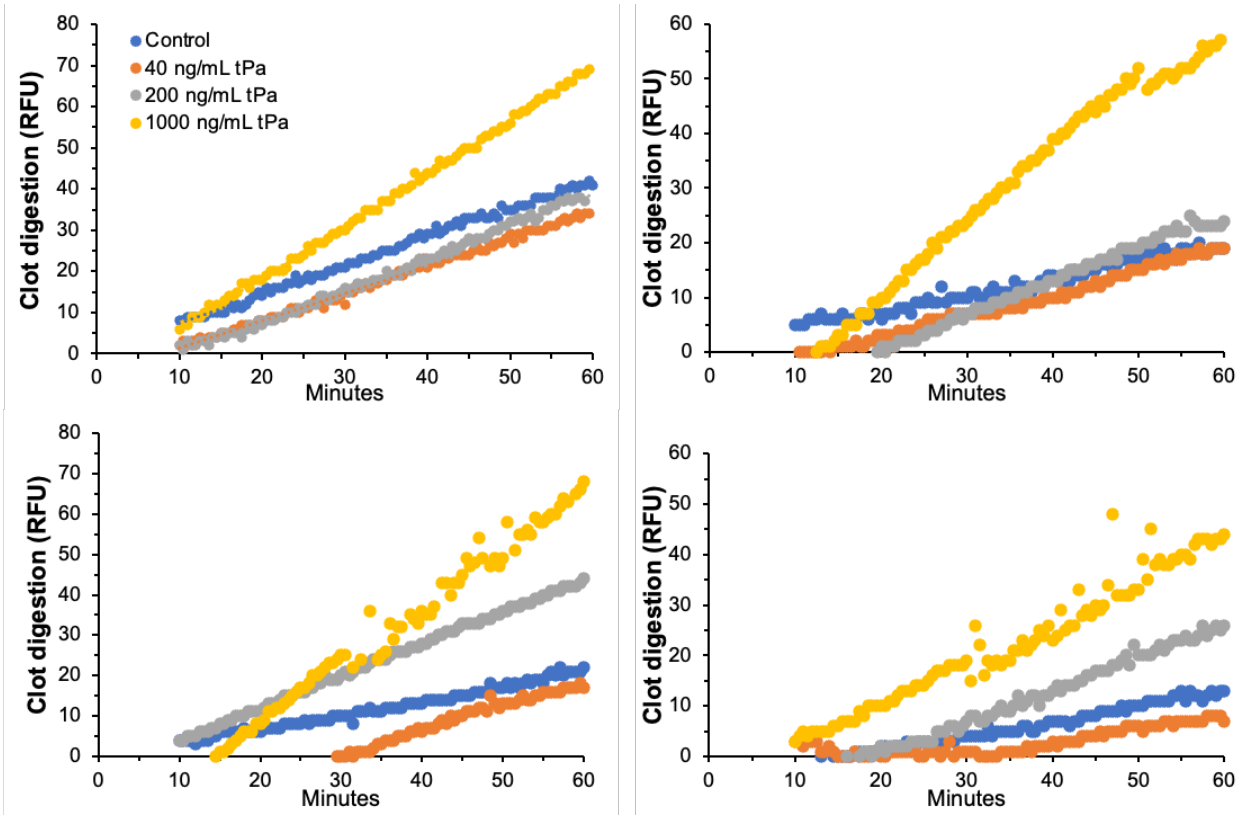

Figure A.23. Scatter plots from four more patients' data. Each point represents a single reading from the fluorometer part of the RT-FluFF assay. Rates of fibrinolysis were derived from the slopes of the linear regions in each graph. Importantly, certain groups had a shortened linear region resulting from a prolonged lag phase; however, rates of FITC release were still able to be extracted from shortened linear phases.

PUBLICATIONS

Justin J. Crowder*, **Ziqian Zeng***, Alissa N. Novak, Nathan J. Alves, and Amelia K. Linnemann. "Stabilization Protects Islet Integrity during Respirometry in the Oroboros Oxygraph-2K Analyzer." Islets (2022).

U.S. Provisional Patent Application (No. 63/230,286): Nathan J. Alves, **Ziqian Zeng**. "Reporter labeled Annular Clot System for Diagnosis and Research." U.S. patent application filed at IU School of Medicine (2021).

Ziqian Zeng, Tanmaye Nallan Chakravarthula, Charanya Muralidharan, Abigail Hall, Amelia K. Linnemann, and Nathan J. Alves. "Fluorescently Conjugated Annular Fibrin Clot for Multiplexed Real-time Digestion Analysis." Journal of Materials Chemistry B (2021) ***(Cover story)***

Ziqian Zeng*, Phuong T. Lam*, Michael L. Robinson, Katia Del-Rio Tsonis, Justin M. Saul. "Design and Characterization of Biomimetic Keratin Aerogel-Electrospun Poly(caprolactone) Scaffolds for Retinal Cell Culture." Annals of Biomedical Engineering (2021): 1-12. ***(Cover story)***

Alexei Christodoulides, **Ziqian Zeng**, and Nathan J. Alves. "In-vitro thromboelastographic characterization of reconstituted whole blood utilizing cryopreserved platelets." Blood Coagulation & Fibrinolysis: an International Journal in Haemostasis and Thrombosis (2021).

Tanmaye Nallan Chakravarthula, **Ziqian Zeng**, and Nathan J. Alves. "Modulating Plasmin Activity using Multivalent Benzamidine Inhibitors." The FASEB Journal, 35 (S1). (2021) **(Published abstract)**

Ziqian Zeng, Tanmaye Nallan Chakravarthula, and Nathan J. Alves. "Leveraging Turbidity and Thromboelastography for Complementary Clot Characterization." JoVE (Journal of Visualized Experiments) 160 (2020): e61519.

Tanmaye Nallan Chakravarthula, John Zagorski, **Ziqian Zeng**, Jeffery A. Kline, Nathan J. Alves. "Equivalence Study of Semaxanib (SU5416) from Different Suppliers." American Journal of Respiratory Cell and Molecular Biology 63.6 (2020): 865-868.

Ziqian Zeng, Mahussi Fagnon, Tanmaye Nallan Chakravarthula, and Nathan J. Alves. "Fibrin clot formation under diverse clotting conditions: Comparing turbidimetry and thromboelastography." Thrombosis Research 187 (2020): 48-55.

Tanmaye Nallan Chakravarthula, **Ziqian Zeng**, and Nathan J. Alves. Effect of PEG Linker Length on Human Plasmin Inhibition by Benzamidine. The FASEB Journal, 34(S1), 1-1. (2020) **(Published abstract)**

'' indicates co-first authorship.*